

**Copyright**

**by**

**Tarek Abu Serie Elshayeb**

**2004**

**The Dissertation Committee for Tarek Abu Serie Elshayeb Certifies that this is the  
approved version of the following dissertation:**

**Integrated Sequence Stratigraphy, Depositional Environments,  
Diagenesis, and Reservoir Characterization of the  
Cotton Valley Sandstones (Jurassic),  
East Texas Basin, USA**

**Committee:**

---

Earle F. McBride, Supervisor

---

Kitty Milliken

---

William Galloway

---

William Fisher

---

Rob Lander

---

Shirley Dutton



**Integrated Sequence Stratigraphy, Depositional Environments,  
Diagenesis, and Reservoir Characterization of the  
Cotton Valley Sandstones (Jurassic),  
East Texas Basin, USA**

**by**

**Tarek Abu Serie Elshayeb, B.Sc.**

**Dissertation**

Presented to the Faculty of Graduate School of

The University of Texas at Austin

In Partial Fulfillment

of the Requirements

For the Degree of

**Doctor of Philosophy**

**The University of Texas at Austin**

**August, 2004**

## **Dedication**

To my parents, my wife **Amany** and to our children, **Mostafa** and **Omar**, my overflowing and endless source of love and life.

## **Acknowledgments**

The Egyptian Cultural and Educational Bureau and the J. Nalle Gregory Chair in Sedimentary Geology of the University of Texas at Austin, provided funding for this dissertation research. This funding is gratefully appreciated.

Thanks for the Geology Foundation, Geological Society of America, Gulf Coast Association of Geological Societies, and American Association of Petroleum Geologists for funding this work.

Dr. Earle McBride supervised this dissertation. I greatly appreciate his constantly available support and generous contribution of his time and effort in research assistance. His patience, scientific ability, and wide experience in diagenesis and all dependent parameters that control diagenetic evolution of sandstones, guided this research. In addition to being a rigorous research advisor, he also gave me plenty of freedom to make and guide my own ideas.

Special thanks to Ms. McBride, the first person I have seen when I came to Austin. She prepared everything for me and my family to live here. She gave us peace of mind and without her, our first days in Austin would have been very difficult.

I am really grateful to my committee members, Dr. Kitty Milliken, Dr. William Galloway, Dr. William Fisher, Dr. Shirley Dutton and Dr. Rob Lander. This dissertation has greatly benefited from their knowledge, experience, and editorial comments.

Dr. Milliken helped with microprobe and SEM analyses and discussion. She also was very helpful in the sample preparations for oxygen isotope analysis. Dr. Bill Galloway helped me in core description and interpreting depositional environments. Dr. William Fisher, in addition to his experience and knowledge of geology, was always a source of friendship and optimism. Dr Fisher also helped a lot in solving my financial problems during this work. Dr Shirley Dutton was always a source of good advice, valuable assistance, and suggestions. She was very open minded and very helpful in discussing any problems concerning this work.

Special thanks to Dr. Rob Lander and Dr. Linda Bonnell, who granted free use and support of Touchstone<sup>TM</sup> diagenesis modeling software. Rob Lander and Linda Bonnell were restless in promptly solving any problems I had in the way.

Thanks are due to Dr. Robert Folk who was always a source of providing keys for specific problems and helped with SEM analysis. He also gave a plenty of time to review the diagenesis part of this work.

A debt of gratitude is given to Dr. Floyd “Bo” Henk who helped me in core description, interpretation of depositional environments, and who taught me how to identify trace fossils. Bo taught me how to put small pieces together to come up with a big view. Moreover, I held my first core workshop with him and he taught me a lot.

I would like to acknowledge Dr. Frank Brown for his help in analyzing the sequence stratigraphy. He spent plenty of his time to review this work. Thanks for Dr.

William Ambrose for his valuable assistance, comments, suggestions, and revision of the depositional environments chapter of this work. Special thanks for my friend Khaled Fouad for his help and support during hard times.

I would like to acknowledge Dennis Trombatore and his staff for essential library assistance, and Greg Thompson for his excellent job in making thin sections for this work.

Special thanks to George Bush, James Donnelly and Robert Sanchez from the Austin Core Research Center at the Bureau of Economic Geology for their sincere help and support to facilitate my core study.

I would like to acknowledge Zachary Sharp for helping on quartz isotope analysis, Fluid Inc. for fluid inclusion analysis, Core Lab for porosity and permeability analysis, and Basline DGSi for organic geochemistry analysis.

I also thank my colleagues of the department of Geological Sciences: Petro Papaziz, Suk-Joo Choh and Jenn Cooke for their help and support during hard times.

Very special thanks to my friends Hamid Ali and Basir Al Fadda for true friendship and helping me and my family when necessary.

I wish to express my gratitude to my wife, Amany Elsayed, who bravely faced the challenge of coming to Texas with me and postponing her graduate study in physical therapy. Amany Elsayed preferred to stay with the family and take care of our kids, Mostafa and Omar. I will be forever in debt to my family for their unconditional love, confidence and motivation through these years.

I will be ever grateful to my Dad and Mom who have supported me with love over all my life, and have given me the reference that make up my personality framework.

Finally, a debt of recognition to a number of people not named here that encouraged me, or just loved me throughout the way

**Integrated Sequence Stratigraphy, Depositional Environments,  
Diagenesis, and Reservoir Characterization of  
the Cotton Valley Sandstones,  
East Texas Basin, USA**

Publication No. \_\_\_\_\_

Tarek Abu Serie Elshayeb, Ph.D.

The University of Texas at Austin, 2004

Supervisor: Earle F. McBride

The cumulative production of the Cotton Valley Sandstones in East Texas Basin as of 1993 was 2,666 BCFG with estimated reserves of 24.2TCFG. The Upper Jurassic-Lower Cretaceous Cotton Valley Sandstone is a thick siliciclastic unit in East Texas Basin. It is characterized by low porosity (<6%) and low permeability (<0.5 md) and requires hydraulic fracturing to yield its gas. This study concerns the sequence stratigraphy, depositional environments and diagenesis of the Cotton Valley Sandstones in order to gain an insight into the processes that influenced their reservoir quality. The research involved the use of 4000 feet of conventional core, 350 well logs, and petrographic and geochemical data on sandstones, shales and organic matter. Various analytical techniques were used, including optical petrography, SEM/EDS, CL, EMP,

XRD, stable and radiogenic isotope geochemistry and fluid inclusions. Six major third-order depositional sequences were identified by correlating SP and resistivity logs on 60 wells. Each sequence has identifiable highstand, transgressive, and/or lowstand system tracts. Sandstones and shales of the transgressive system tract were deposited in strike-oriented barrier island complexes and associated shelf and slope environments. Deposits of the highstand system tracts were most probably deposited in wave-dominated deltaic settings. No cores are available in the lowstand system tracts. Twenty five facies (F1-F25) have been grouped into four main facies associations that represent fully marine (FA1), marginal marine (FA2 and FA3) and back-barrier coastal plain (FA4) environments of deposition.

Cotton Valley sandstones are very fine-to fine-grained, moderately-to well-sorted quartzarenite and subarkose. The Ouachita Mountains and Arbuckle Mountains located north and northwest of the study area are most probably the main sources of sediments for the Cotton Valley clastics. Sandstones experienced extensive diagenesis that altered the original detrital composition of the sandstone and modified initial porosity and permeability.

The paragenetic sequence of the Cotton Valley sandstones include: 1) clay coatings around the detrital grains (chlorite and illite); 2) early pore-filling pyrite; 3) calcite 1 precipitation; 4) quartz cement; 5) dissolution of feldspars; 6) potash-feldspar overgrowths; 7) kaolinite and chlorite cement; 8) oil emplacement; 9) illite; 10) calcite 2; 11) dolomite and anhydrite; and 12) late diagenetic pyrite.



There are two principal internal sources of silica in the Cotton Valley Sandstones, intergranular pressure solution and dissolution along stylolites. The average quartz cement in the Cotton Valley is 11% and the calculated amount of silica derived internally from both pressure solution and stylolites constitute up to 48% of the total quartz cement. The remaining 52% come from sources that could not be quantified. Other significant local sources of silica include dissolution of quartz grains at clay laminae and at contacts between sandstone and interbedded shales, and dissolution of micron-scale detrital quartz within interbedded shales and clay laminae. High content of clay laminae are observed in cores and shale interbeds constitute up to 35% of the total CV rock volume. These sources could not be quantified. A possible external source, a silica-rich fluid expelled from the Bossier shales.

Authigenic carbonates occur as pore-filling cement and replacive phase. Calcite cement is the dominant carbonate type in the Cotton Valley Sandstones. The source of Ca for authigenic calcite is the local dissolution and reprecipitation of the carbonate shell fragments in the sandstones and the oyster-rich lagoonal limestone beds interbedded with the sandstone. The limestone beds, which range in thickness from 35 ft (10.5 m) to 50 ft (15.5 m), served as a good sealing rock as well as a potential source for calcite cement. The Cotton Valley has an average of 20%-35% shales interbedded with the sandstones; these shales could have been a significant source for iron as well as carbonates and quartz cements to the sandstones.

Original porosity loss by compaction was much more than that lost by cementation in the bioturbated *Ophiomorpha*-dominated sandstones and crypto-bioturbated sandstones, whereas porosity loss by cementation was more significant in the cleaner sandstones of the laminated, tidally influenced shoreface and sand flat.

The reservoir quality of the studied sandstones is controlled mainly by depositional environment and subsequent diagenesis. Depositional environment controlled the distribution of clay matrix and oyster fragments. Clay coatings in the Cotton Valley Sandstones had a direct influence on the precipitation of quartz cement. Clay coatings retarded quartz cementation and resulted in a better reservoir quality. It was also observed that shell fragments were the primary source of carbonate cements. So, depositional environment indirectly controlled the distribution of quartz cement and carbonates in various facies.

Three main parameters influenced reservoir quality: (1) the amount of clay matrix introduced by bioturbation, (2) the amount of quartz cement, and (3) the percentage of clay coating. Cotton Valley Sandstones are divided into three main reservoir types: (1) poor reservoir quality: quartz-cemented sandstones, (2) poor reservoir quality: bioturbated sandstones with more than 15% clay matrix; and (3) good reservoir quality: clean bioturbated sandstones with less than 10% clay matrix.

## TABLE OF CONTENT

<b>List of Tables</b> .....	XVIII
<b>List of Figures</b> .....	XIX
<b>CHAPTER 1: PURPOSE OF STUDY</b>	<b>1</b>
1.1. Purpose of Study .....	1
1.2. Study approach and procedure.....	5
1.2.1. Methods.....	7
1.3. Geologic setting.....	10
1.3.1. Introduction .....	10
1.3.2. Regional structural setting .....	11
1.3.3. Local structural setting .....	12
1.3.3. Cotton Valley Group stratigraphic nomenclature.....	14
1.4. Previous work.....	16
<b>CHAPTER 2: SEQUENCE STRATIGRAPHY</b>	<b>25</b>
2.1. Introduction .....	25
2.2. Data.....	29
2.3. Methods.....	30
2.3.1. Stacking pattern .....	30
2.3.2. Stratigraphic surfaces .....	32
2.3.3. Trace fossils .....	35
2.4. Stratigraphic cross sections .....	35
2.4.1. Dip-oriented cross section D-D` .....	38
2.4.2. Strike-oriented and diagonal cross sections .....	41
2.5. Well log core integration .....	46
2.5.1. Cores that penetrated S1 and/or SB1 .....	48
2.5.1.1. SFE # 3 .....	48
2.5.1.2. Blocker Heirs # 1 .....	52

2.5.1.3. Burnett Brothers # 12 .....	57
2.5.1.4. Tallent # 1 .....	57
2.5.1.5. James Anderson # 1 .....	57
2.5.2. Cores that penetrated S2 and/or SB2 .....	61
2.5.2.1. James Anderson # 1 .....	61
2.5.2.2. Jones Gas Unit # 3 .....	64
2.5.2.3. Grace Lowry # 1 .....	64
2.5.2.4. Davidson Foundation # 1 .....	68
2.5.3. Cores that penetrated S3 .....	71
2.5.4. Cores that penetrated S4, SB4, S5, SB5 and S6 .....	71
2.5.4.1. Jones Gas Unit # 3 .....	71
2.5.4.2. Bradshaw # 1 .....	71
2.5.4.3. Jones Gas Unit # 3 and James Anderson # 1 .....	76
2.5.4.4. Davidson Foundation # 1 .....	76
2.6. Sequence stratigraphic model .....	76
<b>CHAPTER 3: DEPOSITIONAL ENVIRONMENT</b>	<b>80</b>
3.1. Introduction.....	80
3.2. Barrier Island .....	82
3.3. Facies and facies associations .....	91
3.3.1. General comments .....	91
3.3.2. Facies association 1: off-shore/shoreface transition .....	92
3.3.2.1. Facies 1: Irregularly interbedded sandstone and shales .....	92
3.3.2.2. Facies 2: Massive to faintly laminated dark grey-black mudstone with fossil shell debris.....	94
3.3.2.3. Facies 3: Intensively bioturbated silty mudstone .....	96
3.3.2.4. Facies 4: <i>Chondrites</i> -dominated mudstone.....	99
3.3.2.5. Facies 5: Bioturbated thin and very thin bedded shale, siltstone and very fine-grained sandstone.....	99
3.3.2.6. Facies 6: Bioturbated, carbonaceous-rich silty sandstone.....	102

3.3.3. Facies association 2: shoreface/offshore .....	104
3.3.3.1. Facies 7: Storm-dominated lower shoreface .....	104
3.3.3.2. Facies 8: Well sorted, cross-bedded/laminated to massive sandstone .....	109
3.3.3.3. Facies 9: Calcite-cemented conglomerates with abundant oysters .....	111
3.3.3.4. Facies 10: Bioturbated <i>Ophiomorpha</i> -dominated sandstone ....	113
3.3.3.4.1. Facies 10A: Horizontally bioturbated <i>Ophiomorpha</i> - dominated sandstone.....	113
3.3.3.4.2. Facies 10B: Vertically bioturbated <i>Ophiomorpha</i> - dominated sandstone .....	115
3.3.3.5: Facies 11: Cryptobioturbated sandstone .....	117
3.3.3.6: Facies 12: Tidal-influenced shoreface/flood-tidal delta .....	119
3.3.4. Facies association 3: tidal inlet 13 .....	121
3.3.4.1. Pebbly conglomerate and bioturbated carbonaceous-rich mudstone .....	121
3.3.5. Facies association 4: Back barrier/coastal plain .....	123
3.3.5.1. Facies 14: Rooted grey sandstone .....	125
3.3.5.2. Facies 15: Rippled-laminated sandstone with carbonaceous matter .....	125
3.3.5.3. Facies 16: Cross-bedded sandstone with carbonaceous laminae .....	127
3.3.5.4. Facies 17: Interlaminated very fine-grained sandstone, siltstone, and claystone .....	129
3.3.5.5. Facies 18: Interbedded sharp-based sandstone and bioturbated sandy siltstone “lam-scam” .....	131
3.3.5.6. Facies 19: <i>Teichichnus</i> -dominated fine-grained sandstone .....	133
3.3.5.7. Facies 20: Laminated to <i>Teichichnus</i> -dominated sandstone.....	135
3.3.5.8. Facies 21. <i>Diplocraterion</i> -dominated interbedded shale and	

sandstone .....	135
3.3.5.9. Facies 22: Dark gray to black oyster-rich mudstone .....	138
3.3.5.10. Facies 23: Intensively bioturbated muddy sandstone/silty mudstone .....	140
3.3.6. Net sand maps .....	140
3.3.6.1. Net sand maps of Ah, Bh, Ch, Dh, and Eh .....	142
3.3.6.2. Net sand maps of Bt, Ct, Dt, Et, and Ft .....	153
3.4. Interpretation of the depositional environments of the Cotton Valley sandstones .....	155
3.5. Barrier island formation .....	164
3.6. Discussion and other alternatives .....	164
<b>CHAPTER 4: PETROGRAPHY AND DIAGENESIS</b>	<b>168</b>
4.1. Introduction .....	168
4.2. Sandstone architectural components .....	169
4.3. Framework grain composition .....	172
4.3.1. Quartz .....	172
4.3.2. Feldspars .....	172
4.3.3. Rock fragments .....	181
4.3.4. Miscellaneous constituents .....	185
4.3.5. Matrix .....	189
4.4. Conglomerate.....	189
4.5. Diagenetic overprint on framework grains and restored composition .....	191
4.6. Provenance .....	196
4.6.1. Petrographic indicators of source area .....	196
4.6.2. Possible source area .....	198
4.7. Burial-thermal history .....	200
4.8. Cements and replacive phases .....	201
4.8.1. General remarks .....	201
4.8.2. Quartz .....	203

4.8.2.1. Sources of silica .....	211
4.8.2.2. Isotope geochemistry .....	218
4.8.3. Carbonate cements .....	224
4.8.3.1. Calcite .....	224
4.8.3.2. Dolomite .....	230
4.8.4. Clay minerals .....	232
4.8.4.1. General remarks.....	232
4.8.4.2. Kaolinite .....	235
4.8.4.3. Chlorite.....	238
4.8.4.4. Illite.....	239
4.8.5. Other authigenic minerals.....	243
4.8.5.1. Feldspars .....	243
4.8.5.2. Pyrite .....	245
4.8.5.3. Anhydrite .....	247
4.9. Porosity and permeability .....	247
4.9.1. General remarks.....	247
4.9.2. Major pore types .....	252
4.10. Secondary porosity development.....	252
4.10.1. General remarks.....	252
4.10.2. Carbonic acids from thermal breakdown of organic matter.....	254
4.10.3. Inorganic carbonic acids.....	256
4.10.4. Organic acids .....	256
4.10.5. Meteoric water .....	257
4.11. Permeability.....	258
4.12. Diagenetic evolution and parasequences .....	270
4.13. Porosity evolution: compaction and cementation porosity loss .....	273

<b>CHAPTER 5: RESERVOIR QUALITY</b>	<b>276</b>
<b>CONCLUSIONS</b>	<b>285</b>
Appendix A: Description and interpretation of cores.....	290
Appendix B: Point-count analysis data.....	329
Appendix C: Electron microprobe analyses of feldspars.....	335
Appendix D: Point-count data: quartz overlap and quartz cement.....	336
Appendix E: Percent of free grain surface area coated by clay.....	337
<b>REFERENCES</b>	<b>338</b>
<b>VITA</b>	<b>361</b>



## LIST OF TABLES

Table. 1: Facies and facies associations of the Cotton Valley Sandstones.....	83
Table 2: Sandstone composition in potential reservoir facies.....	171
Table 3: Present day and restored composition of the Cotton Valley sandstones.....	192
Table 4: Distribution of cements in potential reservoir facies.....	205
Table 5: Comparison between the amount of quartz cement determined by using and without using CL.....	209
Table 6: Percentage of overgrowth of total quartz and oxygen isotopic data For bulk quartz samples.....	210
Table 7: The percentage of thin sections of potential reservoir facies And the percentage of each facies in analyzed cores.....	214
Table 8: The number of stylolites per foot.....	216
Table 9: Oxygen and carbon isotopic data for carbonate samples.....	228
Table 10: Porosity types in different facies.....	249

## LIST OF FIGURES

Figure 1: Regional tectonic map of the north-central Gulf coastal province.....	2
Figure 2: Distribution of the Cotton Valley reservoirs in ARK-LA-TEX.26.....	3
Figure 3: Location map of the study area.....	4
Figure 4: Structure contour map on the top of the Cotton Valley Sandstones (CVS).....	13
Figure 5: Stratigraphic cross section illustrating lithic patterns in northern Louisiana.....	17
Figure 6: Stratigraphic nomenclature, East Texas Basin.....	18
Figure 7: Generalized stratigraphic nomenclature of Cotton Valley Group in Northern Louisiana.....	19
Figure 8: Comparison of the Vail/Exxon depositional model with the Frazier/Galloway stratigraphic model.....	27
Figure 9: Stratigraphic architecture of a simple depositional episode and the resultant genetic stratigraphic sequence.....	28
Figure 10: Depositional architecture and stacking pattern in well 27.....	31
Figure 11: Stacking pattern and stratigraphic surfaces in selected intervals in the study area.....	33
Figure 12: <i>Glossifungites</i> ichnofacies (pipes) formed by <i>Thalassinoides</i> traces.....	36
Figure 13: Stratigraphic cross sections trend in East Texas basin.....	37
Figure 14: Dip-oriented stratigraphic cross-section D-D`.....	39
Figure 15: Stratigraphic cross section C-C`.....	42
Figure 16: Stratigraphic cross section X-X`.....	43
Figure 17: Stratigraphic cross section B-B`.....	44
Figure 18: Stratigraphic cross section along A-A`.....	45
Figure 19: Core legend.....	47
Figure 20: Core-log integration, SFE # 3.....	49
Figure 21a: Stacked tidal inlet-deposits.....	50

Figure 21b: Close-up view of the base of the tidal inlet deposits.....	51
Figure. 22: Core-log integration, Blocker Heirs # 1.....	53
Figure 23: Maximum flooding surface at depth 9354 ft.....	54
Figure 24: Upper shoreface overlain by transitional to inner shelf deposits.....	55
Figure 25: Tidal inlet deposits cut in the lower shoreface.....	56
Figure 26: Core-log integration, Burnett Brothers # 12.....	58
Figure 27: Core-log integration, Tallent # 1.....	59
Figure 28: Core-log integration, Anderson # 1.....	60
Figure 29: Lag deposits at the base of tidal inlet.....	62
Figure 30: Core-log integration, Anderson # 1.....	63
Figure 31: Core-log integration, Jones # 3.....	65
Figure 32a: Core-log integration, Lowry # 1.....	66
Figure 32b: Sequence boundary marks the shift in facies from lagoon to inner shelf.....	67
Figure 33a: Core-log integration, Davidson Foundation # 1.....	69
Figure 33b: Core-log integration, Davidson Foundation # 1.....	70
Figure 34: Core-log integration, Blocker Heirs# 1. ....	72
Figure 35a: Core-log integration, Bradshaw # 1.....	74
Figure 35b: Core-log integration, Bradshaw # 1.....	75
Figure 36: Sequence stratigraphy model of the Cotton Valley Sandstone by Mitchum.....	77
Figure 37: Sequence stratigraphy model of the Cotton Valley Sandstone.....	78
Figure 38: Core distribution in the study area.....	81
Figure 39: Architectural elements of a barrier-island sand body.....	88
Figure 40: Facies 1-storm-dominated inner shelf deposits.....	93
Figure 41: Facies 2-dark grey mudstone with fossil shell debris resembling oysters.....	95
Figure 42a: Facies 3-Inner-shelf deposits exhibiting local continuous wavy bedding.....	97

Figure 42b: Facies 3-Inner-shelf deposits. Interbedded planar laminated siltstone and intensely bioturbated silty mudstone.....	98
Figure 43: Facies 4- <i>Chondrites</i> -dominated inner shelf.....	100
Figure 44: Facies 5-Intensely burrowed interlaminated siltstone and mudstone.....	101
Facies 45: Facies 6-Carbonaceous-rich silty mudstone.....	103
Facies 46a: Facies 7-Storm-dominated shoreface.....	105
Figure 46b: Facies 7-Storm-dominated lower shoreface.....	106
Figure 47: Temporal significance of the idealized storm unit.....	108
Figure 48: Facies 8-Well-sorted massive to cross-laminated sandstone.....	110
Figure 49: Facies 9-Calcite-cemented conglomerates with oyster hash overlying shoreface sandstone.....	112
Figure 50a: Facies 10A- <i>Ophiomorpha</i> -dominated sandstones, horizontal burrows.....	114
Figure 50b: Facies 10B- <i>Ophiomorpha</i> -dominated shoreface, vertical burrows.....	116
Figure 51: Facies 11-Cryptobioturbated sandstone.. ..	118
Figure 52: Facies 12-Tidal-dominated sandstones.....	120
Figure 53: Facies 13-Pebbly bioturbated carbonaceous rich conglomerate.....	122
Figure 54: Facies 14-Rooted grey sandstone with <i>Macaronichnus segregatus</i> .....	124
Figure 55: Facies 15-Rippled-laminated sandstone with carbonaceous matter.....	126
Figure 56: Facies 16-Cross bedded sandstones with carbonaceous matter.....	128
Figure 57: Facies 17-Example of fine-grained back barrier deposits.....	130
Figure 58: Facies 18-Laminated-scrambled facies. Alternating laminated and bioturbated sandstones. ....	132
Figure 59: Facies 19- <i>Teichichnus</i> -dominated sandstones.....	134
Figure 60: Facies 20- <i>Teichichnus</i> -dominated mudstone.....	136
Figure 61: Facies 21- <i>Diplocraterion</i> -dominated interbedded shale and sandstone.....	137

Figure 62: Facies 22-Dark grey to black oyster-rich mudstone.....	139
Figure 63: Facies 23-Soil horizon shows a mix of silt, sand and mud with abundant root traces and carbonaceous matter.....	141
Figure 64: Net sand map for all of the Cotton Valley sequences.....	143
Figure 65: Net sand map of Ah shows strike-oriented sand bodies.....	144
Figure 66: Net sand map of Bt shows strike-oriented sand bodies. ....	145
Figure 67: Net sand map of Bh shows strike-oriented sand bodies.....	146
Figure 68: Net sand map of Ct shows dip-oriented sand bodies.....	147
Figure 69: Net sand map of Ch shows strike-oriented sand bodies.....	148
Figure 70: Net sand map of Dt shows strike-oriented sand bodies.....	149
Figure 71: Net sand map of Dh shows strike-oriented sand bodies.....	150
Figure 72: Net sand map of Et shows strike-oriented sand bodies.....	151
Figure 73: Net sand map of Eh shows strike-oriented sand bodies. ....	152
Figure 74: Net sand map of Ft that does not show any trend for the sand body.....	153
Figure 75: Example of the lower CVS shows shelf and shorefaces deposits. ....	157
Figure 76: Example of the middle CVS shows well-developed, highly bioturbated shoreface and shelf deposits.....	158
Figure 77: Example of the upper CVS shows coastal-plain deposits.....	159
Figure 78: Photo shows North Carolina outer bank .....	160
Figure 79: Photo shows the back barrier of North Carolina outer bank. ....	161
Figure 80: Present day facies distribution along North Carolina outer bank.....	162
Figure 81: Succession of facies through Cotton Valley Formation in the Lowry well no. 1.....	163
Figure 82: Framework grain composition of Cotton Valley Sandstones.....	173
Figure 83: Monocrystalline quartz grains with straight extinction .....	174
Figure 84: Calcitized feldspar grain.....	176
Figure 85: Fresh, yellow-stained potash feldspar.....	178
Figure 86: Partially replaced plagioclase feldspar grain by calcite.....	179
Figure 87: Partial to near complete dissolution of feldspar grains.....	180

Figure 88: Feldspar grain composition based on microprobe analyses .....	182
Figure 89: Metamorphosed siltstone fragment.....	183
Figure 90: Black chert and green chert rock fragments.....	184
Figure 91: Muscovite bent between rigid quartz grains.....	186
Figure 92: Partial dissolution of some heavy mineral grains.....	187
Figure 93: Sandstone with abundant oyster fragments.....	188
Figure 94: Calcite cemented conglomerate.....	190
Figure 95: Present-day and restored framework composition from storm-dominated and cryptobioturbated facies.....	193
Figure 96: Present-day and restored framework composition for tidally influenced shoreface and sand flat sandstones.....	194
Figure 97: Present-day and restored framework composition for bioturbated and laminated sandstones.....	195
Figure 98: Vein quartz and stretched polycrystalline quartz.....	197
Figure 99: Paleogeographic map of Early Cretaceous in south-central And southwestern United States.....	199
Figure 100: Burial and thermal modeling of the Cotton Valley .....	202
Figure 101: Schematic paragenetic sequence of diagenetic processes and products in Cotton Valley Sandstones.....	204
Figure 102: Quartz cement occludes pores .....	206
Figure 103: Combined secondary electron and scanned CL images.....	208
Figure 104: Quartz oxygen isotopic data.....	212
Figure 105: Moderate amplitude stylolite.....	217
Figure 106: Plot between quartz cement and distance to nearest stylolite.....	220
Figure 107: Temperature of quartz cement precipitation.....	223
Figure 108: Calcite type 1 cement.....	227
Figure 109: Temperature of precipitation of calcite cement.....	229
Figure 110: Calcite type 2 cementation.....	231
Figure 111: Temperature of precipitation of dolomite .....	233

Figure 112: koalinite cement.....	236
Figure 113: Calcite dissolution and kaolinite precipitation.....	237
Figure 114: Pore-filling chlorite.....	240
Figure 115: Quartz cement and chlorite coating.....	241
Figure 116: Grain riming and pore-bridging illite cement.....	242
Figure 117: Pyrite cement.....	246
Figure 118: Secondary porosity after calcite dissolutio.....	246
Figure 119: Cross plot of measured and point counted porosity data.....	251
Figure 120: Various types of porosity.....	253
Figure 121: SEM image shows intensive feldspar dissolution.....	255
Figure 122: Cross plot of measured porosity and permeability for all facies.....	260
Figure 123: Cross plot of measured porosity and permeability for the bioturbated <i>Ophiomorpha</i> -dominated sandstones.....	261
Figure 124: Cross plot of measured porosity and permeability for the cryptobioturbated shoreface sandstones.....	262
Figure 125: Cross plot of measured porosity and permeability for sandstones from sand flat setting.....	263
Figure 126: Cross plot of measured porosity and permeability for sandstones from the laminated shoreface .....	264
Figure 127: Cross plot of measured porosity and permeability for sandstones from the storm dominated shoreface showing .....	265
Figure 128: Cross plot of measured porosity and permeability for sandstones from the tidally influenced shoreface .....	266
Figure 129: Permeability values measured at different parts of the lam-scrum facies.....	267
Figure 130: Permeability measurements within and outside the trace fossils reveal bigger values within the traces.....	268
Figure 131: Permeability measurements within different facies.....	269

Figure 132: Burial history curve showing interpreted major diagenetic events.....	271
Figure 133: Diagram illustrate the relation ship between IGV and cement.....	274
Figure 134: Bioturbated sandstones with more than 10 % detrital clay matrix.....	278
Figure 135: Bioturbated sandstones (<10% detrital clay) show good porosity and permeability.....	279
Figure 136: Distribution of quartz cement in various facies. ....	280
Figure 137: Integration of core description, core analysis data and thin section images.....	282



# **CHAPTER 1**

## **1.1. Purpose of Study**

The Challenge of tight gas sandstones is to determine what factors control reservoir quality and the evolution of porosity during diagenesis, and to establish criteria to aid in finding sandstones with the best reservoir quality in the future. Thus, to answer these questions for the Cotton Valley Sandstones a study was made to: (1) construct the sequence stratigraphic framework of Cotton Valley Sandstones by using well logs combined with core data to determine the reservoir architecture in the Woodbine, Carthage, Waskom, Blocker and Dirgin fields, East Texas basin; (2) reconstruct the depositional environment of Cotton Valley Sandstones; (3) to reconstruct the diagenetic evolution of Cotton Valley Sandstones throughout their burial history by linking petrographic and geochemical data on sandstones, shales, and organic matter; 4) to identify the facies/or facies association that has the best reservoir characteristics; (5) and to examine the relationship between reservoir facies and architecture interpreted from stratigraphic sequences, depositional environment and the distribution of various diagenetic phases; to consider the control of depositional environment on diagenesis and its effect on reservoir quality.

The study area covers more than 2000 square miles (3220 square kilometers), and includes all of Harrison, Panola, and Rusk counties, and adjacent portions of Gregg and Upshur counties (Figs. 1-3). The Cotton Valley Group is entirely confined to the

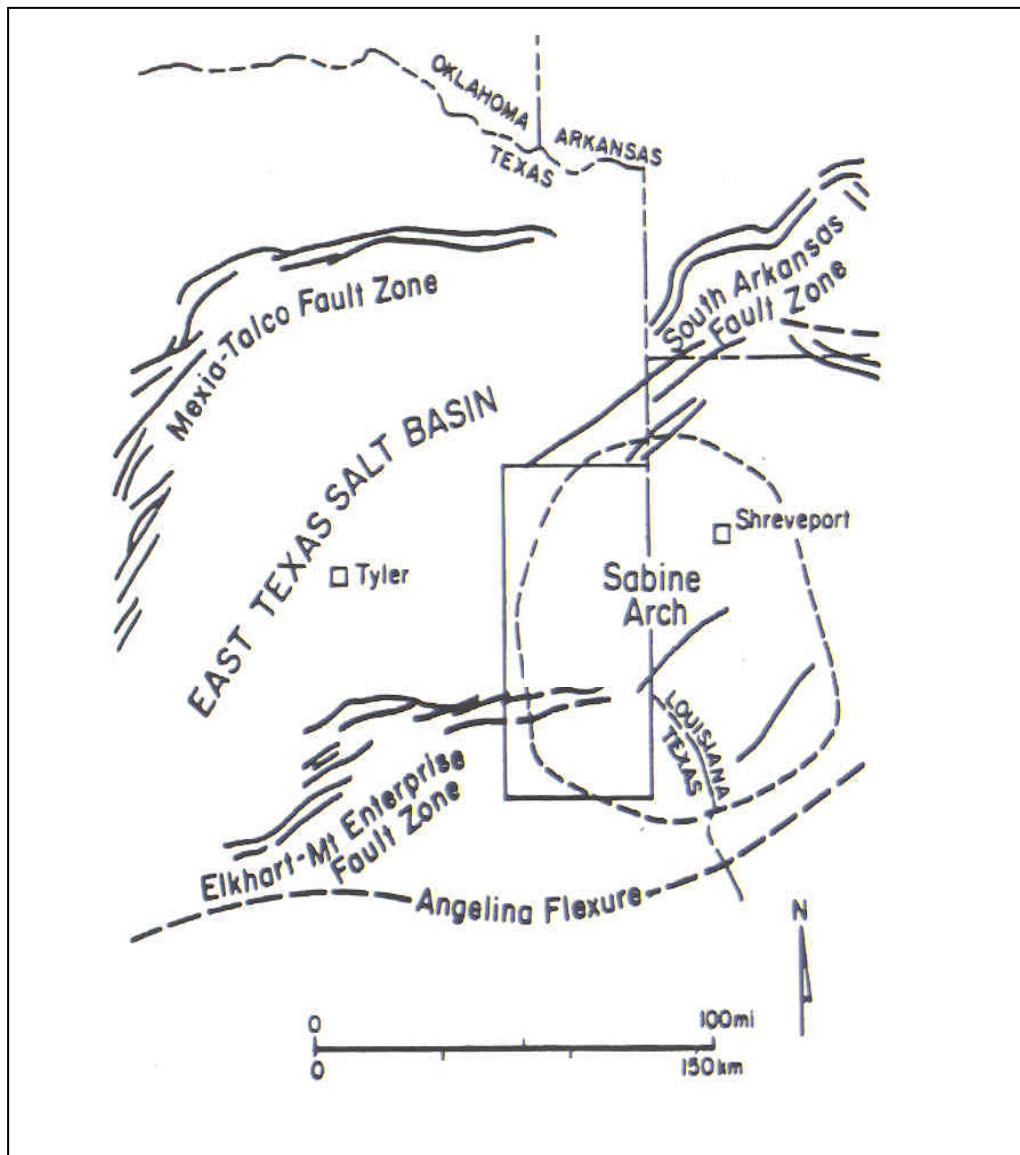


Figure 1: Regional tectonic map of the north-central Gulf coastal province (From Saucier et al., 1985).

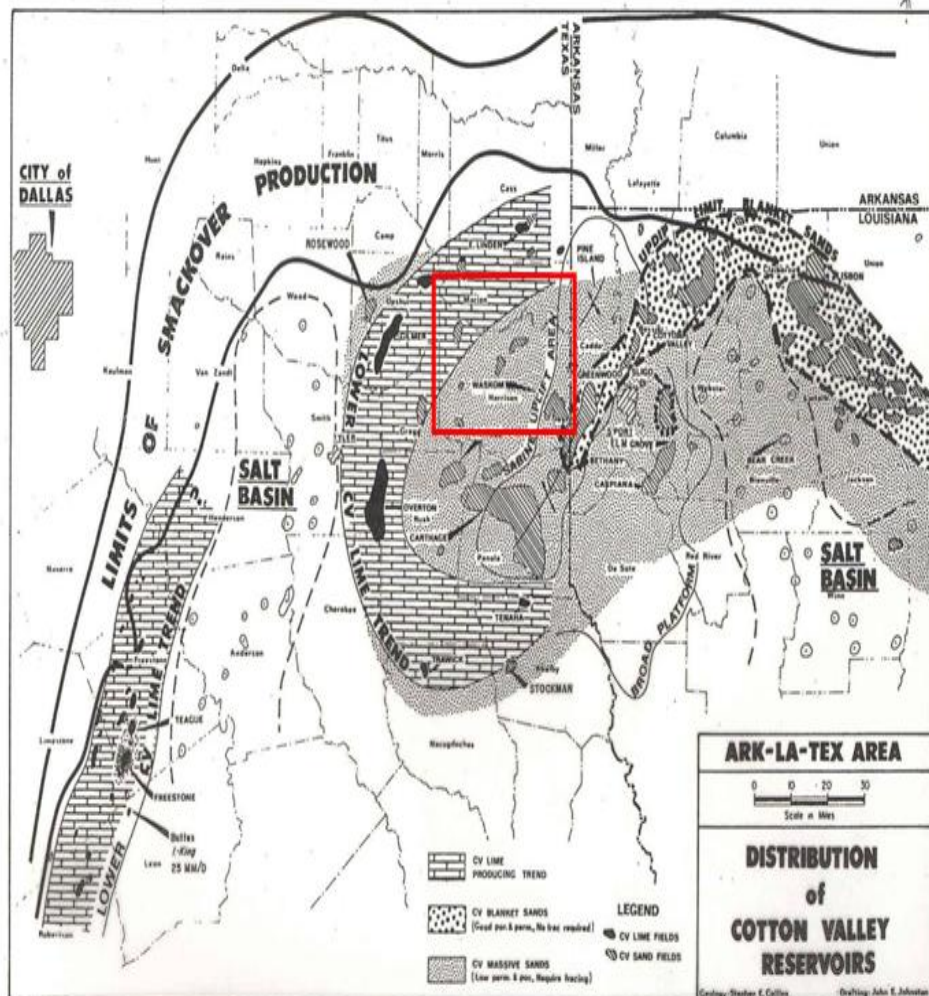


Figure 2: Distribution of the Cotton Valley reservoirs in ARK-LA-TEX Area (after Collins, 1980). Red square is the study area.

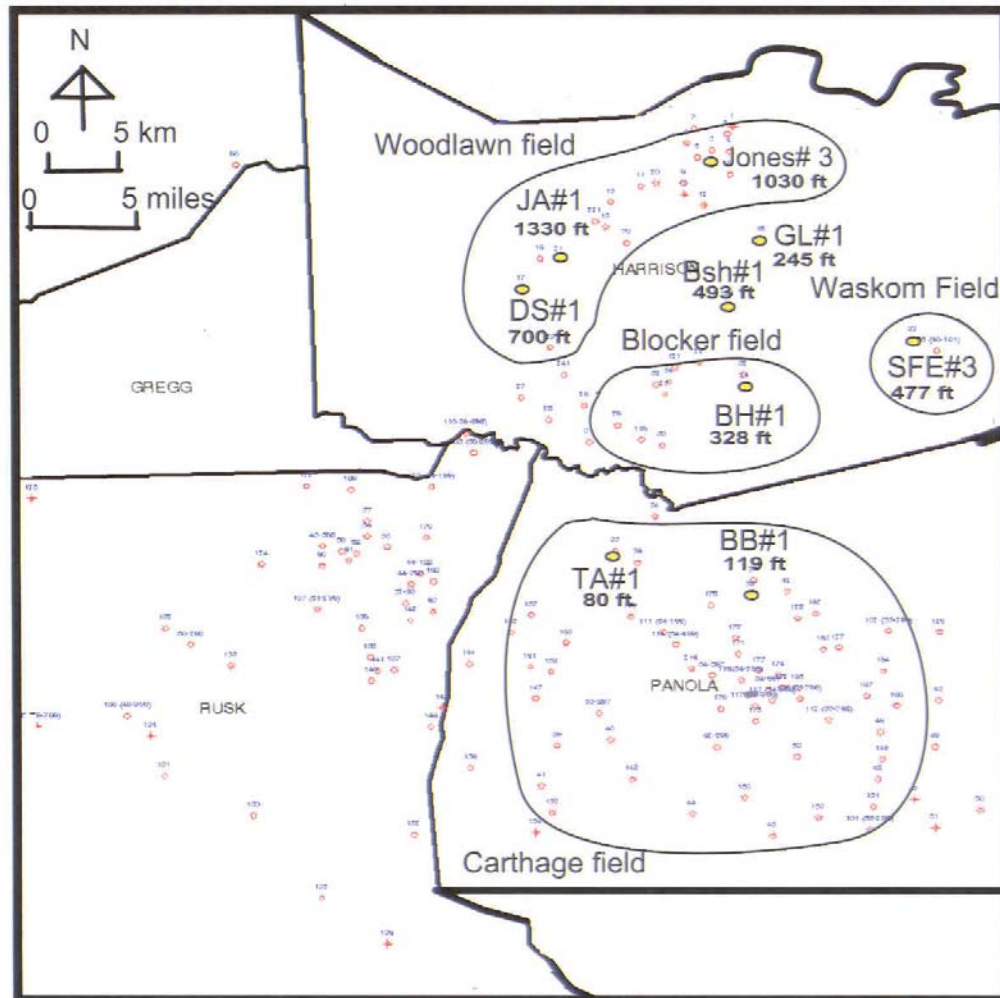


Figure 3: Location map of the study area. JA # 1 = James Anderson well # 1, DS # 1 = Davidson Foundation well no.1., GL # 1 = Grace Lowry well no. 1, BSH # 1 = Bradshaw well no. 1, BH # 1 = Blocker Heirs no.1, TA # 1 = Tallent well no.1., and BB # 1 = Burnett Brothers well no. 1. 700 ft = cored interval. The footage listed is the length of cored interval for the well.

subsurface, so the primary data sources for this study consist of conventional cores and well logs from deep wells. The Cotton Valley Group contains sandstone, shale, conglomerate and limestone. Sandstone interbedded with 20% to 35% shale dominates; limestone occurs as oyster-rich lagoonal carbonate mudstone beds (0.3m -3.5m thick) interbedded with sandstones and shales. In the current study, emphasis is placed on the sandstones of the Cotton Valley. These sandstones are productive of natural gas in the study area, and have been more extensively cored than the other rock types.

## **1.2. Study approach and procedures**

The following approaches were taken in order to achieve the goals of this study.

1. Integration of different sources of data. The Cotton Valley sandstones are mature reservoirs; thus there are numerous well logs, cores, and core analysis data available. Many published studies are also available.
2. Multiscale investigation. With the research goals extending from sequence stratigraphic architecture to detailed reservoir characterization, multi-scale investigations were conducted. Different scales of investigations were made for different aspects of the research interests. Each scale required different techniques and different sets of data.

This study can be approximately divided into three separate but related scales of investigations: facies/subfacies scale; field/reservoir scale; and sequence-stratigraphy scale. The facies and subfacies scale study is aimed at understanding lithologic heterogeneity and its implication to fluid flow within the facies/subfacies elements.

Thus, this scale study is based on “foot by foot” detailed description of cores and detailed petrographic study of representative samples from each facies. The reservoir-to-field scale study is concerned with the facies architecture within the selected mapping areas. It is built on the integrated analysis of all relevant information available, including well logs, and cores. The sequence stratigraphy study is a regional-scale study in nature and aimed at determining the distribution of large-scale stratigraphic elements (system tracts). Data density used for this scale study is usually much lower than that for the reservoir-scale study, but should be high enough to capture the most important sequence stratigraphic elements.

By correlating resistivity and spontaneous potential logs on 180 wells and using the analysis of 4000 feet of conventional core, the major depositional sequences and system tracts have been identified. In each sequence and system tract the various reservoir units have different lithofacies. Each lithofacies has characteristic reservoir sandstone types and distributions, depending upon its depositional environment, diagenesis and its position within sequences and system tracts. Study of the cores includes lithofacies, primary sedimentary structures, fossils, facies relations, textures, compositions and vertical grain-size changes.

These data are correlated and compared to the characteristic response curves on electric logs; sonic, neutron and density logs were used where available. Various kinds of subsurface maps were established, including depth map, isopach, and net sand maps. Study methods include standard petrography (point counting), major and trace element

composition (WDS analysis), CL, fluid inclusion microthermometry, and integration with organic geochemistry and timing of hydrocarbon generation, migration and accumulation. Quartz cement is a common authigenic phase in the studied sandstones and the assessment of its source was considered;

### **1.2.1. Methods**

Identification of diagenetic products and interpretation of diagenetic sequences requires utilization of various microscopic petrographic techniques. One hundred forty seven samples were selected from different facies and from the total depth range available, which is from 8590 ft (2618 m) to 10266 ft (3129 m). Cotton Valley sandstones were studied by using standard thin-section petrography, scanning electron microscopy (SEM) with energy dispersive X-ray spectrometer (EDX), cathodoluminescent petrography, electron microprobe analysis, X-ray analysis, fluid inclusions, and stable isotope analysis.

All the samples were examined using transmitted light microscopy to decide which samples required staining for K-feldspar, calcite and other complementary chemical analysis. Feldspar-rich samples were later cleaned with acetone and stained with Na-cobaltinitrite and calcite-rich samples were stained for calcite using Alizarine Red-S (Friedman, 1971; Houghton, 1980). Point counts of 350 points were done on each of the 147 thin sections to determine detrital and authigenic mineralogy and porosity.

The longest grain diameter and clay coat percentage coverage were measured on 50 grains in a grid. The sorting was determined from the grain-size distribution of 50 grains/sample, and grain-size and clay coat completeness averages were computed (cf. Bonnell and Lander, 2002a).

Stable isotopic analysis of bulk samples of quartz was performed on 15 samples with a wide range of quartz overgrowth percentages as determined by thin section point counts. Samples were treated with  $\text{NaHSO}_4$  and  $\text{H}_2\text{SiF}_6$  by the method of Syers et al. (1968) to isolate detrital quartz and quartz overgrowths. Treated samples were then X-rayed to confirm that only quartz was left. Oxygen was extracted by reacting the quartz (detrital plus cement) with  $\text{BrF}_5$  and then converted to  $\text{CO}_2$  by reaction over hot carbon. The  $\text{CO}_2$  was analyzed by mass spectrometer; the oxygen released is a weighted average of the oxygen in the overgrowth and detrital grain. The isotopic composition of the quartz cement was estimated by extrapolation to 100% quartz cement of the regression line of bulk isotopic composition on percent of quartz cement as percent of total quartz.

Five dolomite-rich sandstones samples and 11 calcite-rich samples were selected to perform carbon and oxygen isotopic ratios. The samples were powdered, X-rayed and reacted with phosphoric acid for 20-24 hours at  $25^\circ\text{C}$ . The extracted gases were purified and analyzed on a PRISM II gas source mass spectrometer. The  $\text{H}_3\text{PO}_4$  fractionation factor was assumed to be 1.01025 (Friedman and O'Neil, 1977).



Isotope values are reported relative to PDB standard. In several of the samples the measured isotopic values represented a combination of early and late calcite.

A wave-length dispersive spectrometry (WDS) analysis of detrital feldspars and albite was carried out on selected samples employing a 10  $\mu\text{m}$  spot size and 15 Kv accelerating voltage. Thin sections were carbon coated, and quantitative composition of feldspars was obtained by using combined wavelength dispersive analysis. Energy dispersive analysis (EDS) was used prior to WDS to check qualitatively the target grain composition.

Primary and secondary standards include natural and synthetic minerals and glasses. Detrital and authigenic feldspars were analyzed for Ca, Na, K, Al, Si, and Ba. Secondary standards used were anorthite (Ca and Al), albite (Na), orthoclase (K and Si), and synthetic Ba-silicate glass (Ba).

Fourteen samples were submitted for fluid inclusion analysis in quartz overgrowths. Only three samples yielded homogenization and freezing temperature data. The freezing temperature was used to calculate the salinity of the pore water that precipitated quartz cement. Fifteen sandstone samples were cleaned and gold coated for scanning electron microscopy and energy dispersive X-ray analysis (EDX). SEM analysis was performed on a JEOL JSM-T330A using an accelerating voltage 20 Kv, and EDX analysis was made by using Kevex delta series EDX microanalyzer. Six mudstone samples were submitted for organic geochemical analysis; only three samples yielded data on vitrinite reflectance and total organic content.

Twelve sandstone polished sections were examined by cathodoluminescence by SEM. Scanned-CL images were obtained using an Oxford instruments photomultiplier-based detector (Model CL 302) installed on the JEOL T330 Scanning Electron Microscope. The parabolic mirror of the CL 302 was inserted approximately 1mm above the surface of the carbon-coated polished thin section. Five photos of different areas were taken for each slide. 400 counts were made on a grid to determine the amounts of detrital and authigenic quartz in each sample and to determine the amount of “overlap” quartz. The number of stylolites per thin section was counted and the amplitude of each one was measured. The volume of quartz dissolved along stylolites was also estimated by point counting the thickness of insoluble residue along stylolites for 26 thin sections (50 counts per slide).

### **1.3 Geologic Setting**

#### **1.3.1. Introduction**

The Cotton Valley Group is an Upper Jurassic to Lower Cretaceous sequence of sandstone, shale, limestone and conglomerate that underlies much of the northern Gulf of Mexico coastal plain. Initial Cotton Valley sandstone hydrocarbon production began in north Louisiana in the 1940s from very porous blanket sandstones which produced from up-dip pinch-outs. Accumulation was by both structural and stratigraphic trapping. Down-dip, the blanket sandstones lose porosity and permeability and grade into a massive sequence of finer grained, low porosity sandstones. All producing Cotton Valley sandstones are generally of two types: (1) porous and permeable blanket

sandstones, which are easily correlatable over many miles and readily produce fluids and gas on open-flow drilling tests; and (2) low-porosity, low-permeability, fine-grained, sandstones which do not flow gas or fluids on drill stem tests, but require fracturing (Collins, 1980). Blanket sandstone reservoirs have been studied by many authors and there are many data published on their reservoir quality. On the other hand, the massive sandstones have been little studied and many problems are still unsolved. Accessibility to well logs, core analysis data, and lots of conventional cores in tight gas sandstones made these sandstones the study of choice.

Downdip and west of the blanket sandstones, Cotton Valley Sandstones occur as thick, stacked sequences-known as “massive sandstones”. Most of these are “tight gas” sandstones, which are gas-bearing rocks that usually have in-situ permeability to gas, exclusive of fracture permeability, of less than 0.1 millidarcy (md). Significant amounts of potentially recoverable natural gas exist in such low-permeability sandstone formations located in sedimentary basins throughout the United States. For example, Cotton Valley wells totaled 2,870 as of 1993. Cumulative production was 2,665.5 BCFG, with an estimated ultimate recovery of 4,999 BCFG (Bartberger et al., 2002).

### **1.3.2. Regional Structural Setting**

Structural features in the study area include the north-trending Sabine Arch, the East Texas Basin, the northeast and east-trending Angelina-Caldwell flexure (Fig. 1), and various structures caused by diapiric movement of salt. The largest structure in the study area is the Sabine uplift, a basement-cored and low-amplitude arch separating the

East Texas and North Louisiana salt basins. With vertical relief of 2000 ft (660 m), the Sabine uplift has a closed area exceeding 2500 square miles (Kosters et al., 1989).

Isopach data across the uplift indicate that it was a positive feature beginning with deposition of the Louann Salt, with renewed activity during the mid-Cretaceous (101 to 98 Ma) and Again during early Tertiary time (58 to 46 Ma) (Laubach and Jackson, 1990; Jackson and Laubach, 1991). As a high area for the past 60 m.y., numerous smaller structural highs on the uplift in the form of domes, anticlines, and structural noses provide traps for hydrocarbon accumulations, including many gas fields in Cotton Valley sandstones. The origin of these smaller structures has been attributed to salt deformation or igneous intrusion (Kosters et al., 1989).

### **1.3.3. Local Structural Setting**

A structure contour map established on the top of Cotton Valley Sandstones shows that Waskom, Woodlawn, Carthage and Dirgin fields are located on gentle structural domes (Fig.4). The Cotton Valley produces primarily from structural traps associated with the Sabine arch and with numerous salt structures (Kosters et al., 1989). A structure contour map on top of the Cotton Valley sandstones in the study area shows elevations of -7550 ft (-2300 m), to more than -9430 ft (-2857.5 m), toward the axis of the East Texas Basin in Harrison, Pannola and Upshur counties (Fig. 4). Development of salt structures in the East Texas basin was active during Late Jurassic and Early Cretaceous time (Seni and Jackson, 1983). One well over the Waskom structure, the Arkla Waskom-Smackover NO. 1, penetrated salt at a depth of 11,341 ft (-3436.6 m).

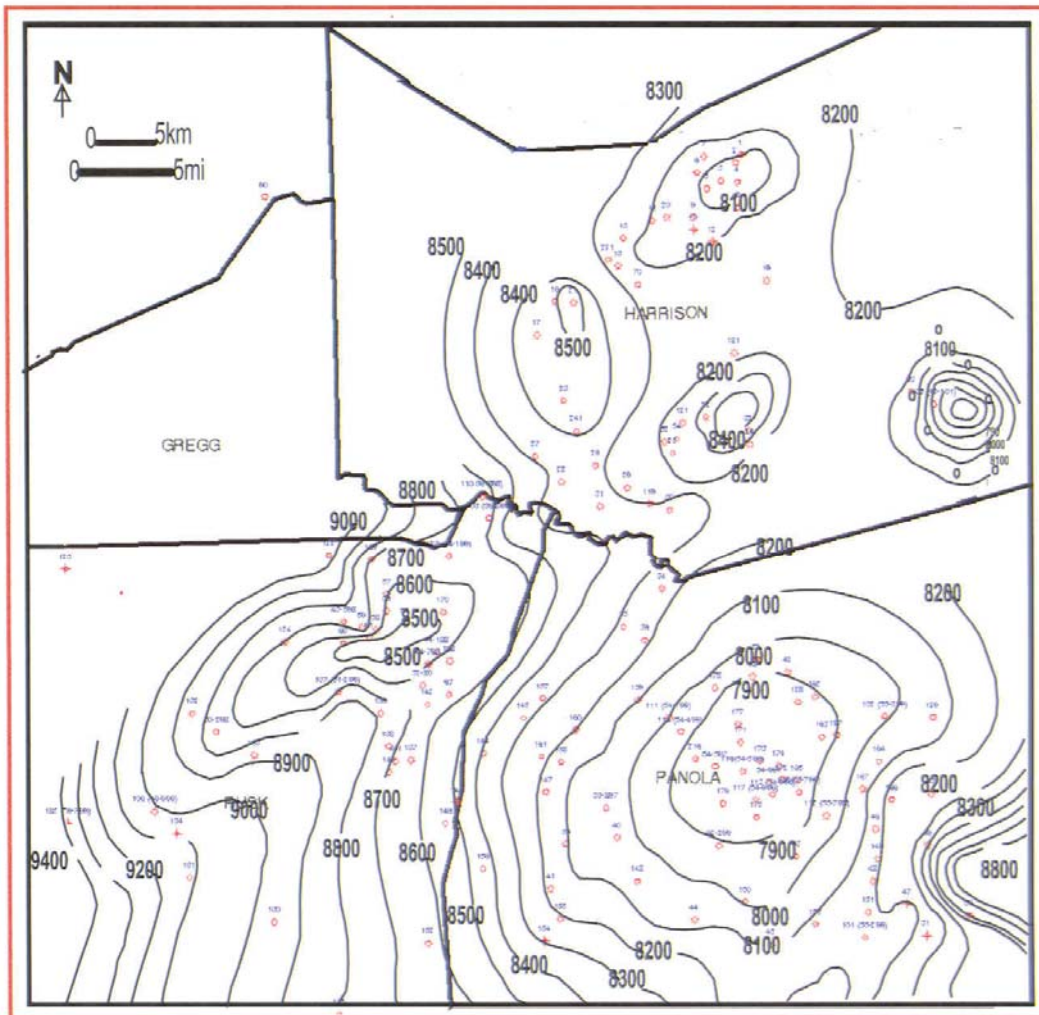


Figure 4: Structure contour map on the top of Cotton Valley Sandstones. Contours in feet below swa level. Contour interval is 100 feet.

#### **1.3.4. Cotton Valley Group Stratigraphic Nomenclature**

Since the first penetration of Cotton Valley strata in northern Louisiana in 1927, complex informal stratigraphic nomenclature developed as numerous Cotton Valley oil and gas fields were discovered across the region through the 1940's. Nomenclature became complex because of local stratigraphic complexities within Cotton Valley strata in northern Louisiana and also because of regional variation in Cotton Valley depositional systems across the north Gulf Basin. Bailey (1983, p. 12) reported that the first published use of the term Cotton Valley as a stratigraphic name was by Shearer (1938). He referred to the non-marine facies of the Cotton Valley, which had been discovered in southern Arkansas, as the Schuler Formation and as the Schuler facies of the Cotton Valley Formation. The first published use of the term Schuler referred to the marine facies of the Cotton Valley (Swain, 1944).

Terminology established by Swain (1944) was used until the complete revision of Cotton Valley stratigraphy by Thomas and Mann (1963) and Mann and Thomas (1964). Mann and Thomas (1964) divided the Cotton Valley Group into five formations: Bossier, Schuler, Terryville, Hico, and Knowles (Fig. 5). The Bossier Formation was redefined to include the dark marine shale and sandstone of the Lower Cotton Valley, but to exclude the nonmarine facies included in the unit by Swain (1944). The Schuler Formation was similarly redefined to include non-marine facies and exclude marine facies. The Terryville Sandstone and the Hico Shale are interpreted by Mann and Thomas (1964) to represent the sandstone and shale components of a barrier island/lagoon system.

The Knowles Limestone, which caps the marine part of the Cotton Valley Group, is described by Mann and Thomas (1964) as “...thin, regionally persistent, dark grey, argillaceous limestones interbedded with dark grey shales” (p. 145-148). Most subsequent reports, including the classic work of Collins (1980), have used Mann-Thomas terminology. Refinements of that terminology have been contributed by Coleman and Coleman (1981) and Eversull (1985).

Cotton Valley lithofacies and associated stratigraphic nomenclature in northern Louisiana and East Texas basins are shown in figure 6. The basal formation of the Cotton Valley Group is the Bossier Shale, a dark calcareous, fossiliferous, marine shale. The Bossier Shale grades upward into Cotton Valley sandstones with interbedded shales. In northern Louisiana, these sandstones consist of stacked barrier-island, offshore-bar, strandplain, and fluvial-deltaic sandstones and are referred to as the Terryville massive-sandstone complex in northern Louisiana by Coleman and Coleman (1981). In eastern Texas, the stratigraphically equivalent unit is called Cotton Valley Sandstone, and it consists of braided-stream, fan-delta, and wave-dominated delta sandstones (Wescott, 1983; Coleman, 1985; Dutton et al., 1993). This study used the term Cotton Valley Sandstone to refer to the massive tight sandstones in the East Texas Basin which is equivalent to the Terryville Formation named by Mann and Thomas (1964). Across the Cotton Valley hydrocarbon-productive trend in eastern Texas and northern Louisiana, the Terryville or Cotton Valley Sandstone averages about 1000 to 1400 ft (303-424 m) in thickness (Finley, 1984; Presely and Reed, 1984).

Sandstone deposition was interrupted in Early Cretaceous time by a regional transgressive event marked by deposition of the Knowles Limestone. In up-dip areas of eastern Texas and south Arkansas, the Knowles Limestone pinches out, and clastic rocks of the Travis Peak, or equivalent Hosston Formation, directly overly Cotton Valley Sandstones. Saucier (1985) considered the Knowles Limestone as the uppermost formation of the Cotton Valley Group, but Coleman and Coleman (1981) included the stratigraphically higher Calvin Sandstone, Winn Limestone, and unnamed sandstones and shales also within the Cotton Valley Group (Fig. 7). It is beyond the scope of this thesis to reevaluate the complex and controversial stratigraphic interpretation of the Cotton Valley Group.

#### **1.4. Previous work**

Because of its importance as a gas reservoir within the East Texas Basin, Cotton Valley Sandstones have been studied by many authors. Collins (1980) has divided all of the producing Cotton Valley sandstones into two different types: 1) porous and permeable blanket sandstones which are easily correlatable over many miles and will give up fluids and gas easily; and 2) low porosity, low permeability, fine-grained, massive undifferentiated sandstones which do not free flow gas but require fracturing. The latter facies, which is the target of this work, is very difficult to define for purposes of outlining limits and productive trends, because they are fine grained, have low permeability and poor regional correlation.



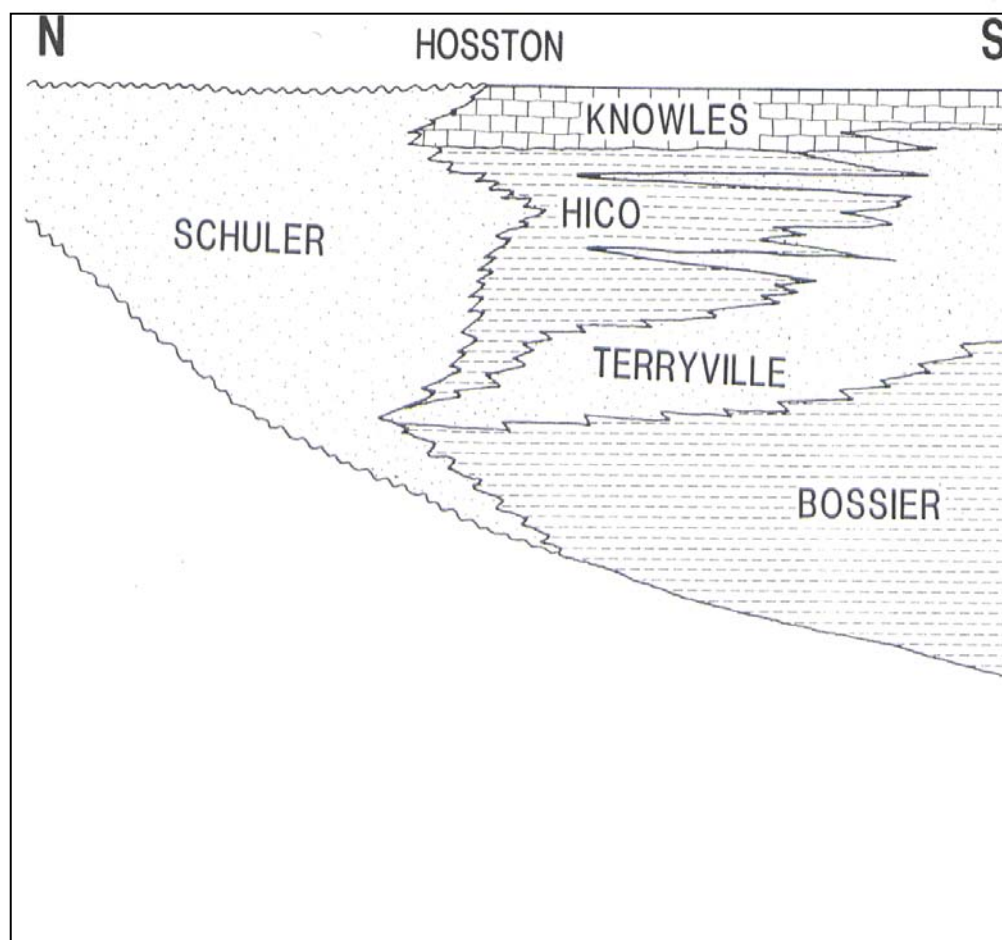


Figure 5: Stratigraphic cross section illustrating lithic patterns in northern Louisiana and nomenclature proposed by Mann and Thomas (1964).

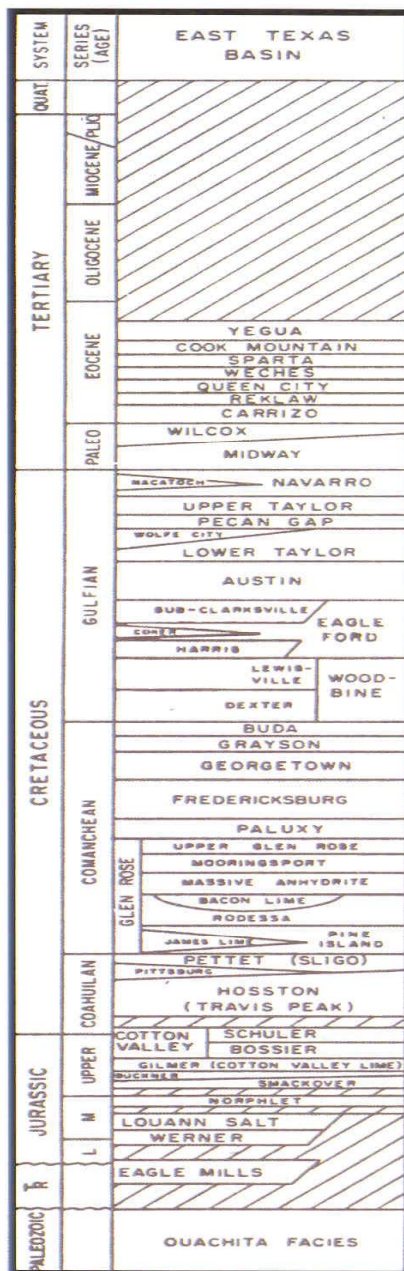


Figure 6: Stratigraphic nomenclature, East Texas Basin (Modified from Galloway et al., 1984).

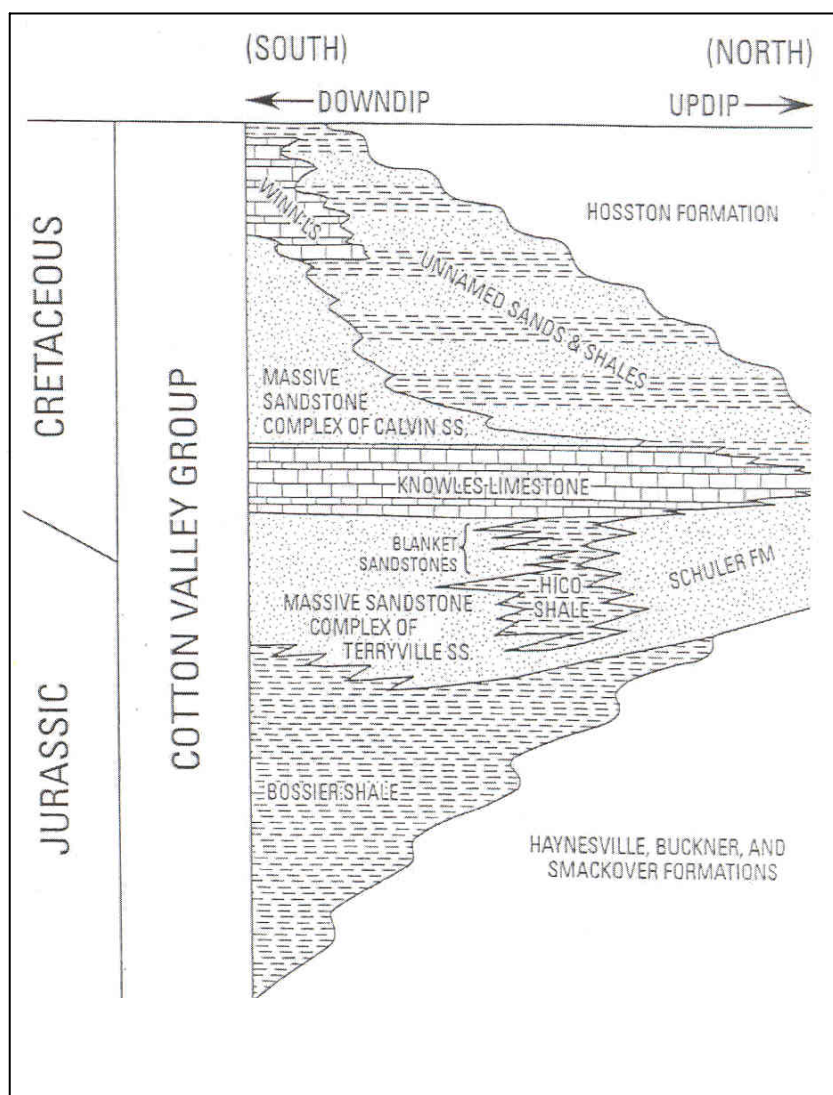


Figure 7: Generalized stratigraphic nomenclature of Cotton Valley Group in East Texas and Northern Louisiana, Modified from Coleman and Coleman (1981).

Williams and Mitchum (1997) identified seven major third-order depositional sequences in Carthage field, east Texas by correlating gamma ray and resistivity logs from 1080 wells. Each sequence has identifiable lowstand, transgressive and highstand system tracts. They identified more than 30 tight-gas sandstone reservoir units in facies spectra of incised valley fill, coastal plain and lagoonal facies.

The work of Williams and Mitchum (1997) has been expanded laterally and vertically by Williams et al. (2001) to cover 31 counties of East Texas and northwest Louisiana. They used digital well log curves for over 2800 wells, of which 1600 wells actually penetrated the top of the Cotton Valley and over 700 penetrated the entire Cotton Valley/Bossier sequence. They were able to extend five Cotton Valley sequences identified by Williams and Mitchum (1997) and two Bossier sequences into large portions of the East Texas Basin.

Bailey (1983) concluded that two main depositional environments were represented in the upper Cotton Valley in the East Texas Basin: 1) wave-dominated delta, and 2) shallow marine shelf. The facies of each environment he divided into various subfacies that correspond with subenvironments. He recognized a total of 14 subenvironmental facies.

The main Cotton Valley reservoir on the Sabine Arch occurs at depths from 9200 (2787 m) to 9350 ft (2833 m) in Waskom field, Harrison County. Sandstones and mudstones in Lower Cotton Valley (Taylor sand) according to Dutton et al. (1992) were deposited in a marine-shoreline setting. The environments represented include: 1) shoreface; 2) microtidal barrier island; 3) lagoon and washover; 4) tidal inlet; and 5)

marsh and lagoon. This vertical sequence was formed by an initial shoreline regression, a subsequent transgression and later relative sea level still stand as indicated by the stacking of barrier and tidal inlet deposits (Dutton et al., 1992). Bailey (1983) and Dutton et al. (1992) studied different parts of the Cotton Valley, which may explain the difference in interpretation of depositional environments. My study indicates that Cotton Valley transgressive system tracts are barrier islands-coastal plain complexes and highstand system tracts are most probably wave-dominated deltaic deposits.

The best reservoir sandstones in the Cotton Valley in the Waskom field are barrier-island deposits oriented parallel with depositional strike and tidal-inlet sandstones oriented perpendicular to depositional strike. Reservoir quality decreases vertically in lagoon and washover deposits above barrier-island sandstones and in abandoned inlet deposits above tidal-inlet sandstones. Marsh and lagoon mudstone deposits cap the sandstone and form a seal for hydrocarbons (Dutton et al., 1992).

McDevitt (1983) studied the petrology and diagenesis of the Terryville sandstones in Northwestern Louisiana and concluded that the massive sandstones are quartz arenites and subarkoses; and quartz overgrowths and calcite cement occluded greater than 90 % of the primary porosity. Dissolution of calcite and feldspars created most of the secondary porosity and after carbonate dissolution there was no significant porosity modification. Dutton et al. (1992) indicated that most of the sandstones studied in Waskom field are subarkose and sublitharenites.

The authors suggested that abundant detrital clay matrix inhibited fluid flow through the Cotton Valley sandstones, thus decreasing rates of feldspar dissolution and preserving much of the original feldspar content.

Wescott (1983) concluded that Cotton Valley sandstones in East Texas Basin could be divided into three groups, which could be related to porosity characteristics. Type I rocks are tightly cemented by quartz and calcite and make a poor reservoir. Type II rocks have high phyllosilicate content and abundant microporosity that may produce gas. Type III rocks have a high content of unstable minerals many of which dissolved to develop secondary porosity. He also suggested that depositional environments were a major control on the diagenesis of the sandstones. Clean, well-sorted sandstones deposited in high energy environments became tightly cemented by quartz overgrowths and sparry calcite. Sandstones deposited in low energy environments contained detrital clays that inhibited nucleation of overgrowths and helped preserve porosity (Wescott, 1983).

Trojan (1985) studied Taylor sandstones of the Cotton Valley Group in Lincoln Parish, Louisiana, and indicated that mechanical compaction has caused a 10 percent reduction of the primary porosity with increasing overburden. He also showed that chemical diagenesis has altered the texture and composition of the sandstone and modified porosity and permeability through cementation, dissolution and authigenic clay precipitation. Hall et al. (1984) studied the Cotton Valley sandstones in the Amoco No. 1 Cullers well (East Texas Basin) and showed that the depositional fabric has modified two principal processes: the reduction of primary porosity by carbonate

cements and quartz overgrowths; and the development of poorly interconnected secondary, intergranular porosity by dissolution of unstable grains. He also indicated that the pore system was further modified by the development of authigenic illite, chlorite and mixed-layer clays.

Black and Berg (1987) reported that the Cotton Valley Taylor “B” sandstone in Kildare field, Cass County, (northern part of East Texas Basin) is interpreted as the distal part of a prograding fan delta based on the vertical sequence in cores. The authors interpreted three major sandstone facies: (1) a massive to laminated, well-sorted sandstone; (2) a laminated, pebbly sandstone; and (3) very fine-grained sandstone interbedded with black shales. They also concluded that carbonate cement was extensive (up to 50% of the total rock) and dissolution of authigenic carbonates resulted in secondary porosity up to 17%.

McGowen and Harris (1984) studied the Cotton Valley and Hosston formations depositional systems and their influence on salt tectonics in the East Texas Basin and concluded that salt mobilization was induced by Cotton Valley and Hosston deltaic deposition. They also reported that parallel salt ridges that formed during deposition of the Cotton Valley and Hosston apparently were the initial stage in the development of salt anticlines and domes.

Wilson and Hensel (1984) suggested that a comparison calculation of various reservoir parameters from well logs and cores provide guidelines for understanding reservoir evaluation in the Cotton Valley Sandstones in East Texas Basin. They also reported that grain size distribution and the degree of shaliness, in addition to porosity

controls permeability and irreducible water saturation. Mcmanus and Tibbetts (1993) reported that Cotton Valley reservoirs in the Carthage field (depth range from 2530-2955 m) consists of six third-order sequences which can be divided into highstand, transgressive and lowstand system tracts. Most of the section is composed of highstand deposits that consist of aggrading to prograding wave-dominated shoreline parasequence sets.



## **CHAPTER 2**

### **SEQUENCE STRATIGRAPHY**

#### **2.1 INTRODUCTION**

Sequence stratigraphic analysis is a multidisciplinary approach that aims to subdivide the sedimentary basin fill into genetic packages bounded by surfaces of erosion or non-deposition. Each genetic package records deposition and preservation under a specific set of conditions. A goal of sequence stratigraphy is to delineate units deposited in time periods ranging from thousands to millions of years and within a broad spectrum of space domains. The discipline includes observation about facies, facies associations, depositional systems, system tracts and depositional sequences.

Sequence subdivision is commonly considered from one of two perspectives; the Vail/Exxon depositional sequence model (Mitchum and Vail, 1977; Vail, 1987; Van Wagoner et al., 1988; Vail and Wornardt, 1991) or the Frazier/Galloway genetic stratigraphic sequence approach (Frazier, 1974; Galloway, 1989a; Galloway and Hobday, 1996). Both perspectives emphasize the definition of genetically related depositional sequences which link coeval depositional systems. One of the primary differences between these two models is the choice of the sequence bounding surfaces used to delineate individual sequences. The Vail/Exxon approach defines a sequence as a relatively conformable succession of genetically related strata bounded by unconformities and their correlative conformities (Mitchum et al., 1977). Galloway and Hobday (1996) define a sequence as a three-dimensional stratigraphic unit consisting of relatively

conformable, genetically related strata bounded in whole or in part by surfaces of nondeposition or erosion (unconformities).

The Vail/Exxon approach emphasizes regressions and relative sea-level lowstand with sequence boundaries defined by subaerial unconformities (Fig. 8). The driving mechanism for these changes in relative sea-level is eustatic sea-level with sediment supply and subsidence rates held constant over time periods on the order of 10 MY or less (Posamentier et al., 1988; Posamentier and Vail, 1988). In the Vail/Exxon model, sequences consist of a succession of a lowstand system tract or transgressive system tract and a highstand system tract, each of which are linked to positions on the relative sea-level curve of Haq et al. (1987). A system tract is defined as “a linkage of contemporaneous depositional systems” by Brown and Fisher (1977).

Based on the nature of the bounding unconformities and the arrangement of strata between sequence boundaries, two types of sequences were recognized in the rock record by van Wagoner et al. (1988): type-1 sequence and type-2 sequence. If sea level falls below a shelf and the basal unconformity of a sequence is associated with significant incision and basinward shift in facies, then the sequence is called a type-1 sequence and the basal unconformity is called a type-1 sequence boundary. Consequently, if the basal unconformity of a sequence is not indicated by significant incision and basinward facies shift but by nondeposition and hiatus, then the sequence is called a type-2 sequence and the basal unconformity is called type-2 sequence

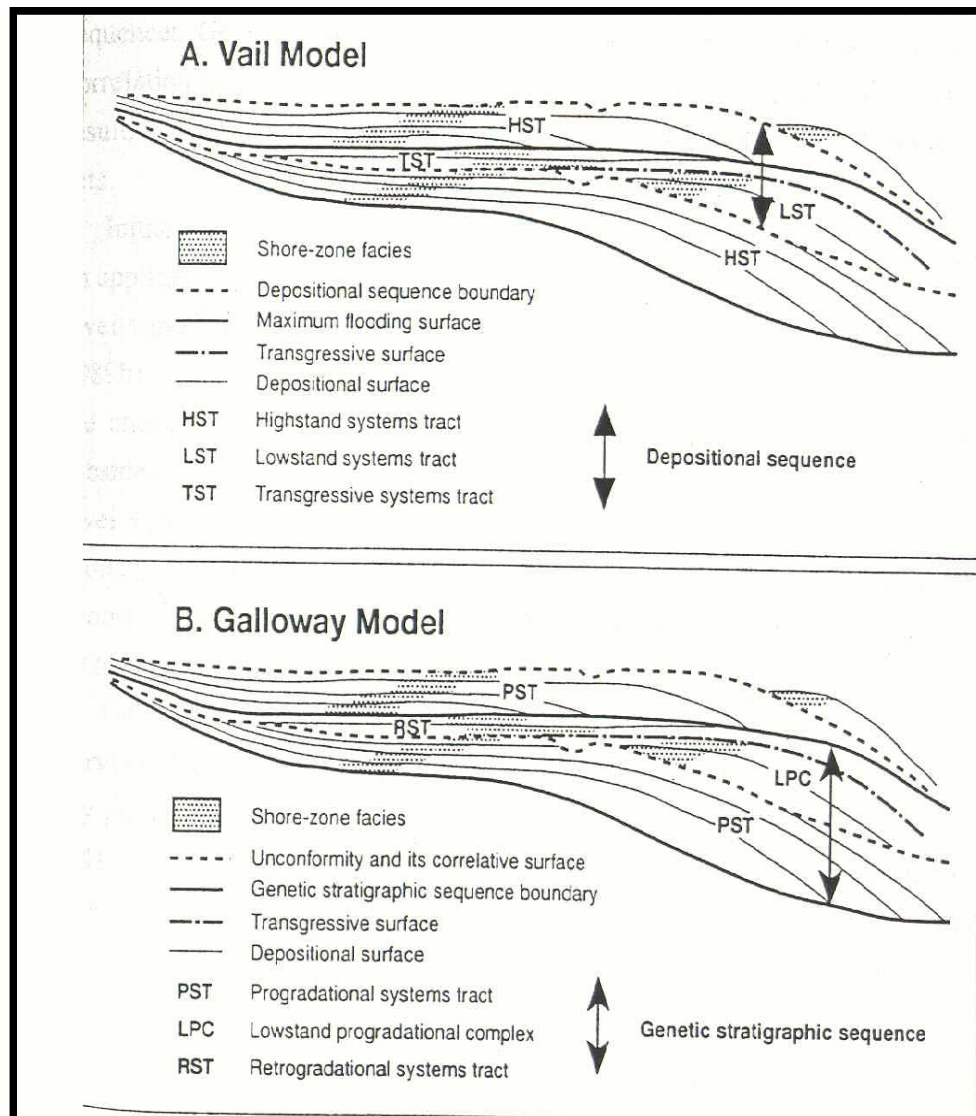


Figure 8: Comparison of the Vail/Exxon depositional model with the Frazier/Galloway stratigraphic model. From Xue and Galloway (1993).

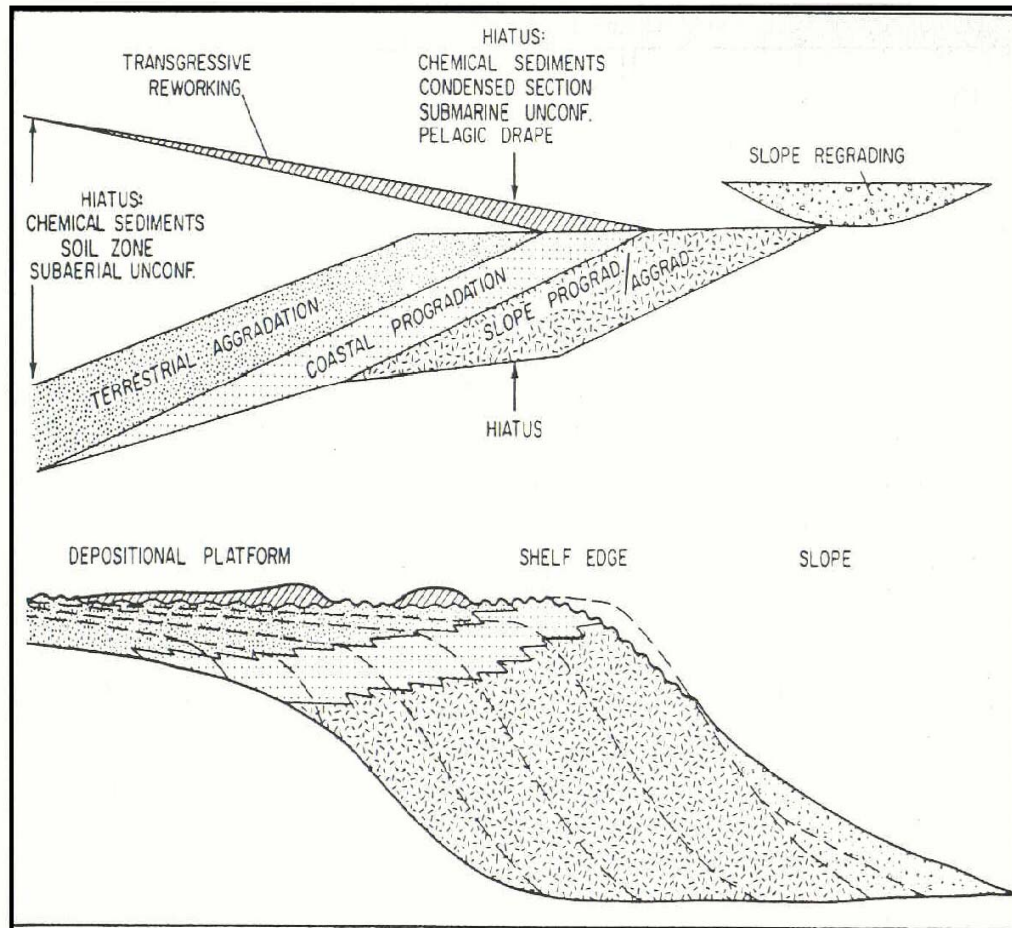


Figure 9: Stratigraphic architecture of a simple depositional episode and the resultant genetic stratigraphic sequence. The upper diagram (episode) has time as the vertical axis and the lower diagram illustrates the stratigraphic architecture and facies associations with depth as vertical axis. From Galloway (1989a, Figure 3).

boundary. In accordance with the above definitions, a type-1 sequence is composed of lowstand, transgressive, and highstand systems tracts; a type-2 sequence is composed of shelf-margin, transgressive, and highstand system tracts (Fig. 8).

Genetic sequence stratigraphy emphasizes the depositional episode as a primary building block in stratigraphic analysis (Frazier, 1974). A complete depositional episode consists of three facies associations which are described in terms of depositional architecture as progradational, aggradational and transgressive facies packages (Fig. 9). Sequence boundaries record periods of nondeposition or very slow deposition associated with maximum transgression and are drawn at composite marine unconformities and/or condensed beds (Galloway, 1989a; Galloway and Hobday, 1996). Condensed beds are defined as thin marine stratigraphic units consisting of pelagic to hemipelagic sediments characterized by very slow sedimentation rates (Loutit et al., 1988). The genetic sequence stratigraphic approach recognizes the same surfaces and strata geometries as the Vail/Exxon model. However, this approach is out of phase with the Vail/Exxon approach by grouping successive progradational (highstand), slope (lowstand) and transgressive deposits as a genetic sequence. I use Vail/Exxon model in this study.

## **2.2. Data**

A total of 150 wells logs are available in the study area and 60 of them were chosen for correlation purposes because of their uniform spacing and depth of penetration. Spontaneous potential, deep-medium-and short-normal induction resistivity log curves are available for each well. Core description of 4000 feet (1212 m) of

conventional cores in nine wells provides the sedimentological data used to calibrate log motif interpretation and adjust the position of the various types of stratigraphic surfaces.

Thus, all of the cored intervals examined in this study are calibrated with well-log data. Among the available log data, spontaneous potential and resistivity log profiles proved most useful for correlation of calibrated cored intervals with wells lacking core data. In this manner, well log profiles of facies associations and bounding sequence stratigraphic surfaces are extrapolated through out the study area, and a sequence stratigraphic frame is generated. Selected methods illustrating this stratigraphic framework include; stratigraphic cross-sections and net sand maps. The contact between the Cotton Valley Sandstones and the underlying Bossier Formation was not studied because most of the drilled wells did not penetrate the Bossier Formation.

### **2.3. Methods**

Electric logs are used to identify the fourth-order system tracts and their bounding surfaces based on stacking patterns, shapes, and petrophysical characteristics. Three types of parasequence stacking patterns of progradation, retrogradation and aggradation are recognized as indicators for change in accommodation space.

#### **2.3.1. Stacking patterns**

Progradation (Fig. 10) is interpreted based on upward-coarsening log response. Progradation commonly is related to the highstand system tract, and was interpreted as such from the presence of an underlying maximum flooding surface and an upper

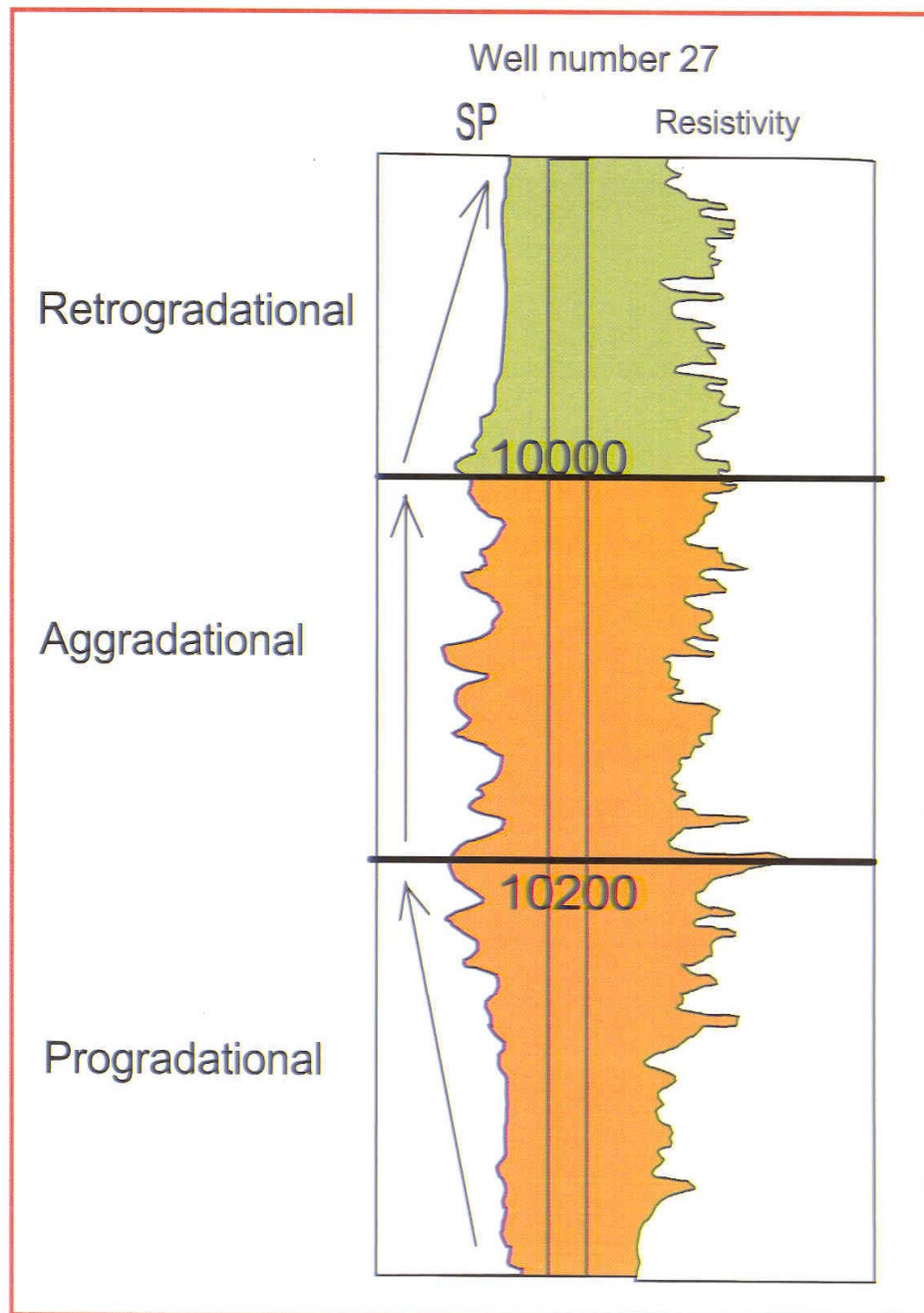


Figure 10: Depositional architecture and stacking pattern in well 27. Depth in feet. Arrows indicate general trend of coarser sand grains.

bounding transgressive surface and/or sequence boundary onto which incised valley fill or transgressive sediments were deposited.

Retrogradation (Fig. 10) is interpreted from an upward-fining log response. Retrogradational stacking patterns were associated with the transgressive systems tract when underlain by lowstand and/or highstand deposits, and overlain by highstand system tract sediments.

Aggradational stacking patterns are interpreted from a cylindrical to blocky log response (Fig. 10). An aggradational stacking pattern is associated with the lowstand systems tract when the lower bounding surface is interpreted as a sequence boundary and the upper surface as a transgressive surface onto which transgressive systems tract sediments were deposited.

### **2.3.2. Stratigraphic surfaces**

The transgressive surface, maximum flooding surface and sequence boundaries are interpreted from the electric log curves. The transgressive surface represents the boundary between the highstand systems tract, or the lowstand systems tract and the first backstepping parasequence of the transgressive systems tract. It was interpreted at the transition between the underlying funnel-shaped or blocky log response of the highstand or lowstand systems tract, and the overlying, fining-upwards bell-shaped response of the spontaneous potential and resistivity log curves (Fig. 11). The transgressive surface can be identified on the spontaneous potential curve as a “kick” or spike. The initial transgressive lag is often heavily cemented with calcium carbonate, which is detected on the resistivity log as a high resistivity “hard” streak.



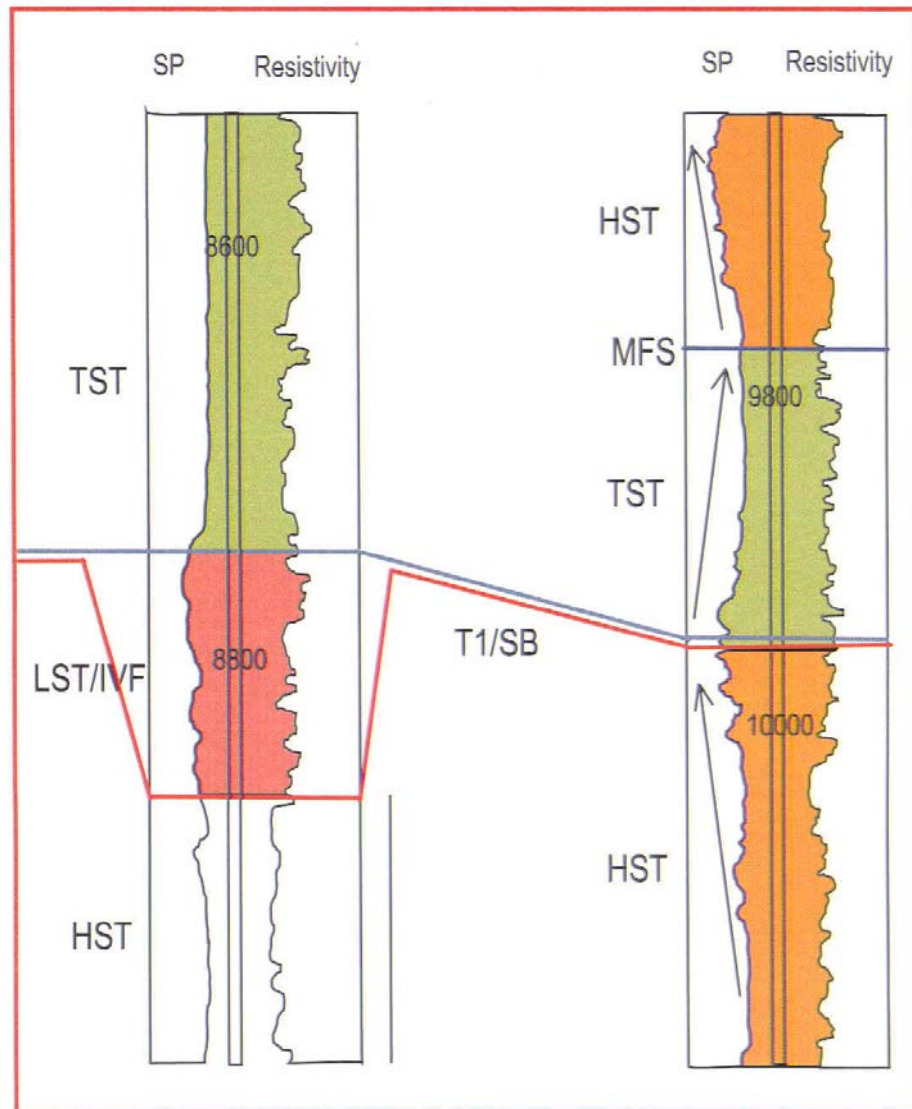


Figure 11: Stacking pattern and stratigraphic surfaces in selected intervals in the study area. Depth in feet. TST is transgressive system tract, LST/IVF is lowstand incised valley fill, HST is highstand system tract, and T1/SB is type 1 sequence boundary (red line).

The boundary between higher resistivity transgressive systems tract shales and lower resistivity highstand systems tract shales is the maximum flooding surface (Fig 11). This surface corresponds to the plane between the fining-upward response of the spontaneous potential curves in the transgressive systems tract and the coarsening-upward log-pattern in the highstand systems tract.

The sequence boundary is identified as the surface located at the base of the incised valley fill deposits. Valleys have a sharp base with a cylindrical or blocky profile. The sequence boundary is picked at the base of the blocky sand on the spontaneous potential curve. On the shelf in the absence of any incision, the transgressive surface and the sequence boundary join to become one surface (Fig. 11). The sequence boundary can be tested in surrounding wells by whether the blocky sediment patterns are aligned along depositional dip or strike. Strike orientation may indicate high-energy shoreface processes, while dip-oriented blocky-sand facies are candidates for incised valley-fill facies. Another test for the presence of incised valley-fill facies is whether or not the highstand sediments were eroded in the vicinity of the incised valley. A crucial test for the presence of a sequence boundary is the scale of the overlying incised valley deposits. Fluvial systems in the highstand and transgressive systems tracts can reach maximum widths of hundreds of meters, while the width of incised valleys are an order of magnitude wider, usually measured in kilometers.

### **2.3.3. Trace fossils**

Trace fossils (or ichnofossils) are biologically produced sedimentary structures

that include tracks, trails, burrows, borings, fecal pellets and other traces made by organisms. The *Glossifungites* (firm ground) ichnofacies is environmentally wide ranging, but only develops in firm, unlithified substrates such as dewatered mud (Fig. 12). Dewatering results from burial and the substrates are made available to tracemakers if exhumed by later erosion (Pemberton and Frey, 1985). In siliclastic settings, most firm-ground assemblages are associated with erosionally exhumed (dewatered and compacted) substrates and, hence, demonstrate erosional discontinuities. The *Glossifungites* ichnofacies is important in both the recognition and genetic interpretation of erosional discontinuities in marine-influenced siliclastic intervals (Pemberton et al., 2001). *Glossifungites* ichnofacies was used in addition to the other tools to verify the erosional stratigraphic sequence boundaries precisely.

#### **2.4 Stratigraphic cross-sections**

In order to reconstruct the sequence and system tracts architecture of Cotton Valley Sandstones, two dip, two strike and one diagonally oriented cross sections were constructed by using well logs correlated with cores where available. The stratigraphic datum is the maximum flooding surface below the top of the Cotton Valley Sandstone. Above this datum highstand system tract of the upper most cotton Valley sequence (S6) occurs. At top of Cotton Valley a transgressive surface occur which marks the base of the transgressive Knowles Limestone. Figure 13 shows the location of the cross sections.

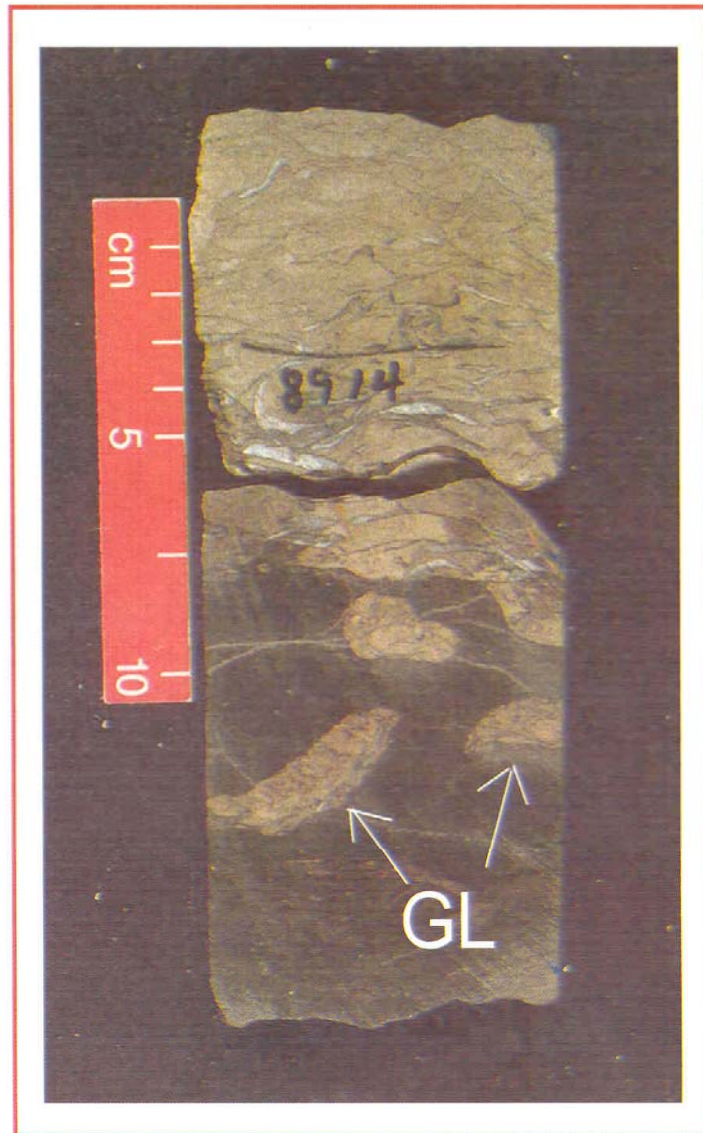


Figure 12: Glossifungites ichnofacies (pipes) formed by Thalassinoides traces (arrows). In the backside of the core these pipes are connected to each other.

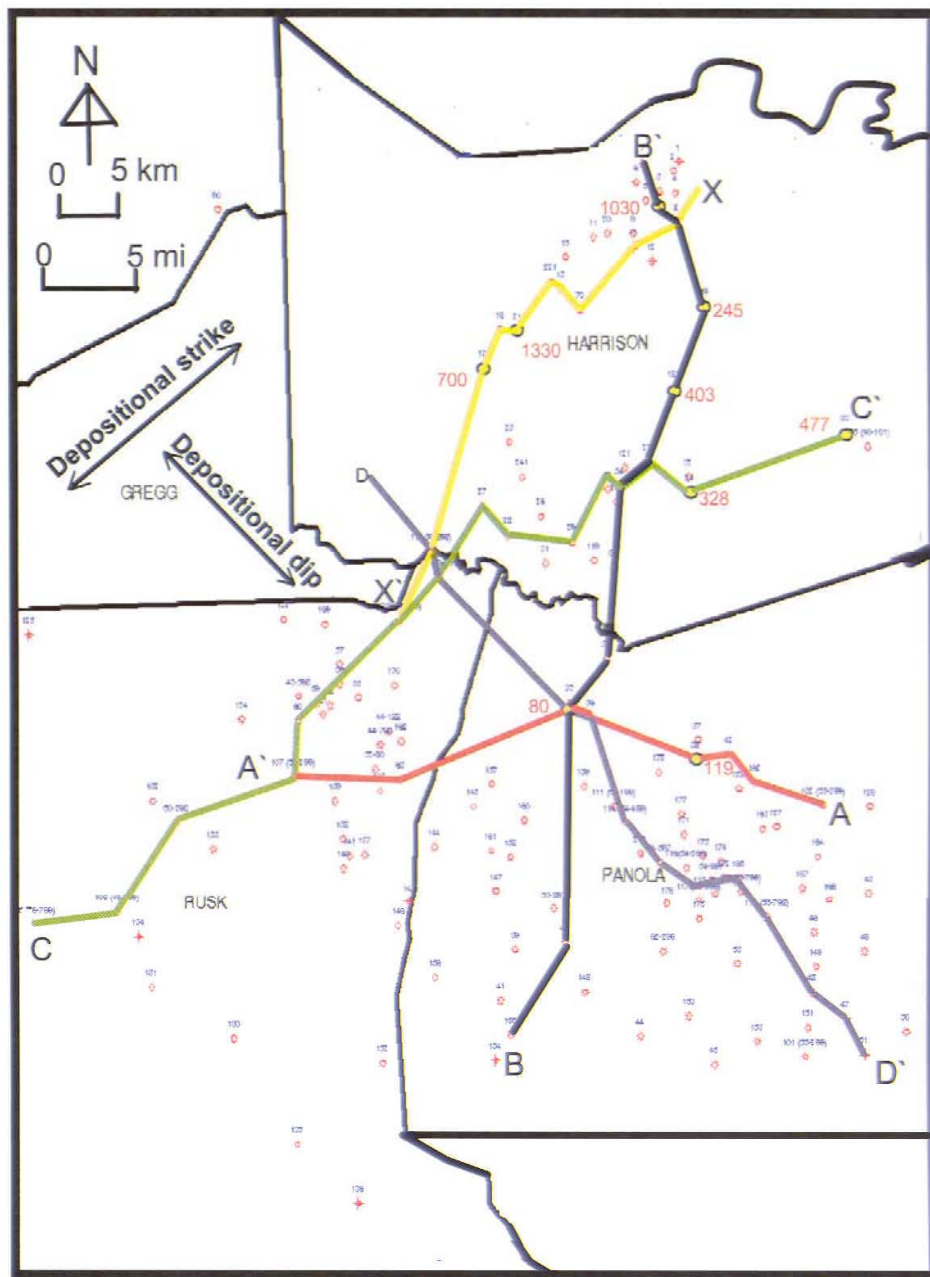


Figure 13: Stratigraphic cross sections trend in the study area.

Core control is more abundant within the strike and diagonal sections than the dip section due to the distribution of cored wells.

#### **2.4.1. Dip-oriented cross section D-D'**

This section (Fig. 14) is oriented north-west to south-east along the depositional dip of the Cotton Valley sandstones. Well number 110 is landward and well number 51 is basinward. The cross section comprises 14 logs over a distance of about 35 miles (63 km). In this trend, one core is available in Tallent # 1 well; the core which penetrates sequence number 2 (S2) will be discussed later in this chapter. Analysis of this core reveals key aspects of the Cotton Valley sandstone sequence stratigraphic architecture:

1) The Cotton Valley Sandstone comprises six third-order sequences, from bottom to top S1-S6, and 13 parasequence sets from bottom to top At to Fh. Each sequence is composed of two or three parasequence sets, highstand, transgressive and/or lowstand systems tracts.

2) The distribution of the parasequence sets within the lowstand, transgressive and highstand systems tracts in sequence 3 reflect type-1 sequences deposited on a basin with a shelf margin. The lowstand prograding wedge and slope and basin floor fans are not observed in other sequences. Mitchum (1997, 2001) in his wider cross section (1073 wells) along the same trend as D-D' interpreted the deep-water sediments for all of his sequences. The following points support the type-1 sequences interpretation.

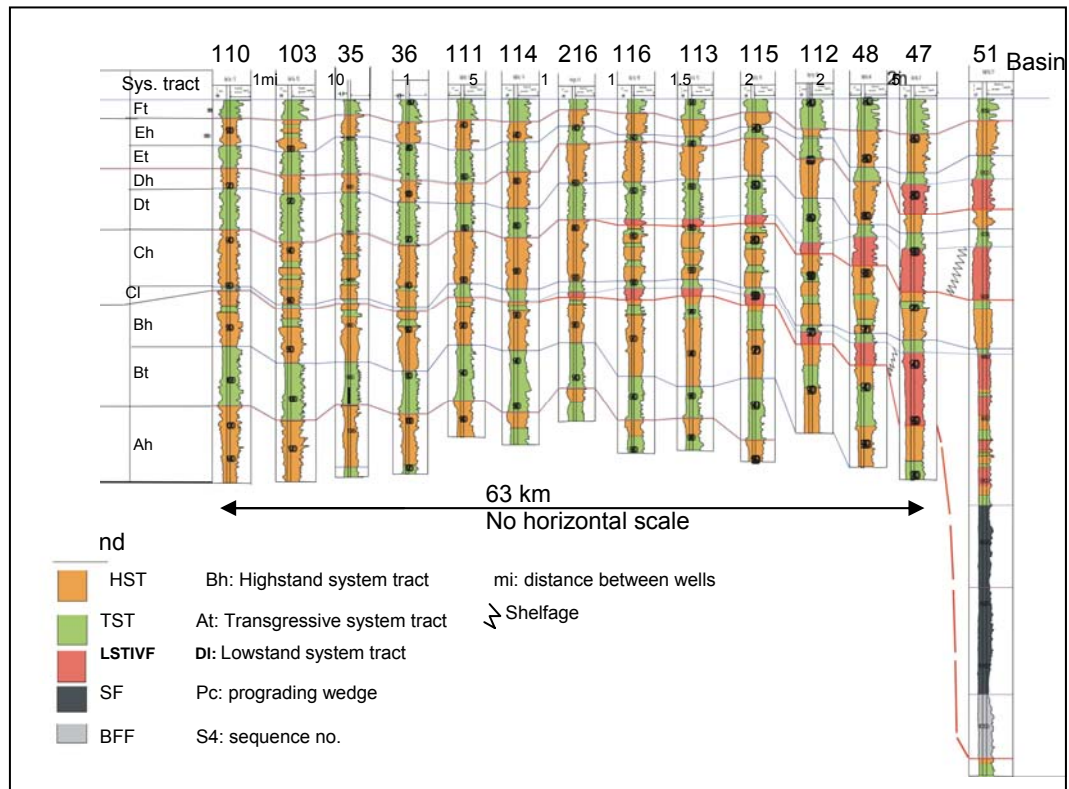


Figure 14: Dip oriented Stratigraphic cross-section D-D'.

a) The Cotton Valley sandstones were deposited in a basin with well-defined shelf, slope and basin floor fans (Fig. 14) which are recognizable in S3 (well 51). The shelf regressed about 30 to 33 miles (54-59 km) between S3 and S4, where incision took place for a short distance into the shelf. For S3, the shelf break is located between wells 48 and 47 where a lowstand prograding wedge, slope fan and basin floor fan are observed in well 51. The shelf break shifts basinward; by S4 it is most probably located between wells 47 and 51. b) A relatively abrupt shelf break separates low-dip shelf-deposits from much more steeply dipping slope deposits. c) Incision in response to sea-level fall below the depositional shoreline break and submarine canyon most probably formed and transported the fluvial sediments from shelf to slope. D) A basinward shift in shoreline or shelf break is also observed in sequences 3 and 4 (Fig. 14).

A type-1 sequence is interpreted to have formed when the rate of eustatic fall exceeded the rate of subsidence at the depositional-shoreline break, producing a relative fall in sea level at that position (Jervy, 1988; Posamentier et al., 1988). In addition to being deposited in a basin with a shelf break, the following additional conditions must exist: 1) sufficiently large fluvial systems to cut canyons and deliver sediments to the basin; 2) enough accommodation rate for the parasequence sets to be resolved; and 3) a relative fall in sea level of a rate and magnitude sufficient to deposit the lowstand systems tract at or just beyond the shelf break (van Wagoner et al., 1990).

Three incised valleys are delineated on section D-D'. On the shelf the incised valleys are bounded below by a sequence boundary/unconformity surface and above by



the transgressive surface. The width of the valleys varies between 2.5 miles and 14 miles (4.5-25.2 km). On the shelf, the transgressive surface and the sequence boundary combined to become one surface (E/T1). Core study reveals the presence of *Glossifungites* ichnofacies and transgressive lag along the E/T1 surface which has significantly coarser-grained gravels and/or oysters that were not derived from the underlying succession. On the slope in well number 51, the base of the basin-floor fan (the base of the lowstand systems tract) is the type-1 sequence boundary and the basin floor fan is overlain down-lap by the slope fan (Fig. 14). Thickness of the basin floor fan plus slope fans is about 800 feet (242 m) and thickness of the overlying prograding wedge complex is about 500 feet (151.5 m).

#### **2.4.2. Strike-oriented and diagonal cross-sections**

Two strike-oriented cross sections are C-C' and X-X'; both trending NE-SW. C-C' section comprises 15 logs over a distance of about 61 miles (109 km); two wells have cores (SFE # 3 and Blocker Heirs # 1: wells number 33 and 23 respectively, Fig. 15). The cored interval in both wells penetrates SB1. Section X-X' comprises nine well logs over a distance of about 27 miles (42 km). Cores are available for wells number 17 and 21 (Fig. 16).

The Davidson Foundation # 1 (well number 17) was cored at two intervals. The lower core # 1 covers most of S3 and parts of S2 and the upper core # 2 penetrates a small interval of HST in S5. The James Anderson # 1 (well No. 21) was cored at four intervals. Core # 1 and # 2 penetrated the lower and upper parts of HST of S1 respectively, core # 3 penetrated the lower part of Bh/S2, and core # 4 cut the upper part

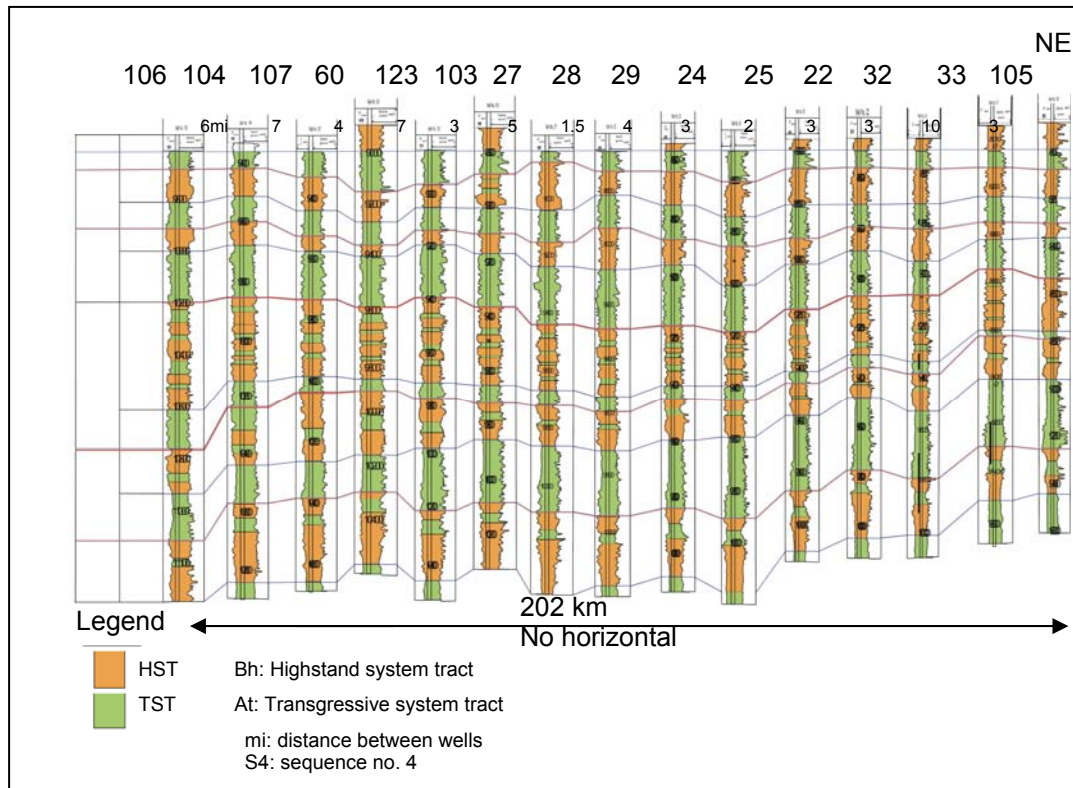


Figure 15: Stratigraphic cross section C-C'.

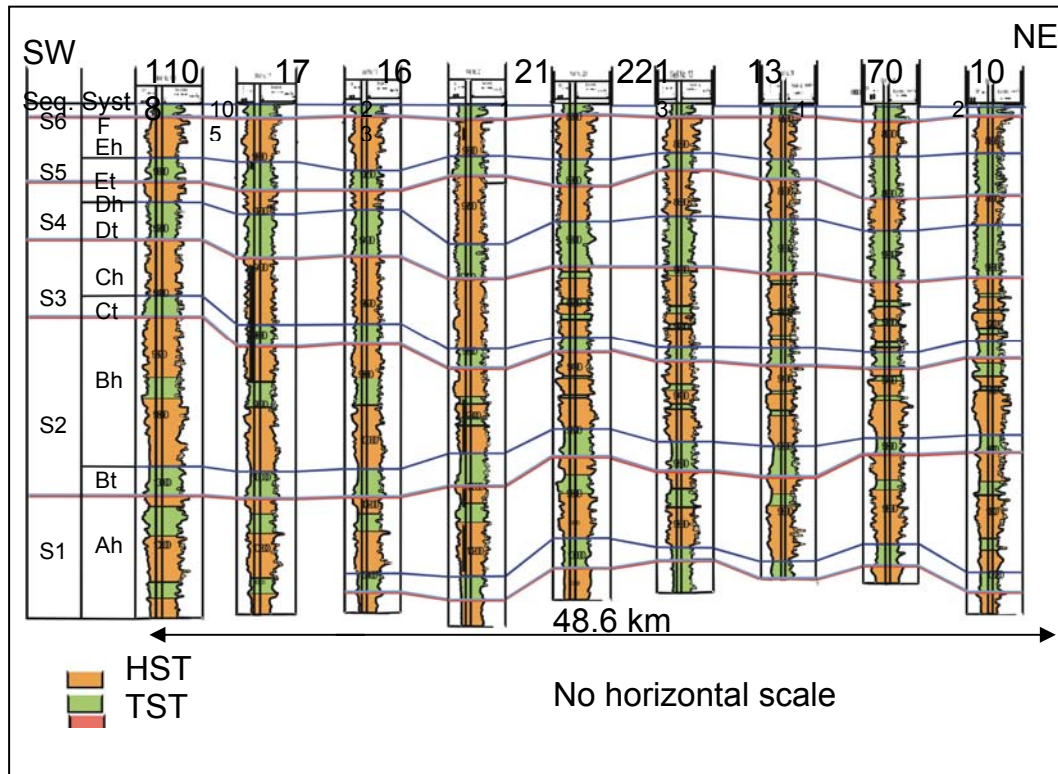


Figure 16: Stratigraphic cross section X-X'.

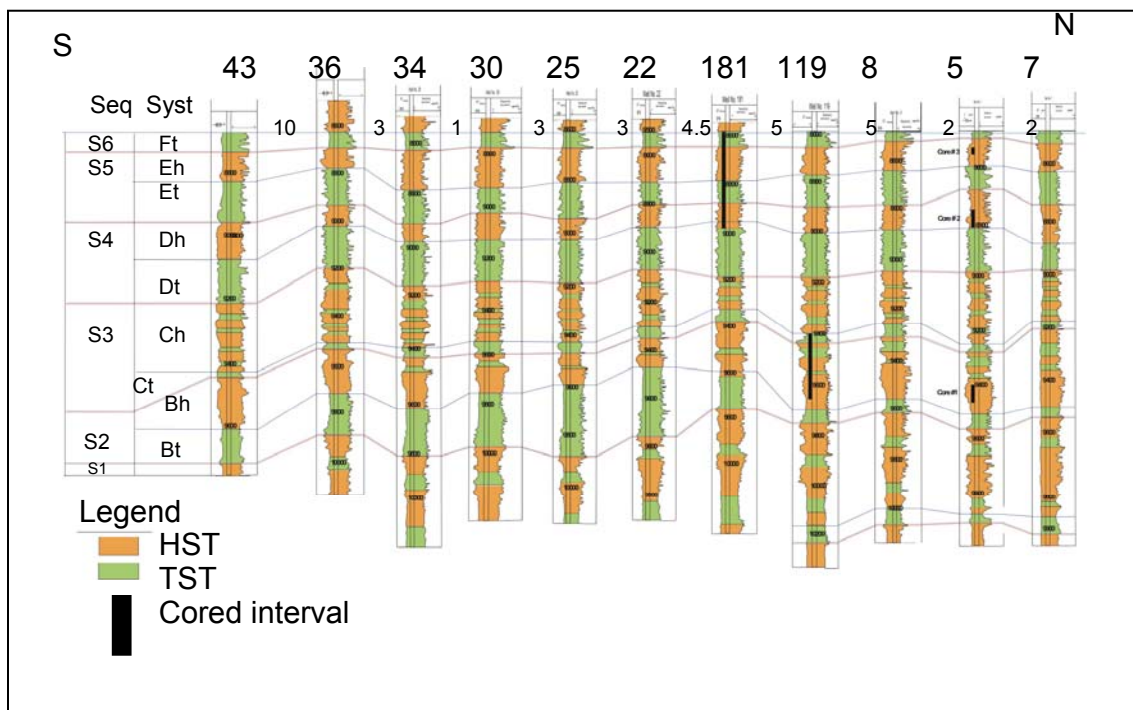


Figure 17: Stratigraphic cross section B-B'.

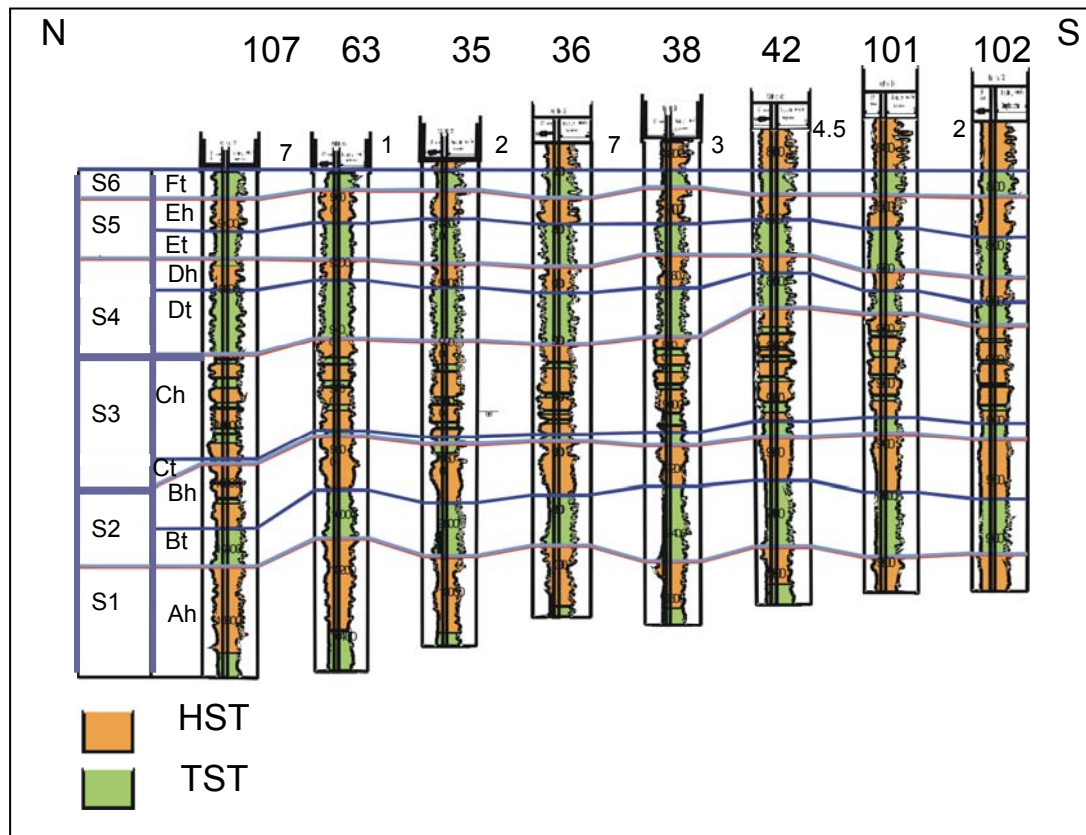


Figure 18: Stratigraphic cross section along A-A'.

of Eh/S5. Two diagonal cross sections close the loop between dip- and strike-oriented sections. Section B-B` (Fig. 17) trends N-S and includes 11 wells over a distance of 42 miles (67 km). This section includes three cored wells; Bradshaw #1, Grace Lowry #1 and Jones #3 (well numbers; 181, 119 and 5, respectively). One of the longest continuous cores in Bradshaw #1 cuts the upper part of the section, including S6, TST of S5 and HST of S4. The Grace Lowry core penetrates TST of S3 and most of HST of S2. Well Jones # 3 (well number 5) was cored at three intervals (1, 2 and 3) which penetrate HST of S2, HST of S4, and HST of S5, respectively. The other diagonal section A-A` (Fig. 18) trends E-W. Eight wells comprise this section over a distance of 37 miles (62 km). Two cored wells in this section are Tallent # 1 (well number 35) and Burnett Brothers # 12 (Well number 38); both cut SB2. Well log to core integration will be discussed in detail after the depositional environment section. Description of the available cores in these sections is discussed in the next section.

## **2.5. Well log-core integration**

Several surfaces that are displayed in cores of the Cotton Valley sandstone could be traced over varying distances. Analysis of the facies above and below these surfaces indicates that they represent fundamentally different depositional environments. Depositional environments are discussed in Chapter III. Features observed in the cores include lithology and grain size, lithofacies, sedimentary structures, trace fossils and accessory components (Fig. 19). No cores cut the lowstand systems tract or submarine fans. Cores are discussed in the order of sequences from S1 to S6 and sequence boundaries from SB1 to SB5.

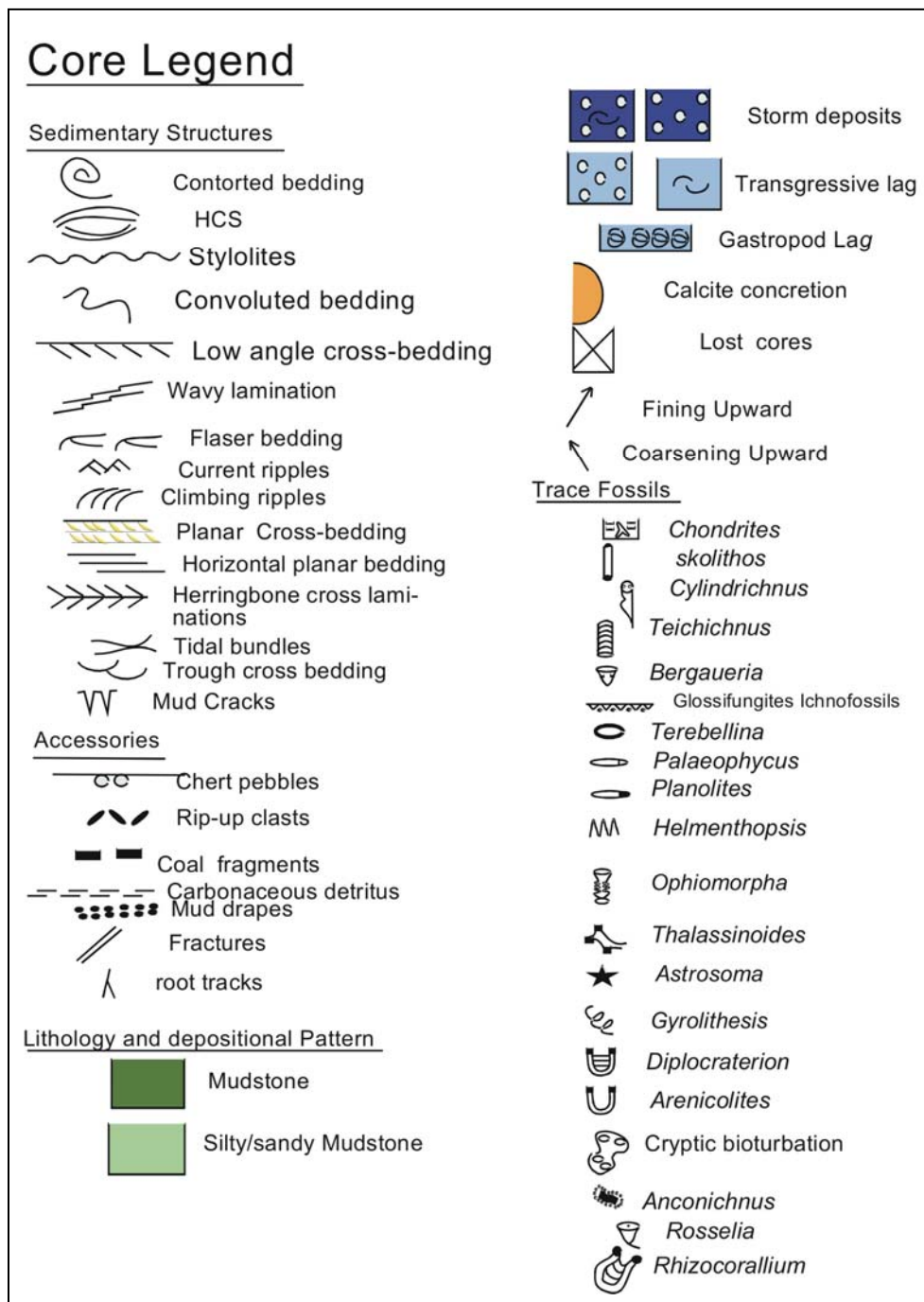


Figure 19: Core legend.

### **2.5.1. Cores that penetrated S1 and/or SB1**

#### **2.5.1.1. SFE #3**

The cored interval in SFE # 3 well penetrated SB1; this well is located in strike cross-section C-C` (Fig. 15). Figure 20 shows that Cotton Valley Sandstones in well SFE # 3 consists of two elements in the vertical direction: the lower progradational interval, which coarsens upward from intensely bioturbated mudstone to fine-grained sandstone composed of small-scale cross lamination and current ripples, and the overlying retrogradational interval which represents deposits of tidal channels and tidal inlets (Fig. 21a). The lower interval is fairly constant in thickness 35-40 feet (10-12 m) throughout the whole area, whereas the upper interval evidently thickens northeastward from 70 ft to 125 ft (21-38 m).

A transgressive lag deposit and *Glossifungites* ichnofacies exist at SB1, which records a vertical shift in facies from high-energy laminated middle-upper shoreface sandstones to intensively bioturbated transitional-inner shelf sandy mudstone (Fig. 20). The lag consists of chert pebbles with abundant mudstone rip-up clasts and organic matter that is 1.5 ft thick. A *Thalassinoides* burrow which is filled by the fine sandstone from the above facies is interpreted as a part of the *Glossifungites* ichnofacies.

Several channelized units bottomed out on this surface. Channelized units are recognized on SP and resistivity profiles as bell-shaped log profiles and on cores as scoured features with lag deposits on them and a fining-upward pattern (Fig. 21b).



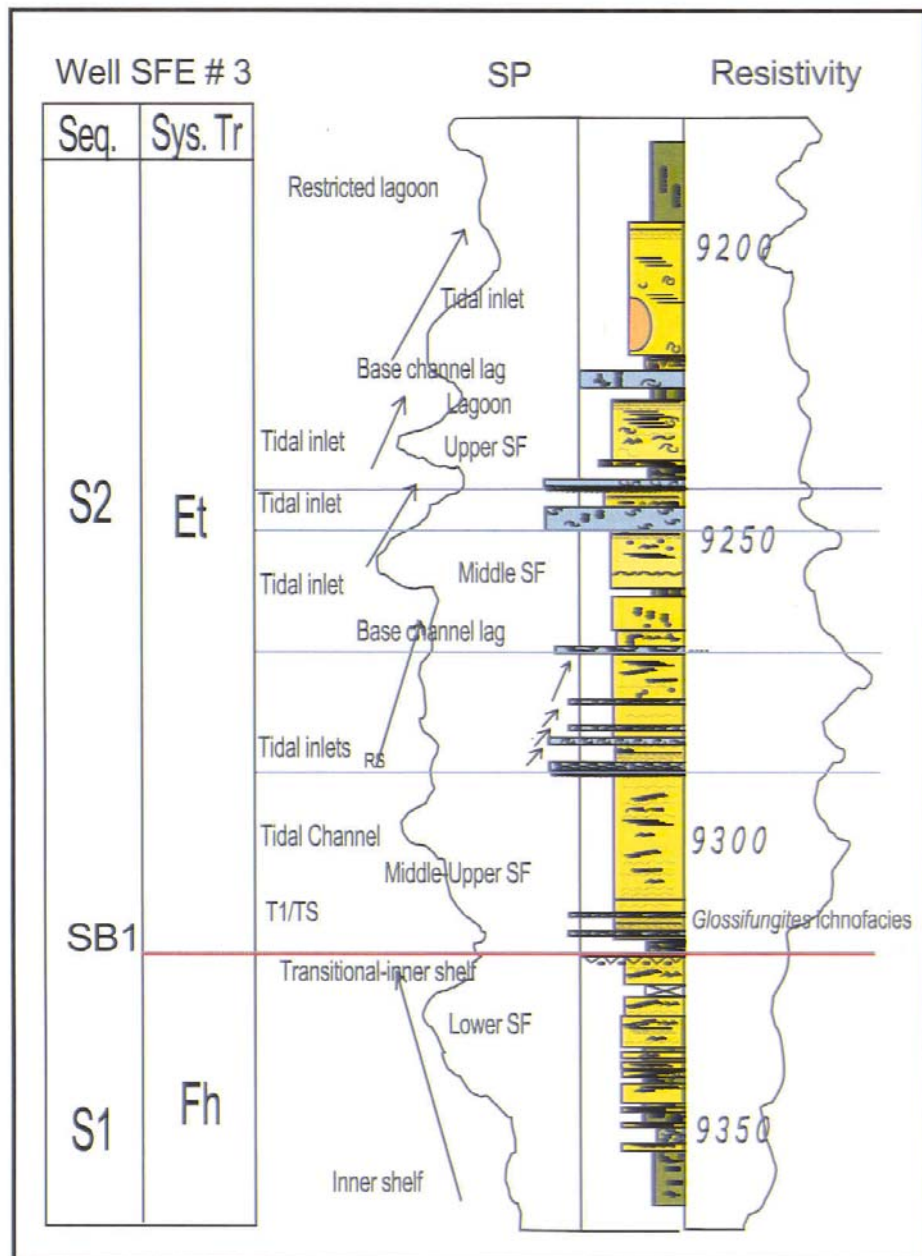


Figure 20: Core-log integration. Depth in feet. See chapter 3 for explanation of system tracts symbols and figure 19 for explanation of sedimentary structures and trace fossils.

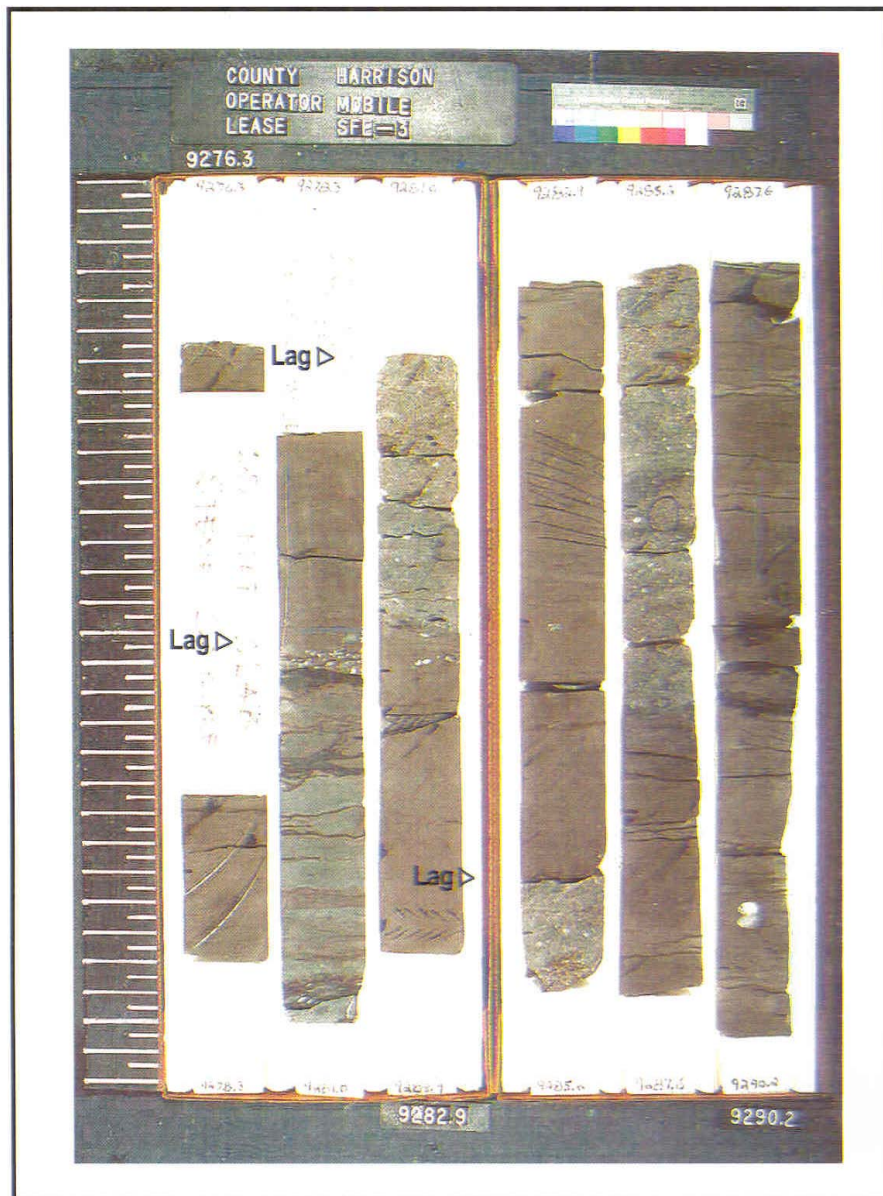


Figure 21a: Vertically stacked tidal inlets. The base of the inlet fill is marked by quartz and chert pebble conglomerate lag with oysters. Well SFE # 3. Left ruler is 3 feet.

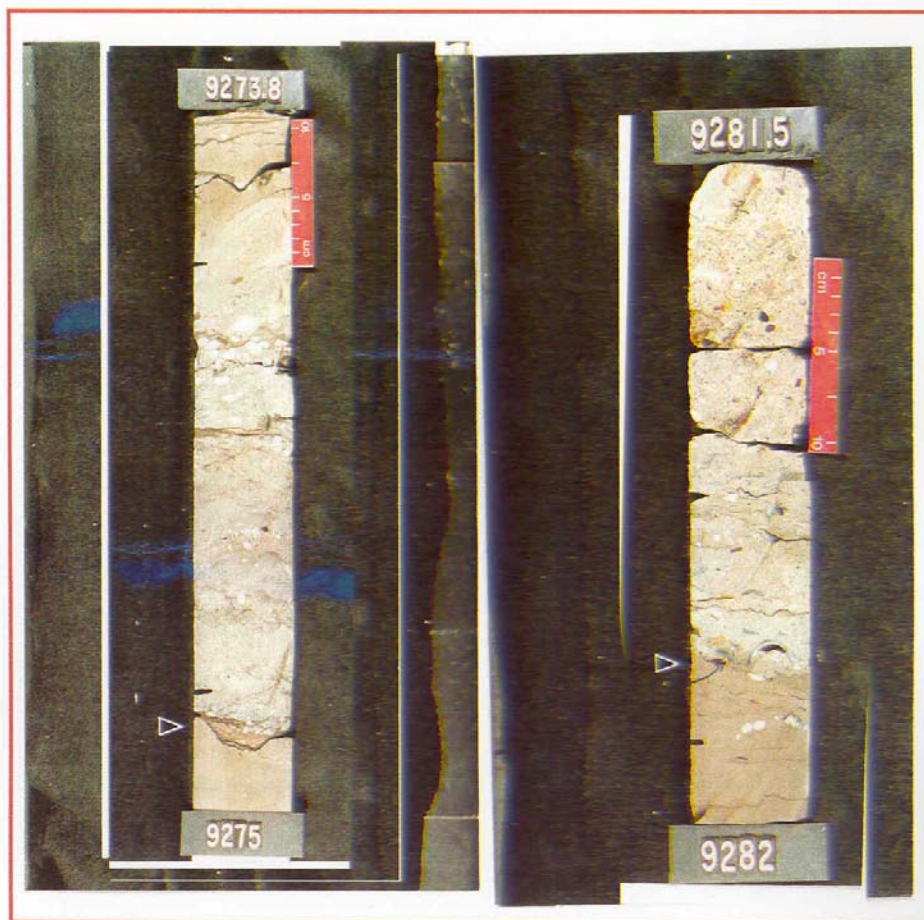


Figure 21b: Close up view of the base of the tidal inlet deposits. Note lag deposits and scouring features (arrows). Well SFE # 3.

The base of each fining-upward channel is a ravinement surface, which is commonly associated with the *Glossifungites* ichnofacies. This is part of the barrier-island/lagoon complex and it will be discussed in chapter III.

#### **2.5.1.2. Blocker Heirs # 1**

This core is located in strike section C-C', just 10 miles (18 km) from SFE # 3 well (Fig. 15). Two vertical elements are observed; the lower progradational interval and the upper retrogradational one with a T1/TS SB1 in-between (Fig. 22). In the lower interval a maximum flooding surface (MFS1) separates transgressive deposits from overlying regressive ones (Fig. 23). The facies below the MFS fine upward from high energy, cross bedded and rippled fine-grained sandstone separated by thin shale partings to black, slightly bioturbated middle shelf mudstone with silty lenses. Facies coarsen above the MFS from middle-shelf mudstone to fine-grained laminated storm-dominated middle to upper shoreface sandstones. Transgressive lag associated with SB1 is composed of thin to 1 foot-thick (0.33 m) chert-pebble conglomerates (maximum pebble size ~2 cm) along with some mudstone rip-up clasts (Fig. 24). The retrogradational interval above SB1 is represented by tidal inlet deposits (Fig. 25). Ravinement surfaces associated with lag deposits are located at the base of each inlet. Minor flooding events are observed in the upper part of the retrogradational interval where oyster lag coincides with deepening of facies from shoreface to inner shelf.



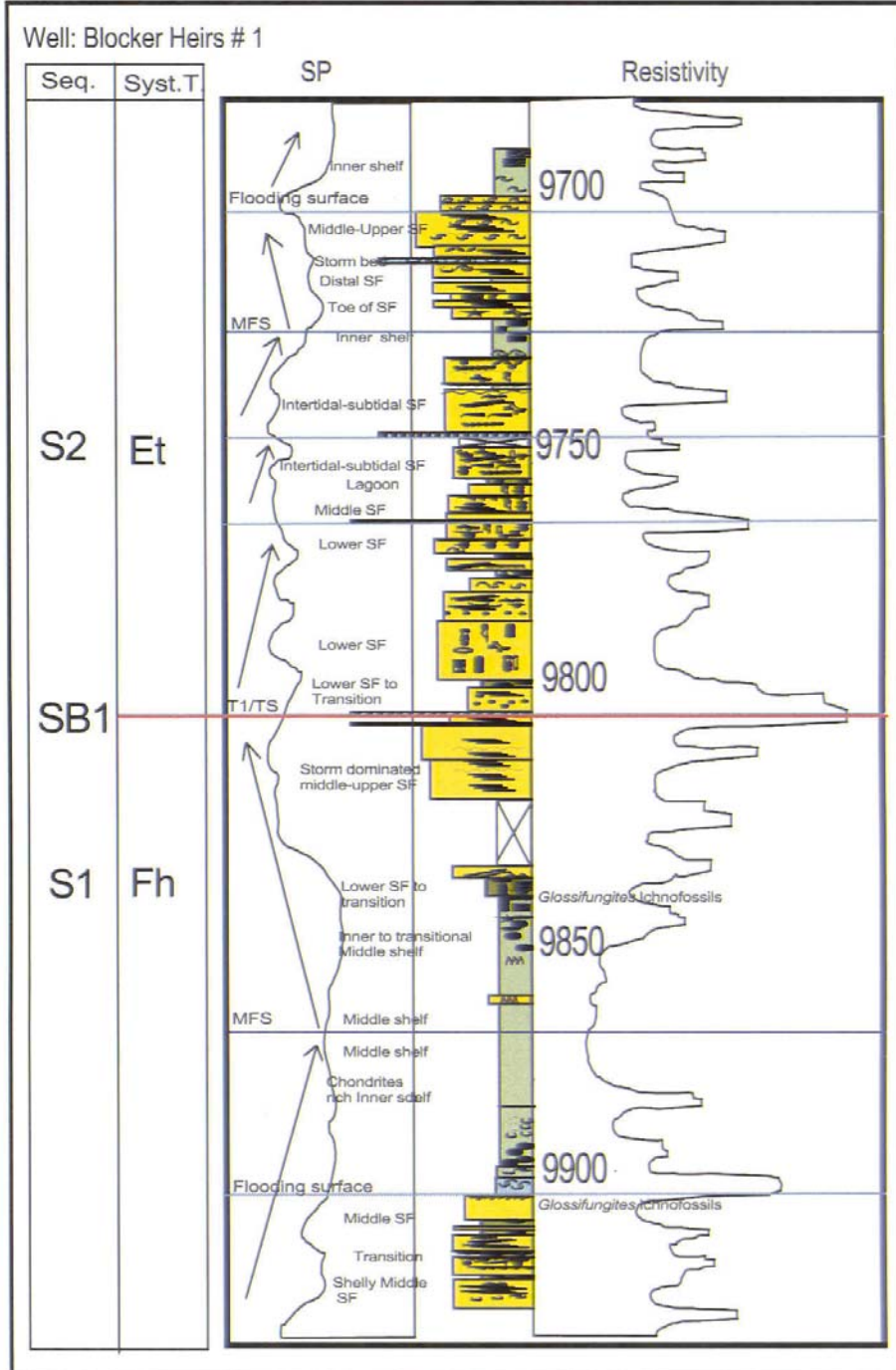


Figure 22: Core-log integration. Depth in feet. See chapter 3 for explanation of system tracts symbols and figure 19 for explanation of sedimentary structures and trace fossils.

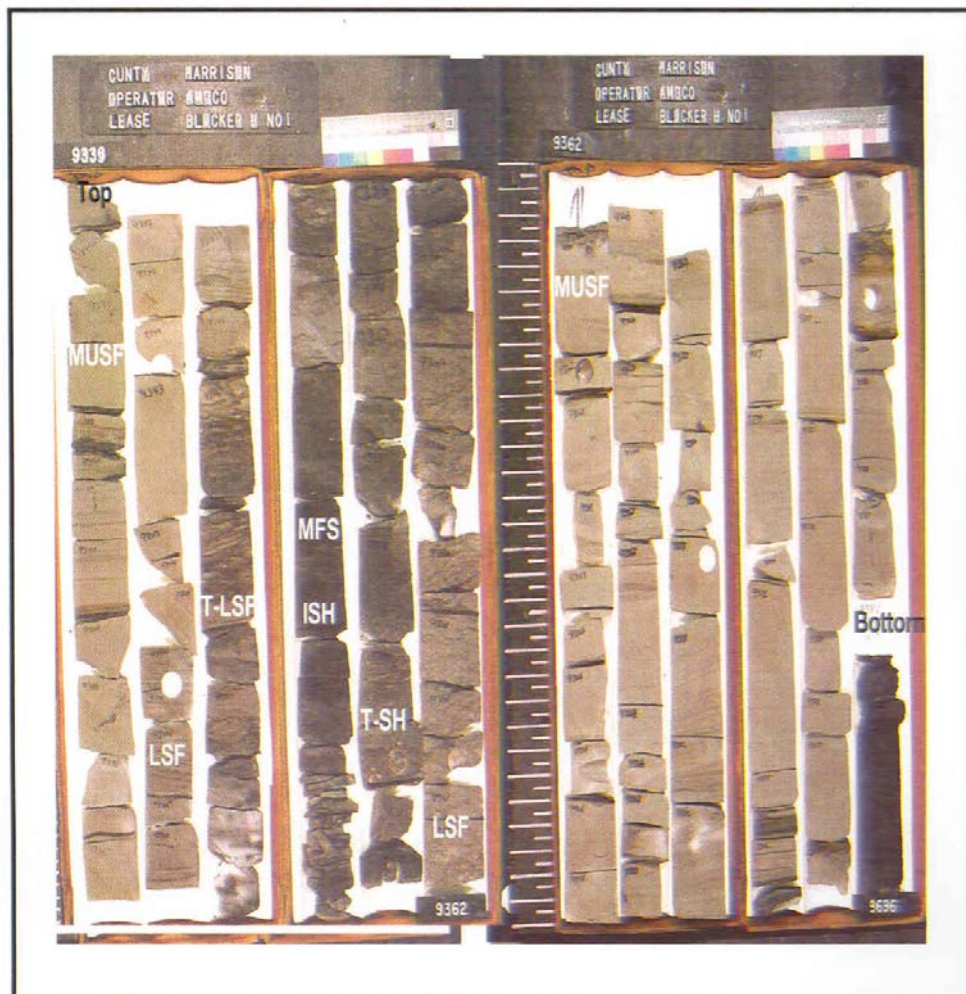


Figure 23: Maximum flooding surface (MFS) at depth 9354 ft. marks the turn around from transgressive to regressive deposits. The sequence of facies from bottom to top are; middle-upper shoreface (MUSF), lower shoreface (LSF), transitional to inner shelf (T-SF), inner shelf (ISH), transitional to lower shoreface (T\_LSF), lower shoreface (LSF) and middle-upper shoreface (MUSF).

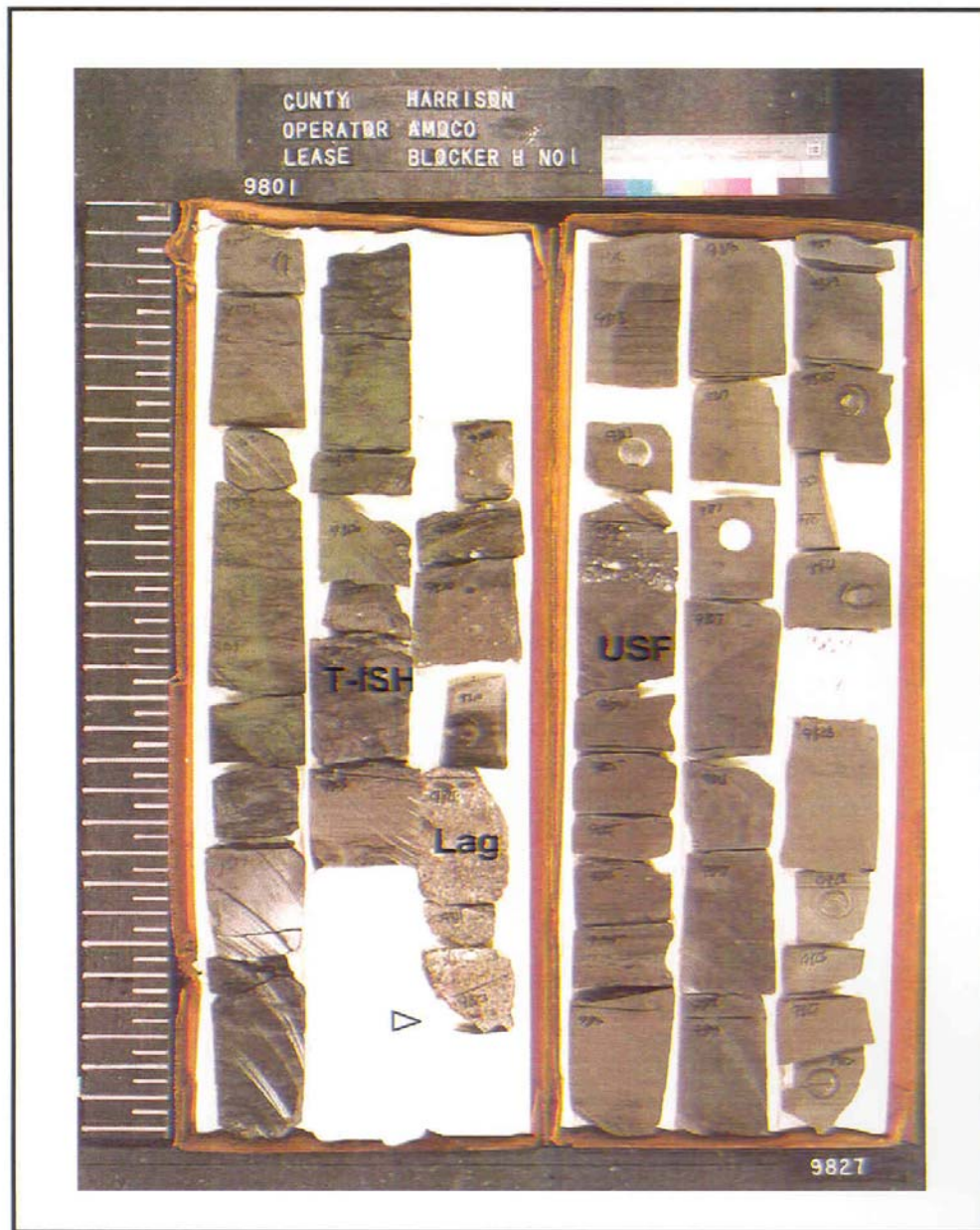


Figure 24: Upper shoreface (USF) deposits are overlain by transitional to inner shelf (T-ISF) sediments recording a sequence boundary (arrow). Note conglomerate lag above the sequence boundary. Blocker Heirs # 1.







#### **2.5.1.3. Burnett Brothers # 12**

This core that is identified in cross-section A-A' (Fig. 18) was divided into two intervals separated by a T1/TS sequence boundary (Fig. 26). The lower interval is progradational (coarsening upward) from low-energy fine-grained bioturbated lower shoreface sandstone to high-energy coarser grained laminated middle-upper shoreface sandstone. *Glossifungites* ichnofacies are recorded at SB1. SB1 is overlain by transitional to inner shelf facies consisting of interlaminated bioturbated sandstone and mudstone. The top part is a lagoonal facies. A regressive surface should occur between the transitional inner shelf and the overlying lagoonal facies, but core at the contact is missing.

#### **2.5.1.4. Tallent # 1**

This core is identified in cross section A-A', 9 miles (16.2 km) west of Burnett Brothers # 12. Figure 27 displays a MFS that separates transgressive deposits from the overlying regressive facies. The transgressive facies fines upward from intensively bioturbated inner-shelf silty mudstone to massive outer-shelf mudstone. The overlying progradational unit coarsens upward from outer- shelf mudstone to middle-upper shoreface sediments.

#### **2.5.1.5. James Anderson # 1**

This core is identified in the cross-section X-X' (Fig. 16). Core # 1 penetrates the lower part of S1. The log response shows two architectural patterns; the lower progradational and the upper retrogradational ones (Fig. 28).

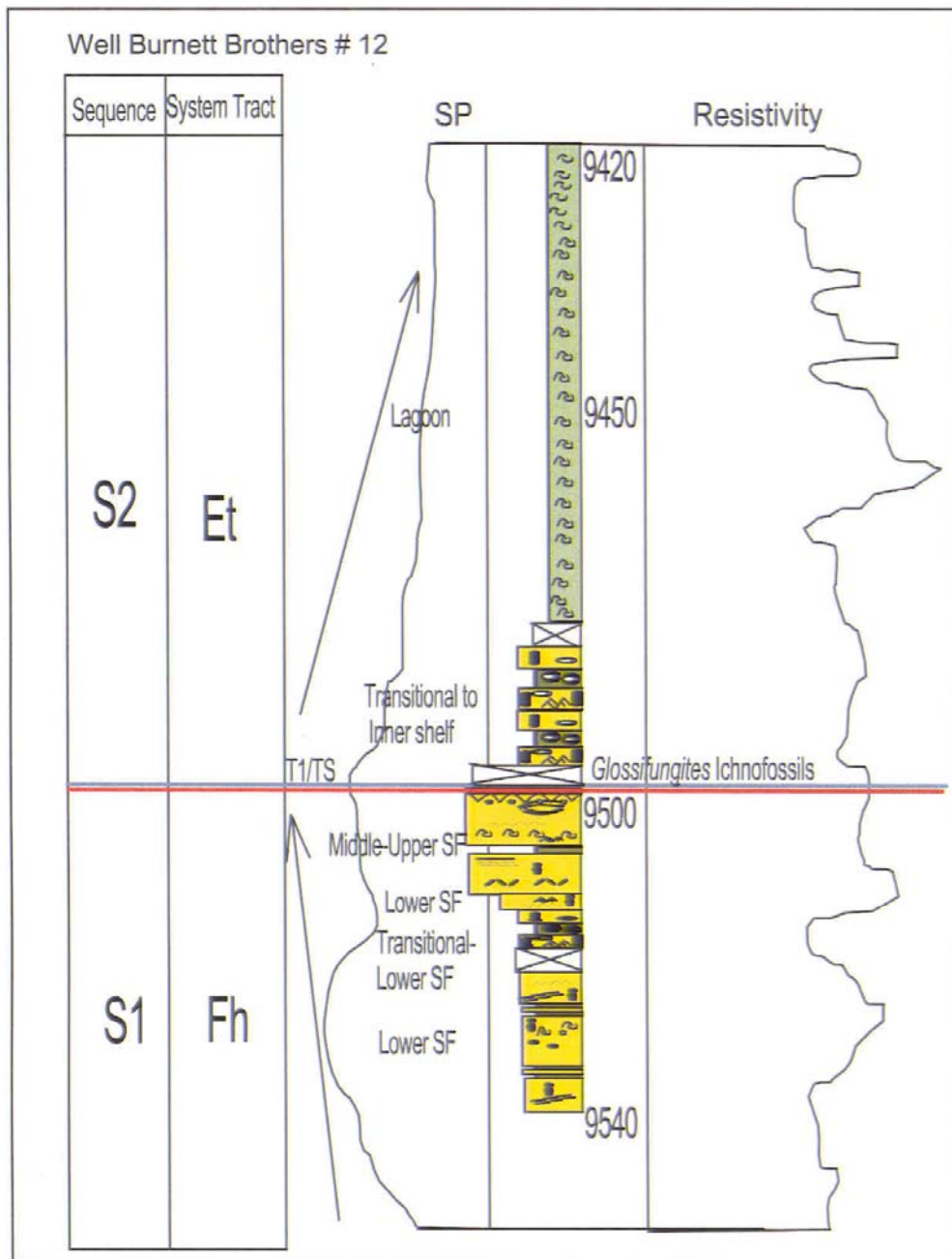


Figure 26: Core-log integration. Depth in feet. See chapter 3 for explanation of system tracts symbols and figure 19 for explanation of sedimentary structures and trace fossils.

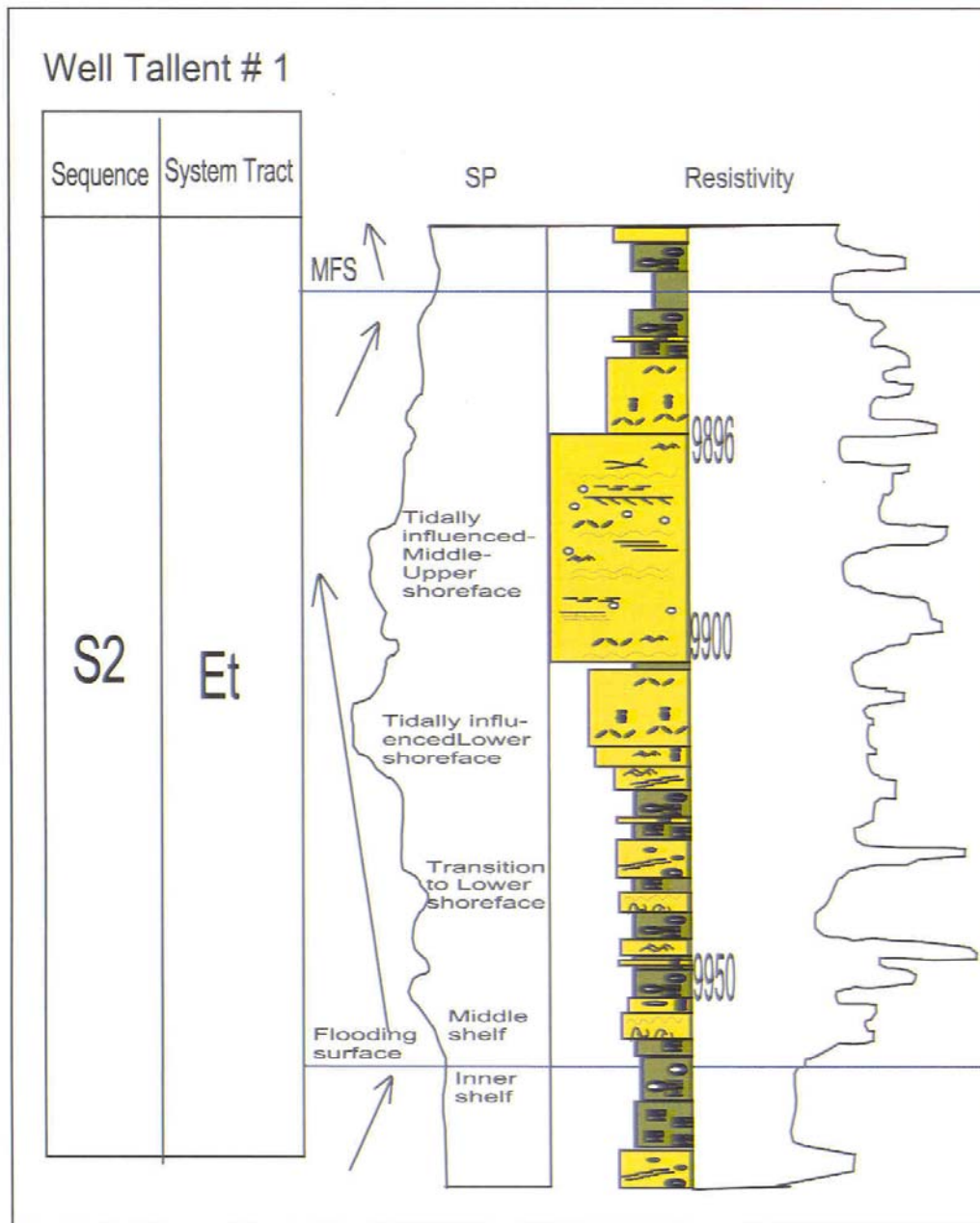


Figure 27: Core-log integration. Depth in feet. See chapter 3 for explanation of system tracts symbols and figure 19 for explanation of sedimentary structures and trace fossils.

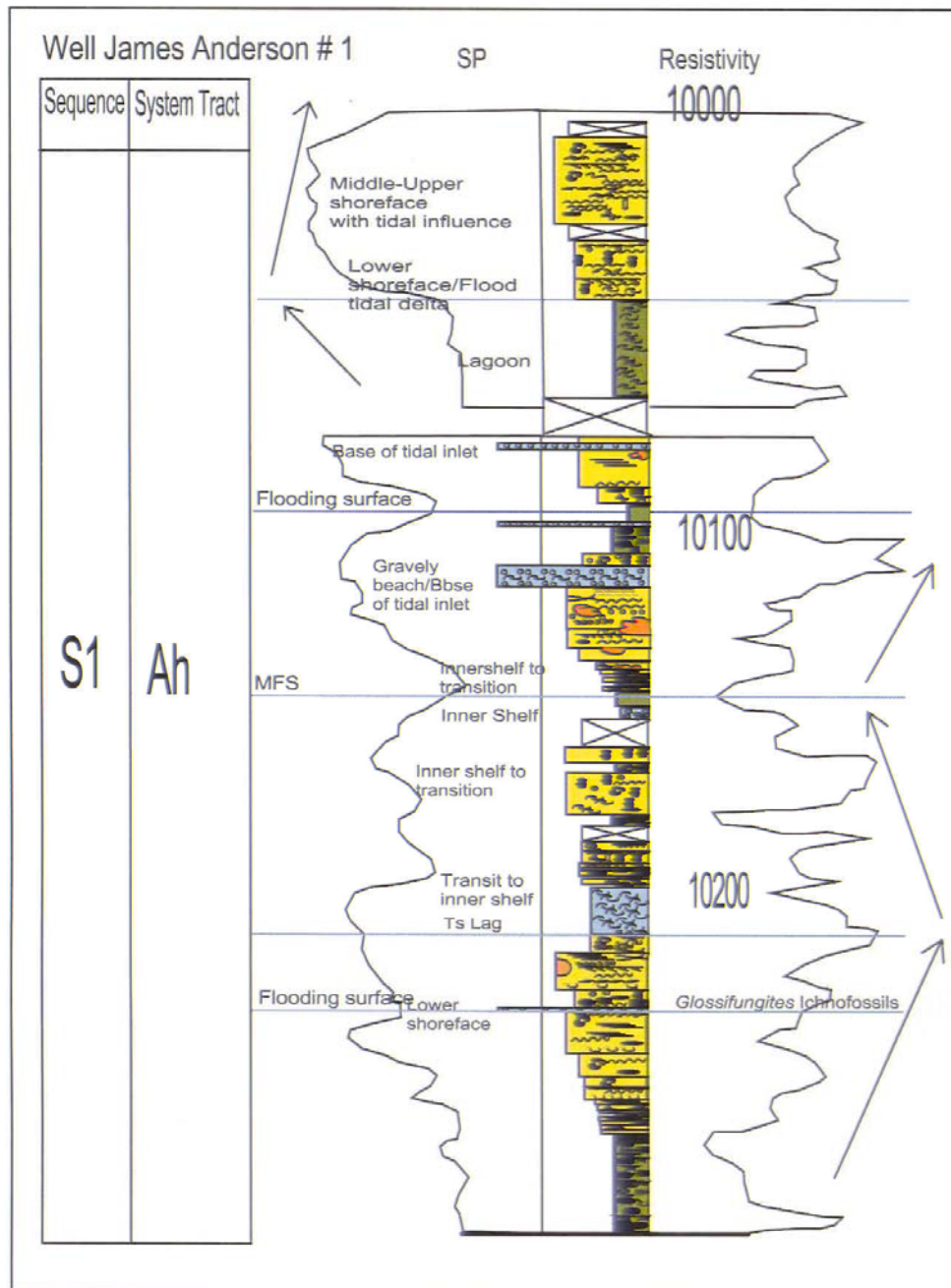


Figure 28: Core-log integration. Depth in feet. See chapter 3 for explanation of system tracts symbols and figure 19 for explanation of sedimentary structures and trace fossils.

The lower interval coarsens upward from intensively bioturbated inner-shelf mudstone to fine-grained, high-energy laminated upper-shoreface sandstone. The upper interval is characterized by fining-upward tidal inlet deposits. A flooding surface may occur at the top of the progradational interval. A ravinement surface with lag deposits is at the base of each inlet deposit. Thickness of the lag sediments vary between 1 and 10 feet (0.3-3.3 m). The lag deposits vary from chert-pebble conglomerates, abundant mudstone rip-up clasts and organic matter (Fig. 29a), to completely cemented oyster shells with some chert pebbles of different sizes (Fig, 29b). No sequence boundary is exhibited and the ravinement surface could not be traced laterally for more than 0.5 miles (0.8 km). In core # 2 (Fig. 28), the blocky log response is interpreted as flood tidal delta deposits.

### **2.5.2. Cores that penetrated S2 and/or SB2**

#### **2.5.2.1. James Anderson # 1**

Core # 3 penetrates most of the high stand system tract in S2. Figure 30 represents three main intervals. A lower progradational, middle retrogradational and an upper progradational unit. A MFS exists between the overlying retrogradational and next progradational one. The lower interval coarsens upward from intensively bioturbated distal mid-shelf mudstone to fine-grained laminated middle shoreface. The overlying retrogradational interval fines upward from middle shoreface to inner shelf and is capped by a MFS. The MFS marks the change from lower retrogradation to upper progradation. The top interval coarsens upward from inner shelf to an *Ophiomorpha*-dominated lower shoreface.

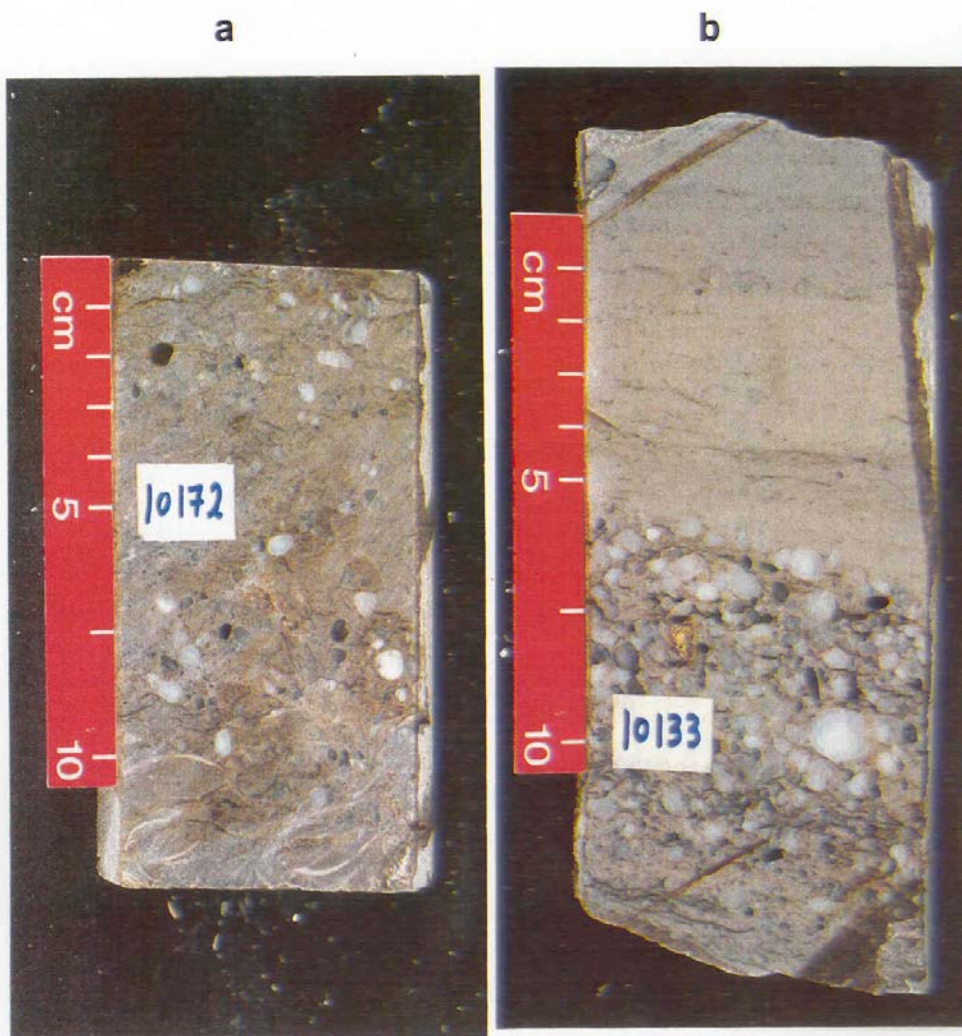


Figure 29: Lag deposits at the base of tidal inlet. a) conglomerate dominated, and b) a mix of conglomerate and shell fragments. Well JA # 1.



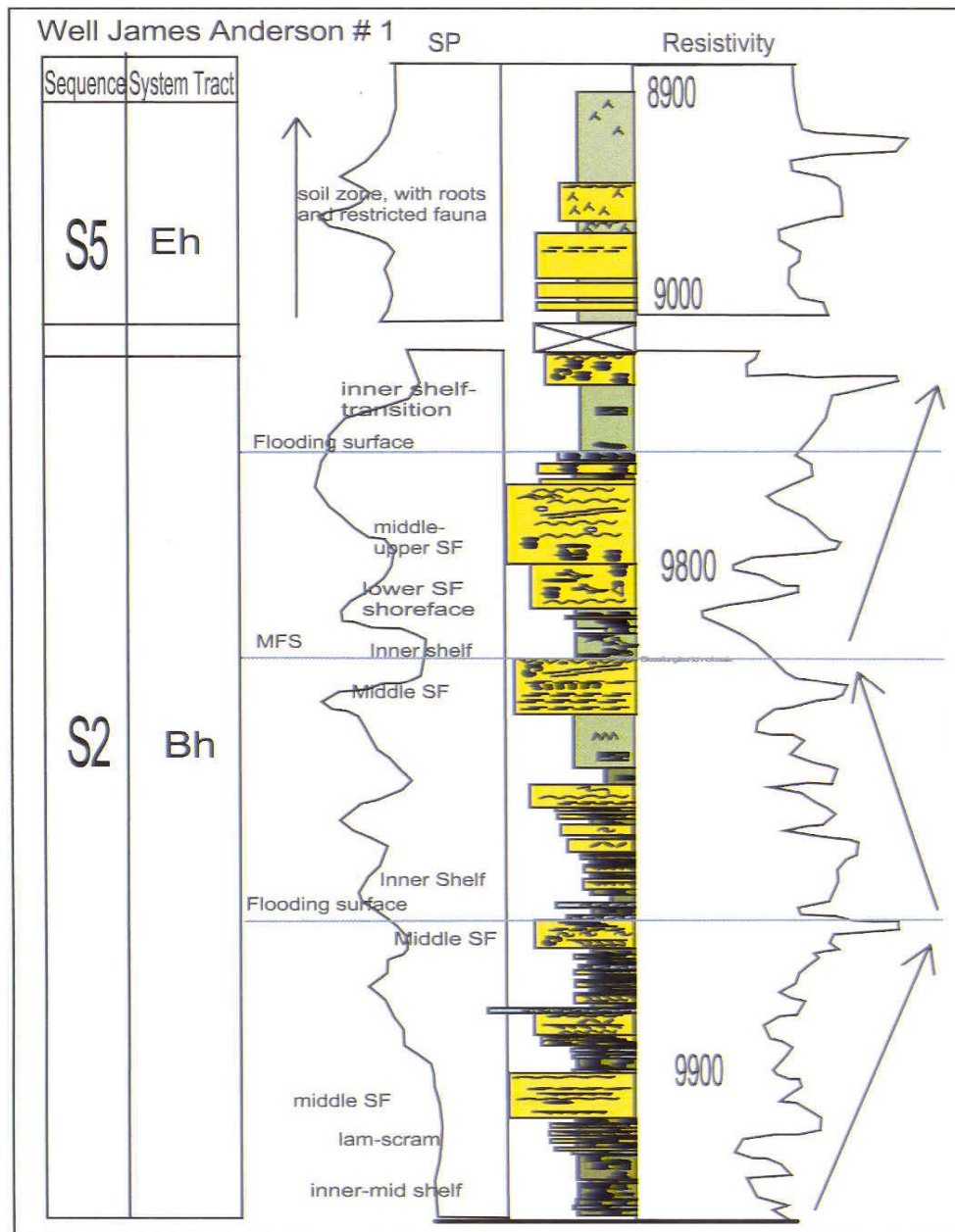


Figure 30: Core-log integration. Depth in feet. See chapter 3 for explanation of system tracts symbols and figure 19 for explanation of sedimentary structures and trace fossils.

### **2.5.2.2. Jones Gas Unit # 3**

Core #1 in this well show in section B-B` (Fig. 17). Figure 31 shows one progradational interval. The rocks coarsen from intensively bioturbated transitional mudstone to lower-shoreface mudstone and sandstone interbeds to fine-grained slightly bioturbated lower-shoreface sandstone with two storm beds events in the lower shoreface.

### **2.5.2.3. Grace Lowry # 1**

The cored well is identified in cross-section B-B`, about 7 miles (11.9 km) south of the James Anderson # 1 (Fig. 17). This core penetrates SB2, which is coincident with oyster lag and a *Glossifungites* ichnofacies (Fig. 32a). Along SB2, there is a vertical shift in facies from oyster-rich lagoonal mudstone to overlying intensively bioturbated inner shelf to transitional facies (Fig. 32b). SB2 separates a lower progradational interval which coarsens upward from middle shelf to shoreface and lagoon and an upper transgressive interval which fines upward from lower shoreface to inner shelf. The lower progradational interval rests on a MFS that is displayed in the lower part of the core. It is associated with a transgressive lag and a vertical shift in facies from lower to middle shoreface to inner shelf. Two storm events are recorded in the progradational section and represented by oyster lags.



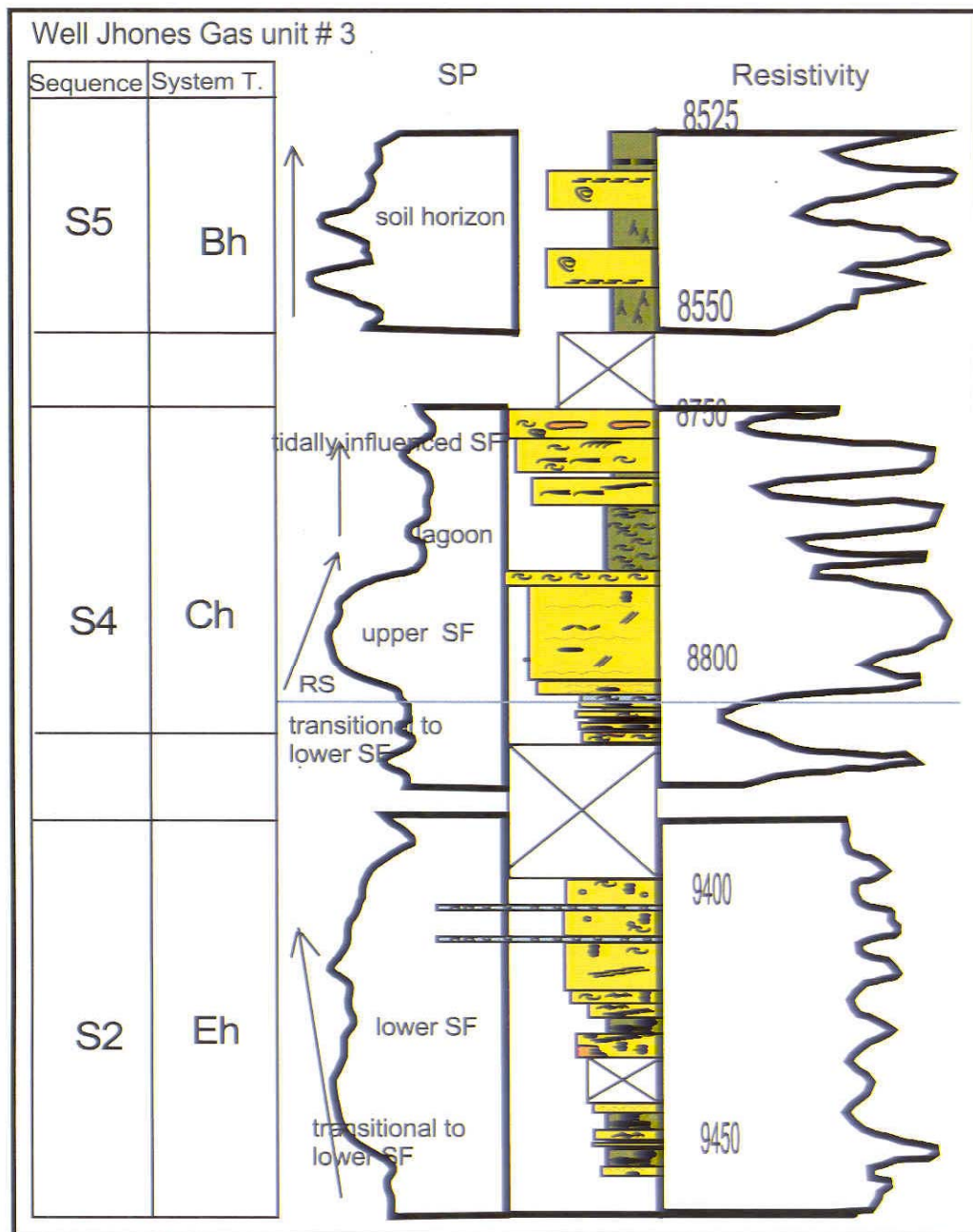


Figure 31: Core-log integration. Depth in feet. See chapter 3 for explanation of system tracts symbols and figure 19 for explanation of sedimentary structures and trace fossils.

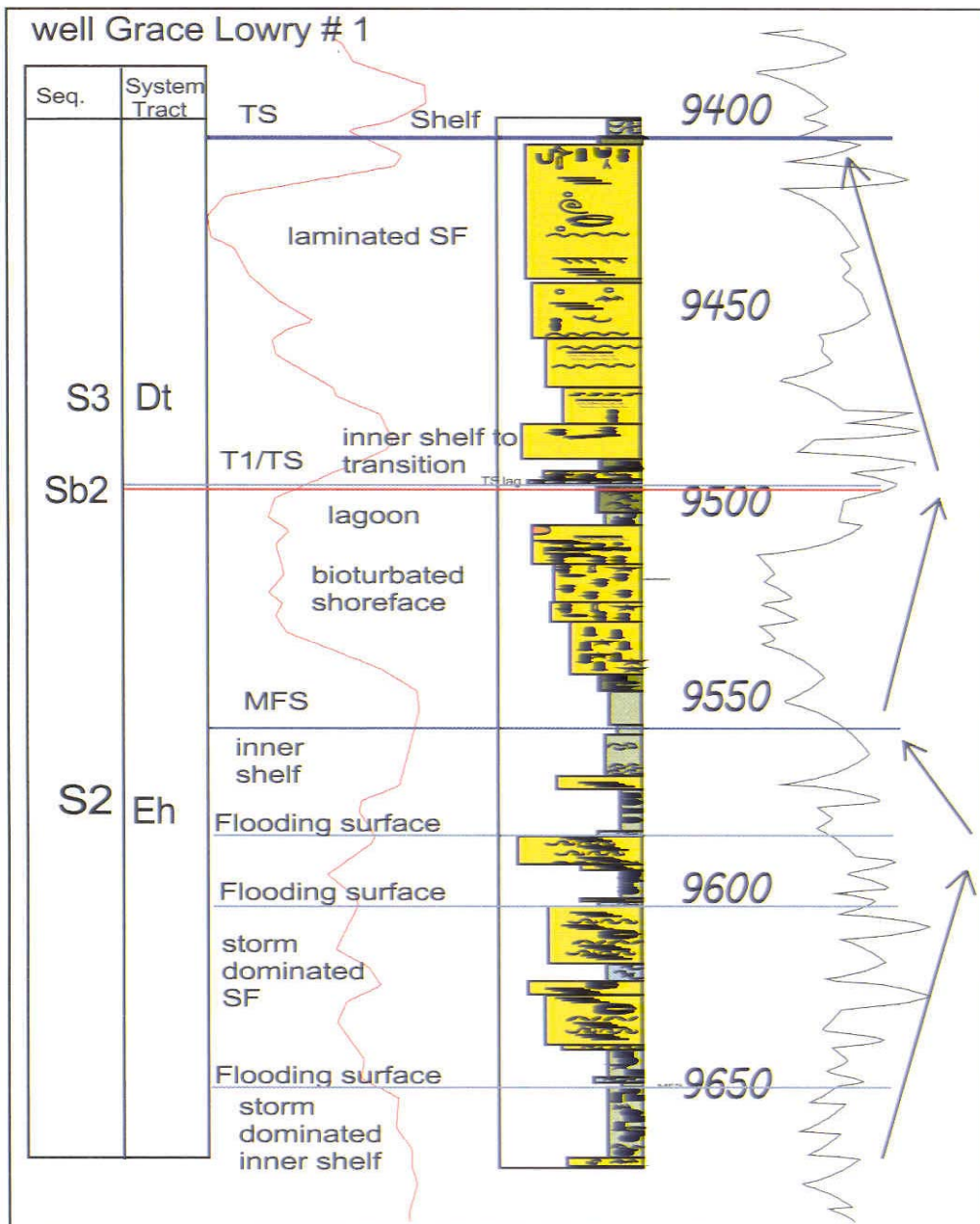


Figure 32a: Core-log integration. Depth in feet. See chapter 3 for explanation of system tracts symbols and figure 19 for explanation of sedimentary structures and trace fossils.

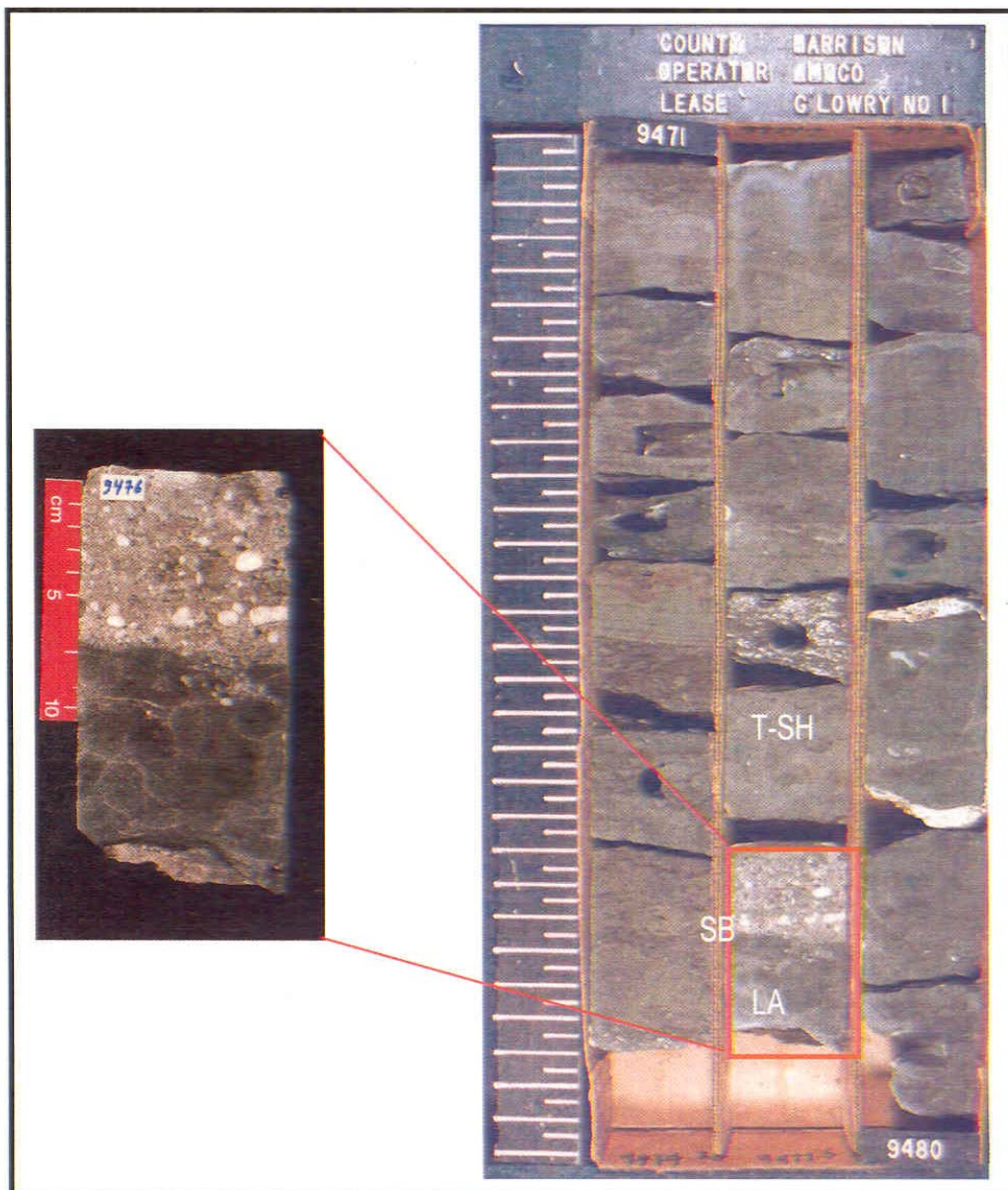


Figure 32b: Sequence boundary (SB) marks the shift in facies from lagoonal mudstone (LA) to the overlying inner shelf-transitional muddy sandstone (T-SF). Well Lowry # 1. Left scale is 3 feet.

#### 2.5.2.4. Davidson Foundation # 1

This is a relatively continuous core that penetrates most of S3 and parts of S2. The well located in cross-section X-X' about 3 miles (5.4 km) southwest of the James Anderson well # 1 (Fig. 16). The suite of facies observed in this core reflects less of a marine influence (tidal flat setting) than the previously mentioned facies (shallow marine to marginal marine and shelf). Figure 33a shows that interval Eh could be divided from, bottom to top, into aggradational, retrogradational and progradational units. The lower aggradational interval is represented in the cores by sand flat, mixed and mud flat and bay mud/sand facies. The second interval passes from fine-grained sand flat to distal bay center mud, which represents a flooding event. The overlying progradational interval coarsens upward from bay center mud into fine-grained sand flat.

SB2 separates the last progradational unit in Eh from the overlying retrogradational unit of Dt, which is a shift in facies from bay-margin mud to bay-center mud. The MFS terminates the last retrogradational interval and is overlain by a progradational one. SB3 contains oyster lag and a *Glossifungites* ichnofacies. Fig. 33b shows that Ch exhibits aggradational and retrogradational architectural patterns. The aggradational pattern exhibits repetition of sand flat, mixed flat, marsh and bay-mud facies. The retrogradational interval fines upward from sand flat into bay mud.

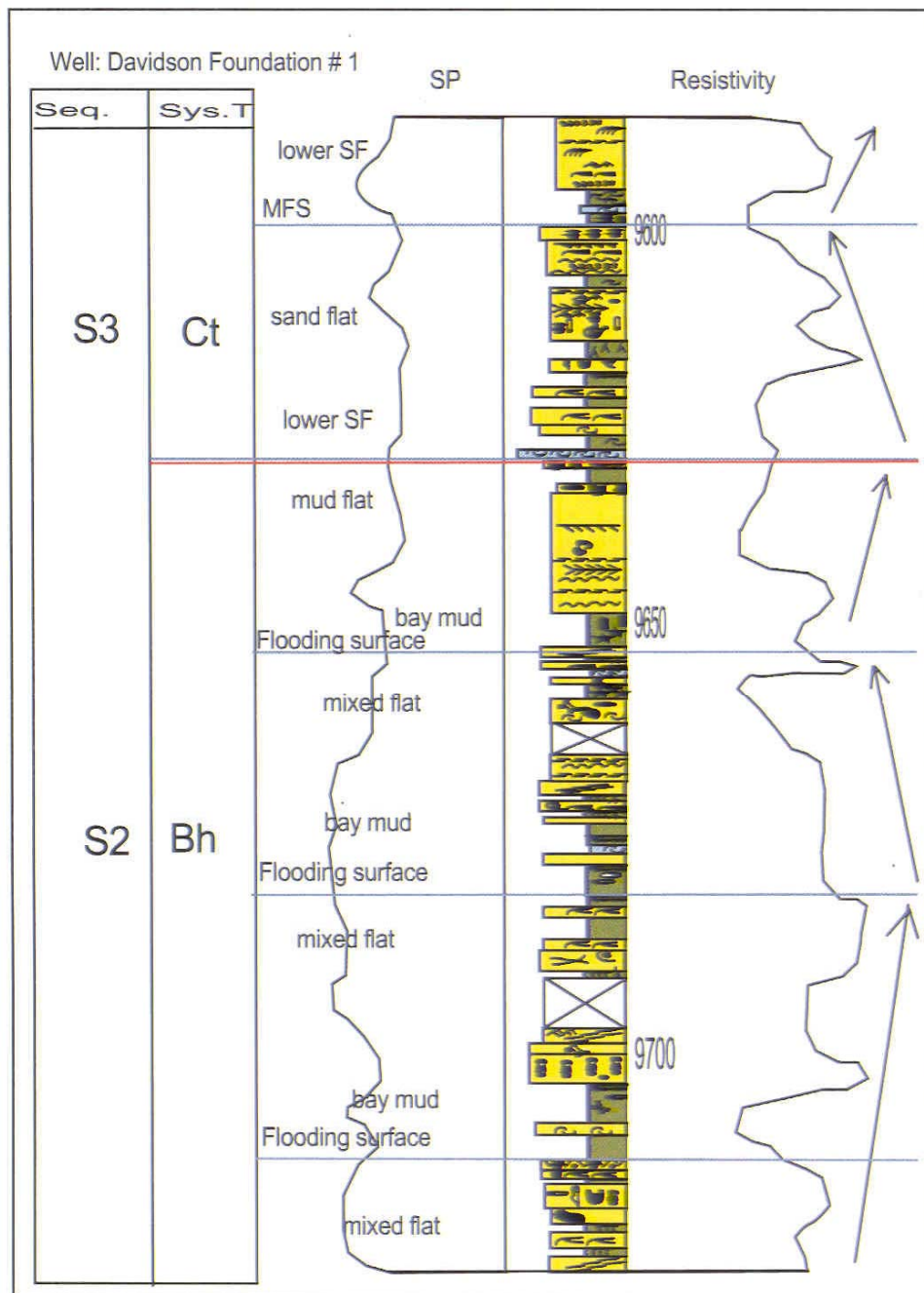


Figure 33a: Core-log integration. Depth in feet. See chapter 3 for explanation of system tracts symbols and figure 19 for explanation of sedimentary structures and trace fossils.



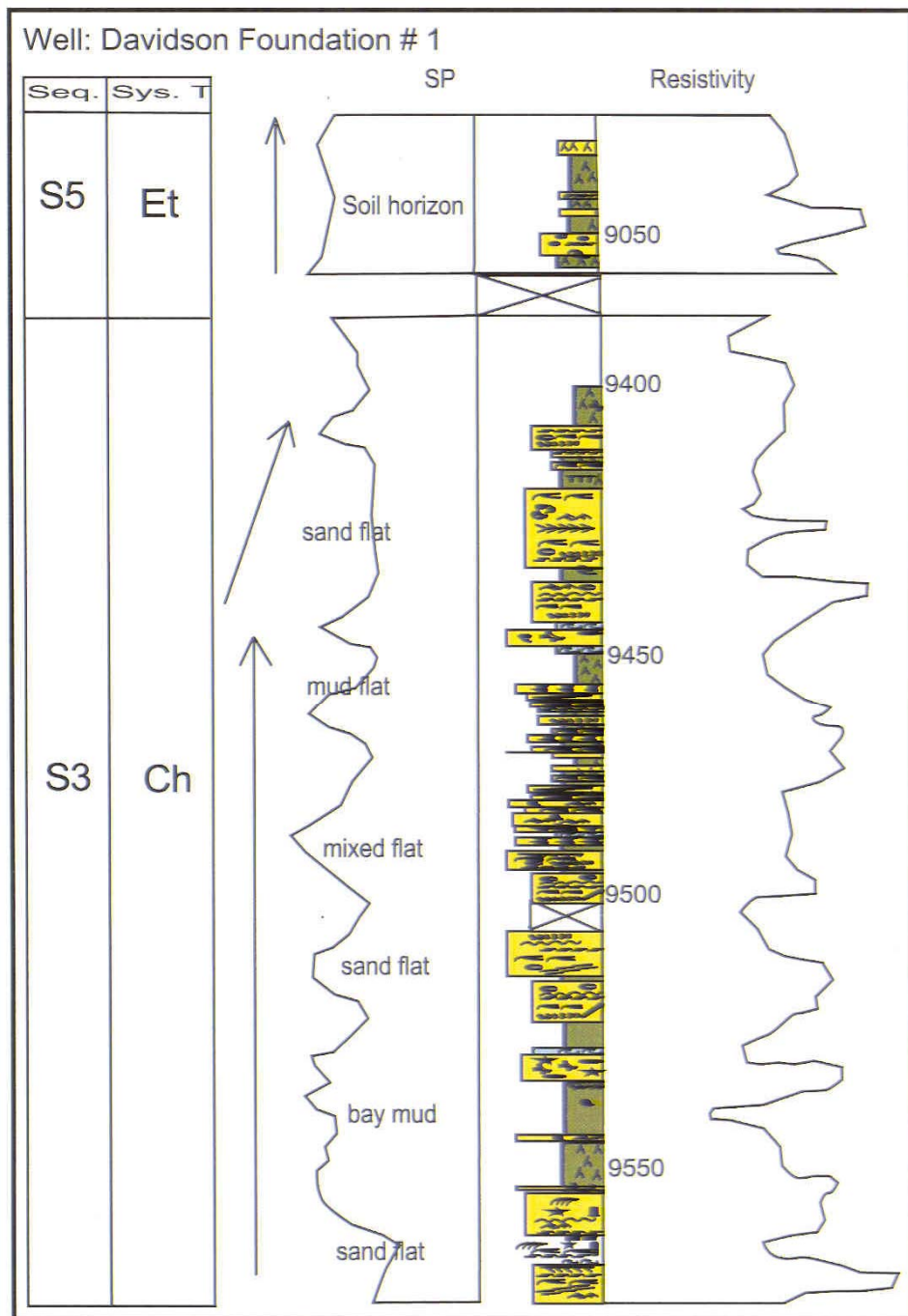


Figure 33b: Core-log integration. Depth in feet. See chapter 3 for explanation of system tracts symbols and figure 19 for explanation of sedimentary structures and trace fossils.

### **2.5.3. Cores penetrated S3**

Core # 2 in the Blocker Heirs # 1 well is the only core that penetrated S3. It is identified in cross-section C-C', about 10 miles (18 km) to the southwest of SFE # 3. Figure 34 show that maximum flooding surface (MFS) separates the lower retrogradational interval from the upper progradational one. The lower interval fines upward from fine-grained middle to upper laminated shoreface sandstone to inner-shelf mudstone. And the upper interval coarsens upward from inner shelf mudstone to lower-shoreface sandstone and transitional to inner-shelf mudstone and siltstone.

### **2.5.4. Cores that penetrated S4, SB4, S5, SB5 and S6**

#### **2.5.4.1. Jones Gas Unit # 3**

Core # 2 penetrates S4 (Fig. 31) and displays a retrogradational interval overlain by aggradational one. The retrogradational interval fines upward and a tidal inlet facies rests on a ravinement surface containing oyster lag. The inlet cuts into transitional to inner-shelf sediments and is filled by upper shoreface sandstones and lagoonal mud. Aggradational stacks of lower and upper shoreface sandstones overlie tidal inlet sediments.

#### **2.5.4.2. Bradshaw # 1**

The second long core in the study area is identified in cross-section B-B'; the core is about 5 miles (9 km) from the Grace Lowry well # 1 (Fig. 17). The Bradshaw core penetrates the transgressive system tract of S6, all of S5, and the highstand system tract of S4.

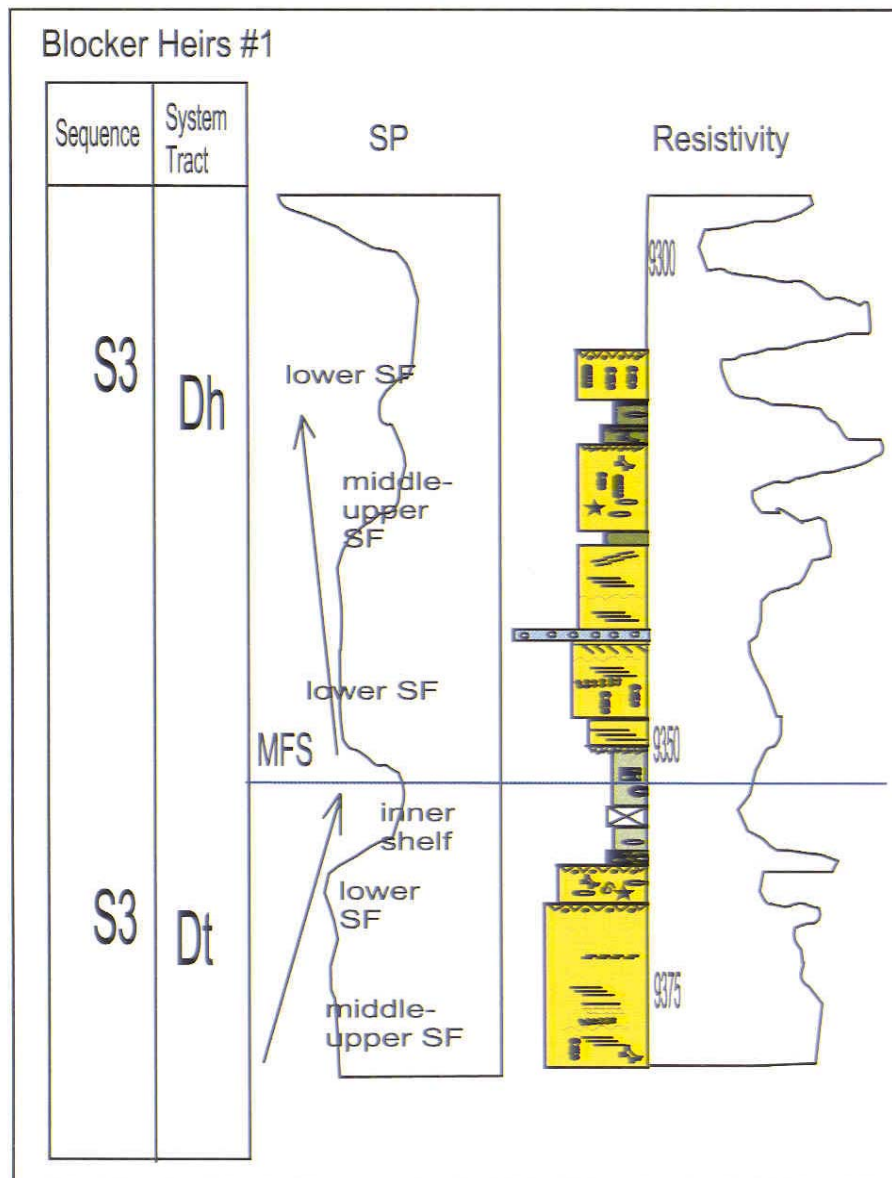


Figure 34: Core-log integration. Depth in feet. See chapter 3 for explanation of system tracts symbols and figure 19 for explanation of sedimentary structures and trace fossils.



Figure 35a exhibits different architectural patterns for the various sequences and system tracts. Dh of S4 comprises two units; a lower retrogradational one which fines upward from lower shoreface sandstone to inner-shelf mud and an upper progradational unit that coarsens upward from inner-shelf mud to subtidal point bar sandstones. MFS separates the two intervals. The progradational unit is capped by SB4, which is associated with a *Glossifungites* ichnofacies and whose facies deepens along the sequence boundary from sand flat into lower shoreface (Fig. 35a).

Two architectural patterns are recognized in the Bt of S5; lower retrogradational and upper aggradational rock units. The retrogradational interval fines upward from lower-shoreface sandstone to lagoonal mudstone (Fig. 35a). It is overlain by lagoonal, marsh and tidal flat facies stacked in an aggradational pattern. Minor regressive and flooding events are recorded. Bh of S5 (Fig. 35b) is a general progradational or coarsening-upward unit except in the lower part, where a MFS is recognized. The MFS separates the lower retrogradational interval in which sediments fine upward from lower shoreface sandstone to inner-shelf mudstone. Minor regressive surfaces and flooding events are recognized. A flooding surface separates sand flat from marine bay mud deposits and a soil horizon from sand flat deposits. A minor regressive surface separates lower shoreface deposits from the upper mixed flat deposits with roots and soil horizon (Fig. 35b).

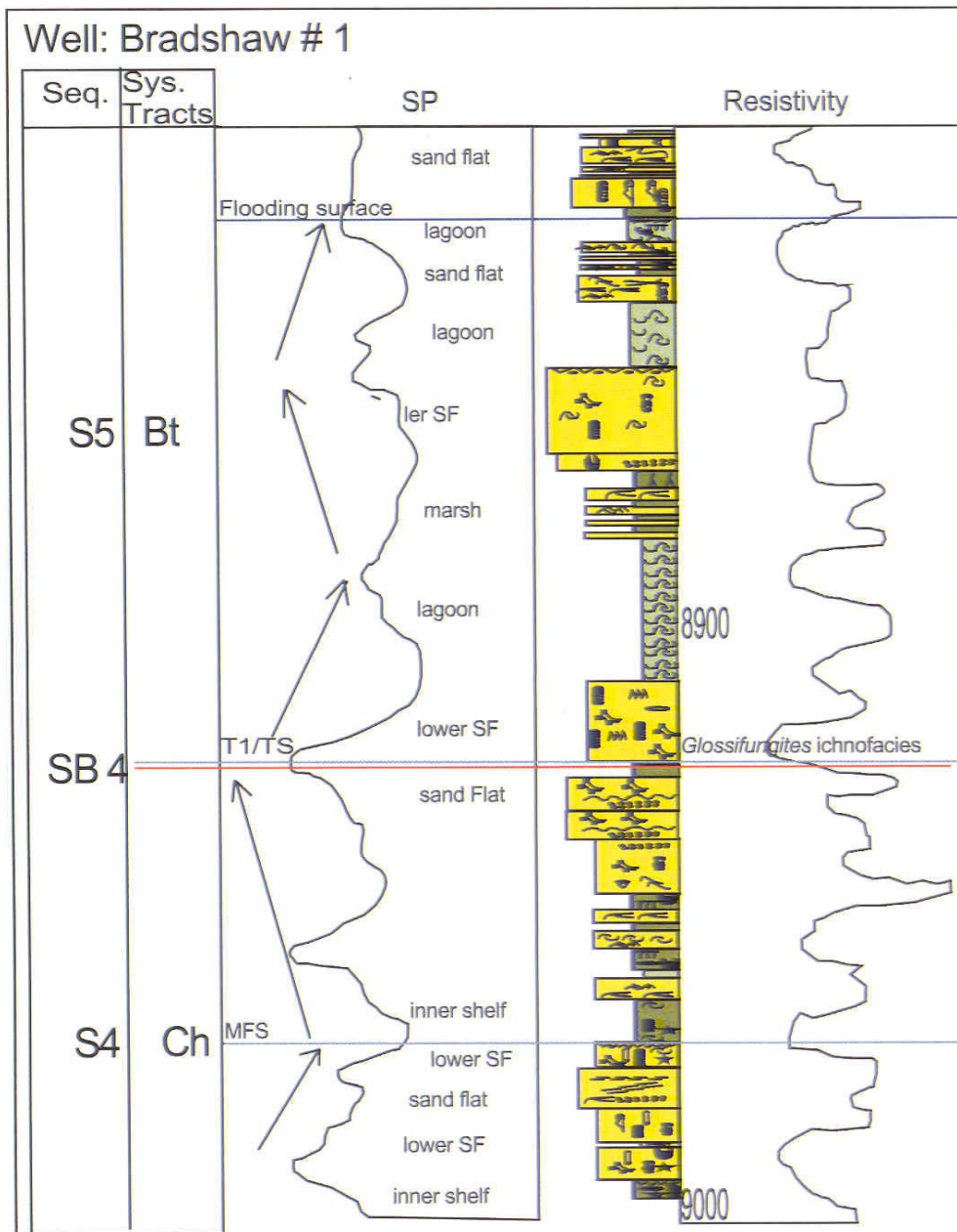


Figure 35a: Core-log integration. Depth in feet. See chapter 3 for explanation of system tracts symbols and figure 19 for explanation of sedimentary structures and trace fossils.

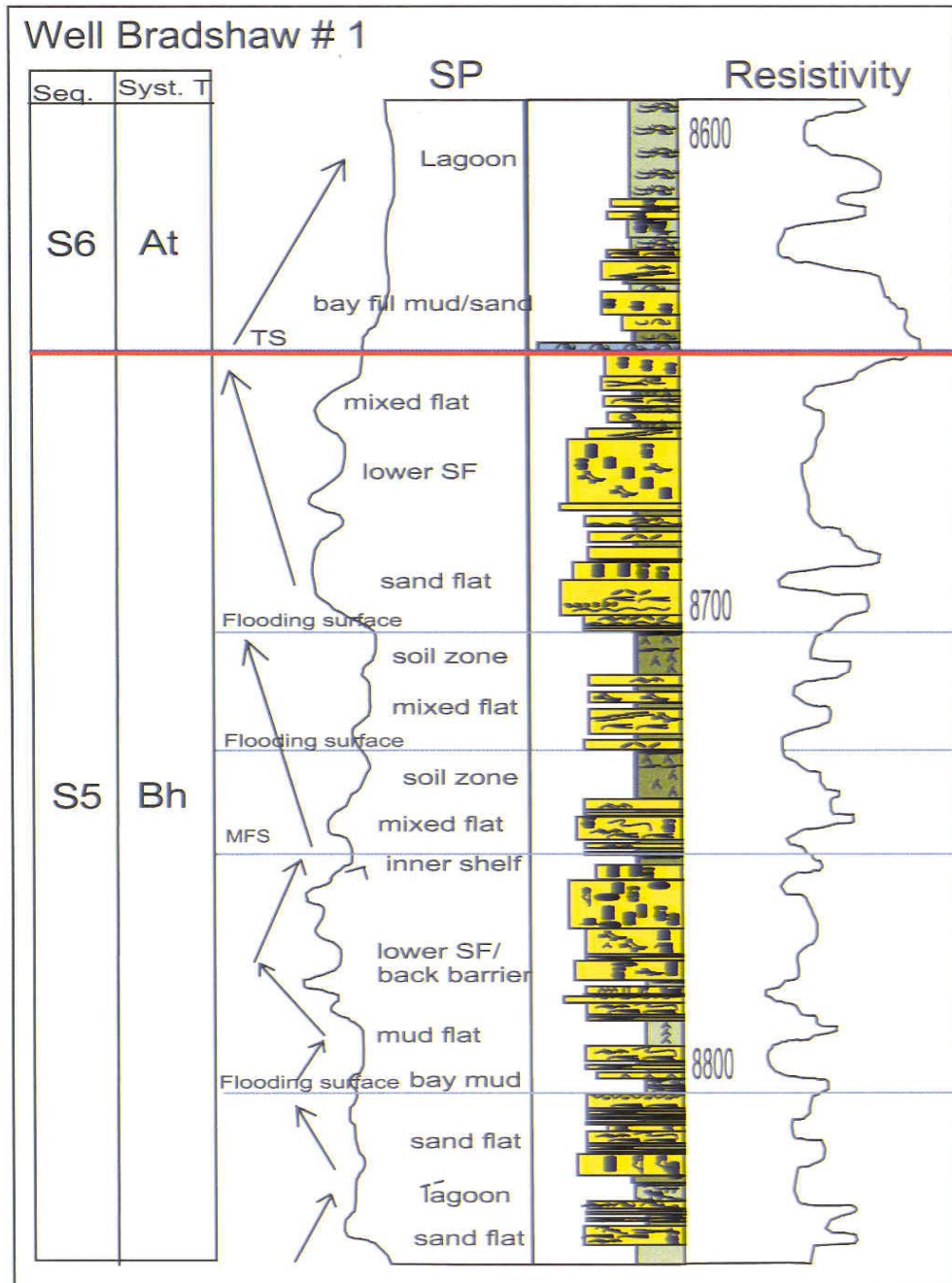


Figure 35b: Core-log integration. Depth in feet. See chapter 3 for explanation of system tracts symbols and figure 19 for explanation of sedimentary structures and trace fossils.

#### **2.5.4.3. Jones gas unit # 3 and James Anderson # 1**

Core # 3 at the top of the cored interval in the Jones gas unit # 3 well (Fig. 31) and Core # 4 in James Anderson # 1 (Fig. 30) penetrate a thin Bh interval of S5 that is aggradational sandstone and mudstone which are interpreted to have developed a soil horizon.

#### **2.5.4.4. Davidson Foundation # 1**

Core # 2 penetrates a thin interval of Et in S5 (Fig. 33b) and shows aggradational patterns of stacked sandstones and mudstones.

### **2.6. Sequence stratigraphic model**

Williams and Mitchum (1997) and Williams et al. (2001) created a sequence stratigraphic model for the Cotton Valley sandstones based solely on log data (Fig. 36). The Cotton Valley model introduced in this study is similar, but is supported with core interpretation. Figure 37 is my sequence stratigraphic model for the Cotton Valley Sandstones in the study area. A sequence is bounded by sequence boundaries, and has lowstand, transgressive, and highstand systems tracts. During the previous rise in sea level, a progradational high-stand system tract is deposited. A relative fall of sea level drops the shoreline below the shelf break and exposes the top of the highstand depositional unit. Erosion occurs, commonly in the form of incision by rivers that adjust their gradient to the lowered base level. This erosional surface and its equivalent on the slope and in the basin form the sequence boundary.

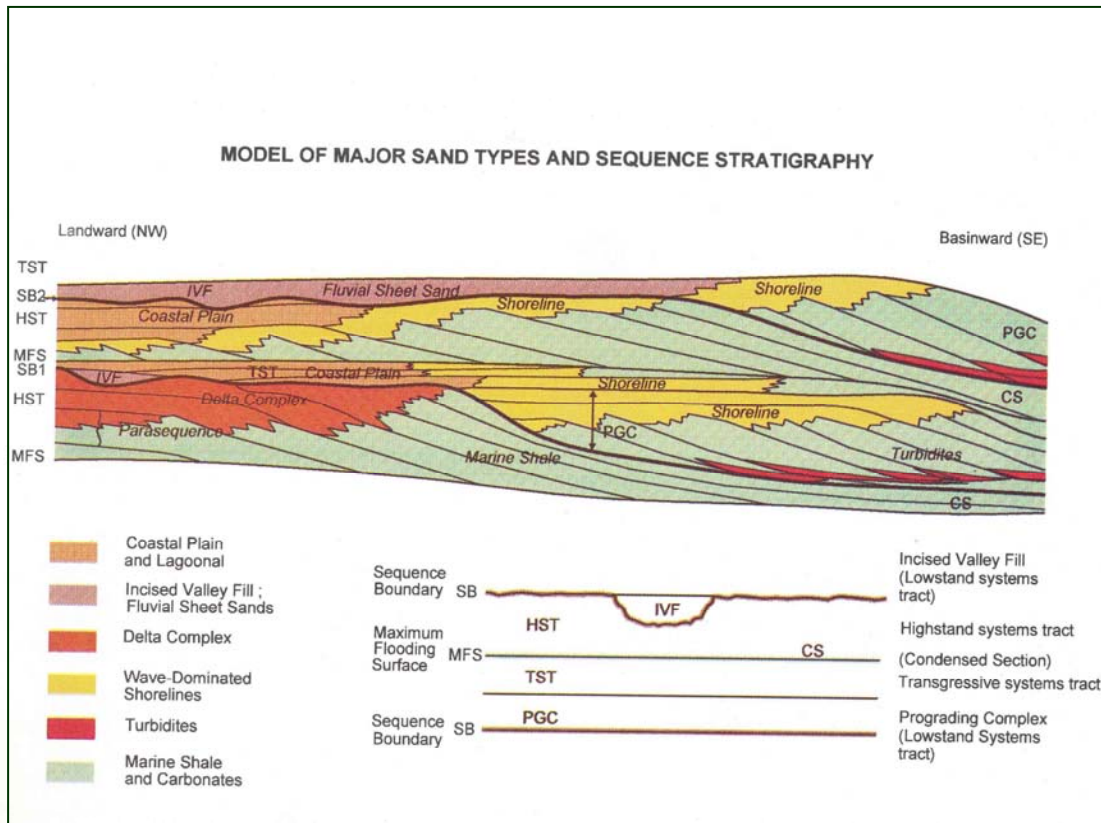


Figure 36: Sequence stratigraphic model adapted for Cotton Valley sequences and major sandstone types with explanatory code (From Williams and Mitchum 1997).

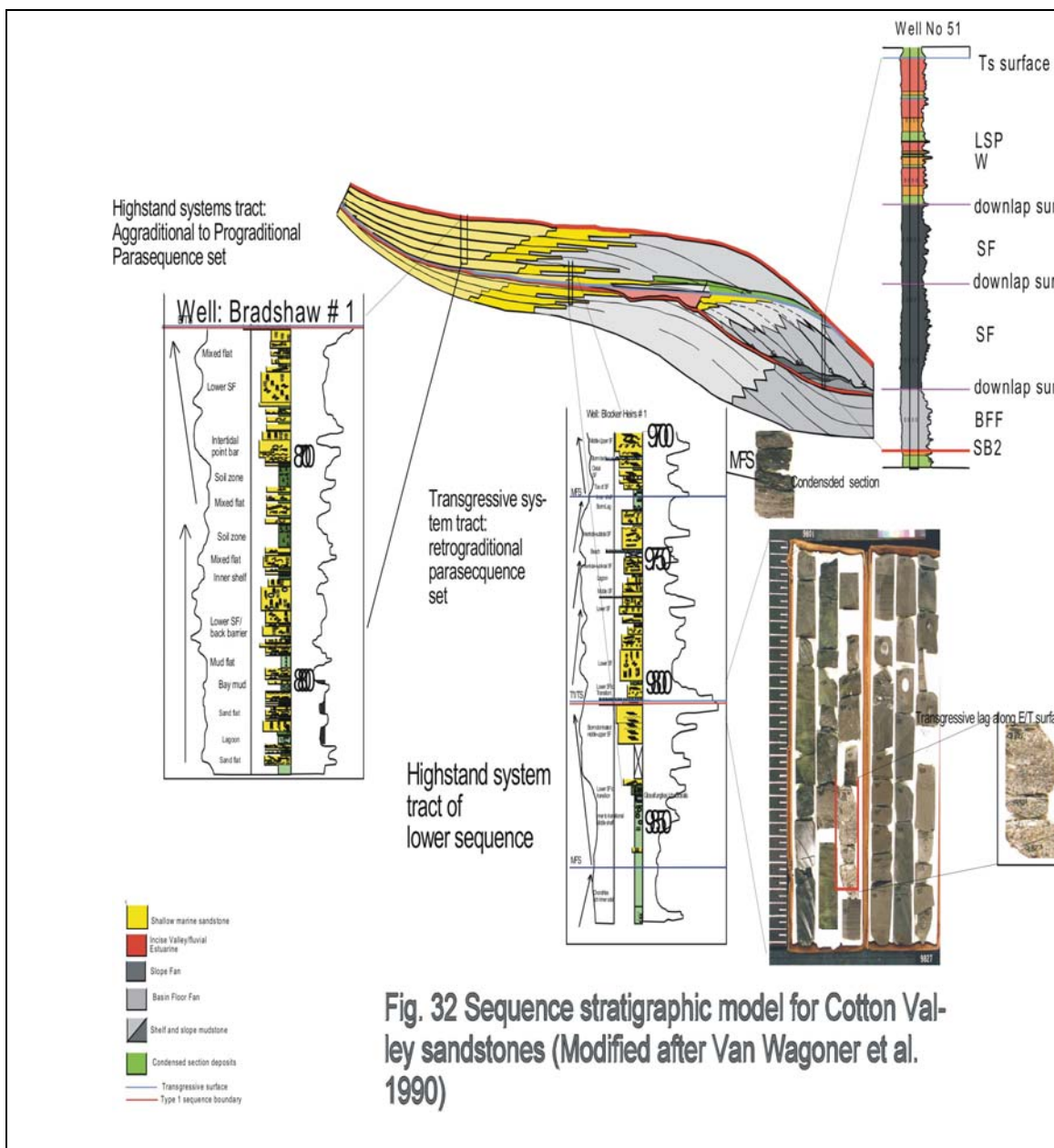


Figure 37: Sequence stratigraphic model of Cotton Valley sandstones (Modified from Van Wagoner et al., 1990).

A deposition of wedge lapping onto the basinward part of the eroded high stand facies is a prograding wedge complex (Vail, 1987). Due to lack of accommodation space at the shelf, the river is not free to avulse, and sediment is focused toward the slope and submarine fans are constructed on the basin floor and slope.

The transgressive system tract is deposited during that part of relative sea- level rise when accommodation space is increasing faster than the rate of sediment supply. The shelf gets flooded, and shoreline sands backstep (retrograde) landward in a transgressive pattern. In the Cotton Valley, transgressive systems are generally thinner than highstand systems tracts. Highstand system tracts are deposited as a relative rise of sea level continues, but at a diminishing rate until sea level reaches a relative stillstand. Another relative fall of sea level begins a new sequence.

## **CHAPTER 3**

### **DEPOSITIONAL ENVIRONMENTS**

#### **3.1 INTRODUCTION**

The depositional systems active during deposition of Cotton Valley Sandstones (CVS) were interpreted in order to reconstruct the paleogeography of the individual genetic stratigraphic sequences. Depositional systems are defined as three-dimensional assemblages of process-related facies that record major paleogeomorphic elements (Galloway, 1989a). They grade laterally into adjacent systems, forming logical associations of paleogeographic elements (Galloway, 1989a). Cotton Valley depositional systems are defined on the basis of lithofacies distribution, log motif, biostratigraphic paleoenvironmental indicators and conventional core description. These data are interpreted within the sequence stratigraphic context illustrated by cross-sections (previous chapter) and interval net-sand maps of the individual sequences. These maps document the shelf-break orientation as well as depositional strike and dip. Conventional core data (Fig. 38) provide direct lithofacies calibration of the log motif and form the basis for the depositional environment interpretation. Complete core descriptions and discussions of depositional facies are provided in Appendix A1.



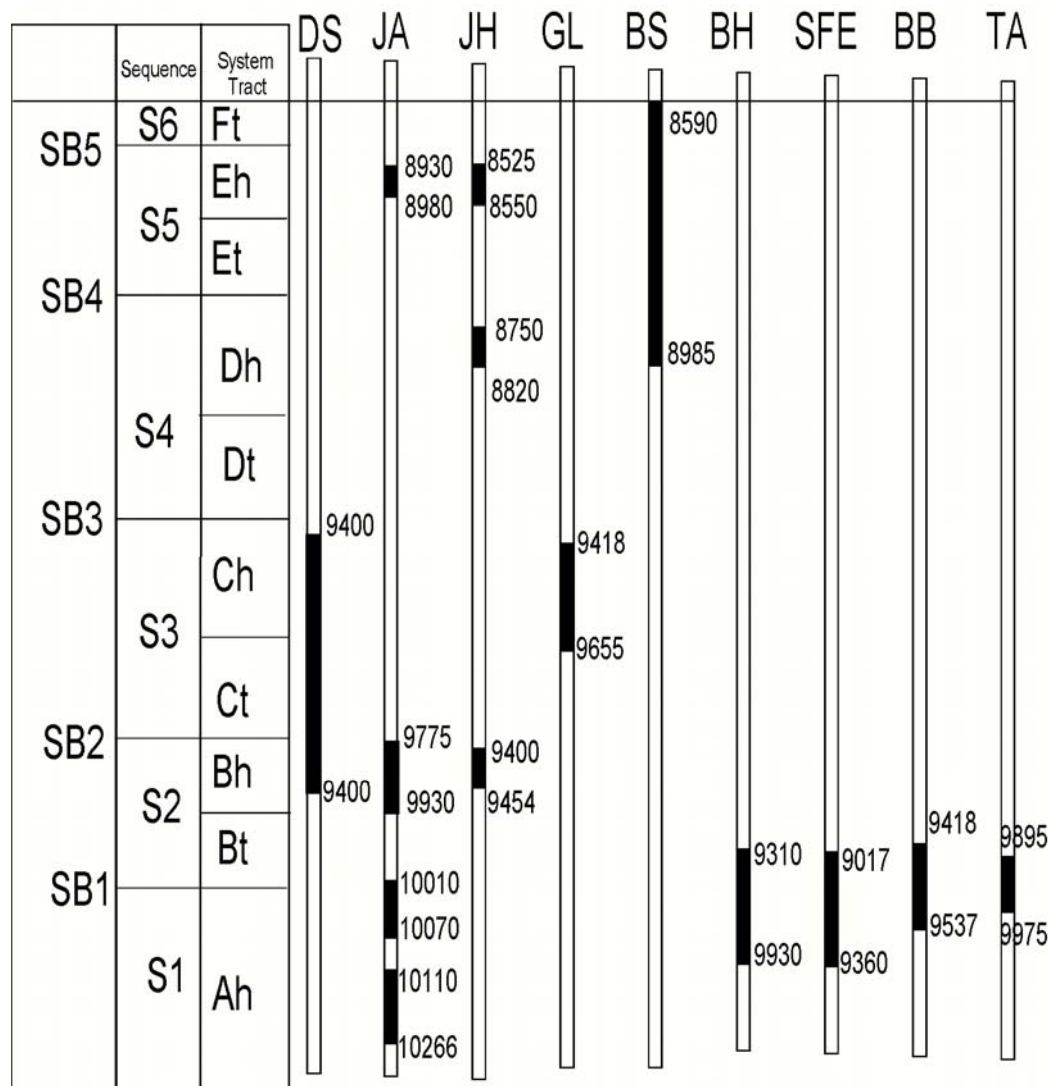


Figure 38: Core distribution in the study area.

Net sand maps along with core description indicate deposition of prograding shorefaces in the highstand system tracts and barrier island/lagoon-shelf systems in the overlying transgressive systems tract. No cores are available in the lowstand system tract.

There is a general shallowing-upward trend in the CVS from fully marine inner-mid shelf at the base to much better developed shorefaces in the middle to soil horizons and subaerial exposure at the top of the formation. A spectrum of depositional systems from coastal plain to inner-mid shelf was developed during deposition of the Cotton Valley Sandstones. No cores are available from the Lowstand incised valley fill or slope fan. By using all available cores in studied wells, Cotton Valley Sandstones are divided into 23 facies; they are combined into six facies associations (Table 1)

### **3.2 Barrier Islands**

Barrier islands are characterized by the presence of a protected body of water (lagoon) behind the barrier. Galloway and Hobday (1983) reported that development of barrier island systems is favored where the continental shelf has a low gradient and where the tidal range is low to moderate. A complex of depositional facies is associated with barrier islands as a result of the exchange of water between lagoon and ocean. The component facies of barrier island systems are: 1) barrier core; 2) inlet fill; 3) flood tidal deltas and associated lagoon; 4) washover-fan/barrier flat; and shoreface/ebb-tidal delta (Fig. 39).

Table 1: Facies and facies associations of Cotton Valley rocks.

Facies Association	Facies
FA1:Offshore/shoreface-transition	F1: Irregularly interbedded sandstone and shale
	F2: Massive to faintly laminated dark grey-black mudstone with fossil shell debris.
	F3: Intensely bioturbated silty mudstone.
	F4: <i>Chondrites</i> -dominated mudstone.
	F5: Bioturbated thin bedded shale, siltstone and very fine-grained sandstone.
	F6: Bioturbated, carbonaceous-rich sandstone
FA2: Shoreface-foreshore	F7: Parallel to subparallel laminated sandstone with HCS
	F8: Well sorted, cross-bedded/laminated to massive sandstone.
	F9: Calcite-cemented conglomerates with abundant oyster debris.
	F10: Bioturbated <i>Ophiomorpha</i> -dominated fine grained sandstone.
	F11: Cryptobioturbated-laminated fine-grained sandstone.
	F12: Tidal-dominated shoreface

Table 1. Continued

FA3: Tidal inlet	F13: Pebbly, bioturbated carbonaceous-rich sandstone.
FA4: Back barrier-coastal plain	F14: Rooted grey sandstone.
	F15: Rippled, Laminated sandstone with carbonaceous matter.
	F16: Cross-bedded sandstone with carbonaceous laminae.
	F17: Interlaminated very fine grained sandstone, siltstone and mudstone.
	F18: Interbedded sharp-based sandstone and bioturbated sandy siltstone.
	F19: <i>Teichichnus</i> -dominated sandstone.
	F20: <i>Teichichnus</i> -dominated mudstone.
	F21: <i>Diplocraterion</i> -dominated interbedded shale and sandstones
	F22: Oyster-rich, dark grey to black mudstone
	F23: Intensely bioturbated muddy sandstone and silty mudstone.

Table 1. Continued

Facies Assoc.	Facies	Lithology	Sedimentary Structures	Ichnofossils	Environment
FA1	F1	Sandy, silty mudstone	Planar lamination and current ripples	<i>Chondrites, Terebellina, Planolites, Teichichnus, Helminthopsis.</i>	Mid-inner-shelf (offshore)
	F2	Oyster-rich mudstone	Massive to faintly horizontal lamination	none	Inner shelf
	F3	<i>Chondrite</i> -dominated mudstone	Remnant of parallel lamination	<i>Chondrites, Terebellina, Teichichnus, Skolithos, Palaeophycus</i>	Inner shelf
	F4	Silty mudstone	Massive	<i>Chondrites</i>	Inner shelf
	F5	Mudstone, siltstone and fine grained sandstone	Parallel lamination, rippled cross lamination	<i>Chondrites, Skolithos, Terebellina, Teichichnus, Paleophycus, Astrosoma</i>	Inner shelf-transition
	F6	Siltstone and fine-grained sandstone	Massive	<i>Ophiomorpha</i>	Transition to lower shoreface

Table 1. Continued

F A 2	F7	Fine-grained sandstone interrupted by shale and pebbly sandstone beds	Parallel, sub parallel lamination, and escape structures	<i>Chondrites</i> <i>Planolites</i> , <i>Palaeophycus</i>	Storm-dominated lower shoreface
	F8	Very fine to upper fine-grained sandstone	Planar, trough and low-angle cross-bedding	<i>Ophiomorpha</i>	Middle-upper shoreface
	F9	Pebbly sandstone with oyster shell fragments	Low-angle planar bedding	none	Foreshore
	F10	Silty sandstones	Massive	<i>Ophiomorpha</i>	Lower to middle shoreface
	F11	Fine-grained sandstone	Parallel and low-angle cross lamination.	Meiobenthic organisms	Middle-upper shoreface
	F12	Fine to medium-grained sandstone	Low-angle cross-bedding, current ripples	<i>Palaeophycus</i> , <i>Skolithos</i> , <i>Thalassinoides</i>	Tidally influenced shoreface/flood tidal delta

Table 1. Continued

FA3	F13	Pebbly fine-grained sandstone	Low-angle cross-bedding, planar lamination	<i>Palaeophycus</i> , <i>Skolithos</i> , <i>Thalassinoides</i>	Tidal inlet
FA4	F14	Very fine-grained sandstone	Faint planar lamination, roots	<i>Macaronichnus segregatus</i>	Tidal flat
	F15	Very fine-grained sandstone	Current ripples, low angle to wavy bedding	<i>Palaeophycus</i> , <i>Planolites</i> <i>Teichichnus</i> ,	Washover
	F16	Fine-grained sandstone	Tabular, trough, and herringbone cross bedding.	none	Tidal channel
	F17	Interbedded sandstone, siltstone, and mudstone.	Horizontal lamination, lenticular, flaser bedding, roots	<i>Ophiomorpha</i>	Tidal flat
	F18	Interbedded sharp based sandstone and bioturbated silty sandstone	Planar to wavy parallel bedding, low angle cross stratification	<i>Ophiomorpha</i> , <i>Teichichnus</i> , <i>Planolites</i> , <i>Diplocraterion</i> , and <i>Thalassinoides</i>	Unrestricted bay
	F19	Sandstone	Massive	<i>Teichichnus</i>	Brackish water
	F20	Mudstone	Rooted	<i>Teichichnus</i>	Restricted brackish/ lagoon
	F21	Fine-grained sandstone	Lenticular and wavy bedding	<i>Diplocraterion</i>	Tidal flat
	F22	Oyster-rich mudstone	Massive	none	Lagoon
	F23	Clayey siltstone and silty mudstone and sandstone	Disturbed fabric, roots	Uncommon	Soil horizon

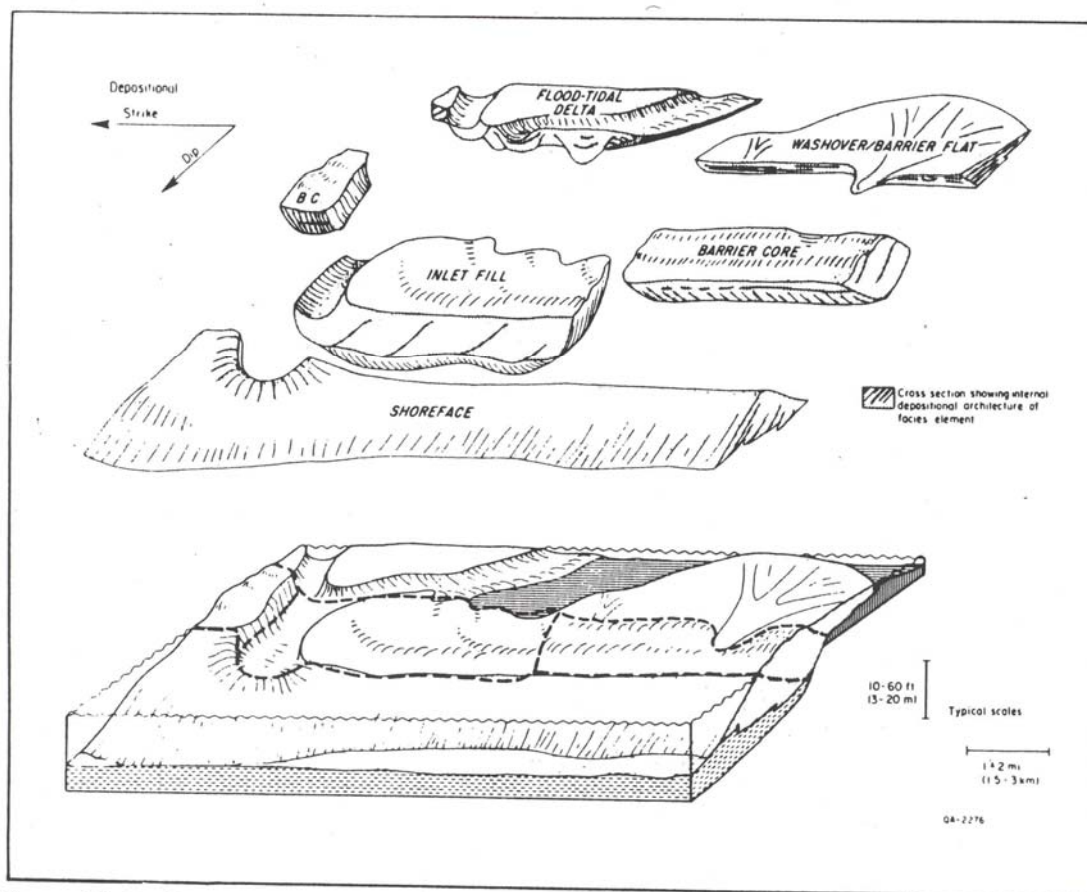


Figure 39: Architectural elements of a barrier-island sand body (from Galloway and Cheng, 1985).



The barrier core is a strike-oriented, massive sand body, separated from the coastal plain by a lagoon. The barrier core is composed of an upward-coarsening sequence of well-sorted upper-shoreface and beach sands. The barrier core complex may exist as a series of low-angle, seaward-dipping foresets. In the subsurface, the barrier core can be identified by an isolated, strike-parallel, thick sand body with an associated funnel-shaped-to-blocky log profile. Identifying characteristics of barrier cores in slabbed-core include an upward-coarsening grain-size profile from the shelf/lower shoreface, and planar to low-angle, discordant laminations of the beach, and by a vertical decrease in the abundance of biogenic structures.

Inlets disrupt the strike-oriented continuity of the barrier core and serve as the conduit through which the waters of the lagoon are exchanged with the waters of the ocean. Inlet-fill facies are characterized by dip-oriented sand-bodies that develop an erosionally-based, upward-fining succession. Upon abandonment, the inlet is filled with muddy sediments underlain by coarse, basal-lag deposits. The inlet-fill facies may be capped by thin, upward-coarsening spit platform deposits. Heron et al. (1984) showed that the frequency of occurrence of inlets is related to the relative amounts of wave to tidal energy. In areas of dominant wave energy, single large sandy ephemeral inlets tend to form and washover fan facies is well developed. In contrast, where tidal energy is dominant, multiple muddy deeply-eroding inlets are formed and the washover-fan is poorly developed.

Inlet facies can be identified in the subsurface as thick, dip-oriented sands with an associated bell-shaped log profile. The log profile may also be blocky or serrate,

depending on the location of the well to the accretionary foresets of the inlet fill.

Abandoned channel facies may show upward-fining profiles from a sharp base, due to preservability of basal lag deposits. An upward-coarsening to spiky log shape above the inlet fill is associated with the spit platform. In core, the inlet fill facies can be identified by the upward-fining grain size profile, above an erosional base. Dominant sedimentary features include basal rip-up clasts/shell hash, trough cross-strata, and planar laminations and ripple cross laminations.

The flood tidal-delta facies has two major elements: 1) thin upward-coarsening landward-progradational sequence that is produced by sediment washing through the inlet into the muddy lagoon, and 2) thin cross-cutting, upward-fining, lenticular tidal channels. In plan view, the overall complex is lobate and pinches-out on the landward side of the inlet fill facies into lagoonal mud. Log profiles are serrate in nature due to interfingering with lagoonal mud and fluctuating sediment supply. Tidal channel fills have an upward-fining grain size profile above a coarse basal lag and may have landward and seaward-dipping cross beds. The tidal delta platform has an upward-coarsening grain size profile and has both landward-and seaward-dipping cross beds. Lagoonal deposits are dominantly the result of suspension sedimentation of silt and mud.

The washover fan/barrier flat facies forms on top of and along the lagoonal side of the barrier facies as a result of storm washover and eolian processes. The overall complex has a lobate shape and pinches-out on the landward side of the barrier core facies into lagoonal mud. In cores, horizontal beds, trough cross-strata and bioturbation zones, in an overall upward-coarsening grain-size profile are observed.

The shoreface facies fronts the entire barrier island system and lies transitionally above shelf mud. The shoreface is characterized by upward-coarsening silt to fine sand and with seaward-dipping bedding, and a strike-parallel depositional trend. Ebb-tidal deltas form along the seaward margin of the inlet fill. In the Gulf Coast basin, ebb-tidal deltas are poorly developed and merge with the shoreface.

### **3.3. Facies and Facies Associations**

#### **3.3.1. General comments**

Cotton Valley Sandstones are divided into facies based upon physical and biological characteristics observed in core. Among the defining features inherent to each of the facies are lithology, grain size, and physical and biogenic sedimentary structures. I recognized 23 facies and they are characterized here from basinward to land-ward beginning with facies F1 (irregularly interbedded sandstone and shale) and extending to F23 (soil horizon). Some facies are very similar and best recognized on the basis of associated facies.

Facies associations are groupings of genetically related facies that have been deposited and modified by both sedimentary and biological processes active within an environment of deposition (Galloway, 1989a). Sediments are subject to varying degrees of physical and biological reworking. The degree to which sediments become reworked following deposition is dependent upon a range of physical and biological processes that are inherent to the environment of deposition. Evidence of these processes in core is present as a distinctive succession of facies. The Cotton Valley Sandstones depositional environments encompassing the marine and marginal marine realm are characterized by

four facies associations that exhibit a distinctive succession within cores. These four facies associations are as follows: FA1: off-shore/shoreface transition; FA2: barrier shoreface and foreshore; FA3: tidal inlet; and FA4: back barrier/coastal plain (Table 1).

### **3.3.2. Facies Association 1: Off-shore/shoreface transition**

Facies Association 1 reflects the lowermost and middle intervals of the Cotton Valley Sandstone and it was not recognized in all cores from the upper part of the CVS. The succession records a transition from proximal offshore to lower shoreface. Deposits of FA1 are bioturbated sandy siltstone and silty shale grading into very fine-to fine-grained sandstone. FA1 is typically overlain by coarser-grained facies of FA2. FA1 is missing from the upper part of the Cotton Valley Sandstones and replaced by FA4. Facies common to FA1 are F1, F2, F3, F4, F5, and F6 (Table 1).

#### **3.3.2.1. Facies 1: Irregularly interbedded sandstone and shale**

**Sedimentological characteristics:** This facies generally consists of sandstone layers 1-30 cm thick interbedded with laminated shale. This facies occurs in all of the cores cut the lower and middle Cotton Valley. It commonly overlies the inner shelf facies (F2, F3, and F4 mudstones) and overlain by F5 mudstones and sandstones. Overall unit thickness is highly variable and ranges from 5 to 25 ft (1.5-7.5 m) and displays many erosional contacts (Fig. 40). The fair-weather deposits are clay, silt and very-fine-grained sandstone thoroughly overprinted by different types of ichnofossils, periodically punctuated by storm deposits which are recorded as fine-grained sandstones with

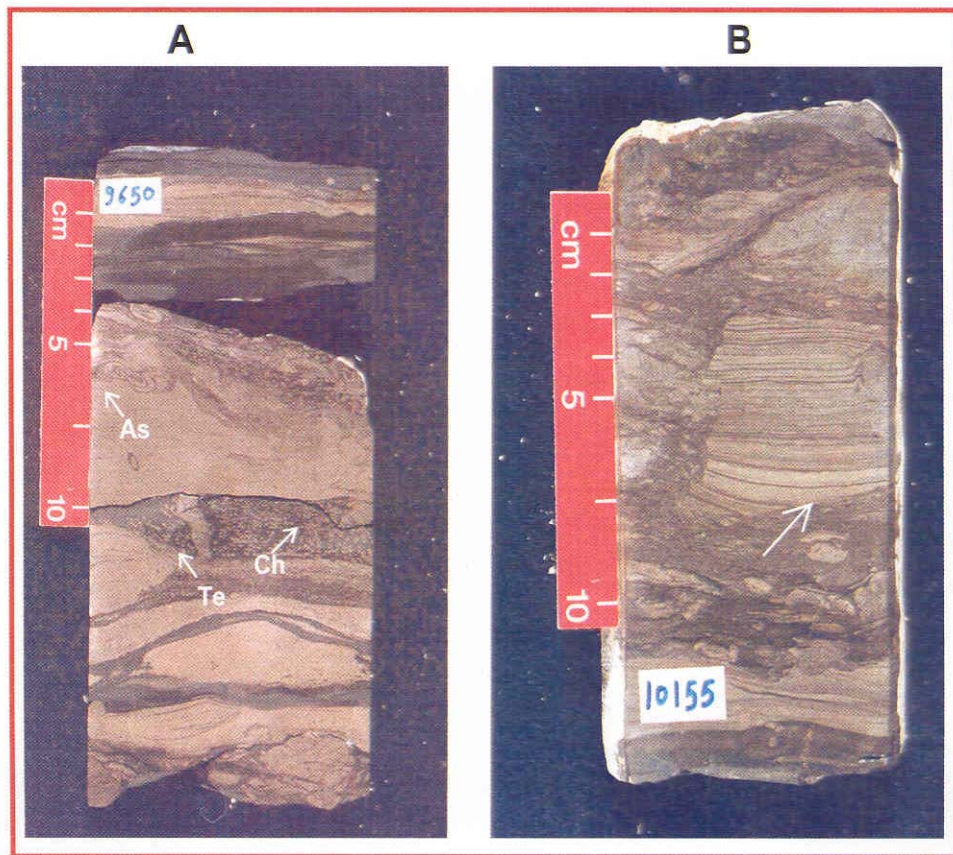


Figure 40: Facies 1-Storm-dominated inner shelf exhibit interlaminated sandstone and mudstone with continuous wavy lamination and variable burrow intensity. A: GL # 1, 9650 ft. As = *Astrosoma*, Te = *Teicichnus*, Ch = *Chondrites*. B: JA #1, 10155 ft. Arrow = event beds.

bioclastics and sharp contacts. Grain size ranges from clay to very fine-grained sandstone. Sandstone beds are amalgamated with numerous internal erosional surfaces. Beds exhibit low-angle planar lamination with uncommon current ripples.

**Ichnological characteristics:** Trace fossils in this interval are sparse and low in diversity. Traces are most commonly found near bedding contacts between shale and sandstone. Trace fossil abundance generally increases upwards rock is truncated by a sharp surface. Trace fossils include *Chondrites*, *Teichichnus*, *Terebellina*, *Planolites*, and *Helminthopsis*.

**Interpretation:** Facies 1 is interpreted to represent deposition in an offshore setting dominated by storms and waves. Episodic sedimentation is the result of major storms or hurricanes (Pemberton et al., 1992). In this facies, event deposits are indicated by numerous and irregular bedding contacts and increased upward abundance of trace fossils below the overlying storm bed. This episodic sedimentation is interpreted as a result of deposition dominantly during storm and post-storm recovery events, which indicate alternating slow and rapid deposition with erosion (Howard, 1975). Shale deposition is likely representative of post-storm setting of fines or normal fair-weather deposition.

#### **3.3.2.2. Facies 2: Massive to faintly laminated dark grey-black mudstone with fossil shell debris**

**Sedimentological characteristics:** F2 consists of 0.25-1.5 m of dark-gray-to-black calcareous and massive to faintly laminated mudstone (Fig. 41). This facies commonly associated with maximum flooding surface. It overlies F5 sandstones and mudstones or



Figure 41: Facies 2-Dark grey mudstone with fossil shell debris resembling oysters (arrows). GL # 1, 9558.5 ft.

F8 sandstones and overlain by F5 sandstones and mudstones. In this facies broken fragments of large (up to 7 cm) bivalve mollusks are observed (Fig. 41). Finely interstratified siltstone and claystone appear to be the most common sediment type.

**Ichnological characteristics:** Trace fossils are rare.

**Interpretation:** Facies 2 was deposited mainly by fallout from suspension of clay and silt below wave base. This shale represents a condensed section formed on the continental shelf during maximum transgression. Lack of burrowing activity may be due to completely or partially anoxic conditions.

### **3.3.2.3. Facies 3: Intensively bioturbated silty mudstone**

**Sedimentological characteristics:** This lithofacies consists of dark silty shales thoroughly homogenized by biogenic reworking. F3 which ranges in thickness from 0.1-0.5 m overlies inner shelf facies (F2 and F4) mudstones and overlain by F5 siltstones, shales, sandstones and mudstones. Remnant of very fine-grained sandstone beds are observed locally and undulatory parallel laminae are preserved (Fig. 42a). Thicker beds tend to show sharp, erosive bases, with moderately to well-developed parallel laminations (Fig. 42b). These preserved beds are interpreted as distal storm beds (cf. Pemberton et al., 2001).

**Ichnological characteristics:** Trace fossils in this interval are sparse and low in diversity. Common ichnogenera include *Chondrites*, *Terebellina*, *Skolithos*, *Paleophycus* and *Teichichnus*.

**Interpretation:** This facies is interpreted as deposits of the lower offshore (inner-shelf) setting. The offshore zone is regarded to lie below minimum (fair-weather) wave base



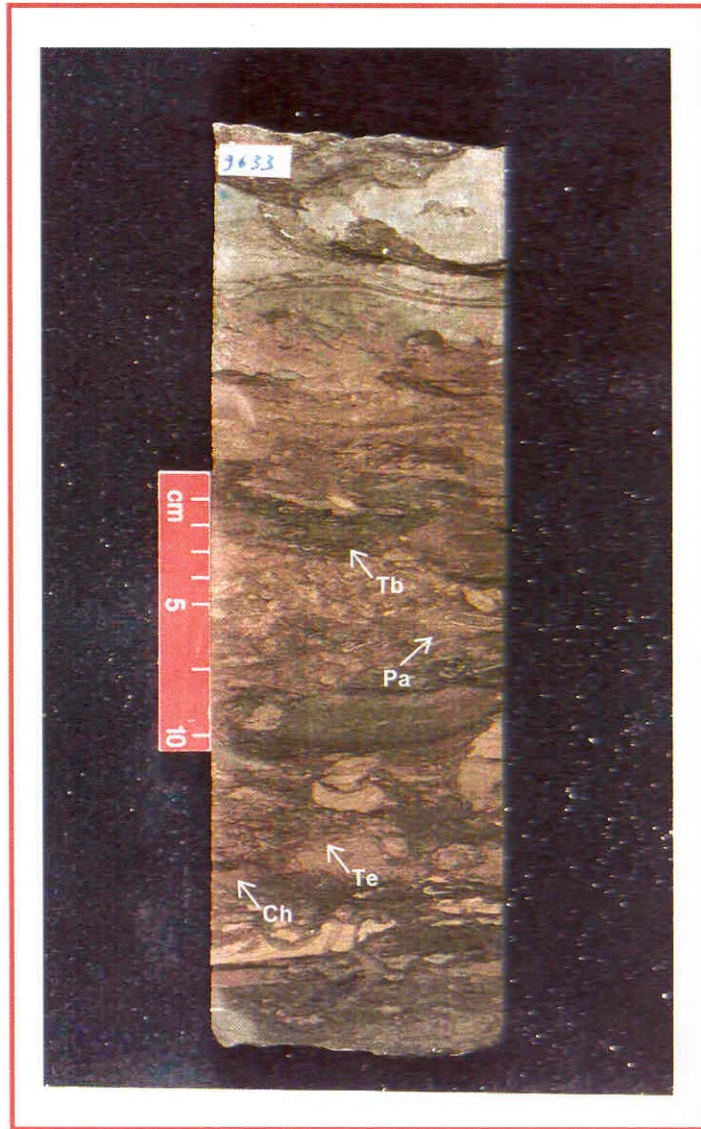


Figure 42a: Facies 3-Inner shelf deposits exhibiting local continuous wavy bedding. GL # 1, 9633 ft. Te = *Teichichnus*, Ch = *Chondrites*, Tb = *Terebellina*, and Pa = *Palaeophycus*.

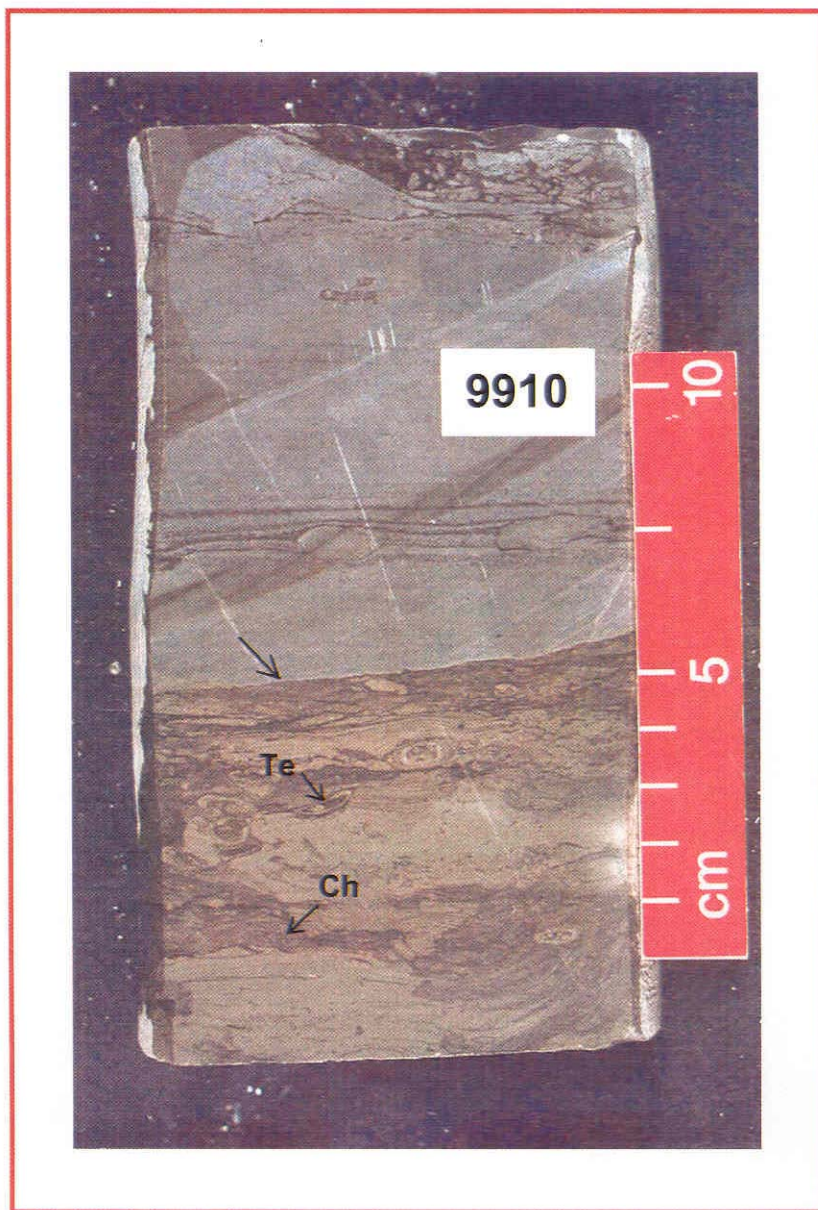


Figure 42b: Facies 3-Inner shelf deposits. Interbedded planar laminated siltstone and intensely bioturbated silty mudstone. Note sharp erosional contact (arrow). JA # 1, 9910 ft. Ch = *Chondrites*, Te = *Terebellina*.

and above maximum (storm weather) wave base. The distal storm beds are deposited below fair-weather wave base, physical processes during non-storm periods are not competent to modify them, and hence, such beds have a high preservation potential (Dott, 1983, 1988; Wheatcroft, 1990).

#### **3.3.2.4. Facies 4: *Chondrites*-dominated mudstone**

**Sedimentological characteristics:** This facies is commonly massive in appearance and is composed of dark gray silty mudstone (Fig. 43). F4 ranges in thickness from 0.1-2 m and commonly overlies F2 black mudstone and is overlain by F5 siltstones, shales and sandstones. In some cores transgressive lag separated this facies from the underlying shoreface sediments of Facies Association 2.

**Ichnological characteristics:** *Chondrites* sp. (Fig. 43) is abundant and commonly is the only trace fossil observed suggesting that it is one of the pioneer animal traces in these sediments.

**Interpretation:** Monospecific association of *Chondrites* has been interpreted to be indicative of low oxygen zones (Pemberton et al., 2001). F4 is interpreted to have been deposited in a lower offshore/inner shelf setting.

#### **3.3.2.5. Facies 5: Bioturbated thin and very thin bedded shale, siltstone and very fine-grained sandstone**

**Sedimentological characteristics:** Extensive mixing of shales, siltstones and very fine-grained sandstones through the activity of bottom-feeding organisms characterize these deposits. F5 ranges in thickness from 0.1-0.4 m. It overlies inner shelf facies (F1-F4) mudstones and overlain by F6 sandstones and mudstones. Bioturbation mottling, green



Figure 43: Facies 4-*Chondrites*-dominated inner shelf. JA # 1, 9816.5 ft. Arrows = *Chondrites*.



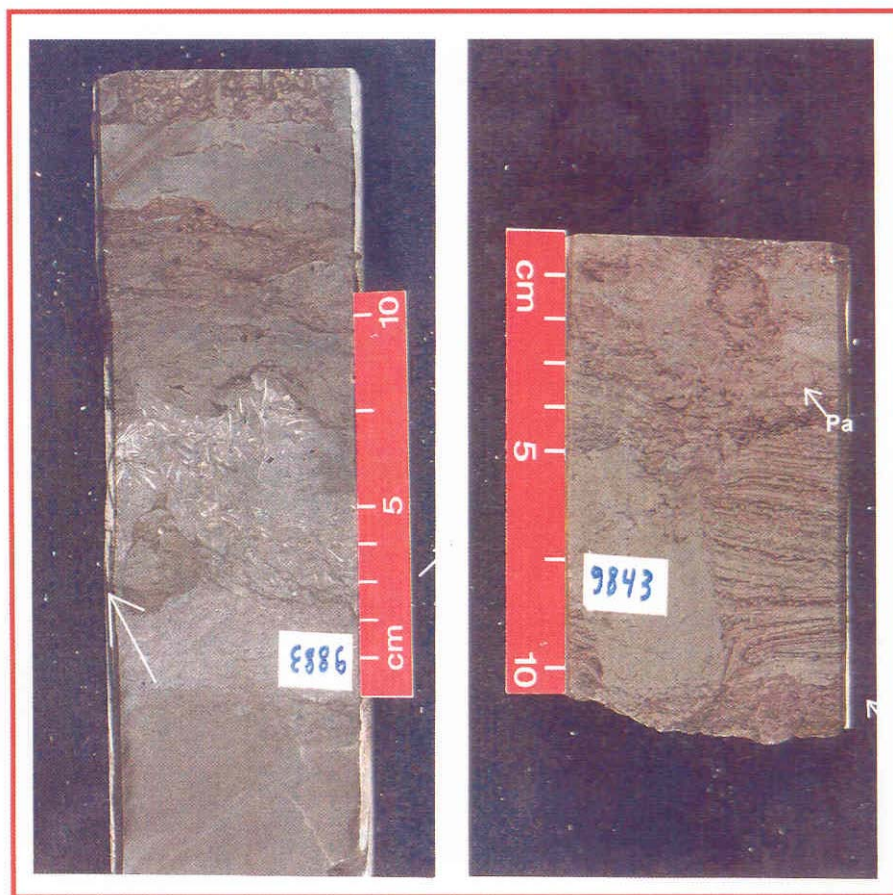


Figure 44: Facies 5-Intensely burrowed interlaminated siltstone and mudstone. A: JA # 1, 9883 ft. Arrow = big crustacean burrow filled with oysters. B: JA # 1, 9843 ft. Ba = *Bergaueria*, Ch = *Chondrites*, Pa = *Palaeophycus*.

shales, trails and burrows are ubiquitous (Fig. 44). Where preserved, primary sedimentary structures in beds of millimeters to centimeters thickness consist of parallel laminae ripple cross laminations, and wavy bedding.

**Ichnological characteristics:** Ichnofossils commonly encountered are *Chondrites*, *Terebellina*, *Palaeophycus*, *Skolithos*, *Helmenthopsis*, *Astrosoma*, and *Teichichnus*.

**Interpretation:** Facies 5 was deposited in an inner shelf to shoreface transition zone. The high trace fossil content and diversity and shale color change from black to green observed in this facies is attributed to greater oxygenation of the bottom water associated with increasing current activity.

#### **3.3.2.6. Facies 6: Bioturbated, highly carbonaceous-rich silty sandstone**

**Sedimentological characteristics:** This facies ranges in thickness from 0.2 m to 1.5 m and consists of bioturbated siltstone to very fine-grained sandstone with abundant carbonaceous debris and laminae (Fig. 45); bioclastic debris is rare. F6 commonly overlies F5 siltstones, shales and sandstones and is overlain by varied deposits of shoreface sandstones of F7, F8, and F10. The most diagnostic feature of F6 is the prevalence of horizontally oriented almond-shaped burrows; these burrows have a thin, organic-rich lining, commonly flat bottoms and passive fills. Such characteristics favor crabs over shrimp as the trace-producing organism (Hubbard et al., 1999).

**Ichnological characteristics:** Although a monospecific assemblage of these *Ophiomorpha*-like crab burrows dominates the ichnological signature of F6, there are other traces present. These include *Astrosoma*, *Palaeophycus*, *Teichichnus*, *Thalassinoides*, and *Planolites*.

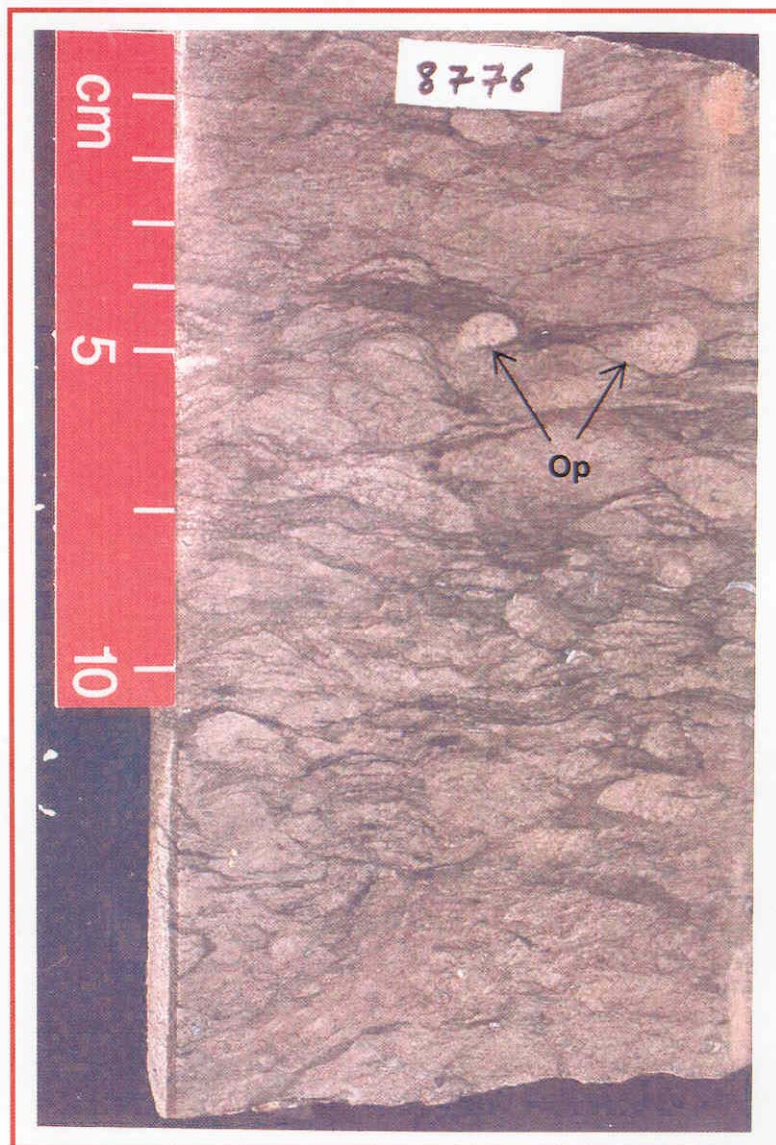


Figure 45: Facies 6-Carbonaceous silty mudstone. JA # 1, 8776 ft. Note horizontally-oriented almond-shaped burrows. Op = *Ophiomorpha*.

**Interpretation:** This facies is interpreted as deposits of a transition to lower shoreface.**3.3.3. Facies Association 2: shoreface/offshore**

Facies represented by FA2 are distributed throughout the Cotton Valley Sandstone unit within the study area and commonly overlie offshore deposits of FA1. It comprises lower fine-to-medium-grained sandstone and conglomerate that are partially or completely cemented. The variability of grain size distribution, sedimentary structure, bedding thickness and contact relationships between facies within FA2 reflects the dynamic and complex nature of nearshore systems. Facies common to FA2 are: F7, F8, F9, F10, F11, and F12.

#### **3.3.3.1. Facies 7: Storm-dominated Lower shoreface**

**Sedimentological characteristics:** F7 is fine-grained sandstone displaying gently inclined parallel to subparallel laminations (Fig. 46a). The grains are typically well sorted and very fine to fine in size. Stratigraphic thickness ranges between 0.4 m to as much as 2 m. F7 overlies F6 sandstones and mudstones and overlain by F8 sandstones and F9 conglomerates. Bedding contacts are typically sharp and erosive. Contacts between laminations are distinguished based upon mineralogy and texture emphasized by dark laminations composed of micaceous flakes and organic detritus (Fig. 46b). Lighter laminations are composed of quartz, silt and authigenic clay minerals.

Vertical successions of F7 are commonly interrupted by discrete beds of massive and bioturbated mudstone and pebbly sandstone which do not exceed 0.2 m thick. Physical structures are typically absent in both rock types. F7 directly overlies organic-rich mudstone and is capped by a bioturbated sandy shaley siltstone.



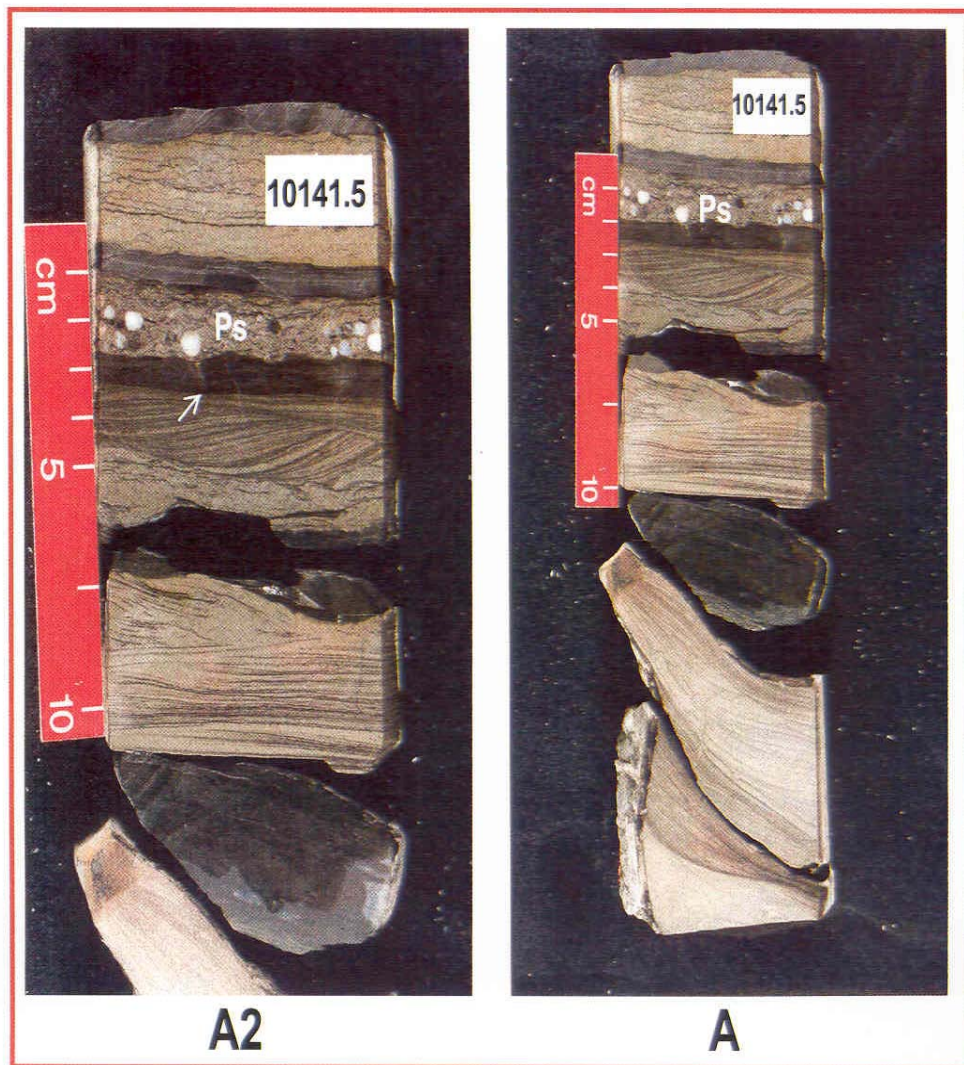


Figure 46a: Facies 7-Storm-dominated shoreface. A: JA # 1, 10145.5 ft. Arrow = sharp contact. Ps = Pebbly sandstone. A2 is close up view of A.

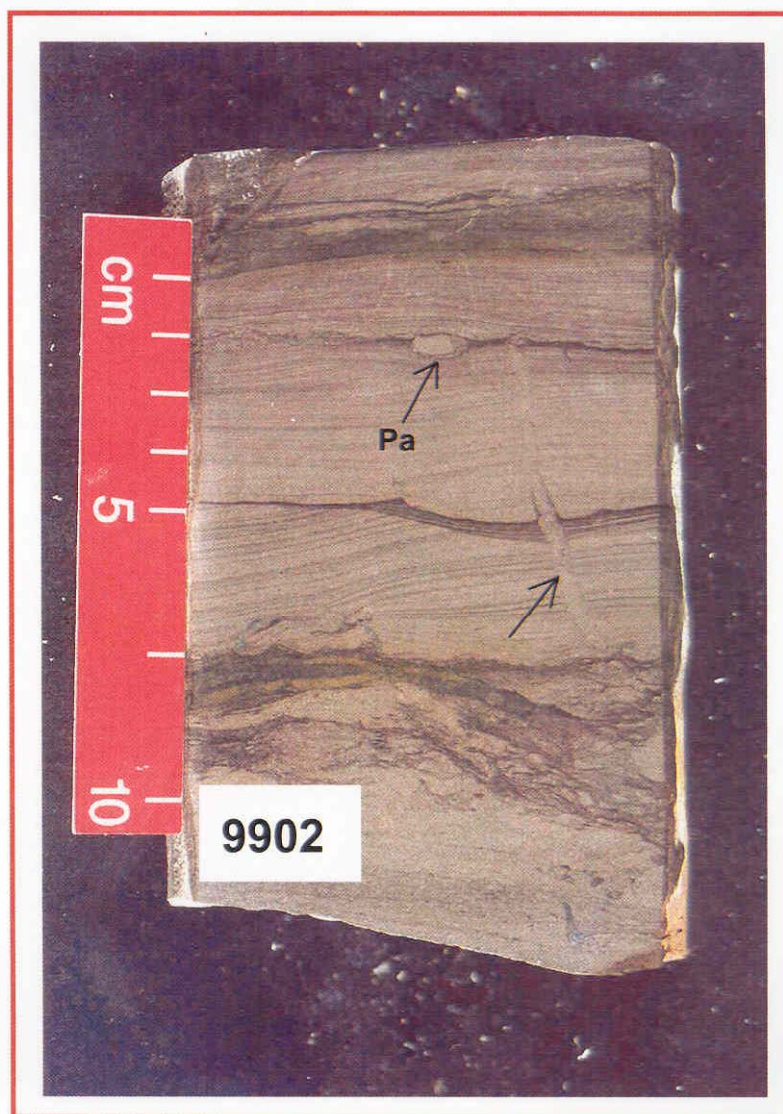


Figure 46b: Facies 7-Storm-dominated lower shoreface. JA # 1, 9902 ft. Pa = *Planolites*, arrow = escape structure.

This facies is heavily mottled by bioturbation where no recognizable features of primary bedding survived except rare discontinuous wavy carbonate laminations.

**Ichnological characteristics:** The trace fossil assemblage is dominantly composed of horizontally-oriented burrows including *Chondrites*, *Planolites*, *Paleophycus* and escape structures.

**Interpretation:** The sedimentary succession within F7 is interpreted to represent a shoaling-upward setting chiefly of storm deposits within the lower shoreface. F7 contains amalgamated and stacked bed sets of low-angle sub-parallel planar lamination interpreted as hummocky cross-stratification (HCS). HCS has generated much debate regarding its origin and the exact nature of the process controlling its formation (Duke et al., 1991). One hypothesis suggests that HCS results from the fallout and subsequent remolding of hummocks and swales by elevated wave orbital motions (Duke, 1985). Others have proposed that the development of HCS bedding is strongly dependent upon combined flows generated by a strong geostrophic current superimposed upon oscillatory wave motion (Swift et al., 1983). Regardless of the exact nature of the depositional processes involved in HCS formation, it is commonly believed that HCS bedding is formed below fair-weather wave base during intense storms.

Disruption of the fine-grained background deposits of F7 by the coarse-grained beds is interpreted as the product of episodic of sediments carried into the lower shoreface by rip currents during peak storm activity. Figure 47 shows an idealized hummocky sequence. Peak storm wave oscillation and reworking is represented by

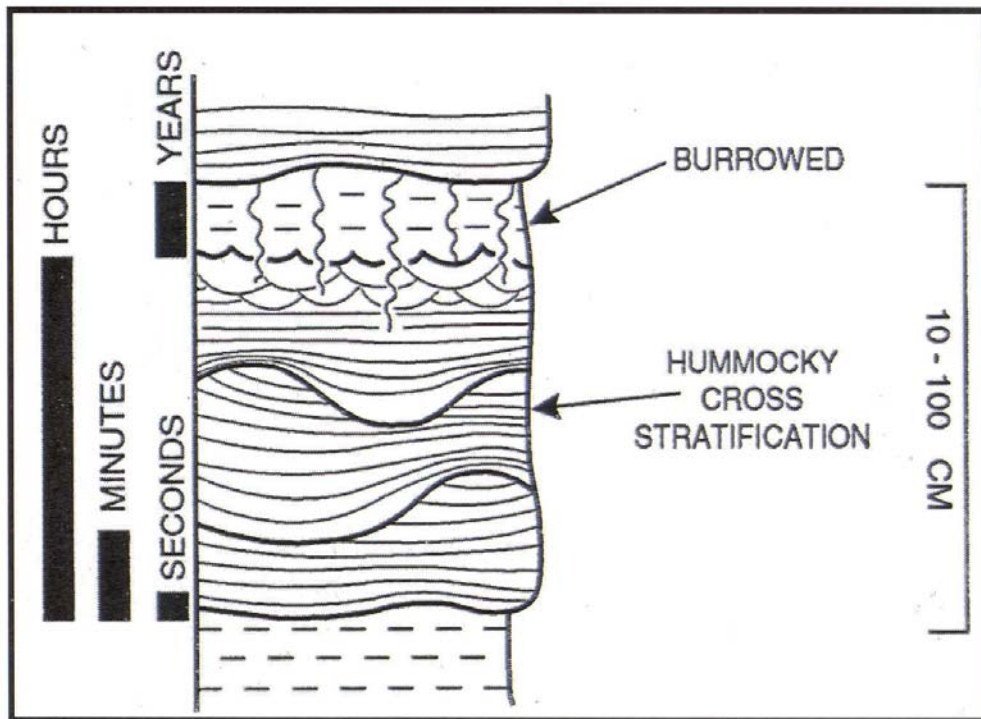


Figure 47: Temporal significance of the idealized storm unit (modified from Dott, 1983).

Amalgamated beds of laminae sets within the lower portion of the sequence. The lower portion is overlain by wave-ripple laminae sets representing the waning stage of the storm. The time scale within which amalgamated HCS bed sets and capping bed of wave ripples sets is shown in Figure 47. Beds deposited above the lower sequence become burrowed by organisms during periods of relative quiescence following storm activity. Over a time scale of weeks, months or even years of storm inactivity, the uppermost succession may become completely bioturbated (Pemberton et al., 1992; Pemberton and MacEachern, 1997).

#### **3.3.3.2. Facies 8: Well sorted, cross-bedded/laminated to massive sandstone**

**Sedimentological characteristics:** F8 is composed of well-sorted, very fine to fine-grained sandstone. Intervals of this facies consist of amalgamated sharp based sandstone bodies with average thickness of 4.5 m. F8 commonly overlies F7 and F10 sandstones and is overlain by F9 conglomerates. Grain-size profiles are generally blocky, but a subtle upward-coarsening trend to lower-medium sandstone is discernable. Mudstone laminae are rare.

High- and low-angle foreset laminae are defined by argillaceous material or slightly finer grain sizes (Fig. 48). Some of the cross beds show an alternation of thick and thin sandy laminae separated by thin argillaceous matter. In the absence of mudstone, there is a slight upward fining of the sandstone that defines the couplets. Physical structures include planar parallel and wavy bedding, tabular and trough cross bedding in which thicknesses are greater than 7 cm. Some intervals within this facies



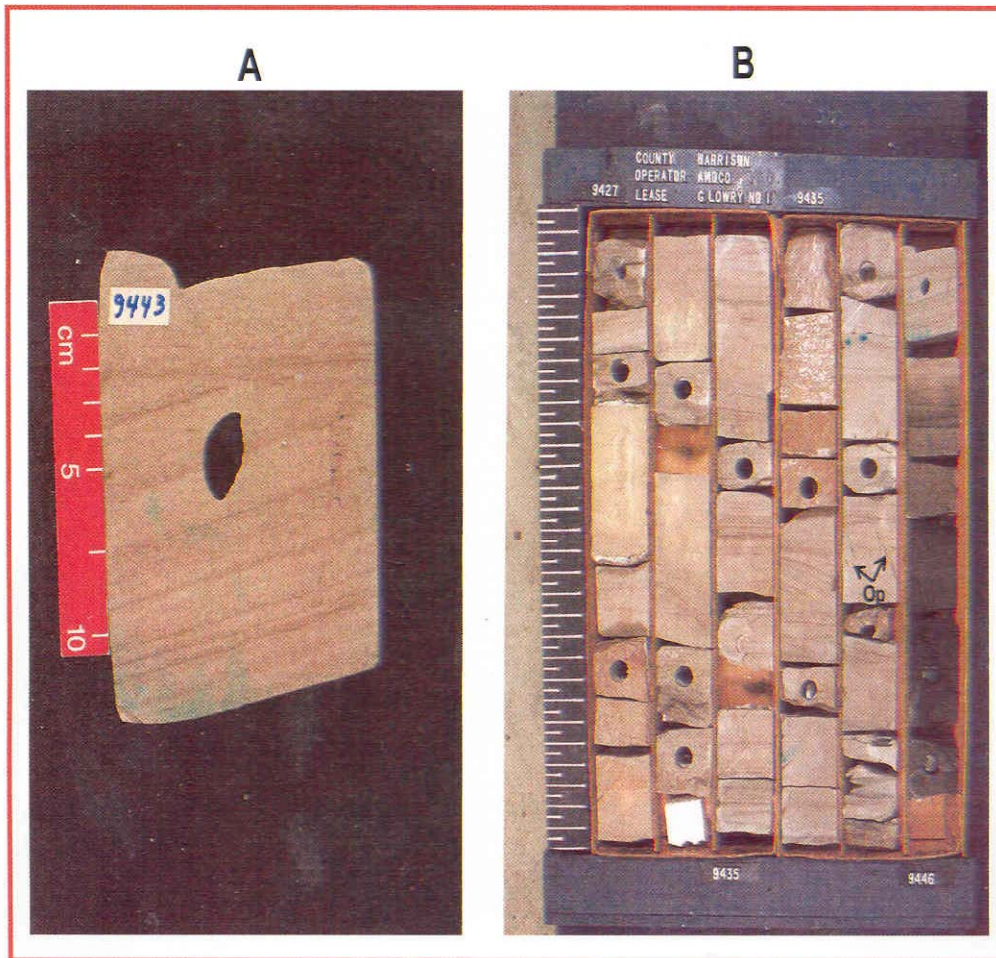


Figure 48: Facies 8-Well-sorted massive to cross-laminated sandstone. A: GL # 1, 9443 ft. Note tabular cross bedding. B: GL # 1, 9427-9446 ft. Op = *Ophiomorpha nodosa*. Left scale in B is 3 feet.

contain bedding that appears fuzzy or blurry. Other intervals are totally devoid of physical structures and thus appear massive.

**Ichnological characteristics:** Rare *Ophiomorpha* are observed.

**Interpretation:** This facies is interpreted to be deposited in the lower to middle shoreface. The amalgamation of the sandstone bodies indicates storm-dominated currents as the principal control of the laminated to massive deposits. The presence of *Ophiomorpha* and fine-grained carbonaceous debris indicate high-energy shoreface deposition.

### **3.3.3.3: Facies 9: Calcite-cemented conglomerates with abundant oysters**

**Sedimentological characteristics:** This facies overlies F8 sandstones and is overlain by sand flat deposits of the back-barrier and ranges in thickness from 0.06 to 0.9 m. It consists of a polymodal matrix to clast-supported conglomerate. Pebble clast types identified in cores include chert and quartz. This facies is very important in interpretation of provenance of the Cotton Valley sandstones.

The lower contact of the unit is variable, gradational and sharply erosive contacts are observed (Fig. 49). This facies contains abundant oysters and carbonaceous material. Granules are more spherical than pebble-size material, which is dominantly disk shaped. Bedding is massive with a lack of well-defined sedimentary structures. However, this observation is likely due to limited size of core.

**Ichnological characteristics:** Bioturbation was very rarely observed in this facies. There are two likely reasons for this.



Figure 49: Facies 9- Calcite-cemented conglomerates with oyster hash overlying shoreface sandstone (SF). A: SFE # 3, 9284 ft. B: SFE # 3, 9287 ft. Note coal fragments (left arrow) and oyster hash (circle).



The coarseness of the sediment may have prevented preservation of the burrows, or the burrows are more difficult to discern where there is little grain size variation between the burrow fill and the matrix. A big crustacean burrow filled by oyster debris is present in one core.

**Interpretation:** Facies 9 is interpreted to represent deposition in the foreshore environment. Due to the coarseness of the deposits, trace fossils are not well preserved. Although beach deposits are not commonly preserved, it has been noted that in strongly progradational sequences there is a greater chance of preservation (Dickenson et al., 1972).

#### **3.3.3.4. Facies 10: Bioturbated *Ophiomorpha*-dominated sandstone**

**Comments:** This facies is divided into F10 A and F10 B; the main difference is the degree of bioturbation, nature of *Ophiomorpha* and physical structures. F10 commonly overlies F6 sandstones and mudstones and is overlain by F8 and F11 sandstones.

##### **3.3.3.4.1. Facies 10 A: Horizontally Bioturbated *Ophiomorpha*-dominated sandstone**

**Sedimentological characteristics:** F10 A consists of heavily bioturbated sandstone with silty intervals ranging in thickness from 0.3 to 5 m. The most diagnostic feature of F10 A is the prevalence of horizontally oriented burrows (Fig. 50a). These burrows have a thin, organic-rich lining. The sandstone is massive apparently from intense bioturbation.

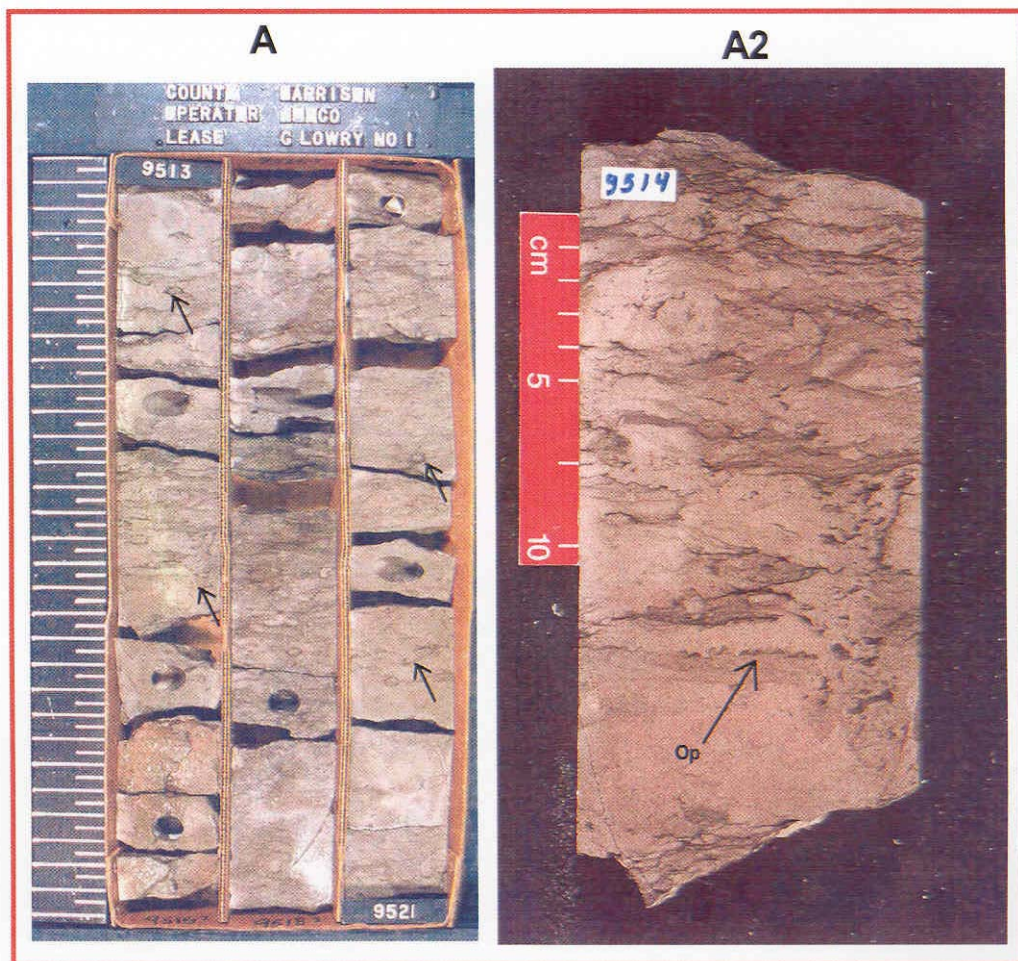


Figure 50a: Facies 10a-*Ophiomorpha*-dominated sandstones. A: GL # 1, 9513-9521 ft. Arrows = horizontal *Ophiomorpha* burrows. A2: GL # 1, 9514 ft. Op = *Ophiomorpha*. Left scale is 3 feet.

**Ichnological characteristics:** *Ophiomorpha* is the dominant trace fossil in this facies.

The bioturbation within F10 A appears two-tiered, but on closer inspection, the different burrow types exhibit a more intimate relationship (Fig. 50a). The background bioturbation consists of horizontal to slightly inclined sand-filled *Ophiomorpha* burrows that have a thin to relatively thick, dark lining. In some *Ophiomorpha* sp. burrows the wall lining is multilayered and silt filled. Vertical burrows with thin and relatively thick dark lining are also observed.

#### **3.3.3.4.2. Facies 10 B: Vertically Bioturbated *Ophiomorpha*-dominated sandstone**

**Sedimentological characteristics:** F10 B is identical to F8 and consists of 0.3-1.5 m thick stacked sequences of fine-grained sandstone that contains granule- to pebble- size chert clasts and quartz (Fig. 50b). The chert clasts are dispersed through out the sandstone. Locally, chert pebbles occur as 1 cm thick laminae. The degree of bioturbation is less than F10 A and current ripples are observed.

**Ichnological characteristics:** Heavily lined vertical or deep-penetrating *Ophiomorpha nodosa* is the only trace fossil observed in this facies.

**Interpretation:** Lack of physical structures and intense bioturbation in F10A indicates deposition in the lower shoreface. Conversely, the presence of coarser grained sediments, lesser degree of bioturbation and the presence of heavily lined, deep-penetrating *Ophiomorpha nodosa* in F10 B are an indication of middle-to-upper shoreface environment. Howard (1975) and others have noted that *Ophiomorpha* systems tend to shift from horizontal to vertical in orientation as energy levels increase.

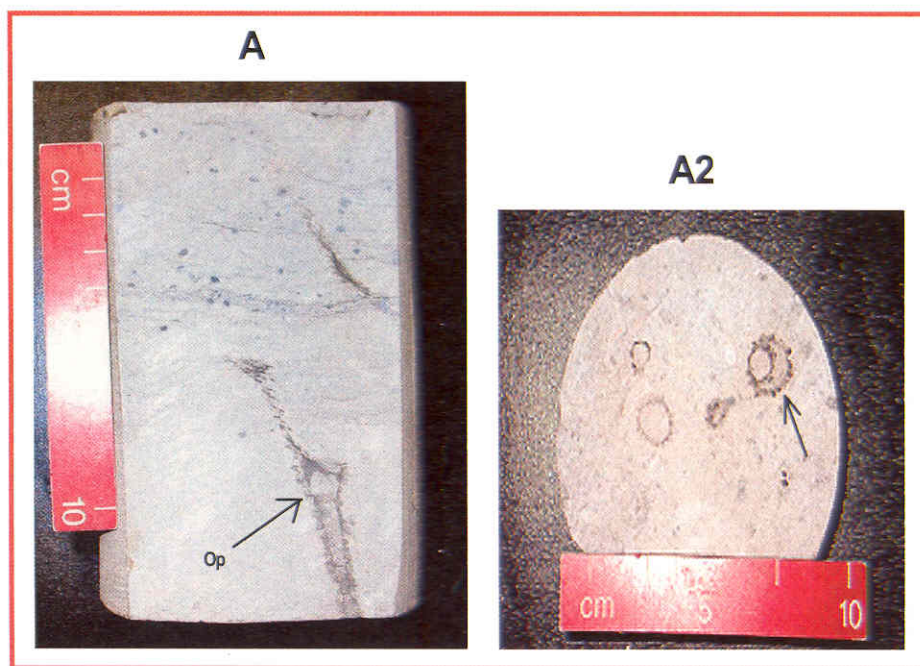


Figure 50b: Facies 10b-*Ophiomorpha*-dominated shoreface. A: JA # 1, 10137 ft. Op = *Ophiomorpha*. B: JA # 1, 10137 ft., cross sectional view of A. Arrow = double lining *Ophiomorpha*.

#### **3.3.3.5. Facies 11: Cryptobioturbated sandstone**

**Sedimentological characteristics:** Cryptic-bioturbation is the most diagnostic feature for this sandstone (Fig. 51). Crypto-bioturbation is defined as a small-scale disruption of grain fabric by microscopic and macroscopic organisms and there is a tendency to preserve rather than to destroy the physical sedimentary structures (Pemberton et al., 2001). This facies is thoroughly bioturbated and yet shows remarkably little distortion of original bedding. F11 is composed of very well sorted, very-fine to fine-grained sandstone. Intervals of this facies consist of amalgamated sharp-based, sandstone bodies. Grain-size profiles are blocky, but a subtle upward-coarsening trend to lower-medium sandstone is discernable. Mudstone laminae are rare. Physical structures include planar parallel lamination and low-angle cross bedding. This facies ranges in thickness between 0.3 to 1.0 m and overlies the different types of shoreface sandstones of F7, F8 and F10 and is overlain by F9 conglomerates.

**Ichnological characteristics:** Cryptobioturbation is observed.

**Interpretation:** Cryptobioturbation is one of the most common and widespread forms of burrowing in ancient marine sandstones (Pemberton et al., 2001). Cryptobioturbation and physical sedimentary structures indicate that this facies was deposited in a high-energy middle to upper shoreface. The occurrence of F 11 overlying lower to middle shoreface sediments supports this interpretation. Cryptic-bioturbation is believed to be indicative of the life activity of meiobenthic organisms



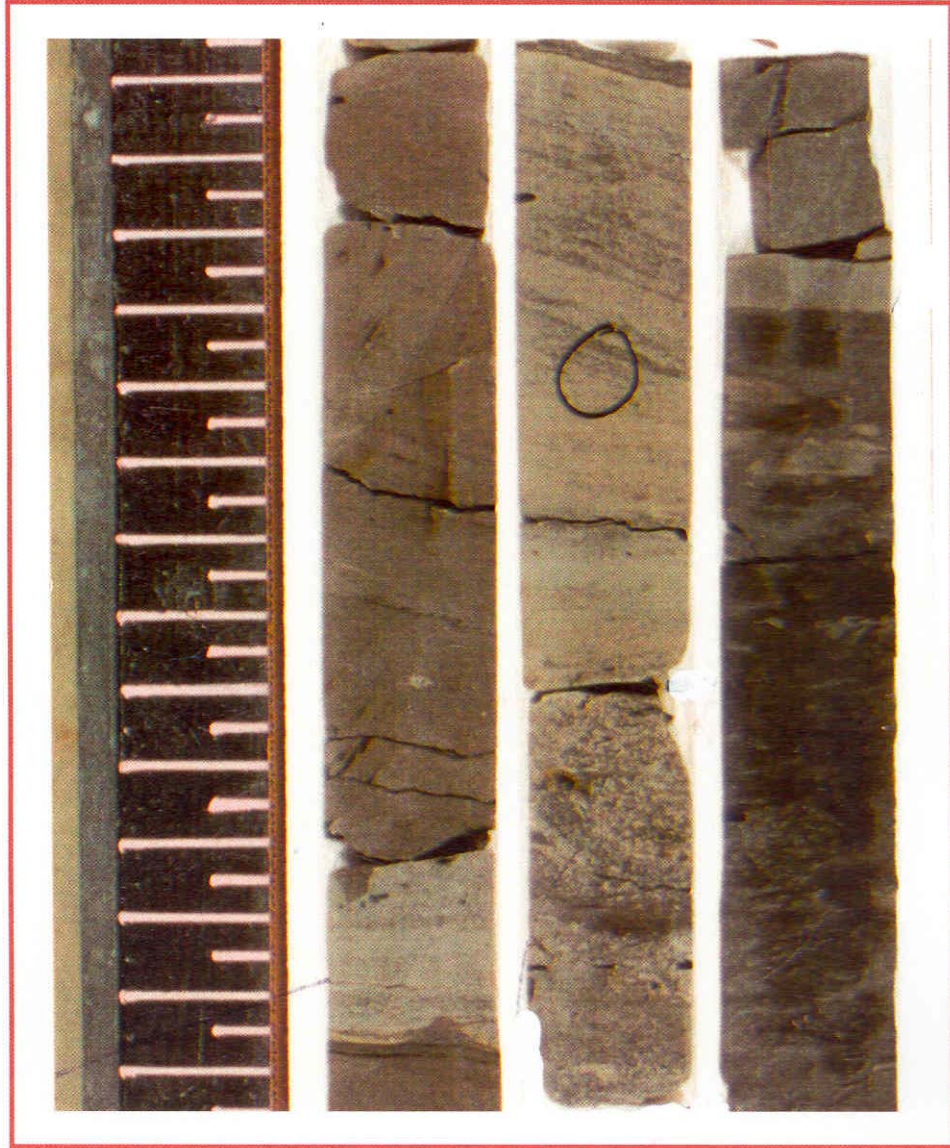


Figure 51: Facies 11-Cryptobioturbated sandstones. Note fuzzy lamination (circle) due to bioturbation. SFE # 3, 9310-9314 ft. Major ticks in left scale is 10 cm.

that are present interstitially within the substrate pen-contemporaneously with deposition (Howard and Frey, 1975). As the name suggests, cryptic-bioturbation is of small scale, as are the trace makers to which the bioturbation is attributed. Meiofauna is believed to account for the fuzzy lamination that is characteristic of cryptically bioturbated substrates (Howard and Frey, 1975).

#### **3.3.3.6. Facies 12: Tidal-influenced shoreface/Flood-tidal delta**

**Sedimentologic Characteristics:** Facies 12 consists of well-sorted, fine-to lower medium-grained sandstone. It varies in thickness between 0.6-5.0 m and overlies lagoonal and bay fill deposits and is overlain by marine transgression indicated by inner shelf facies or transgressive lag. Although F 14 looks blocky, there is a general upward-coarsening trend. Physical sedimentary structures increase upwards and bioturbation is restricted to the lower part of this facies. Low-angle to planar parallel stratification is typical of facies 14. Wavy bedding, low-angle cross bedding and current ripples are common. Carbonaceous matter is locally observed. A large number of stylolites are recorded in many cores (about 180 stylolites in 5 feet section) which may indicate the former presence of clay laminae. Double mud drapes and oscillatory climbing ripples are also observed (Fig. 52).

**Ichnological Characteristics:** The lower part of this facies indicates low burrowing density and cryptic bioturbation. Trace fossils present are *Skolithos*, *Paleophycus*, and *Thalassinoides*.

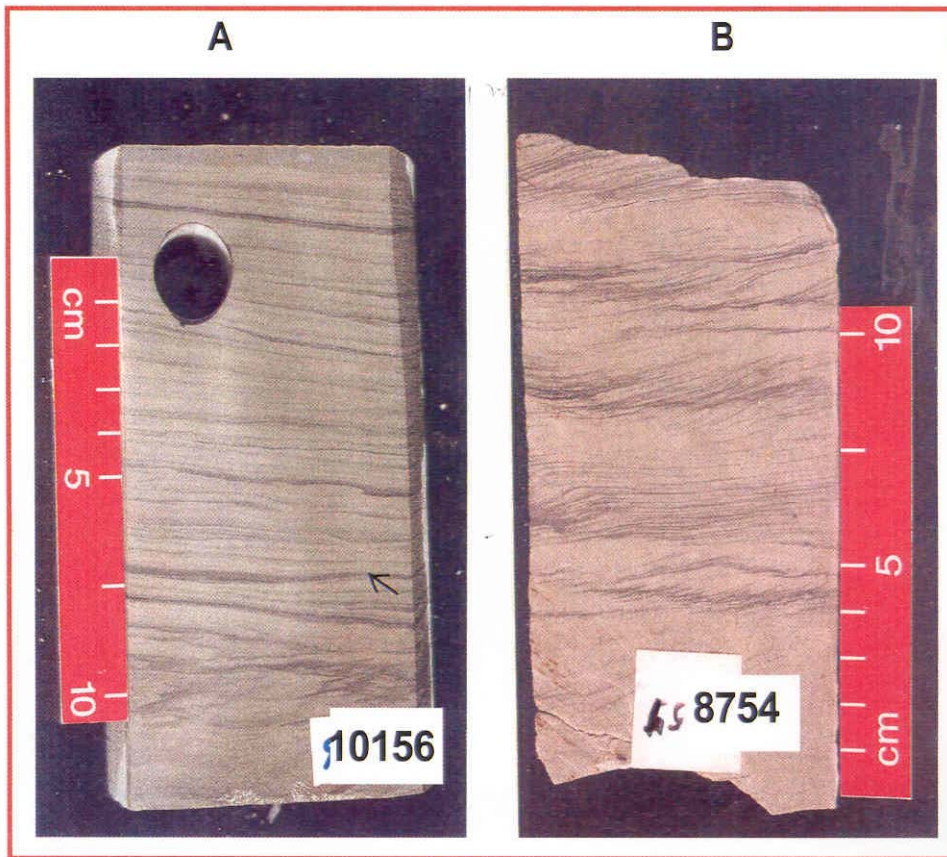


Figure 52: Facies 12-Tidal-dominated sandstone. A: JA # 1, 10156 ft. B: BSH # 1, 8754 ft. Core shows double mud drapes (arrow) typical of tidal setting.



**Interpretation:** The presence of double mud drapes and oscillatory climbing ripples indicate tidal influence. Double mud drapes are indicative of diurnal tides. Kvale and Archer (1991) indicated that oscillatory ripples are examples of a very thin tidal bundle sequence. The occurrence of both wave- and tide-generated sedimentary structures in Facies 12 and its position overlying lagoonal mud indicates it formed in a flood-tidal delta.

#### **3.3.4. Facies association 3: Tidal inlet**

FA3 stratigraphically overlies FA1 and is capped by F4 and represents sediments that were deposited during a distinct episode of sediment supply and relative change in sea level. Deposition of FA3 was closely related to and influenced by processes active during deposition of FA2. As a result, FA3 facies succession contains many of the facies that included in FA2. FA3 is characterized by a fining-upward succession that is overlain by organic-rich, shaley fine-grained facies association FA4. The upper contact of FA3 is commonly deeply rooted, indicating a period of subaerial exposure. F13 is the only facies in FA3.

##### **3.3.4.1. F13: Pebbly conglomerate and bioturbated carbonaceous-rich sandstone**

**Sedimentologic Characteristics:** Pervasively bioturbated sandstone comprises facies 13.

The most diagnostic feature of this interval is the rounded quartz and chert pebbles scattered throughout and in stringers (Fig. 53) and ranges in thickness from 5 to 15 cm. F13 is commonly observed at the base of tidal inlets in most of the cores. It overlies varied types of shoreface sandstones (F8, F10, and F11) and commonly overlain by



Figure 53: Facies 13-Pebbly bioturbated carbonaceous conglomerate. JH # 3, 9406 ft. Op = *Ophiomorpha*. Note no traces in conglomerate.

back barrier deposits. These pebbles reach up to 2 cm in diameter and the carbonaceous matter is common. A prominent lag of pebbles and/or bioclastic debris occurs above the sharp, scoured lower contact of F13. Shelly material very rarely occurs with lag deposit. Localized occurrence of coal fragments are also found in F13. Bioturbation is intensive in the fine-grained sandstone and absent in the conglomerate.

**Ichnological characteristics:** Discernable trace fossils include *Ophiomorpha*, *Palaeophysis*, and *Thalassioides*.

**Interpretation:** The channelized nature (sharp base and basal lag) and restricted occurrence are indicative of deposition in a barrier inlet. The high degree of bioturbation and absence of any physical structures implies that energy conditions varied greatly within the inlet. The presence of pebbles suggest high energy at time of deposition, but the degree of bioturbation implies the waning of energies (due to channel switching and periodic channel abandonment) allowing for burrowing organisms to inhabit the environment.

#### **3.3.5. Facies association 4: Back Barrier/Coastal plain**

Facies Association 4 is underlain by Facies Association 3 or 2 and primarily comprises a relatively conformable succession of sand-rich and shale-rich, fine-grained facies. Facies Association 4 is observed only in cores cut the upper part of the Cotton Valley. This unique variety of hydrodynamic and biological processes was likely responsible for deposition of FA4 as indicated by a wide range of physical and biogenic sedimentary structures. Facies encountered within FA4 are in facies F14-F23.

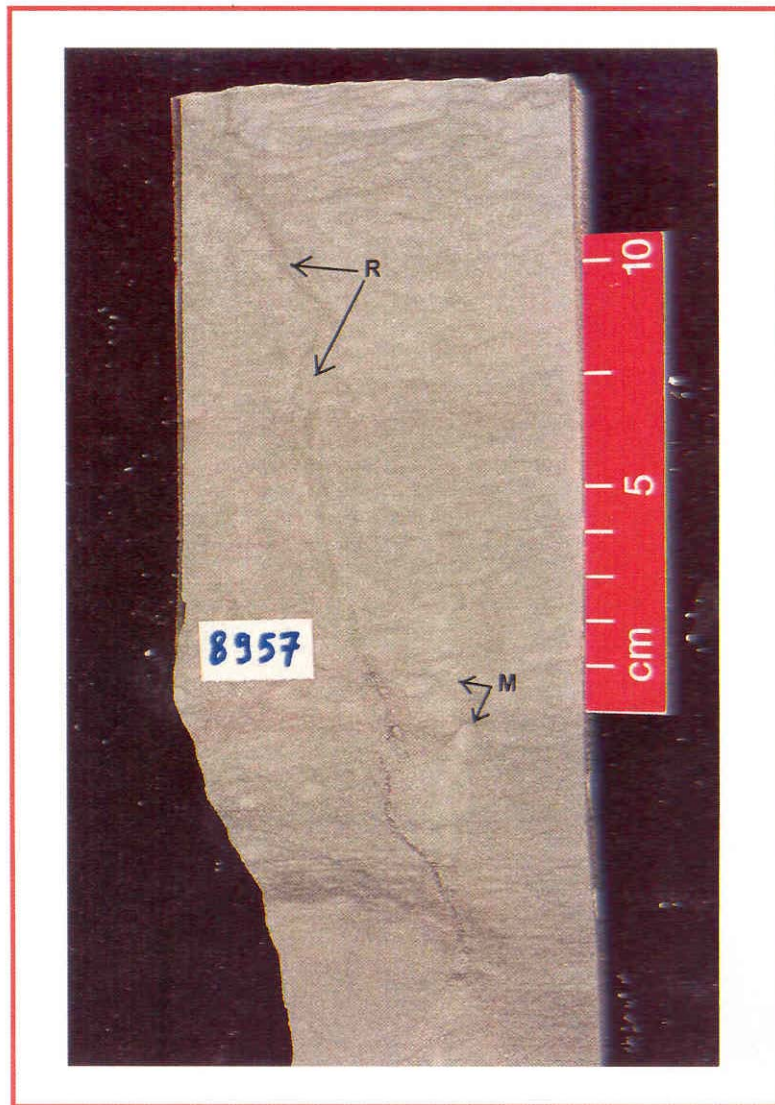


Figure 54: Facies 14-Rooted grey sandstone with *Macaronichnus segregatus* (M). JA # 1, 8957 ft. R = Root.

#### **3.3.5.1. Facies 14: Rooted grey sandstone**

**Sedimentological characteristics:** This facies consists of fine-to lower medium-grained sandstone, though it is dominantly fine-grained sandstone. This facies is intensely bioturbated and rooted and attains a maximum thickness of 0.6 m. It overlies bay sand and mud and is overlain by mixed or mud flats. In spite of extensive bioturbation, faint planar lamination is apparent in some intervals (Fig. 54).

**Ichnological characteristics:** Trace fossil abundance and diversity is typically very low; the exception to this is the extensive occurrence of *Macaronichnus segregatus* which is the dominant traces in this facies. *Thalassinoides* is also present.

**Interpretation:** *Macaronichnus segregatus* is a common element of high-energy shoreface successions (MacEachern and Pemberton, 1992). It commonly occurs at the toe of shoreface deposits (Saunders et al., 1994), although it has also been reported from a variety of other settings, such as the lower shoreface (Curan, 1985) and within tidal channel deposits (Clifton, 1978). This facies is believed to be deposited in tidal flat setting (Floyd "Bo" Henk, 2003 personal communication). The close proximity of this facies to deeply rooted interbedded sandstone and mudstone supports this interpretation.

#### **3.3.5.2. Facies 15: Rippled-laminated sandstone with carbonaceous matter**

**Sedimentological characteristics:** Ripple-laminated, fine-to upper fine-grained sandstone with abundant clay and carbonaceous laminae constitute this facies (Fig. 55).

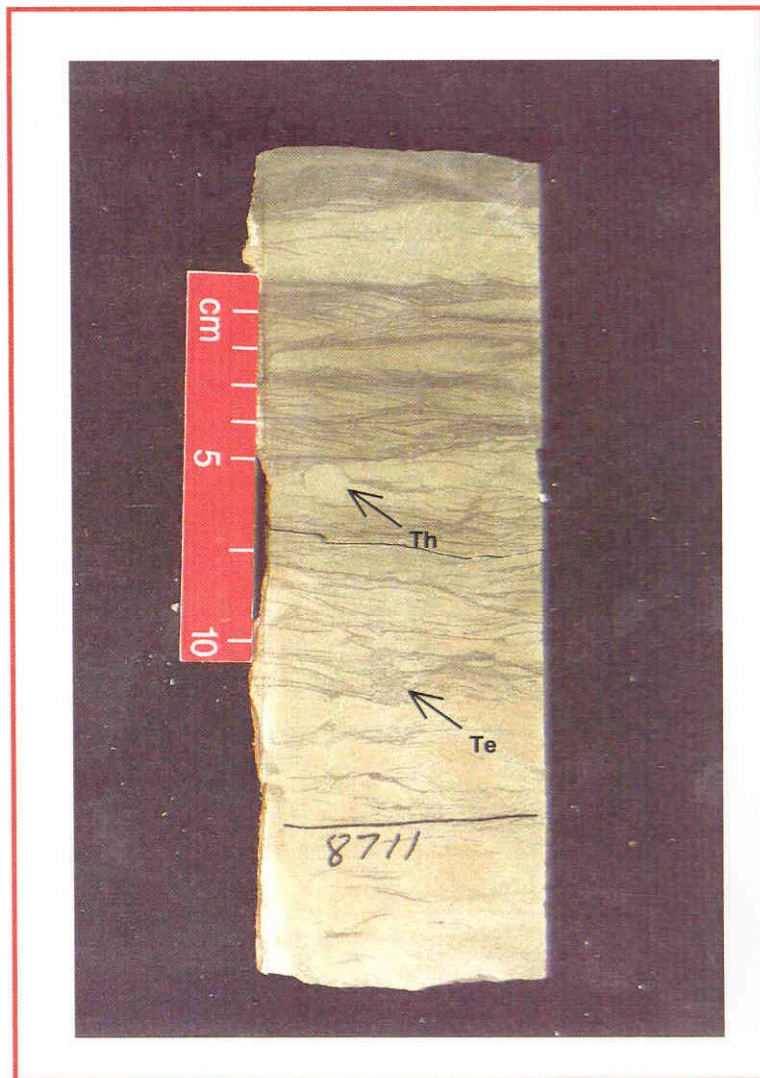


Figure 55: Facies 15- Rippled-laminated sandstone with carbonaceous matter. *BSH # 1*, 8711 ft. *Te* = *Teichichnus*, *Th* = *Thalassinoides*.



Shell debris is rare. The sandstone beds are thin (up to 0.5 m) and occur as isolated sharp-based units within facies FA4. This facies overlies bay mud and sand or shoreface sandstones and is overlain by lagoonal mudstone and ranges in thickness from 0.3-1.5 m. Physical structures are dominated by low-angle bedding in the lower portion of F15 intervals, but grade upward into wavy and rippled bedding. Carbonaceous and clay laminae accent ripples.

**Ichnological characteristics:** The trace fossil suite consists of rare *Planolites*, *Teichichnus*, and *Palaeophycus*.

**Interpretation:** The sandstone beds are interpreted as washover deposits extending into lagoonal mudstone. These thin sandy units with planar and rippely bedding were deposited during major storm events that breached the barrier. During fair-weather conditions, the lobate or sheet-like sands were colonized, as seen in the presence of trace fossils near the top of individual sandstone beds. Washover deposits have a high potential for preservation in transgressive successions, especially when interbedded with lagoonal facies (Pemberton et al., 2001).

#### **3.3.5.3. Facies 16: Cross-bedded sandstone with carbonaceous laminae**

**Sedimentary characteristics:** F16 consists almost entirely of very fine-grained, well-sorted sandstone (Fig. 56). It overlies varied types of tidal flat facies (sand flat, mixed flat and mud flat) and is overlain by lagoonal and bay mudstones. The thickness of these sandstone bodies ranges from 0.3 to 2.3 m. Sandstones are mostly cross laminated beds truncated at the top and tangential at the base.

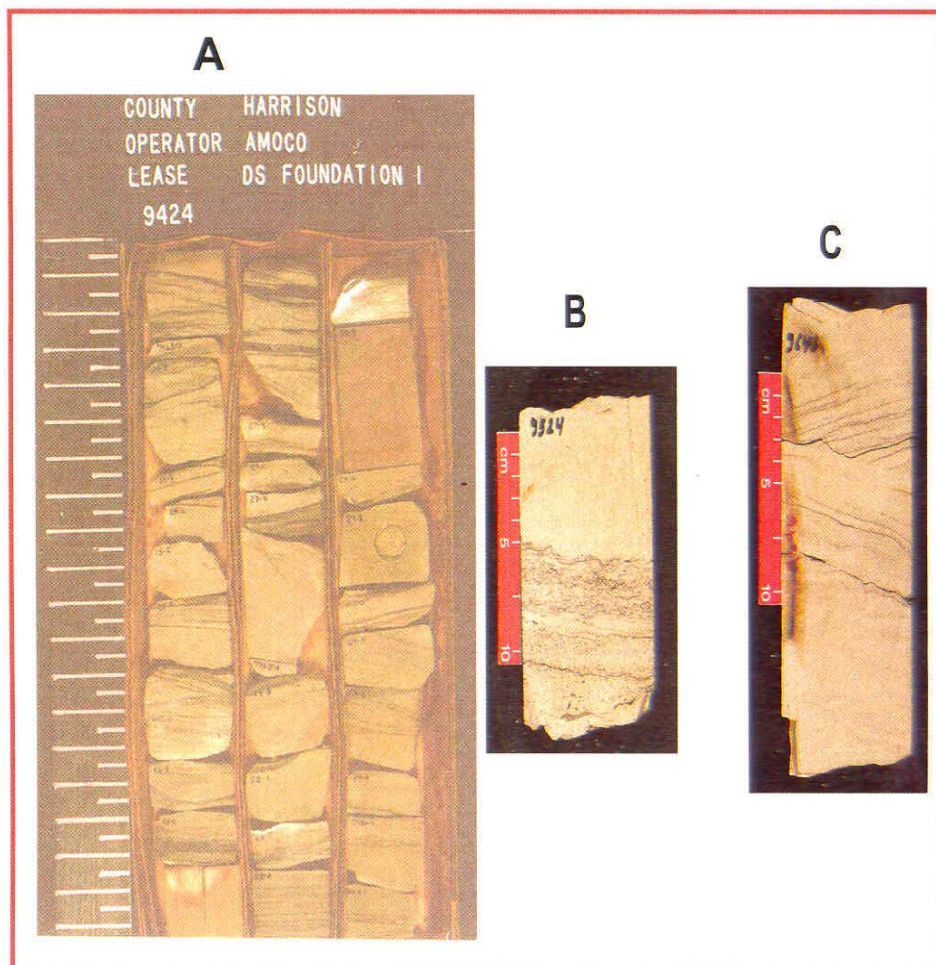


Figure 56. Facies 16-Cross bedded sandstone with carbonaceous matter. A: DS # 1, 9424-9430 ft. Low-to high-angle cross lamination. B: DS # 1, 9524 ft. Abundant ripples and carbonaceous matter. C: DS # 1, 9646 ft. Herring bone cross-bedding. Left scale is 3 feet.



Laminae of detrital carbonaceous clay are common in steeply dipping sets of cross strata. The sandstones exhibit a sharp base with upward-fining texture and abraded shell fragments (rare) and clay clasts near the base (Fig. 56b). Herringbone cross-bedding is also observed (Fig. 56c).

**Ichnological characteristics:** Trace fossils are rare to absent.

**Interpretation:** F 16 is interpreted to be tidal channel sandstones. The well sorted, cross-bedded sandstones indicate deposition by high-energy, strongly directed currents. The herringbone cross bedding indicates that these sands were deposited by opposed currents interpreted to be flood and ebb tidal currents.

#### **3.3.5.4. Facies 17: Interlaminated very fine-grained sandstone, siltstone, and claystone**

**Sedimentary characteristics:** F 17 consists of interlaminated very fine sandstone, siltstone and claystone characterized by an upward decrease in grain size and increase in clay content (Fig. 57a). It overlies bay mud and sand and is overlain by marsh deposits. F17 ranges in thickness from 3 to 8 m in all cores that penetrated the upper part of the Cotton Valley. Thin, horizontal laminations and very fine-grained rippled beds are present throughout most of the sequence. Local convoluted bedding is also observed. Sediments at the top are partly to entirely bioturbated and range in color from dark grey to olive green silty mudstone (Fig. 57b).

**Ichnological characteristics:** *Ophiomorpha* (rare) is the only observed trace fossil in facies 17. Rootlets occur in moderate to high abundance and commonly exist in specific horizons.

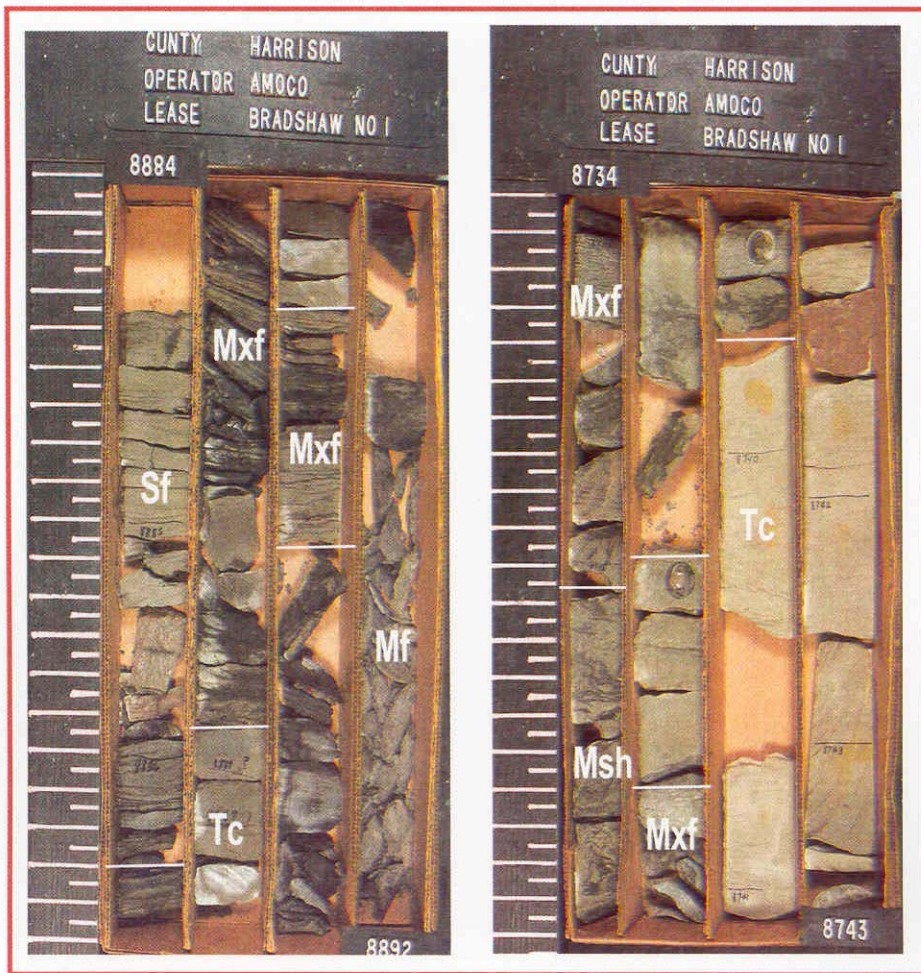


Figure 57: Facies 21-Example of fine-grained back barrier deposits, including, mud flat (Mf), mixed flat (Mxf), sand flat (SF), marsh (m), and tidal chanel (Tc) deposits. Left scale is 3 feet.

**Interpretation:** F 17 is attributed to deposition on tidal flats (sand, mixed and mud flats) and marshes. Horizontal laminations and very fine-rippled beds indicate deposition by weak fluctuating currents. The low diversity of biogenic traces is due to numerous stresses, such as fluctuating currents, extremes in salinity and periodic desiccation (in the muddy intervals), and sporadic deposition (cf. Weimer et al., 1982).

#### **3.3.5.5. Facies 18: Interbedded sharp-based sandstone and bioturbated sandy siltstone “Lam-Scram”**

**Sedimentological characteristics:** Facies 18 consists of sharp-based sandstones gradationally overlain by bioturbated silty sandstone and sandy siltstone (Fig. 58). Sandstone beds commonly have a scoured base, with carbonaceous material in the form of flakes and wispy laminae. F18 ranges in thickness from 0.2 to 1.5 m and overlies bay mudstone and sandstone and is overlain by tidal flat sediments. Planar to wavy parallel bedding and low-angle cross stratification are typical. The upper boundary of the sandstone beds is commonly burrowed and gradational in nature. The overlying silty sandstone is completely bioturbated by diverse trace fossil assemblages.

**Ichnological characteristics:** Forms encountered in the bioturbated silty sandstones include *Ophiomorpha*, *Teichichnus*, *Planolites*, *Diplocrateron*, and *Thalassinoides*.

**Interpretation:** The “Lam-Scram” (laminated to scrambled) appearance of Facies 18 is typical of storm beds alternating with associated fair-weather deposits (Howard, 1972). Scoured-based sandstones gradationally overlain by bioturbated, fine-grained sediments are characteristics of tempestites.

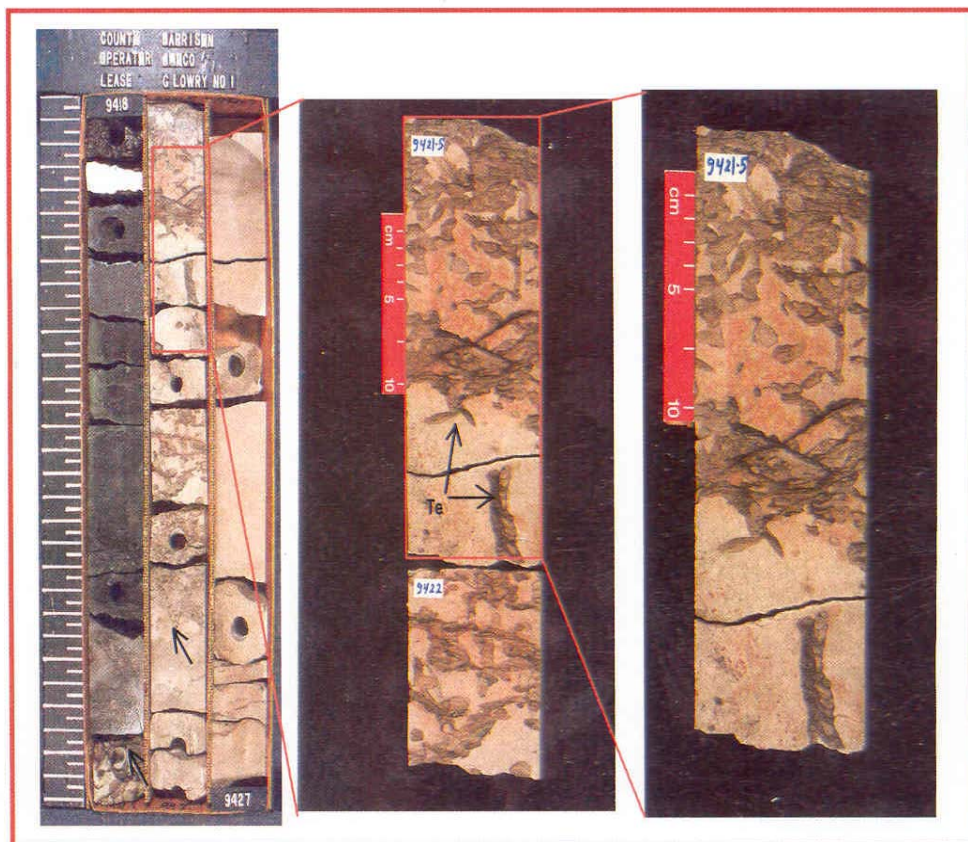


Figure 58: Facies 18-Laminated-scrambled facies. Alternating laminated and bioturbated sandstones. Bsh # 1, 8653 ft. Th = *Thalassinoides*.

The occurrence of these event beds suggests that deposition was moderately storm-dominated (cf. Pemberton et al., 2001). An unrestricted embayment exhibits the necessary conditions for such depositional characteristics. Bays that are completely open to the ocean have a fully marine ichnological signature.

#### **3.3.5.6. Facies 19: *Teichichnus*-dominated fine-grained sandstone**

**Sedimentological characteristics:** Bioturbated fine-to upper-fine-grained sandstone is very distinctive to facies 19. It commonly has reddish brown coloring accentuated in burrow linings (Fig. 59). This facies is thin, reaches up to 1 m thick, and is rare. It gradationally overlies bay fill sandstones and underlies dark gray to black lagoonal mudstones. This facies is devoid of physical structures.

**Ichnological characteristics:** *Teichichnus* sp. is abundant and commonly is the only trace fossil observed in these deposits, suggesting that it is one of the pioneer animal traces in these sediments.

**Interpretation:** The low species diversity and dominance of just one ichnogenus in facies 21 is characteristic of brackish-water environment (Pemberton and Wrightman, 1992). Fewer organisms are able to adapt to these stressed systems, and therefore trace fossil suits tend to be composed of forms attributed to very few species. This facies is interpreted to have been deposited in a brackish bay-like environment. The presence of bay-fill sand below and lagoonal mudstone above this facies support this interpretation.



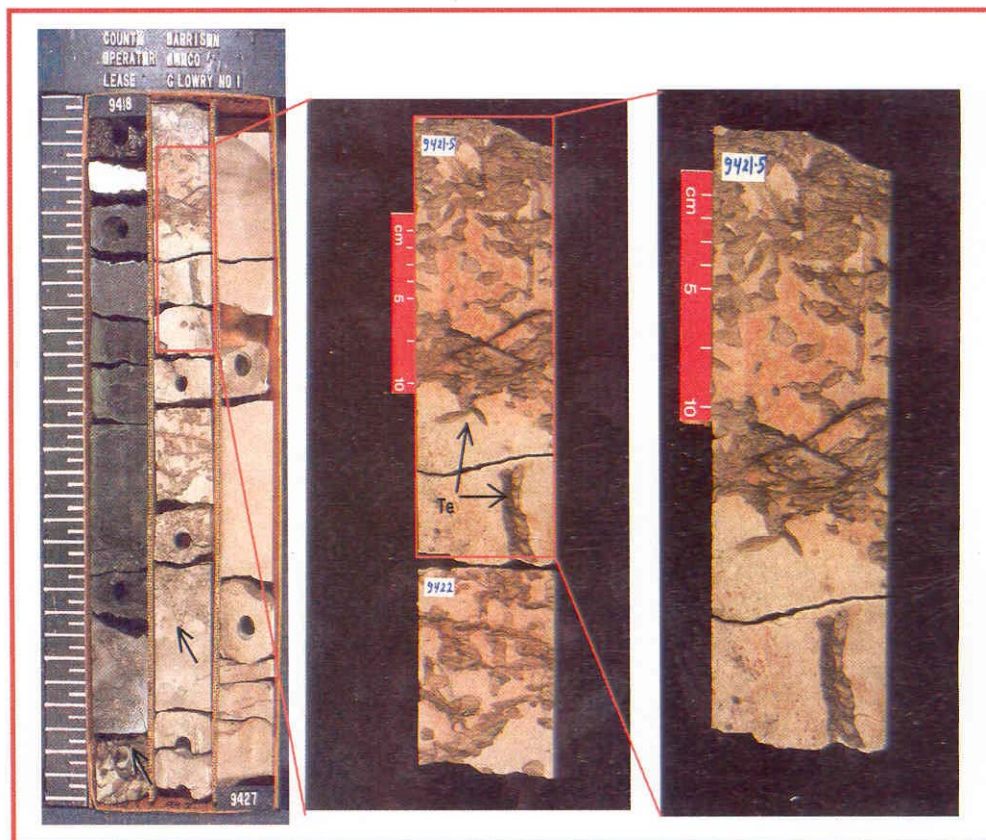


Figure 59: Facies 19-*Teichichnus*-dominated sandstones. A: GL # 1, 9418-9427 ft. Note the gradational contact between this facies and both of the underlying and overlying facies. B: GL # 1, 9421.5-9422 ft. Te = *Teichichnus*. C: Close up view of B. Left scale is 3 feet.

#### **3.3.5.7. Facies 20: Laminated to *Teichichnus*-dominated sandstone**

**Sedimentological characteristics:** F20 is a dark gray to black, faintly laminated, carbonaceous mudstone; siltstone and sandstone comprise less than 20% (Fig. 60). This facies is very rare. F20 ranges in thickness between 0.1 to 0.3 m. It commonly gradationally overlies sand flat sandstones and is overlain by lagoonal mudstone.

**Ichnological characteristics:** *Teichichnus* sp. is abundant and commonly is the only trace fossil observed in these deposits.

**Interpretation:** The low diversity and dominance of one species only in F 20 is characteristic of brackish water environment (Pemberton et al., 2001). This facies is interpreted to have been deposited in a restricted marine lagoon.

#### **3.3.5.8. Facies 21: *Diplocraterion*-dominated interbedded shale and sandstones**

**Sedimentologic Characteristics:** Bioturbated fine-to upper-fine grained sandstone of F 21 is another distinctive unit within FA4. It commonly has gray, light to dark brown, and reddish-brown coloring with vertical burrows (Fig. 61b). It consists dominantly of sandstone, with minor shale interbeds. F21 overlies tidal flat facies (mixed and mud flat) and is overlain by sand flat sandstones (Fig. 61a). It ranges in thickness from 0.1-0.4 m. In many cases the succession fines upwards, but it is truncated by other coarser facies. Bedding is often difficult to observe in the shale layers, but when interlaminated with fine sandstone the bedding is observed to be planar. Local lenticular to wavy bedding is also observed.

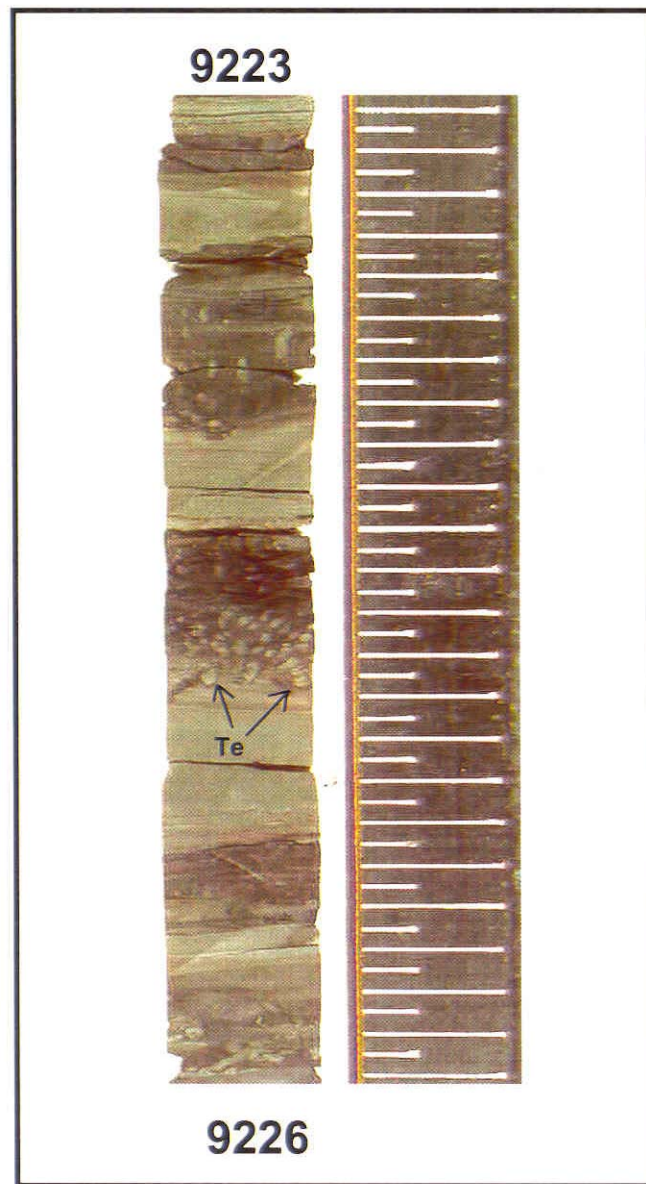


Figure 60: Facies 20-*Teichichnus*-dominated mudstone.  
SFE # 3, 9223-9226 ft., Te = *Teichichnus*. Right scale is 3 feet.



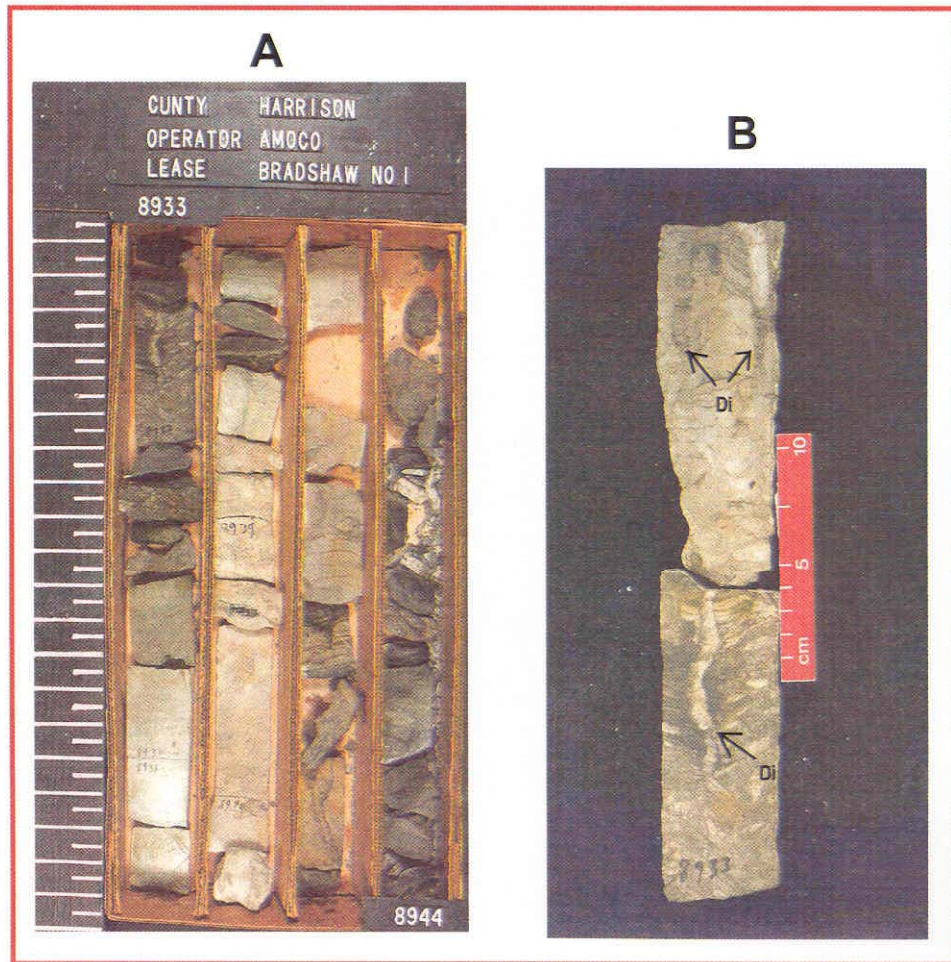


Figure 61: Facies 21-*Diplocraterion*-dominated interbedded shale and sandstone. This facies is interbedded with tidal flat deposits as in A. B: BSH # 1, 8933 ft. Di= *Diplocraterion*. Left scale is 3 feet.

**Ichnological characteristics:** Bioturbation is generally sparse but may be locally abundant. Typical diversity in these areas is low and typically consists of monospecific assemblages. *Diplocraterion* dominate the trace fossil assemblage of this unit. Other traces include *Planolites* and *Teichichnus*.

**Interpretation:** Facies 21 displays characteristics that are consistent with a quiescent environment with little influence of current energy. Physical sedimentary structures indicate that the primary current shaping these sediments was likely tidal in origin. Lenticular and wavy bedding are often intimately associated with tidally influenced deposits. The low diversity and monospecific nature of biogenic traces in Facies 21 indicates brackish-water conditions. This facies may have been deposited in a tidal flat or tidally influenced bay. Close association of this facies to mud flat deposits supports the tidal flat interpretation.

#### **3.3.5.9. Facies 22: Dark gray to black oyster-rich mudstone**

**Sedimentary characteristics:** F22 is fossiliferous limestone containing abundant thick-shelled pelecypod fragments which closely resemble oysters in morphology (Fig. 62). The matrix is composed chiefly of micritic calcite with lesser amounts of silt and clay. Most bioclasts show excellent preservation and shells have retained their delicate ornamentation. This facies vary in thickness between 0.5-3.5 m and commonly overlies F13 sandstones and all facies in Facies association 4 and is overlain by marsh deposits and soil horizons.

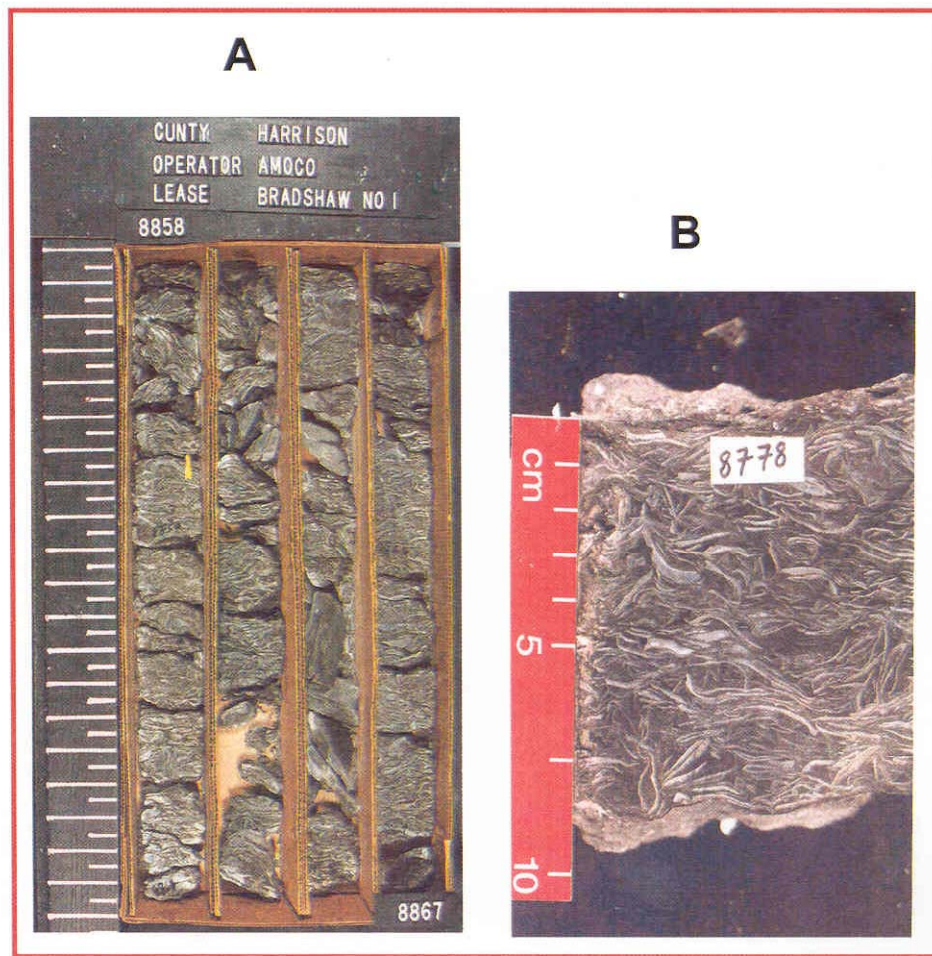


Figure 62: Facies 22-Dark grey to black oyster-rich carbonate mudstone. Most bioclasts show excellent preservation and remain articulated. A: BSH # 1, 8858-8867 ft. B: JH # 3, 8778 ft. Left scale is 3 feet.

**Ichnological characteristics:** Physical sedimentary structures and bioturbation may have been obliterated by the abundance of shell fragments.

**Interpretation:** F22 is interpreted to have been deposited in a lagoon in which fine-grained carbonate was being generated.

#### **3.3.5.10. Facies 23: Intensively bioturbated muddy sandstone/silty mudstone**

**Sedimentary characteristics:** F23 is a yellowish-orange and gray, massive to highly bioturbated, clayey sandstone and silty mudstone (Fig. 63). Oxidized sediments dominate with large burrows and root traces. The unit is 10 feet thick and commonly caps all facies in Facies association 3.

**Ichnological characteristics:** Roots are dominant, and trace fossils are difficult to identify.

**Interpretation:** Facies 23 is a well-developed soil horizon produced during prolonged subaerial exposure. The dominance of oxidized sediment indicates subaerial exposure. The soil horizon masks the original depositional features and structures, which makes a paleoenvironmental interpretation difficult.

#### **3.3.6. Net sand maps**

Net-sand maps are used to identify sand-body geometry and distribution; information used to interpret depositional history. Figure 64 shows a compiled net sand map for all of the sequences. It shows strike-oriented sand body geometry with maximum thickness of 700 ft (212 m). Yellow areas reflect the depocenters at the time of the Cotton Valley deposition.





Figure 63: Facies 23-Soil horizon shows a mix of silt, sand and mud with abundant roots (R) and carbonaceous matter (C). JH # 3, 8541 ft.

Net-sand maps are also constructed for all of the system tracts in different sequences (Figs. 65-74) including the highstand system tracts and the overlying transgressive system tracts (Ah, Bt, Bh, Ct, Ch, Dt, Dh, Et, Eh, and Ft). No core was available from the lowstand systems tract in the study area.

Eleven net sand isopach maps were constructed for the various system tracts. Net-sand maps can be divided into two groups. The first group is for HST system tracts where the netsand thickness is measured in the interval between the lowermost sequence boundary and the lower MFS. And the second group is the TST and the net sand thickness is measured between the sequence boundary and the next younger MFS.

#### **3.3.6.1. Net sand maps of Ah, Bh, Ch, Dh, and Eh**

The highstand systems tract net-sand maps (Figs. 65, 67, 70, 72, and 74) display thick strike-elongated sandstone bodies trending north east-southwest. The thickness of the sand bodies decreases upward from Ah to Eh. The average thickness ranges between 180 ft (60 m) and 100 ft (30.3 m). The overlying TST net-sand isopach maps also exhibit trends aligned parallel with depositional strike, but TST sandstone bodies do not exceed 100 ft (30.3 m) thick. The overall gross-thickness and net sand thickness in the highstand system tract is much greater than in the transgressive system tract.



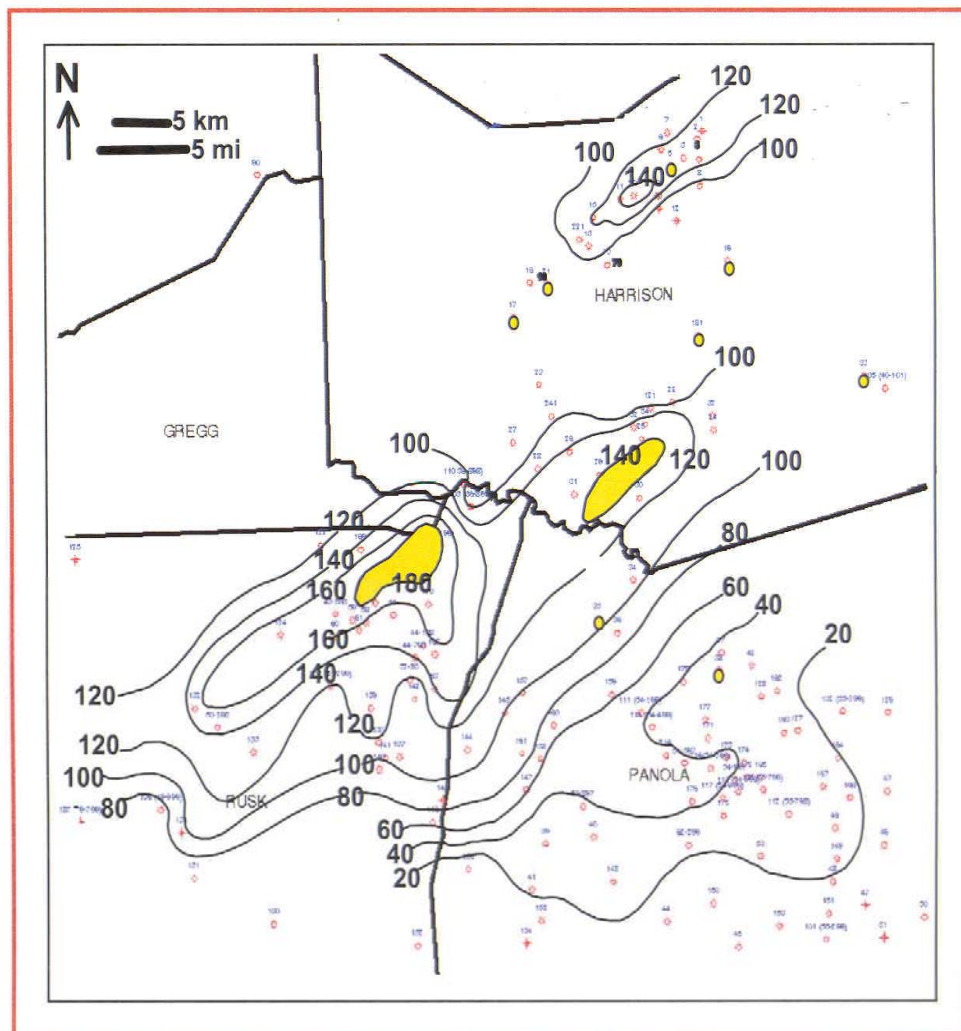


Figure 65: Net sand map of Ah system tract shows strike-oriented sand bodies. Major “thicks” range from 140 to 180 ft (yellow areas). Contour interval is 20 ft.



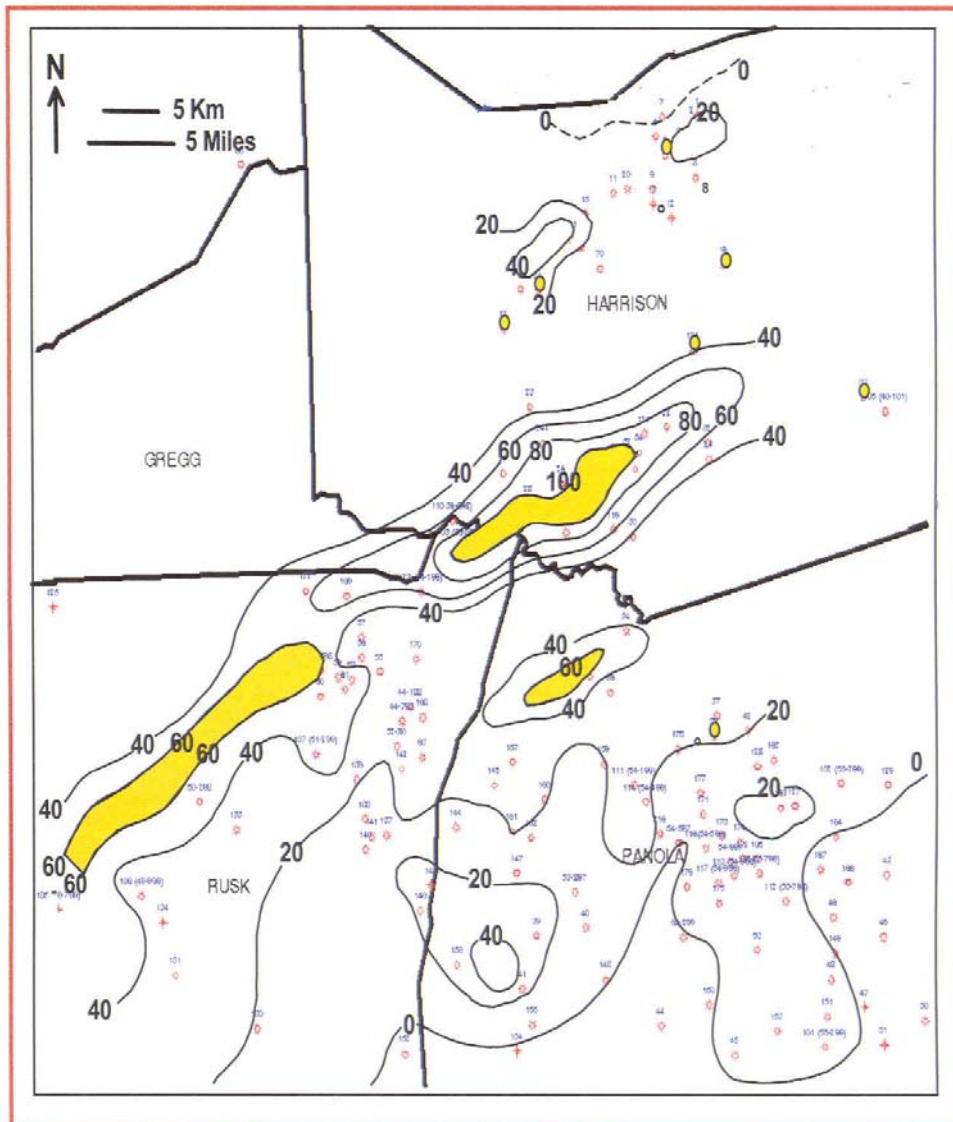


Figure 66: Net sand map of Bt system tract shows strike-oriented sand bodies. Major “thicks” range from 60 to 100 ft (yellow areas). Contour interval is 20 ft.

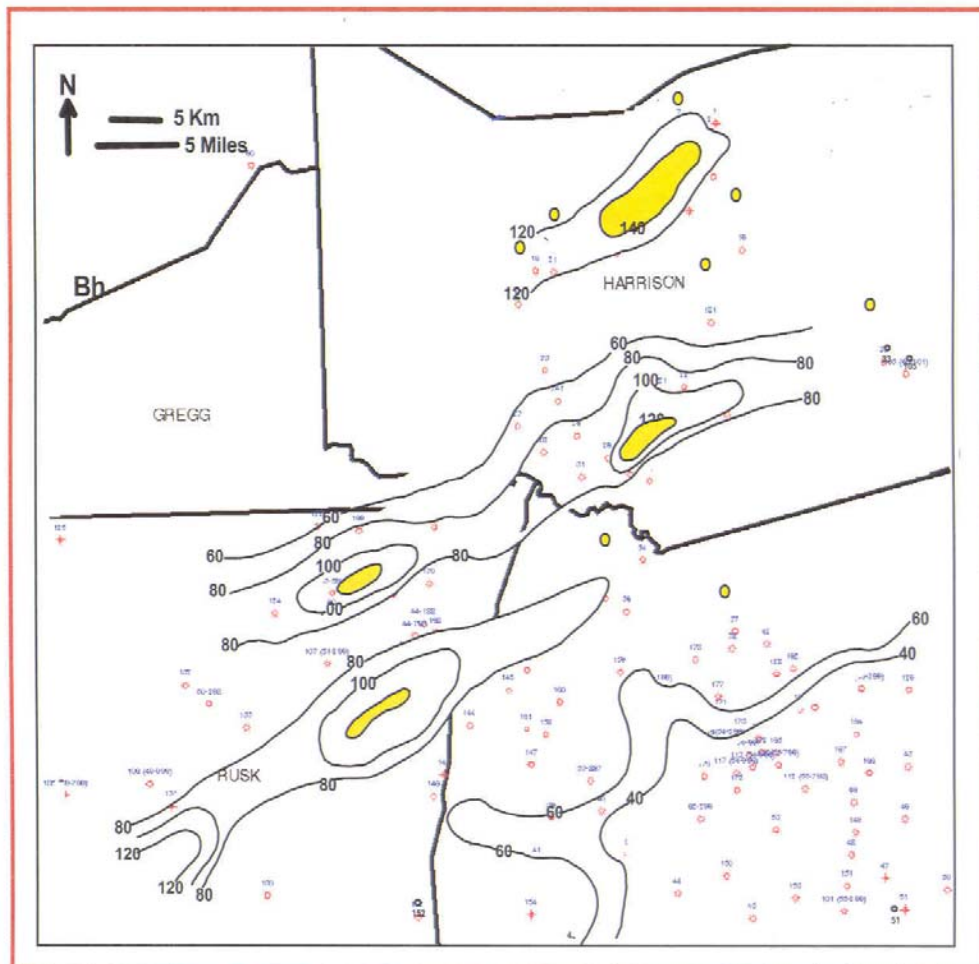


Figure 67: Net sand map of Bh system tract shows strike-oriented sand bodies. Major “thicks” range from 100 to 120 ft (yellow areas). Contour interval is 20 ft.

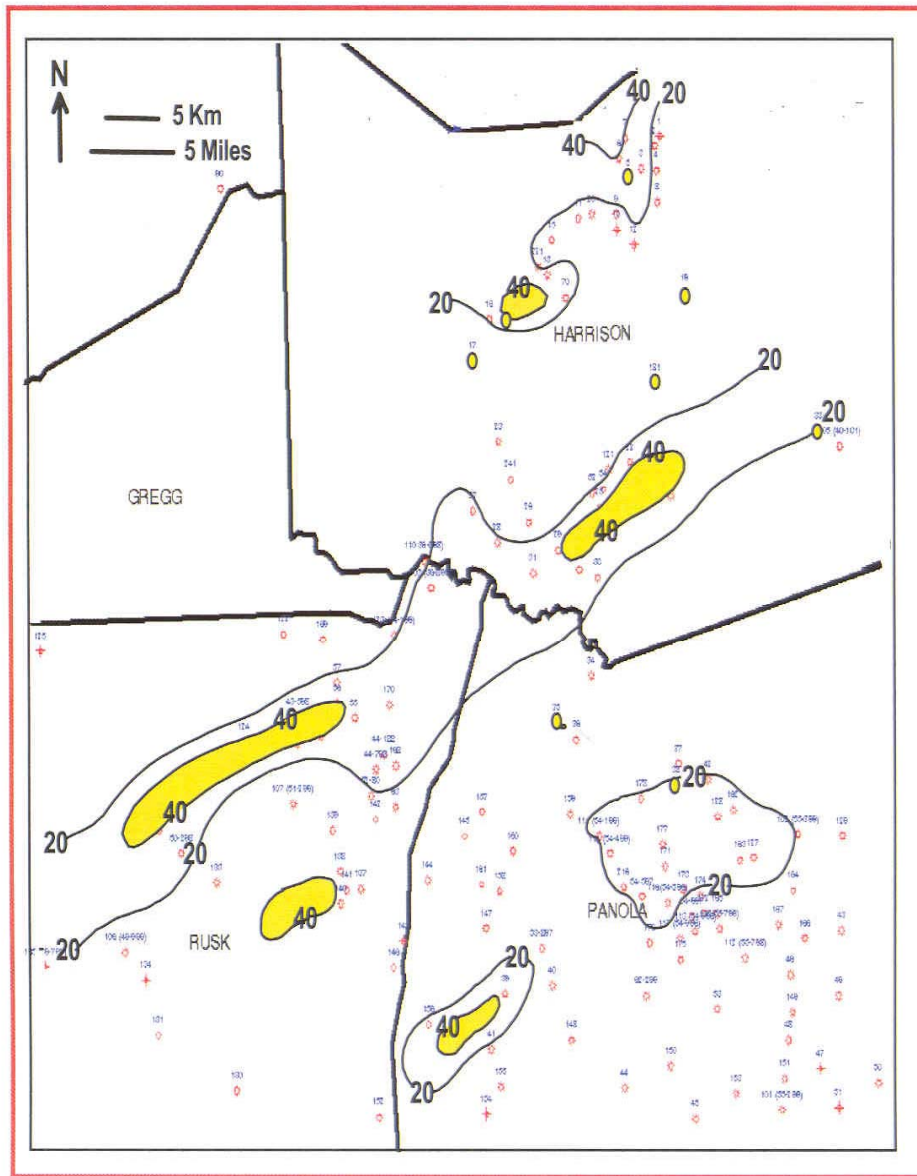


Figure 68: Net sand map of Ct system tract shows strike-oriented sand bodies. Major “thicks” range from 40 to 60 ft (yellow areas). Contour interval is 20 ft.

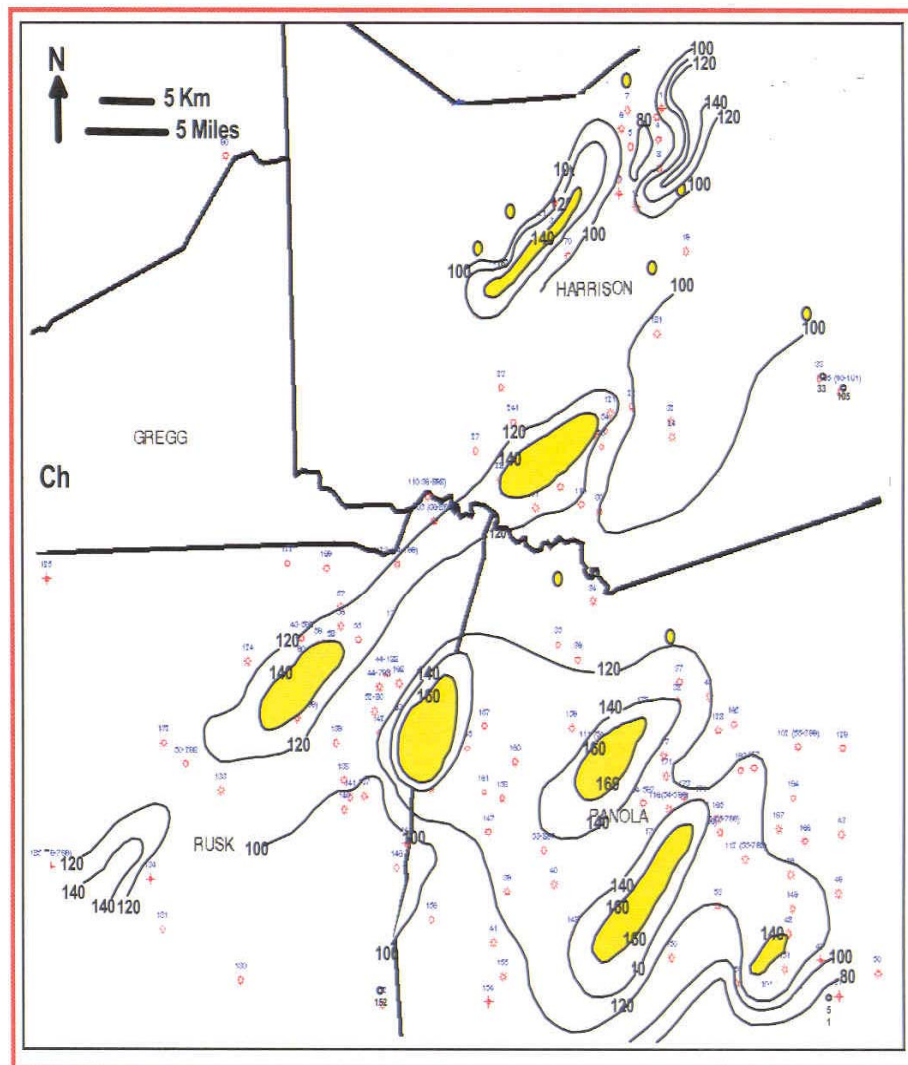


Figure 69: Net sand map of Ch system tract shows strike-oriented sand bodies. Major “thicks” range from 140 to 160 ft (yellow areas). Contour interval is 20 ft.

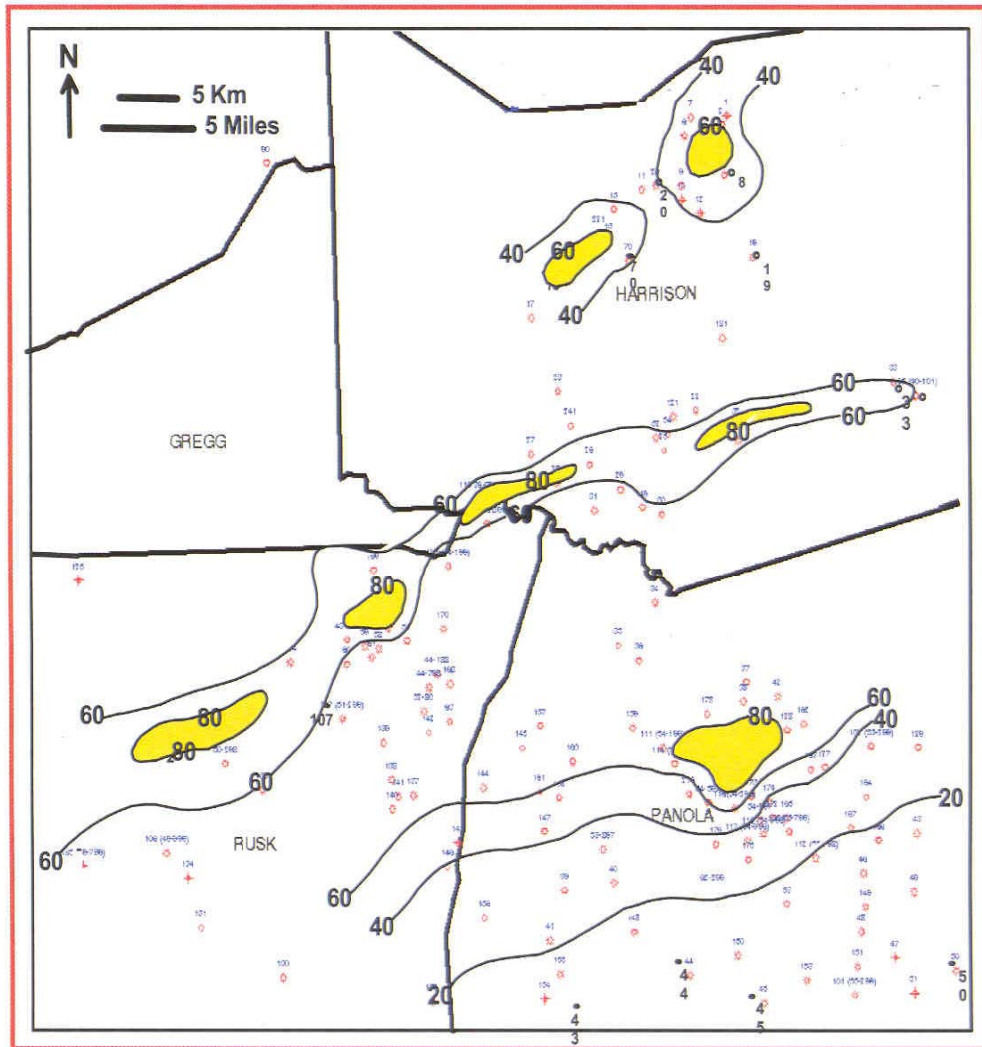


Figure 70: Net sand map of Dt system tract shows strike-oriented sand bodies. Major “thicks” is 80 ft (yellow areas). Contour interval is 20 ft.



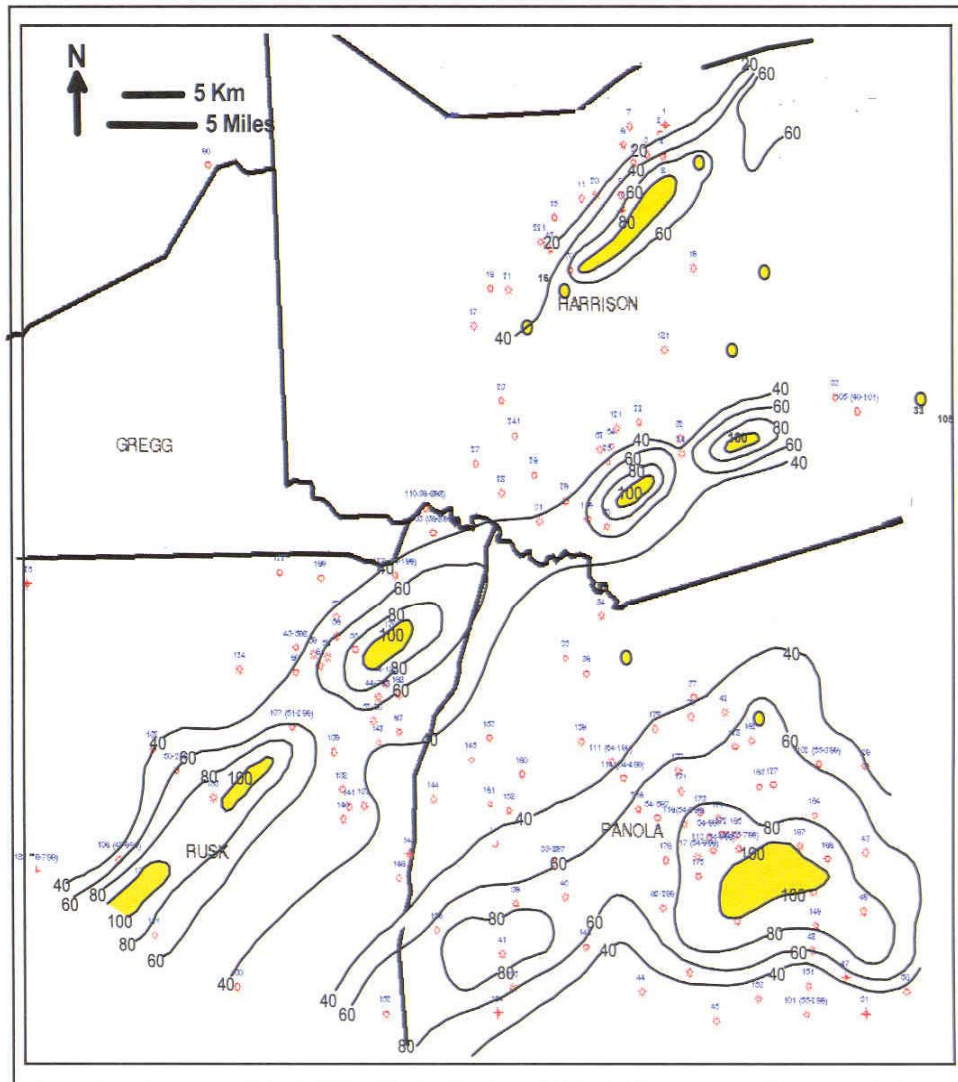


Figure 71: Net sand map of Dh system tract shows strike-oriented sand bodies. Major “thicks” range from 80 to 100 ft (yellow areas). Contour interval is 20 ft.

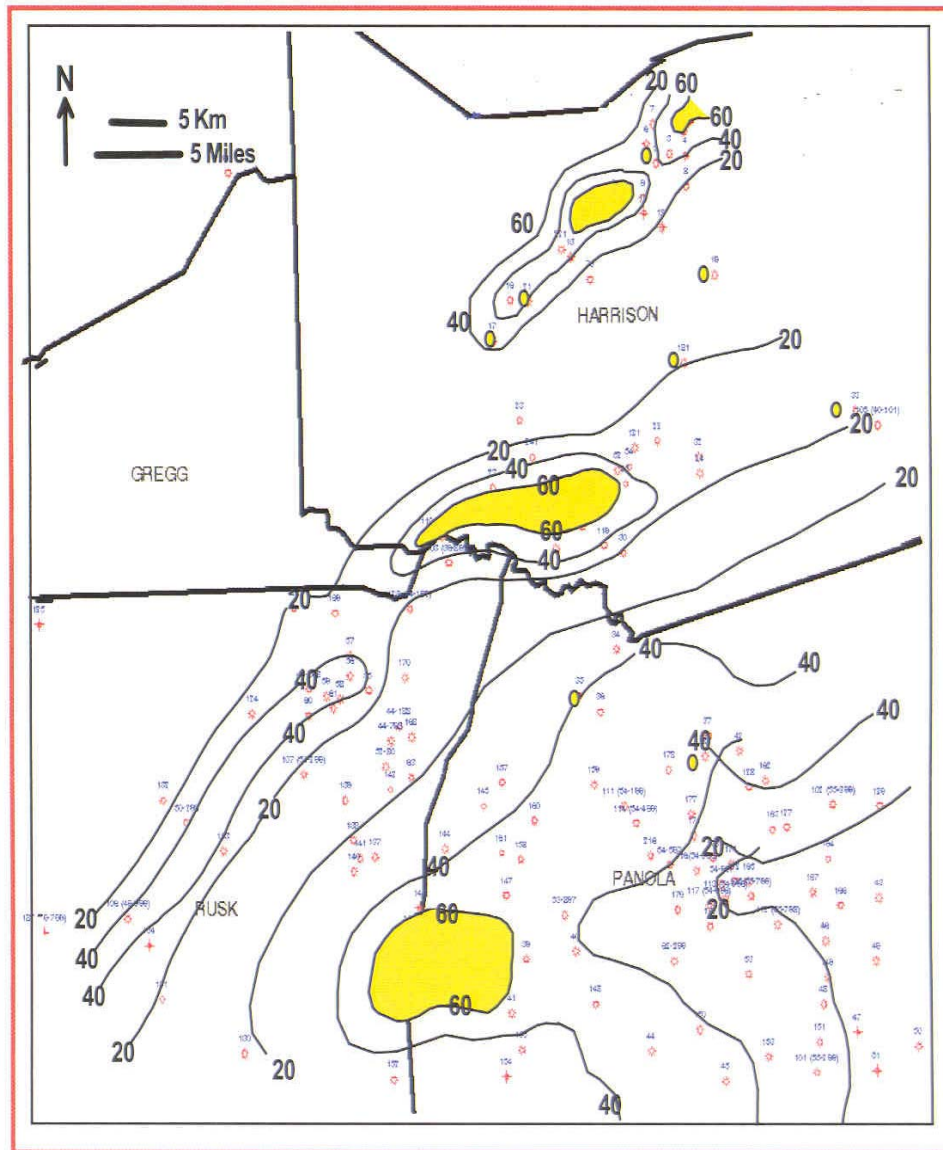


Figure 72: Net sand map of Ah system tract shows strike-oriented sand bodies. Major “thicks” range from 40 to 60 ft (yellow areas). Contour interval is 20 ft.

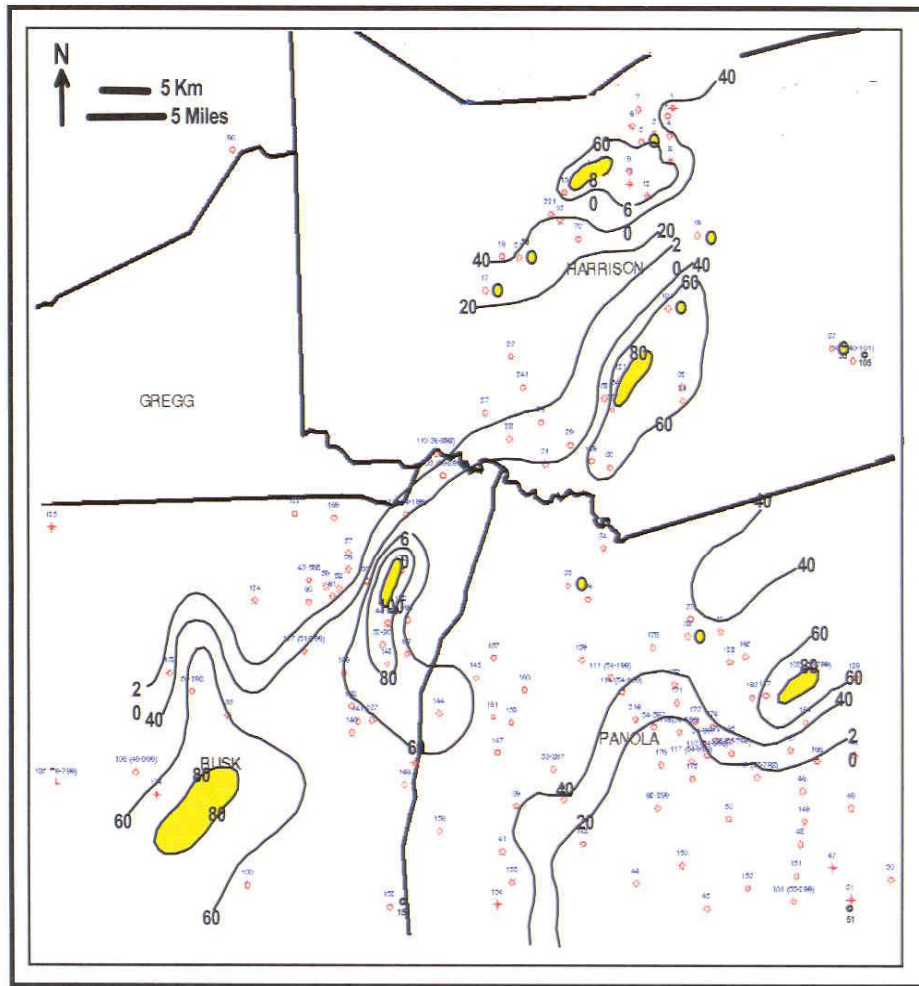


Figure 73: Net sand map of Eh system tract shows strike-oriented sand bodies. Major “thicks” are 80 ft (yellow areas). Contour interval is 20 ft.



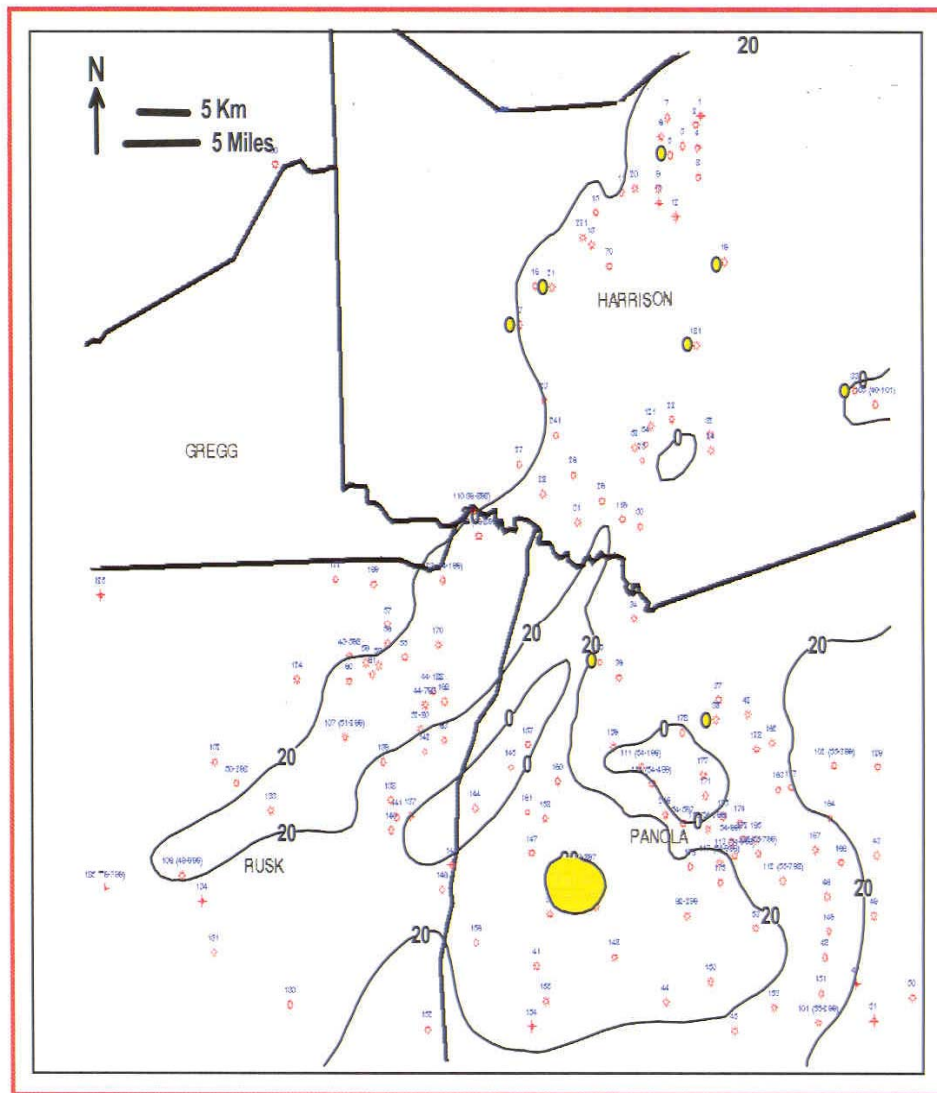


Figure 74: Net sand map of Ft system tract shows strike-oriented sand bodies. Major “thicks” is 20 ft (yellow areas). Contour interval is 20 ft.

### **3.3.6.2. Net sand maps of Bt, Ct, Dt, Et, and Ft**

Net sand maps of the TST exhibit strike-oriented sand bodies that range in thickness from 100 ft (30.3 m) in Bt to 60 ft (19 m) in Et (Figs. 66, 69, 71, 73, and 74). The netsand map of Ft does not show any particular trend and the maximum sand thickness is 35 ft (10.6 m). The thickness of the sand decreases basinward and landward. This facies represent complex coastal marine deposits.

The tendency of the strike-oriented sand body to occupy the same position along A-A trend reflect stability of shoreline which is most probably structurally controlled. A close relationship is observed between major thicks of the pre-existing highstand system tract sediments and the respective overlying transgressive systems tract sandstones. TST barrier-island sandstones are consistently deposited directly above net sand “thicks” of the underlying highstand system tract. Redeposition of the underlying highstand system tract and lowstand system tract sediments contributed to the volume of sediments deposited in the overlying barrier systems of the transgressive system tract.

Reineck and Singh (1968) indicated that reworked sediments contributed to approximately 50% of the sediments deposited along transgressive shorelines. Therefore, based on the relationship of the transgressive system tracts with the underlying highstand system tracts, it appears that a major sediment contribution was remobilized from underlying sediments from beneath the transgressed surface during Cotton Valley time.

### 3.4. Interpretation of the depositional environments of the Cotton Valley Sandstones

Based on the previous discussion about the various lithofacies observed in the cores, abundance of fully marine trace fossils, and strike-oriented sand body geometry, the CVS is interpreted to have been deposited in barrier island-lagoon-shelf systems. Figure 75 shows an example of the lower CVS in Blocker # 1 well. This interval represents coarsening- and shallowing-upward seaward prograding barrier islands followed by shelf flooding or marine transgression over the shoreface. Oyster lag is part of the transgressive episode.

The middle CVS interval (Fig. 76) shows well developed, thicker barrier island shorefaces deposited in lower energy than the lower Cotton Valley and have stepped out into the inner shelf. Bioturbated *Ophiomorpha*-dominated and cryptobioturbated shorefaces which are dominant in the middle CVS show the best reservoir characters.

The upper part of the CVS (Fig. 77) shows much evidence of back barrier bay-fill and lagoonal deposits. The maximum marine regression in the upper Cotton Valley is marked by marsh and root grounds. The lowermost sandstones of the upper Cotton Valley, which look similar ichnologically as well as sedimentologically to the shoreface deposits in the lower and middle CVS, are interpreted as subtidal parts of flood tidal deltas which prograded landward into bay mud.

Net sand maps of most of the TST demarcate mesotidal barrier-lagoon systems. The barrier-islands strike NNE-SSW. Tidal-inlet channels associated with flood-tidal delta interrupt the barrier systems. Due to lack of well control points, it is difficult to document the presence of tidal inlets and flood tidal deltas in the maps. However, they

are recognized in cores. The Bt (Fig. 66) net sand map is made up of three primary components; a barrier-island located on the basinward edge of a lagoon and tidal-inlet channels that connect the lagoon with marine shelf deposits. The zero sand-line is located to the southeast of the map area and delineates a sand pinchout. Sparse well control in the northwest corner of the mapped area did not allow the proximal system or landward part to be mapped.

The barrier islands are interpreted to have been mesotidally influenced. This interpretation is inferred on the presence of short barriers with tidal flats and tidal marshes, and recognition of large numbers of tidal inlets in cores. The average net sand thickness of the barriers is 70 ft (21m). The tidal inlets are closely associated with the barrier island sand bodies. Flood tidal deltas and washover fans are interpreted from cores.

The outer banks of North Carolina are believed to be a present-day analogue for the CVS transgressive depositional system (Fig. 78). The occurrence of large back-barrier bays, flood deltas, oysters and marshes in the landward margins of the bay support this interpretation. Moreover, flood tidal deltas building into fully marine waters with water depths 20-40 ft (6.5-13.5 m) (Fig. 79) and fringes of the deltas resemble lower shoreface ichno-assemblages (Elshayeb and Henk, 2003; and Henk and Elshayeb, 2004). The barrier island profile along the outer bank of North Carolina (Figs. 80 and 81) is very similar to that interpreted for the CVS barrier-shorefaces profile. No beach or dune deposits are preserved in the CVS, but they were likely eroded during marine transgression (Henk and Elshayeb, 2004).

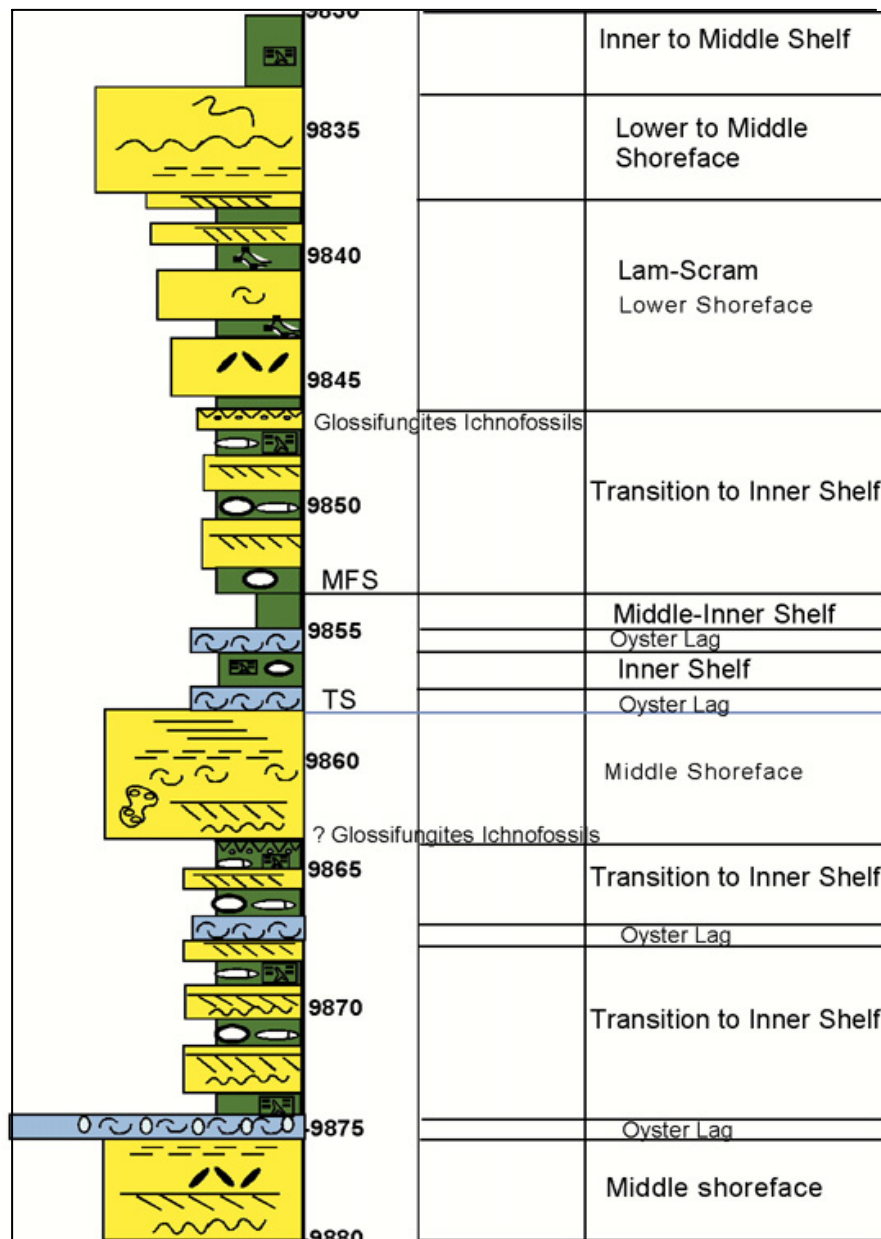


Figure 76: Example of the lower CVS composed of shelf and shoreface deposits. See figure 18 for explanation of symbols.

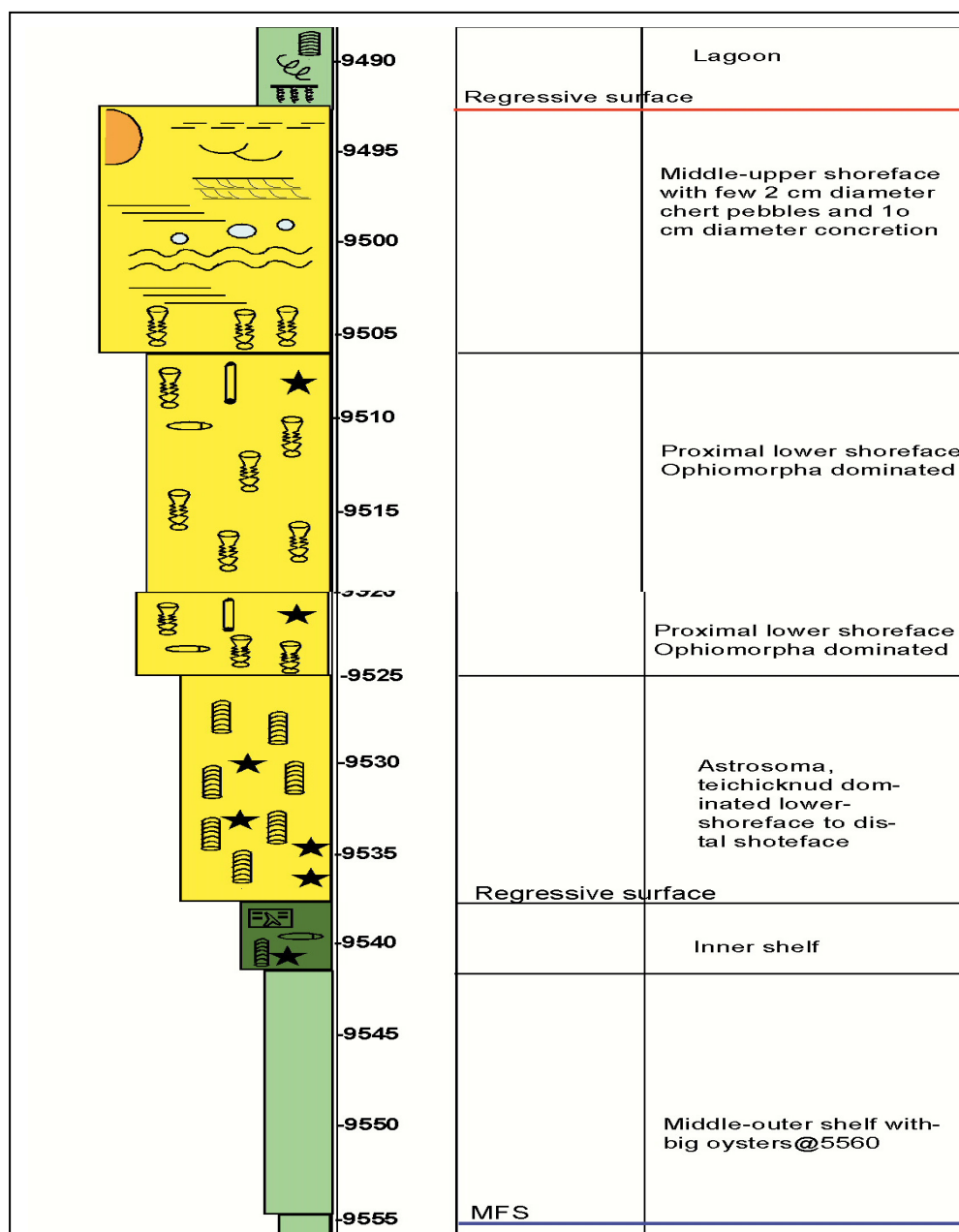


Figure 77: Example of middle CVS showing well-developed, highly bioturbated shoreface and shelf deposits. See figure 18 for explanation of symbols.

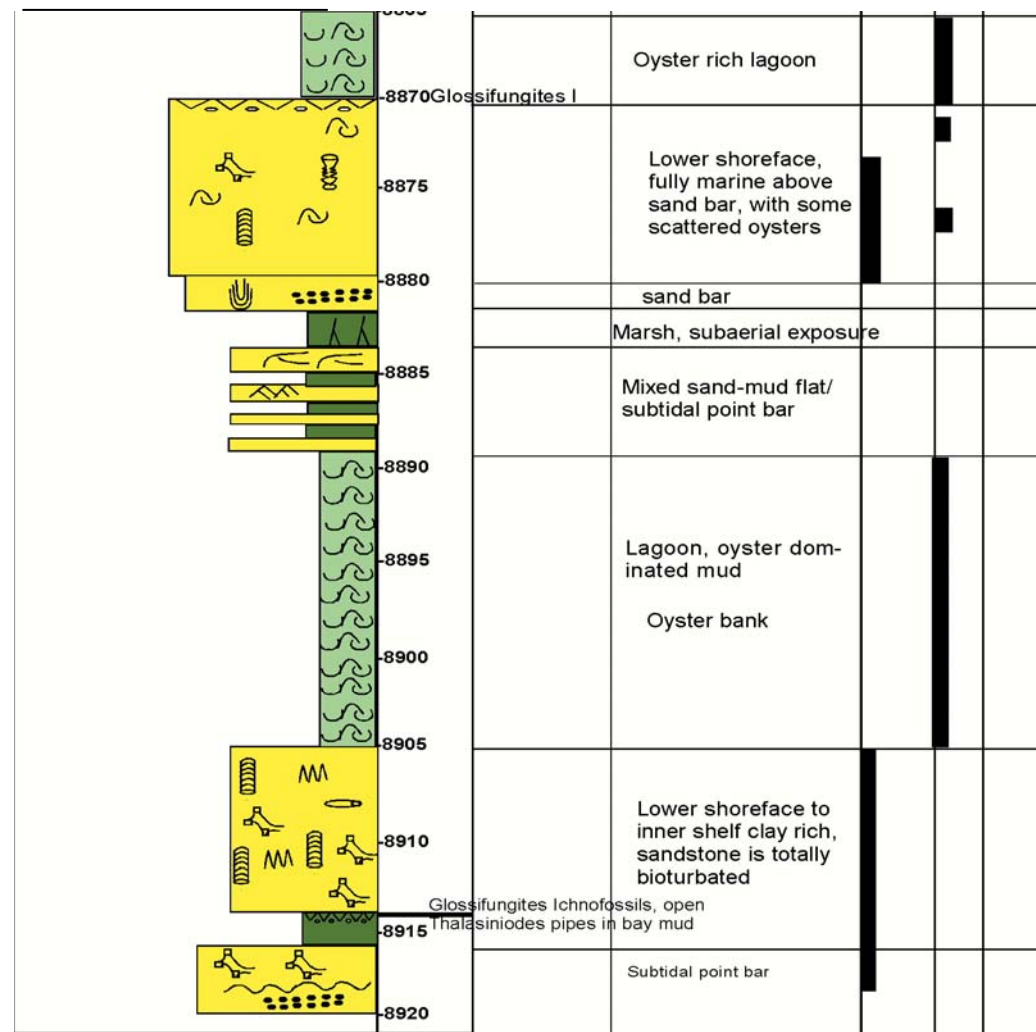


Figure 78. Example of the upper CVS showing coastal plain deposits. See figure 18 for explanation of symbols.





Figure 78: Photo shows North Carolina outer with well developed barrier island, large back barrier and flood tidal deltas. (From Henk and Elshayeb, 2004).

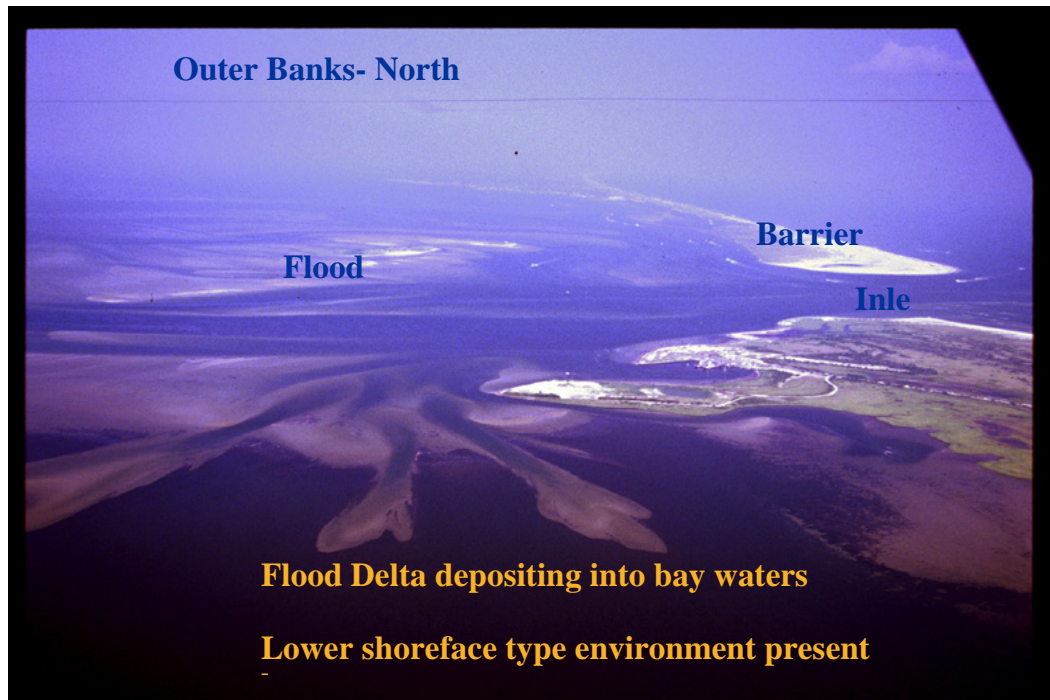


Figure 79: Photo shows the back barrier of North Carolina outer bank. Note flood tidal delta deposits in bay and lagoon mud. (From Henk and Elshayeb, (2004).

## Outer bank - North Carolina



Figure 80: Present-day facies distribution along the North Carolina barrier islands. (From Henk, 2004).

# Grace Lowry # 1

Amoco

9480-9565 ft

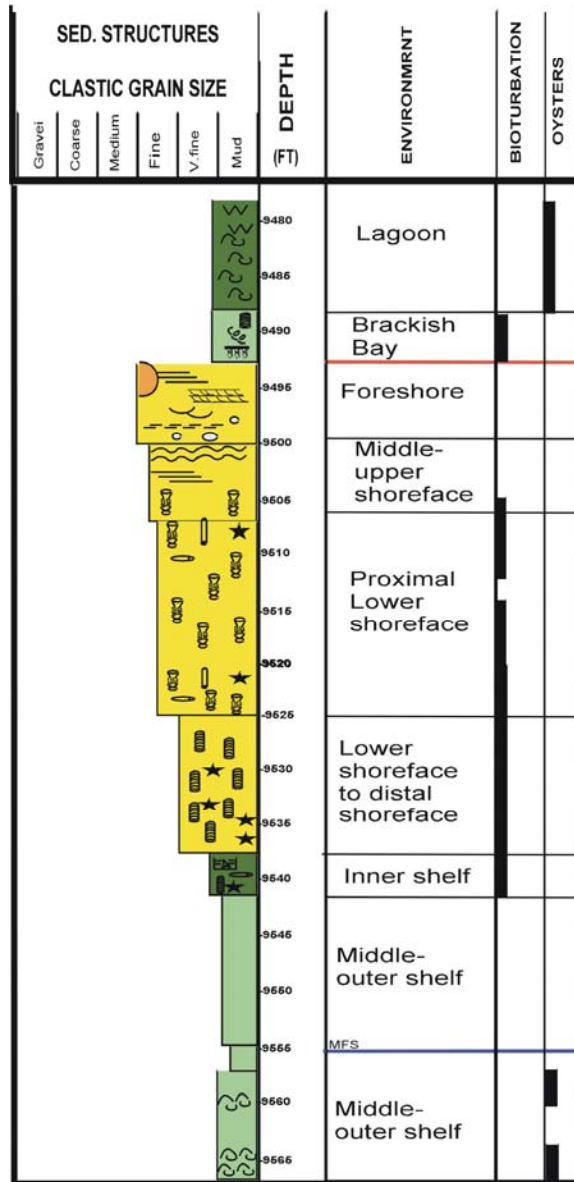


Figure 81: Succession of facies through Cotton Valley Formation in the Lowry well no. 1. In this location the entire depositional sequence has been cored.

### **3.5. Barrier Island Formation**

There has been much debate regarding the formation of barrier island systems. The origin of barriers has been attributed to at least three distinct mechanisms (Hoyt, 1967; Swift, 1975; Wilkinson, 1975): 1) vertical growth and emergence of offshore bars, 2) longshore spit growth across an embayment, and 3) flooding of coastal lowlands behind former beach ridges. These mechanisms of barrier formation are effective in either stillstand or transgressive settings. However during relative sea level fall, the back barrier portion quickly fills in and the advancing shoreline takes the form of a strand-plain (Roy et al., 1994). Galveston Island is the most extensively studied modern progradational barrier island. However, the lagoon in Galveston Island was formed during an overall transgression of the shoreline (Morton, 1979). Currently, a global rise in relative sea level and coastal subsidence are the only known processes that allow the maintenance of a lagoon.

### **3.6. Discussion and other alternatives**

The depositional environments of the CVS in the East Texas Basin are interpreted by many authors who studied different gas fields. Most of them agreed on the marine-shoreline setting for the CVS. Dutton et al. (1992) interpreted CVS in Waskom field (Harrison County) as marine-shoreline deposits including: 1) shoreface; 2) microtidal barrier island; 3) lagoon and washover; 4) tidal inlet; and 5) marsh and lagoon. This interpretation is compatible with my interpretation, however, their interpretation for the microtidal barrier island was based on only one core from well SFE # 3 (Cargill well no. 15).

Varva et al. (1990) interpreted the depositional environment of the CVS (Taylor) in the Oak Hill field, Rusk County (northeast Texas) as barrier island with back-barrier, foreshore and inner shelf subenvironments. The authors's interpretation was based on a study of 5 cored wells. They identified two barrier island complexes, each of which was terminated by a marine transgression that reworked the upper portion of the complex. This interpretation fits with my interpretation and supports the barrier island-shelf model.

Black and Berg (1987) interpreted the lower Cotton Valley Group in Kildare field, northeast Texas as a distal part of fan delta. The authors divided the Cotton Valley Group into three main facies; 1) beach facies of massive to laminated sandstone; 2) channel facies of conglomeratic sandstone; and 3) an offshore sandstone and interbedded black shales. The authors did not report any kind of bioturbation in any of their facies and reported that wave action was dominant at time of deposition. Fan delta deposits were not present in my study area. Presley and Reed (1983) reported that facies within Cotton Valley group grade from terrestrial in the north to marine in the south. In the central and southern parts of the East Texas Basin, deltaic and shoreline systems of the Cotton Valley Sandstone grade southward into offshore Bossier shales and limestones.

Bailey (1983) interpreted the upper part of the Cotton Valley in Harrison, Rusk and Panola counties, East Texas Basin, as wave-dominated deltaic and shallow marine deposits. The author also reported that the deltaic deposits of the upper Cotton Valley resemble the deposits of barrier/lagoon systems. He identified facies very similar to those interpreted in the current study, but he lists distributary channel and intensely



bioturbated channel-mouth bar facies. The distributary channels interpreted by Bailey (1983) could also be interpreted as stacked tidal inlets. The high rate of deposition at a channel mouth bar makes it a much stressed environment for organisms to live and results in rare bioturbation. The high diversity and intensity and large size of the fully marine trace fossils within the studied sandstones rules out the channel mouth bar interpretation. I believe these sandstones are parts of the barrier island shorefaces.

Eubanks (1986) interpreted the Cotton Valley Terryville sandstones in Carthage field, Panola County, as the product of a prograding fluvial-wave influenced delta. The author recognized distributary channel, mouth bar, distal bar, prodelta shale and shoreface sandstone deposits as the major facies. He also reported that isopach maps of the major sandstone bodies indicated distributary mouth bar deposits trend parallel and normal to depositional strike and distal bar deposits and shoreface deposits trend parallel to strike. Although I disagree with Bailey (1983) and Eubanks (1986) on their interpretation of distributary channel and channel mouth bar facies, I believe that a wave-dominated delta is an acceptable model for the highstand/or lowstand sediments of the CVS.

In the current study the barrier island model is the best fit for the sediments in the transgressive system tracts. In the highstand system tracts, stacked shorefaces with marine flooding shales in-between are recognized. These strike-oriented sand bodies prograded seaward and show no evidence of lagoonal facies. These shoreface sediments may be part of a big wave-dominated deltaic system or strand plain. There is not enough data to favor one interpretation over another. During formation of the lowstand system

tract, there should have been some active fluvial systems. It is difficult to explain the occurrence of cobbles and pebbles in the CVS without involving fluvial input. Moreover, the presence of slope fan and basin floor fan (with considerable amounts of sand) indicates that fluvial systems at that time were heavily loaded with sediments. So, small or large deltas may have been formed during lowstand and highstand times.

On the other hand, the absence of any fluvial deposits in more than a mile of cores (especially the high stand system tracts), the occurrence of large diversity of fully marine trace fossils, and the strike-oriented sand body geometry indicate strong marine influence on these sediments. Any deltas that formed were apparently completely reworked by wave action as well as intensively bioturbated by marine organisms.

Although a wave-dominated deltaic system might be a good interpretation for the high stand/or lowstand sediments, more data are required to verify that interpretation. The Ouachita Mountains and Arbuckle Mountains, located north and northwest of the study area, are most probably the main source of sediments for the Cotton Valley Sandstones.



## **CHAPTER 4**

### **PETROGRAPHY AND DIAGENESIS**

#### **4.1. INTRODUCTION**

The main goal of this chapter is to identify and quantify the main diagenetic processes affecting reservoir quality, and to reconstruct the diagenetic evolution of Cotton Valley Sandstones throughout their burial. Because of the availability of large amount of cores throughout the basin (4300 feet, 1310.6 m), the Cotton Valley offers a superb opportunity for evaluating diagenetic evolution within the same unit through time at different depths. The success of massive hydraulic fracturing redefined the porosity-permeability cutoff for economic reservoirs, so that companies now explore and produce gas from formations which were once uneconomic. Vertical and lateral variation in porosity and permeability values within the Cotton Valley Sandstones are related to original depositional environment and subsequent diagenesis.

Diagenesis has altered the original composition of the sandstone and modified the porosity and permeability through mechanical compaction, cementation, and dissolution and authigenic clay precipitation. The relative timing of the various diagenetic processes was determined as well as the relative importance of compaction versus cementation in loss of porosity with depth. Quartz overgrowths and carbonate cements are the most significant authigenic phases that controlled the petrophysical properties of the Cotton Valley Sandstones. Major local sources of silica for quartz cement are intergranular

pressure solution and stylolites. The relative importance of these sources was quantified.

The Cotton Valley Sandstones I studied were deposited in a shallow marine setting and are divided into many facies and facies associations (see chapter 3). Hence, they present a commendable chance for empirical analysis, focusing upon the effect of depositional environment on diagenesis and reservoir quality. Only potential reservoir facies were selected for this analysis, including sandstones in the various types of shorefaces and sand flat.

#### **4.2. Sandstone architectural components**

In the following section, the four architectural components of a sandstone, framework grains (F), matrix (M), cement (C), and porosity are described in that order. Sandstones were selected from different facies including, bioturbated-*Ophiomorpha*-dominated shoreface, cryptobioturbated shoreface, laminated shoreface, tidally influenced shoreface, and storm-dominated shoreface. Sandstones from the sand flat were also selected to represent the possible reservoir rock in the back-barrier setting. The overall average sandstone architecture for the Cotton Valley Sandstones is  $F_{70.5}M_{4.5}C_{19.9}P_{5.1}$  (Table 2). Facies from different depositional environment exhibit some variation in architecture and composition. Framework grains are mainly quartz, feldspars, and a variety of rock fragments and heavy minerals. The framework composition varies between 63.5% in the storm dominated shoreface and 76.5% in the cryptobioturbated shoreface. Matrix is essentially dispersed detrital clay. Sandstones from the bioturbated shoreface and the tidally influenced shoreface facies have the highest average of clay matrix (7% and 5% respectively) and the storm-dominated

shoreface sandstones are cleaner with an average of 2%. Cryptobioturbated, laminated shorefaces and sand flat sandstones have an average matrix content of 4%.

Authigenic minerals in the Cotton Valley Sandstones occur as pore filling and grain-replacement phases. Quartz cement and calcite are the most significant authigenic phases; dolomite, kaolinite, illite, chlorite and minor amounts of anhydrite, feldspar, albite, and pyrite are also present. The highest percentage of total cement, 32% and 22.5%, occur in sandstones of the storm-dominated and laminated shorefaces, respectively. Cryptobioturbated sandstones have the lowest amount of cement (12%). Sandstones from the bioturbated *Ophiomorpha*-dominated shorefaces have an average cement of 13.5%. Sandstones from the tidally influenced shoreface and sand flat have an average cement of 19.5%.

Various types of porosity are observed in the Cotton Valley sandstones, including, intergranular, intra-granular, moldic, oversized, and micropores. Secondary porosity constitutes up to 75% of the total porosity, but averages 68.1%. Microporosity accounts for about 19% and primary porosity is about 6%. The cryptobioturbated sandstones show the highest average thin section porosity of 7.5% among the other facies. On the other hand, sandstones from laminated and storm-dominated shorefaces possess the lowest average porosity (4.5% and 2%, respectively). Causes for the variations in porosity and reservoir quality will be discussed in porosity reservoir quality sections.

Table 2: Sandstone composition in potential reservoir facies. F = framework grains, M = matrix, C = cement, and P = porosity. Values are percent of rock volume.

Facies	F	M	C	P
Bioturbated	73.0	7.0	13.5	6.5
Cryptobioturbated	76.5	4.0	12.0	7.5
Laminated	70.0	4.0	22.5	3.5
Tidal Shoreface	70.3	5.0	19.7	5.0
Storm shoreface	63.5	2.5	32.0	2.0
Sand Flat	70.0	4.5	19.5	6.0

### **4.3. Framework grain composition**

The sandstones are quartzarenite and subarkose and the present day average composition for the various facies is  $Q_{87.9}F_{10}R_{2.1}$  (Fig. 82). Diagenesis overprinted the original detrital composition through pervasive dissolution and/or replacement of unstable grains (feldspars and rock fragments). The effect of diagenesis on changing the sandstone composition and the restored composition will be discussed later on the diagenetic overprint on framework grains and restored composition section.

#### **4.3.1. Quartz**

Quartz grains are the predominant framework constituent in all of the studied sandstones. Point-count data indicate that quartz comprises from 85% to 91% (average 87.9%) of the framework constituents. Approximately 97% of quartz grains are single crystals (Fig. 83) with straight or slightly undulose extinction. Monocrystalline quartz grains with abundant vacuoles and vermicular chlorite are also observed. Polycrystalline quartz grains generally show more than five subcrystals with crenulated crystal boundaries, but some of them show polygonal crystal boundaries.  $\delta^{18}O_{SMOW}$  values of pure detrital quartz averages 13.5‰ (see quartz isotope section).

#### **4.3.2. Feldspars**

Feldspars range from 7 to 12% and comprise an average 10% of the framework components. Feldspar content was greater at the time of deposition because some feldspar has been lost by dissolution and replacement by carbonate and kaolinite. Textural evidence, such as partially dissolved and replaced feldspars, moldic pores, oversized pores and large carbonate cement patches indicate that original feldspar content

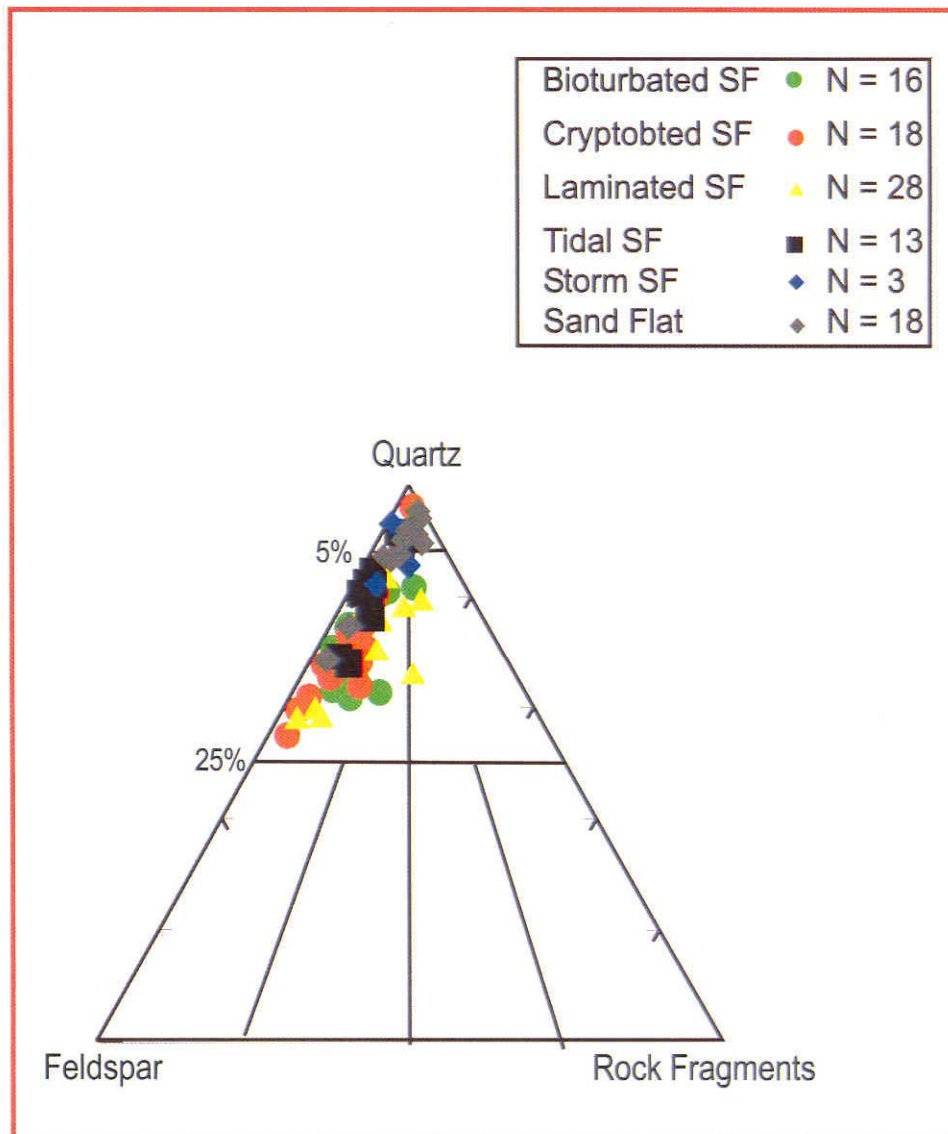


Figure 82: Framework grain composition of Cotton Valley sandstones, based on the classification of Folk (1980). Present-day composition of the sandstones is mainly subarkose and quartz arenites. N is the number of samples.

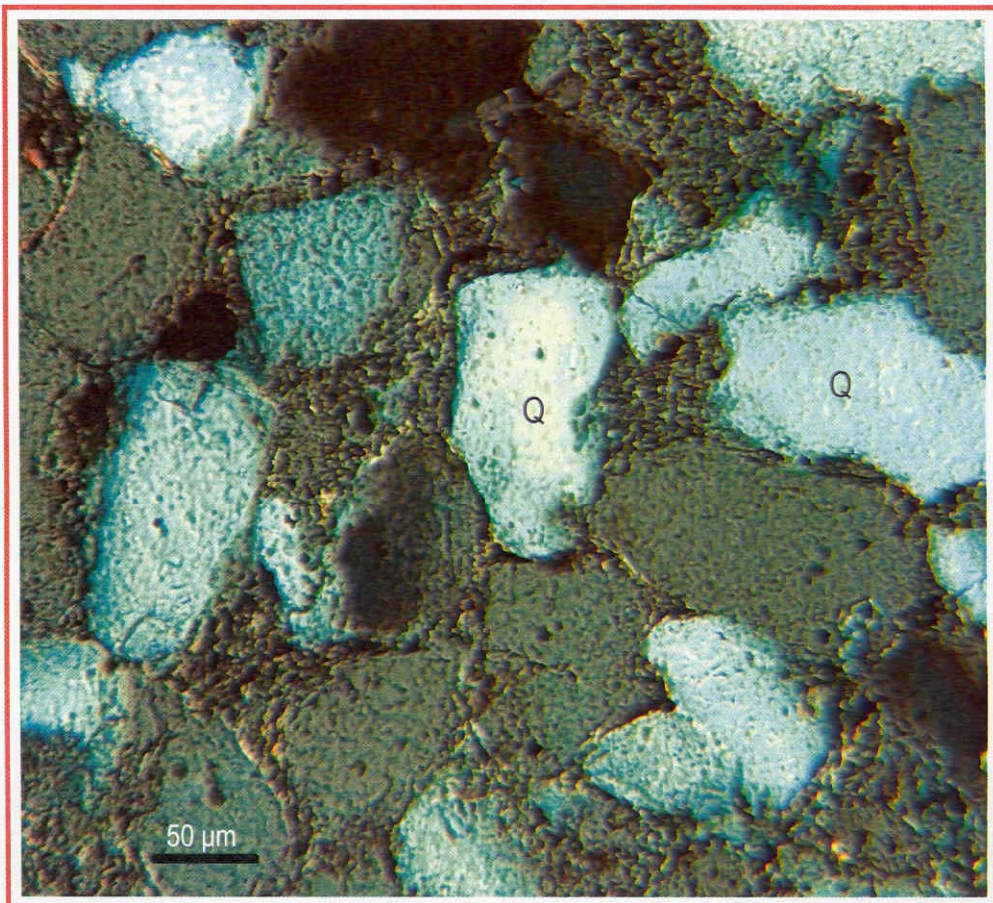


Figure 83: Thin section image showing monocrystalline quartz grains (Q) with straight extinction. BSH # 1, 8652 ft.

was much more abundant at time of deposition. Replaced feldspar grains (by calcite and/or kaolinite) ranges from 0 to 2.5% (average 1.5%) of the total feldspars. pure detrital quartz averages 13.5 ‰ (see quartz isotope section). Feldspar lost during diagenesis ranges from 4 to 8% (average 6.2%).

Two criteria are commonly used to differentiate between totally replaced feldspar grains and intergranular calcite cement: firstly, oversized patches of calcite cement, especially those that show a ghost of the original feldspar grain from the presence of insoluble residue (Fig. 84); secondly, calcite pseudomorphs, where the original feldspar grain boundary is outlined by an original grain coating.

The original abundance of feldspars was estimated as follows:

$$FO = K-f + P + OP/3 + MP/3 + IP + mP/2 + RC + RD + RK \quad (\text{Souza, 1999})$$

Where:

FO = original feldspar content

K-f = potassium feldspar

P = plagioclase

OP = oversized pores

MP = moldic pores

IP = intragranular pores

mP = micropores (visual microporosity that associated with feldspar replaced by kaolinite, not intergranular kaolinite cement).

RC = replacive calcite

RD = replacive dolomite



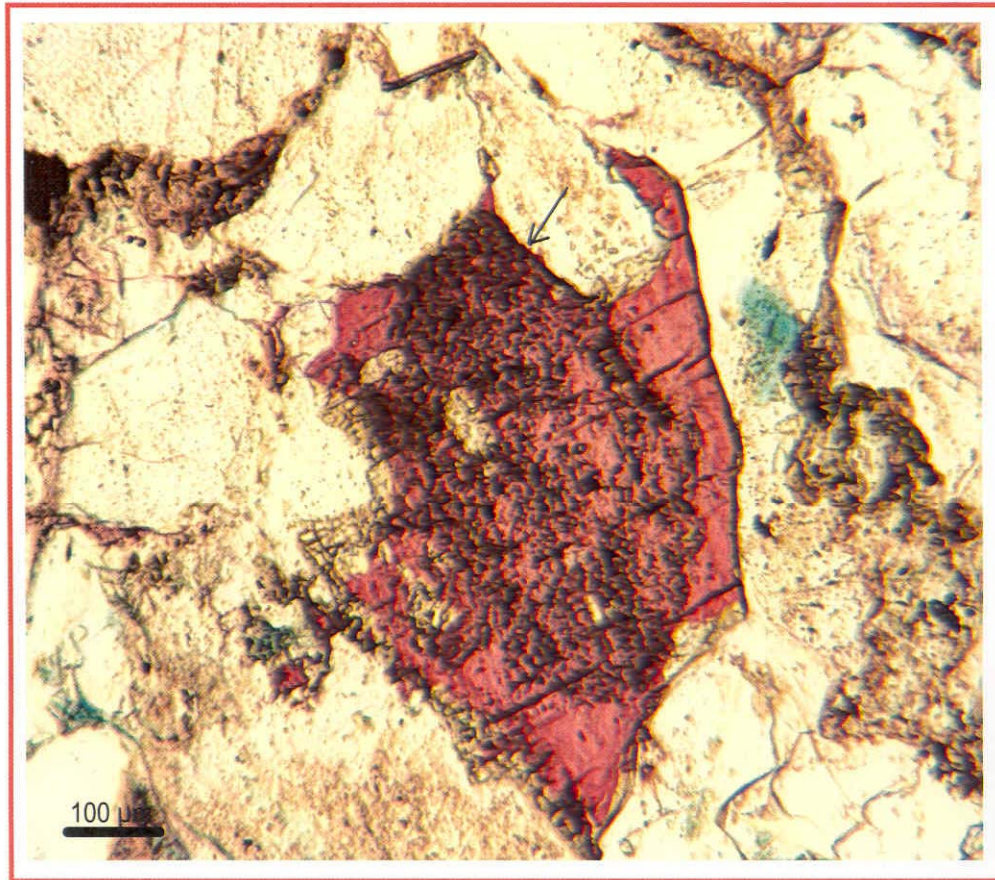


Figure 84: Calcitized feldspar grain. Note insoluble residue (arrow) left after feldspar dissolution and replacement. JH # 3, 8809 ft.

RK = replacive kaolinite.

Only one-third of the oversized pores were conservatively interpreted to be primary porosity in origin and 1/3 of moldic pores were thought to be grains other than feldspar and rock fragments. Only one half of the visual microporosity (associated with feldspars replaced by kaolinite, not intergranular kaolinite cement) was considered to be feldspar in origin.

Orthoclase and plagioclase are dominant feldspars and microcline is minor. The condition of feldspars is highly variable: some grains are fresh, other grains have been partially to totally dissolved and replaced (Figs. 85, 86, and 87). The presence of fresh detrital feldspar is rather surprising, because burial to depths of 10,000 ft (3030 m) commonly results in extensive feldspar dissolution or albitization. Dutton (1987) suggested that abundant clay matrix may have inhibited fluid flow through Cotton Valley sandstones, thus decreasing rates of feldspar dissolution. Also, the chemical analyses of Cotton Valley formation waters suggest they are in equilibrium with quartz, K-feldspar and K-illite (Dunnay, 1981).

Plagioclase grains range from fresh to sericitized and vacuolized. Many plagioclase grains show albite twinning; other grains show chessboard twinning that is the product of albitization (Gold, 1984). Microprobe analyses (appendix C) indicate that feldspars in the shallowest cores (BSH # 1, 8693 ft) are nearly completely albitized (>90% of the analyzed feldspar grains), however, yellow stained K-feldspar could be observed in thin section. However, sample (BSH # 1, 8935 ft) has no albite. So, the percentage of albite among probed grains is highly variable (between 0 and 90%).

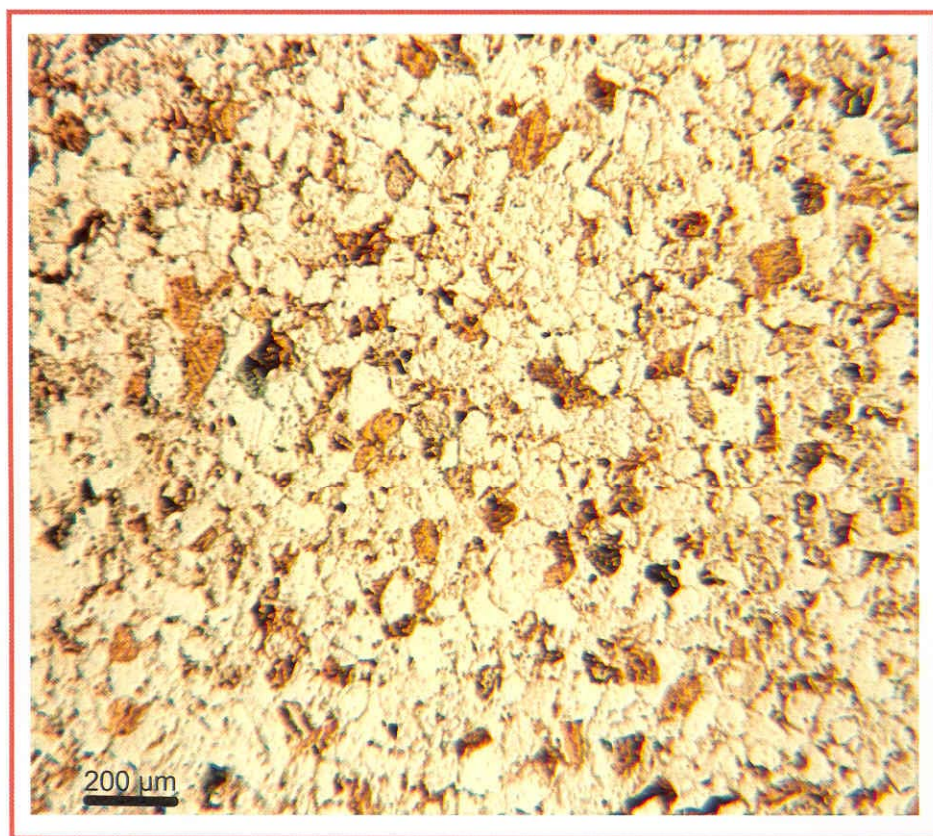


Figure 85: Plane-light thin section image showing fresh, yellow-stained potash feldspar. GL # 1, 9459 ft.



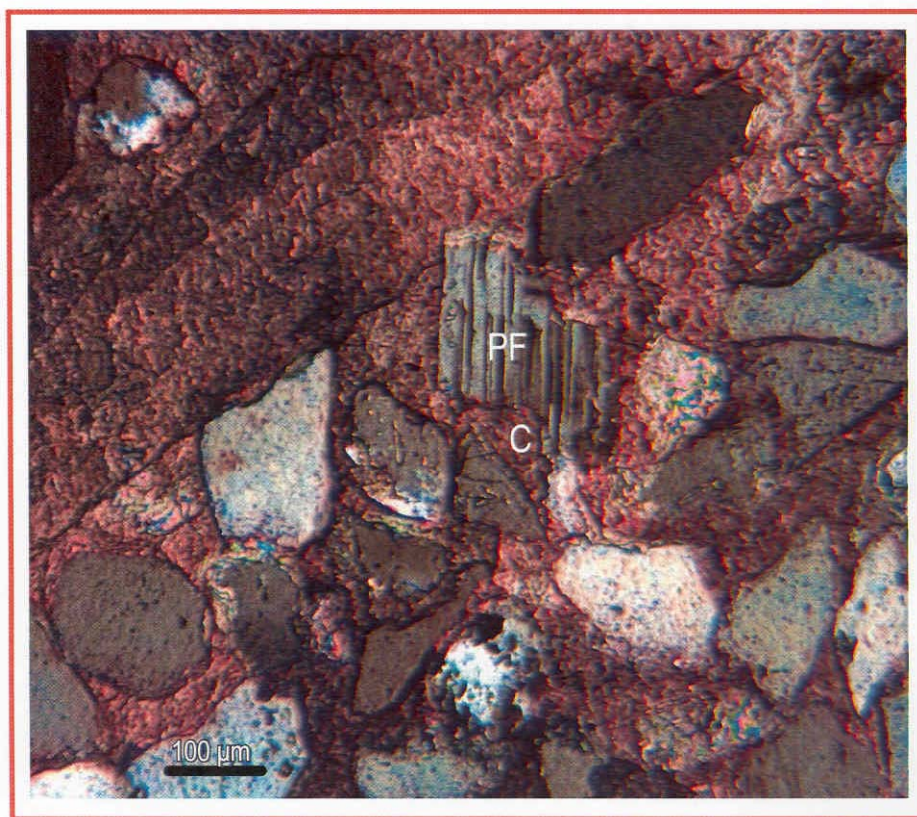


Figure 86: Half crossed-polars view showing partially replaced plagioclase feldspar grain (PF) by calcite ©. BH # 1, 9829 ft.

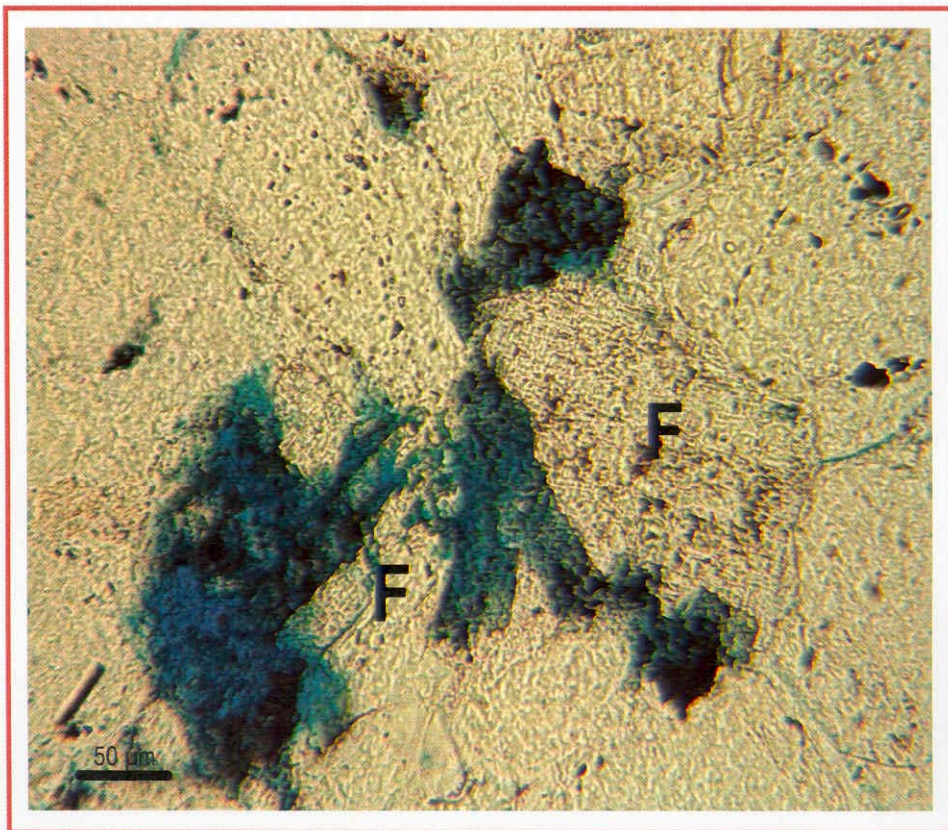


Figure 87: Photomicrograph showing partial to nearly complete dissolution of feldspar grains (F). Blue areas are porosity. BSH # 1, 8760 ft.

Microprobe analyses indicate that unalbitized K-feldspars have an average composition of Or > 93 and albitized grains have Ab > 92 (Fig. 88).

#### **4.3.3. Rock fragments**

Rock fragments range from 1 to 3% (and average 2%) of the framework composition. Lithic components of the Cotton Valley are primarily chert and low rank metamorphic rock fragments (Figs. 89 and 90). Sedimentary and plutonic rock fragments are also observed. Chert occurs as ordinary, black organic-rich and microporous chert (green) in thin section. Black chert has 2-3% impurities of organic carbon and the green colour of some microporous chert fragments is due to invasion of microporosity by epoxy. Metamorphic rock fragments include metamorphosed chert, metamorphosed sandstone (schist) and metamorphosed siltstone (slate). Quartz grains composed of an aggregate of crystals and with biotite or muscovite flakes between the crystals are considered as metamorphic rock fragments. Sedimentary rock fragments are sandstone and siltstone. Many samples contain traces of phosphatic rock fragments, which may be locally derived. Bailey (1983) reported the occurrence of volcanic rock fragments, but I found none. The original content of rock fragments was estimated as:

$$RO = SRx + MRx + OP/3 + MP/3 \quad (\text{Souza, 1999})$$

Where:

RO = original rock fragments content

SRx = siliceous rock fragments

MRx = metamorphic rock fragments

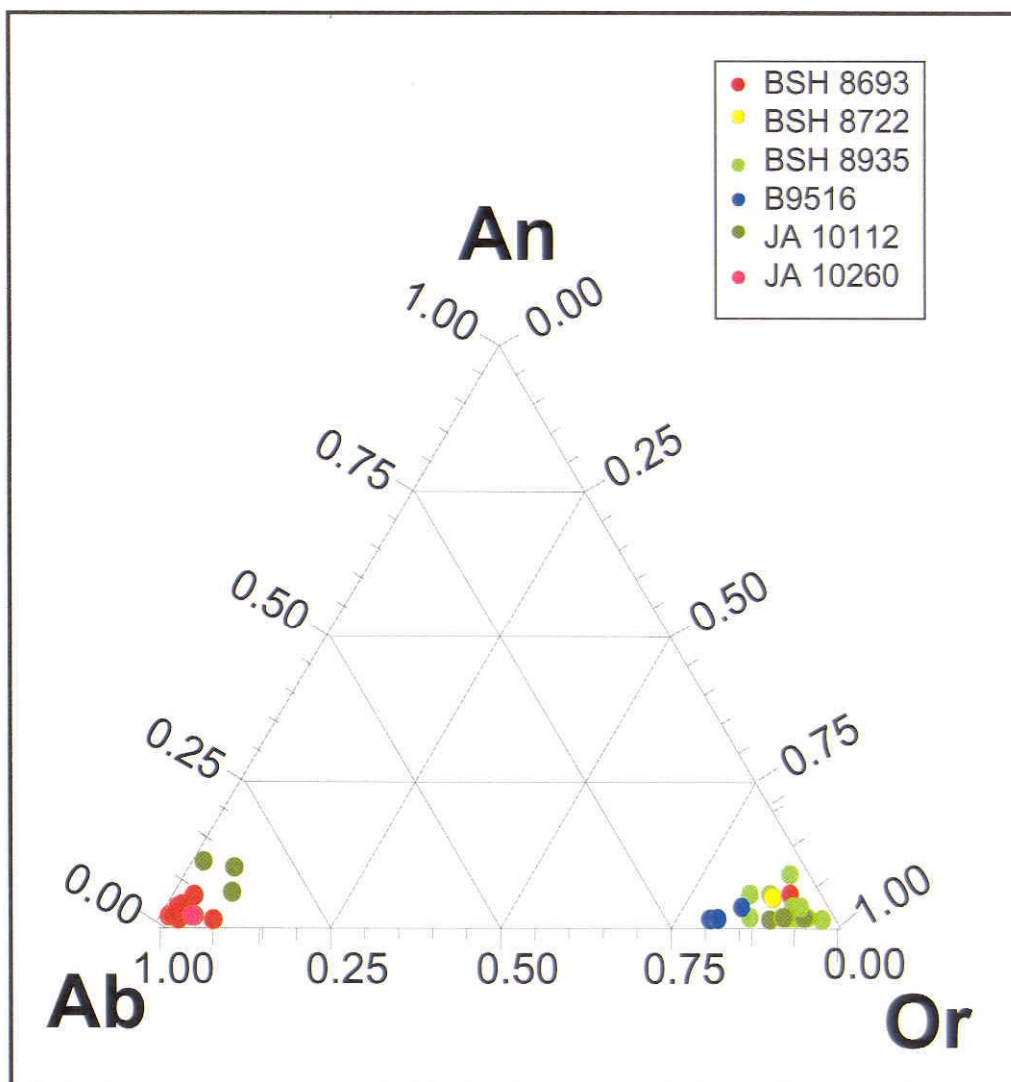


Figure 88. Feldspar grain composition based on microprobe analysis of six sandstone samples from depth range between 8693 ft (2634 m) and 10260 ft (3109 m).



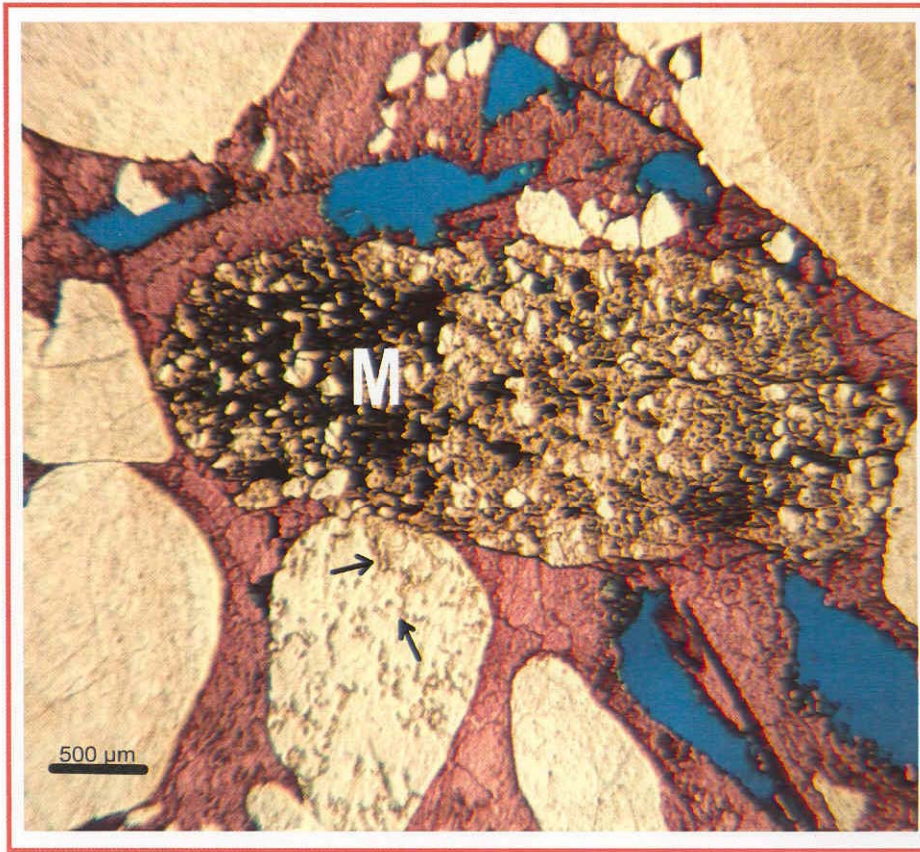


Figure 89: Photomicrograph showing metamorphosed siltstone fragment (M). Note red stained calcite and vermicular kaolinite (arrows). Blue areas are porosity. BH # 1, 9811 ft.



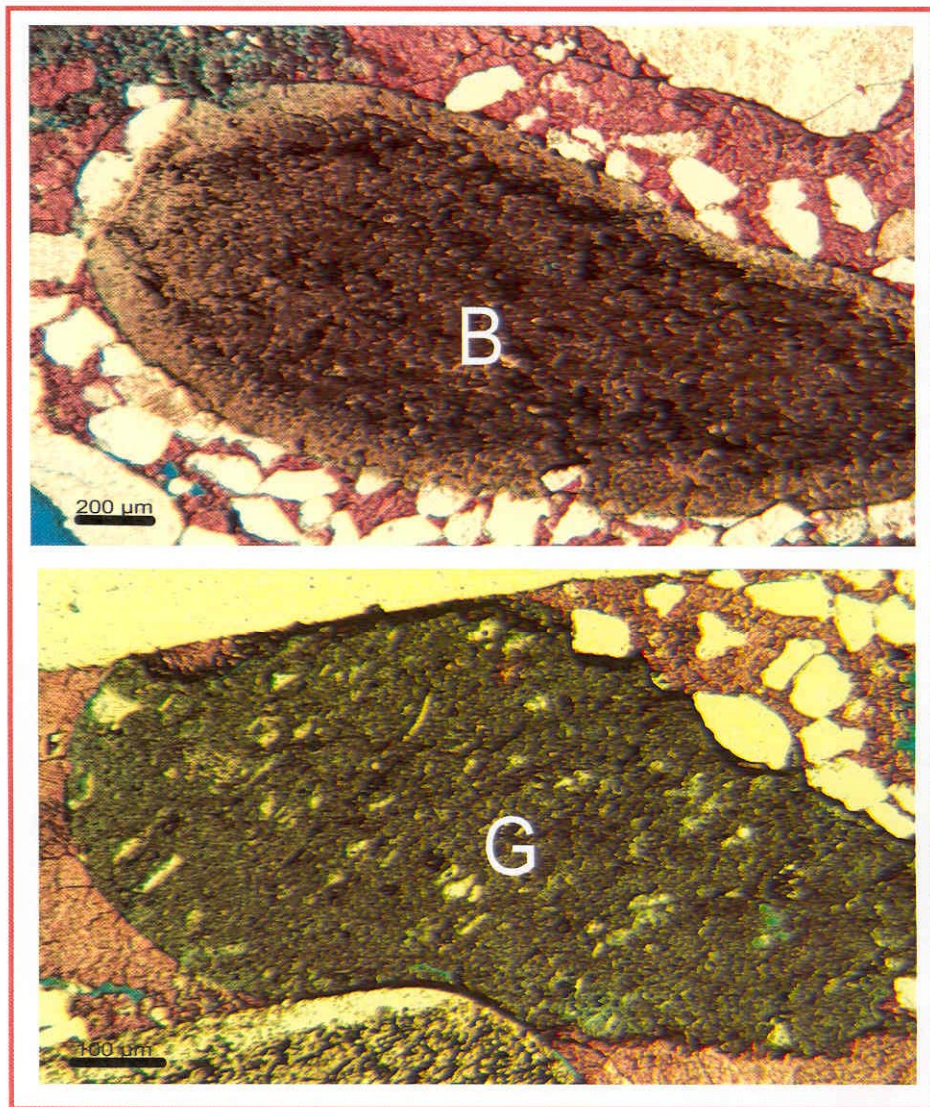


Figure 90: Photomicrograph showing black chrt (B) and green chert (G). Note red stained calcite. Samples from BH # 1, 9811 ft.

OP = oversized pores

MP = moldic pores

A maximum of 1% of rock fragments was lost during diagenesis.

#### **4.3.4. Miscellaneous constituents**

Mica, heavy minerals, carbonaceous organic matter, and fossil fragments make up an average of >1 % of the framework grains. Muscovite is the major type of mica observed in the Cotton Valley sandstones. Muscovite is common along stylolite surfaces and grains have been bent or broken by compaction (Fig. 91). It also appears to be dissolved or replaced. Zircon and tourmaline are the most abundant varieties of heavy mineral. Although they are extremely stable, and survive long transport, they show some evidence of dissolution (Fig. 92). Carbonaceous organic matter is locally significant and includes plant leaves, stems and roots. Solid hydrocarbon (bitumen) was observed as a minor component in few samples in the sand flat facies. Bitumen filled the available pores at the time of its formation. It is a late diagenetic phase that post-dates quartz and carbonate cements. Its relative age suggests late diagenetic oil emplacement.

Carbonate fossils, especially large oyster shells, are a significant component in some sandstones. Oyster shells are composed of fibrous calcite (Fig. 93) or have been replaced by dolomite. Other fossils, like gastropods and pelecypods, are also observed.

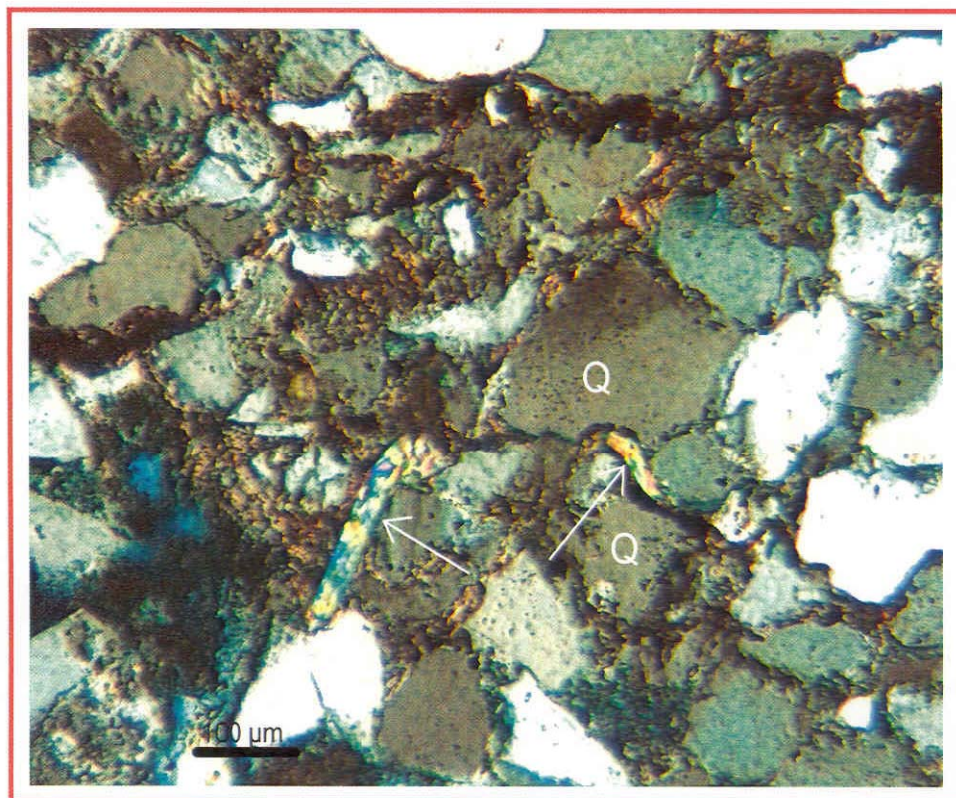


Figure 91: Crossed-pollars photomicrograph shows muscovite (arrows) bent between rigid quartz grains (q). BH # 1, 9749 ft.



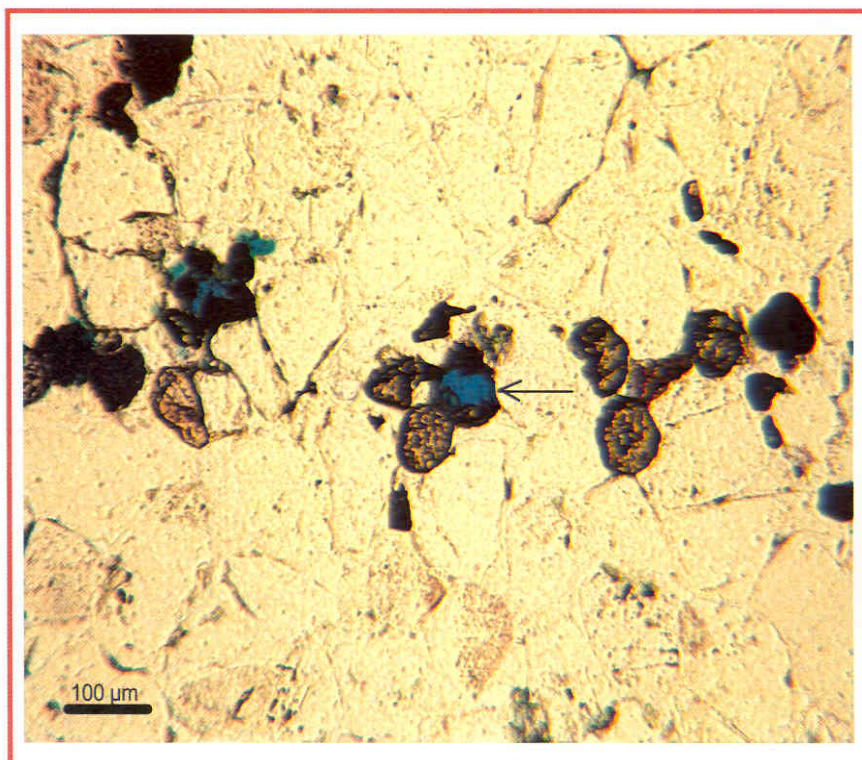


Figure 92: Partial dissolution of some heavy mineral grains (arrow). BSH # 1, 8817 ft.



Figure 93: Sandstone with abundant oyster fragments. JH # 3, 8779 ft.

#### **4.3.5. Matrix**

Detrital clay matrix (dispersed detrital clay among framework grains) is a volumetrically significant component in all facies (Table 2). It varies between 4% and 7% in the bioturbated shorefaces and 6% and 7% in the laminated and tidally influenced shorefaces. Sand flats have an average of 5% and the storm-dominated sandstones have an average of only 2.5%. Clay matrix occurs dispersed among the framework grains. Wilson and Pittman (1977) summarized different sources for detrital clay. They indicated that detrital clay might be syndepositional (dispersed matrix, sand-sized floccules, mud clasts) or might be introduced subsequent to deposition as a result of bioturbation. The latter may explain the origin of clay matrix in the bioturbated shorefaces. Most of the detrital clay now is illite (cf. Wescott, 1983).

#### **4.4. Conglomerate**

Conglomerates are minor in the Cotton Valley and range in thickness from 5 cm to 25 cm and average 15 cm. They are commonly observed at the base of tidal inlets or associated with transgressive surfaces. They are polymodal, matrix- to clast-supported conglomerates. Clasts are subrounded to rounded and reach up to 2 cm in diameter (Fig. 94). Clasts are mainly chert (black and green types) and metamorphic rock fragments (metamorphosed chert, metamorphosed sandstone and siltstone), whereas, sedimentary (sandstone) and plutonic (interlocked aggregates of quartz and K-feldspar and plagioclase) clasts are minor. Oyster fragments are also observed. Conglomerates are completely cemented by calcite, which ranges from 21.5% to 29.5% and averages 25.8% of the total framework. The average intergranular volume (IGV)

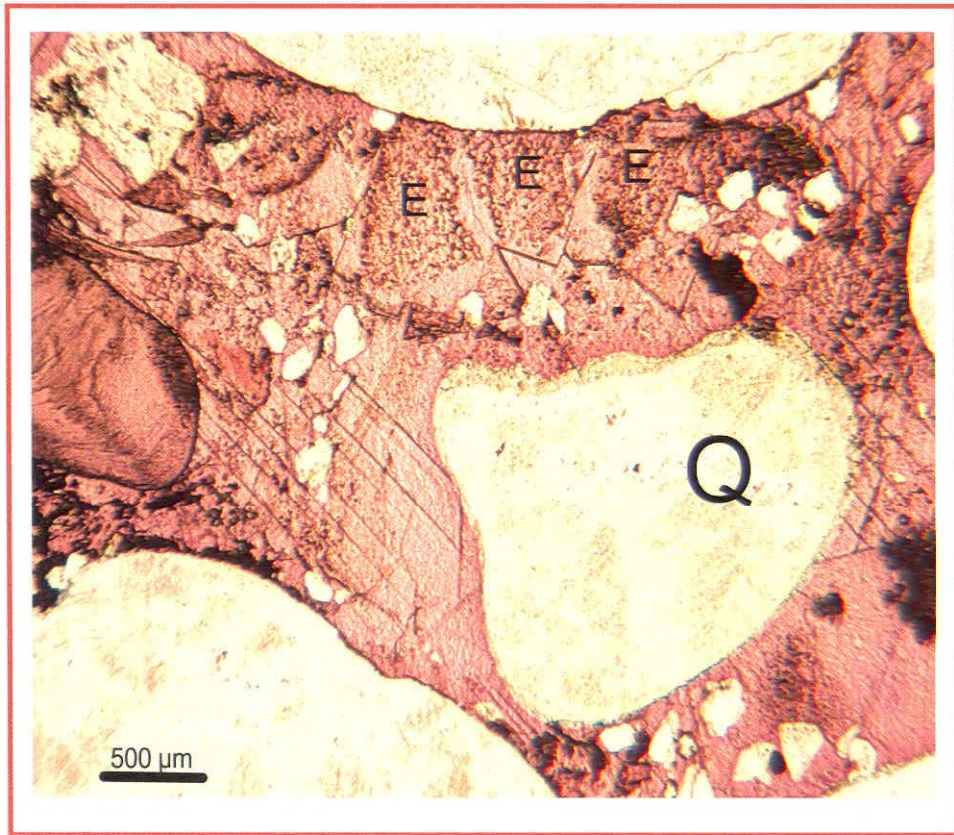


Figure 94: Photomicrograph showing calcite-cemented conglomerate. Q is quartz, calcite is red stained. Note sand grain matrix and echinoderm fragments (E) which provide nucleation substrates for calcite cement.



for conglomerates range from 21.1% to 30.7% with an average of 28.5% which is the highest IGV found in all samples.

#### **4.5. Diagenetic overprint on framework grains and restored composition**

Mineral composition of sandstones may be significantly altered by dissolution, or replacement during diagenesis (Pettijohn et al., 1987). Dissolution of feldspars and replacement by carbonates and kaolinite and other clay minerals are the most significant processes that modified the original sandstone composition.

Feldspar dissolution is the major process that has substantially modified the original framework composition as evidenced by the presence of intragranular and moldic pores. Other metastable grains like chert, chalcedony, as well as heavy minerals, show evidence of partial dissolution. Other diagenetic processes that alter the framework composition include kaolinitization and replacement by carbonates.

The framework composition of the Cotton Valley Sandstones was originally arkoses and subarkose with average composition of  $Q_{81.2}F_{16.2}R_{2.6}$  and were altered to subarkose and quartzarenite with an average composition of  $Q_{87.9}F_{10}R_{2.1}$  (Table 3). Figures 95-97 show restored composition for each facies. The average amount of feldspars lost during diagenesis ranges from 4% in the storm-dominated shoreface sandstones to 8% in the cryptobioturbated shoreface and tidally influenced shoreface sandstones. Sand flat and bioturbated shoreface sandstones lost 6% of the original feldspar content and laminated shoreface sandstones lost about 5% of the original feldspars (Fig. 95).



Table 3: Present-day and restored sandstone composition of the Cotton Valley sandstones. Values are percent of framework.

Facies	Quartz present	Feldspar Present	Rock fragments present	Quartz restored	Feldspar restored	Rock fragments restored	Feldspar lost	Rock fragments lost
Bioturbated	90	8	2	83	14	3	6	1
Cryptobioturbated	87	12	1	78	20	2	8	1
Laminated	86	11	3	81	16	3	5	0
Tidal influenced	85	12	3	76	20	4	8	1
Storm-dominated	91.5	7	1.5	87	11	2	4	0.5
Sand flat	88	10	2	82	16	2	6	0
Average	87.9	10	2.1	81.2	16.2	2.6	6.2	0.5

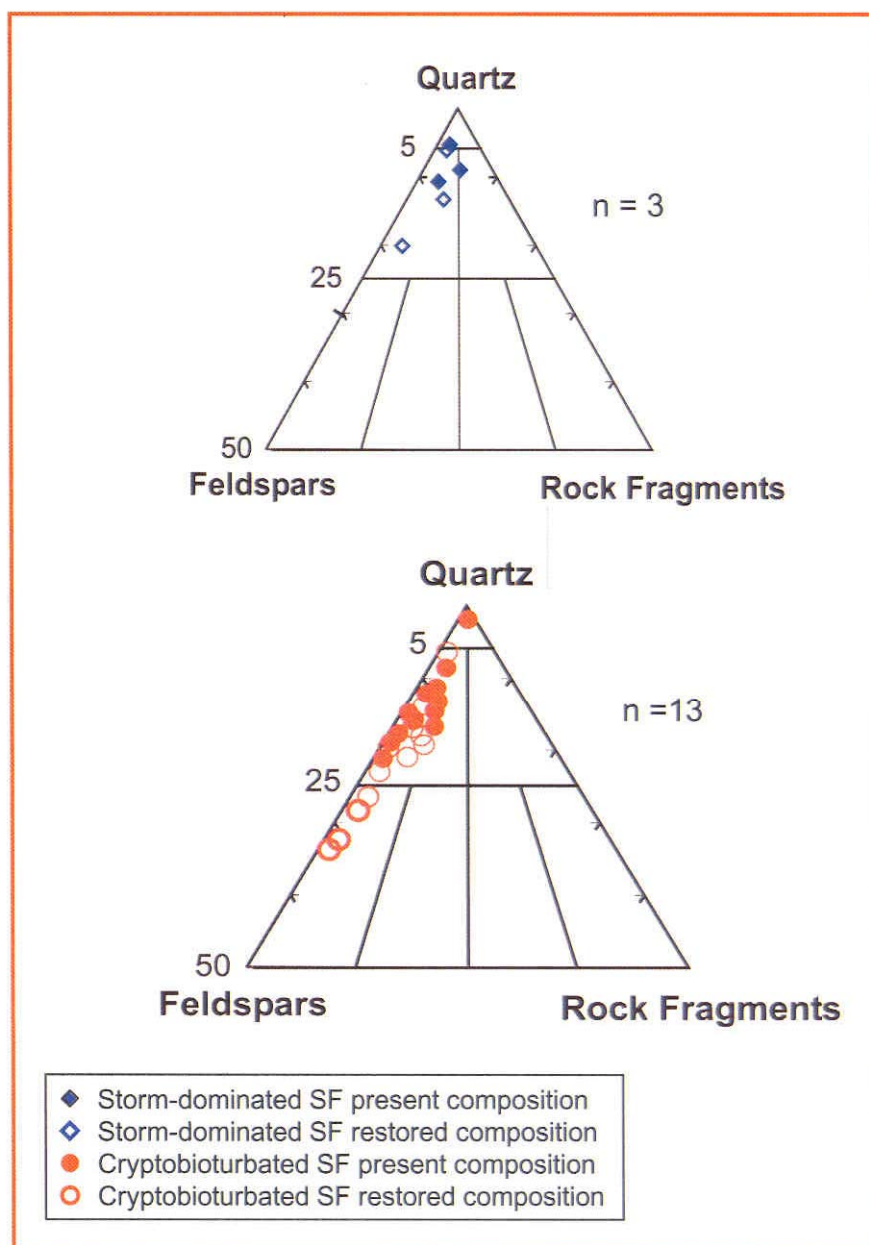


Figure 95: Present-day and restored framework grain composition of sandstones from the storm-dominated and cryptobioturbated shorefaces. SF is the shoreface sandstones, n = is the number of samples.

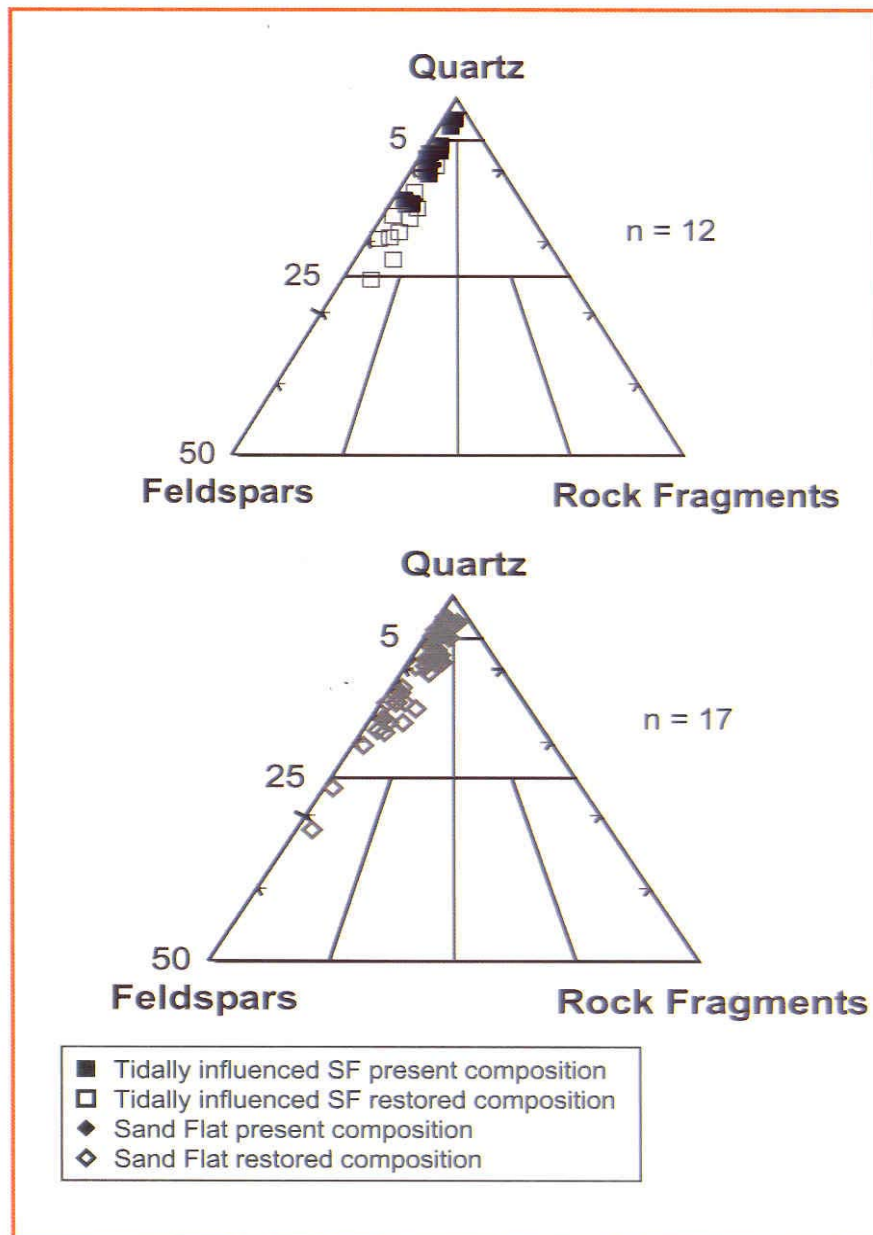


Figure 96: Present-day and restored framework grain composition of sandstones from the tidally influenced shoreface and sand flat. SF is shoreface sandstones., n = number of samples.

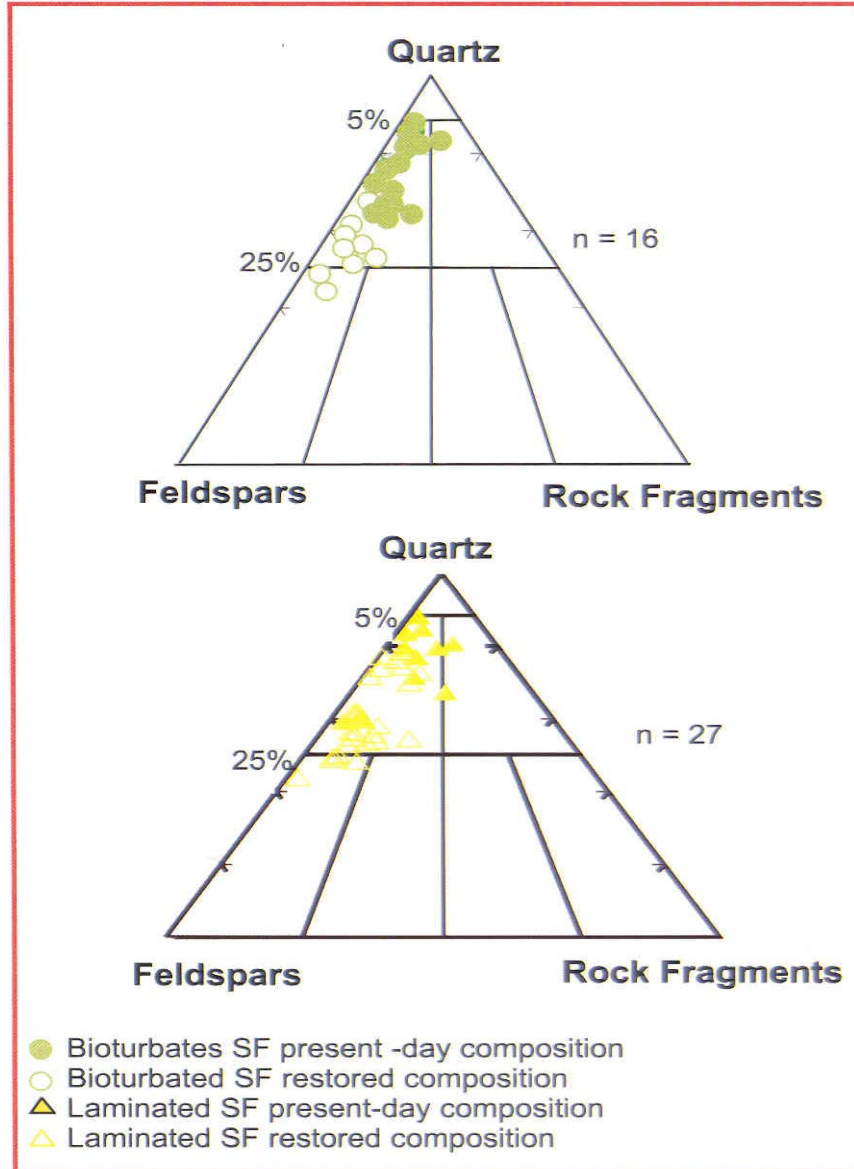


Figure 97: Present-day and restored framework grain composition of sandstones from the bioturbated and laminated shoreface. SF is shoreface sandstones., n = number of samples.

Significant amount of AL, Si and K was released to the pore water by feldspar dissolution. In 100 cc of sandstone 6.2% of feldspar lost

So,  $6.2\% \times 2.56 \text{ g/cc (density of feldspar)} = 15.87 \text{ g of K-feldspar}$

$15.87\text{g}/278.2 \text{ g/mole (molecular weight)} = 0.057 \text{ moles}$

So, in  $\text{KAlSi}_3\text{O}_8$

The amount of K released to pore water  $= 0.057 \times 1 = 0.057 \text{ moles}$

The amount of Al released to pore water  $= 0.057 \times 1 = 0.057 \text{ moles}$

And the amount of Si released to pore water  $= 0.057 \times 3 = 0.171 \text{ moles}$

#### **4.6. Provenance**

##### **4.6.1. Petrographic indicators of source area**

Vein quartz and stretched polycrystalline quartz grains observed in the CV are diagnostic of a source rock (Fig. 98). Sheared polycrystalline quartz is diagnostic of metamorphic source lithology and vein quartz is diagnostic of quartz veins, which can be found in metamorphic rocks, pegmatites or sedimentary rocks (Folk, 1974).

Pebble-size rock fragments are the best clues to provenance. Low grade metamorphic fragments (metamorphosed chert, metamorphosed sandstone and siltstone) and chert (black and green) fragments are abundant. Whereas, sedimentary rock fragments (sandstone and siltstone) and plutonic fragments (aggregates of quartz and feldspars) are minor. These types of rock fragments indicate metamorphic, sedimentary and plutonic rocks in the source area.

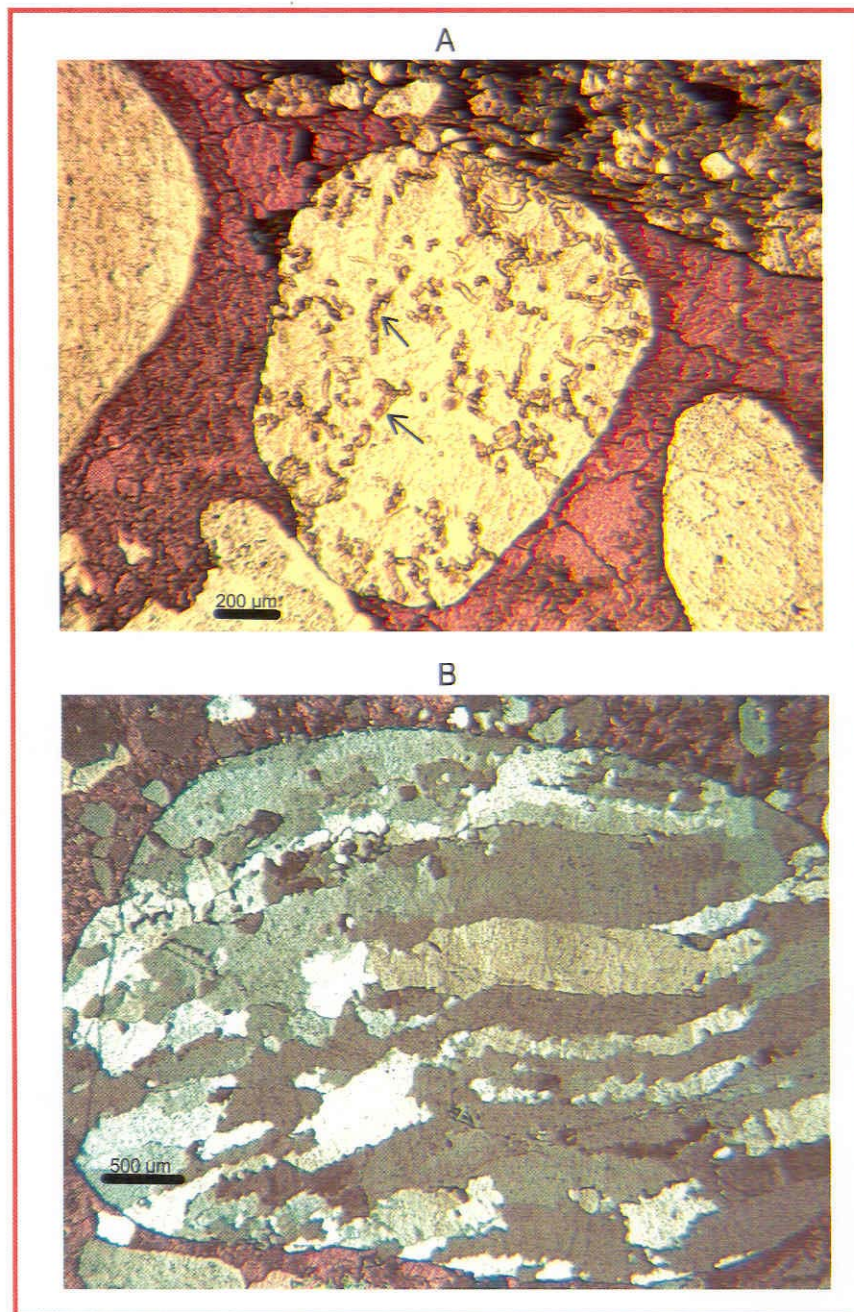


Figure 98: Photomicrograph showing (A) vein quartz with vermicular chlorite (arrows) and (B) stretched polycrystalline quartz grain. Both images from BH # 1, 9811 ft.

The presence of untwined plagioclase feldspars is an indicator of a metamorphic origin (Pittman, 1970). The other feldspar types in Cotton Valley sandstones (potash-feldspar and polysynthetically twinned plagioclase) may be of plutonic or volcanic origin.

#### **4.6.2. Possible source area**

McGowen and Harris (1984) concluded that deposition of Cotton Valley terrigenous clastics in the East Texas Basin was the result of a reactivation of a source area along the northern and western margins of the basin began during the Early and Late Jurassic. The Llano Region of Texas and the Ouachita, Arbuckle, and Wichita Mountains of Oklahoma and Arkansas were all highlands during the Late Jurassic and Early Cretaceous (Imlay, 1943). Figure 99 shows the Paleogeologic map of the Early Cretaceous of the south-central and southwestern United States (Saucier, 1985). Areas drained by the ancestral Mississippi River, including the Appalachian Mountains, have also been proposed as a potential source area (Forgoston, 1954; Bailey, 1983. p. 132).

The Ouachita Mountains, located 120 miles (193 km) northwest of the study area, is most probably the main source of quartz and rock fragments for the Cotton Valley Sandstones, but not the source for feldspars. The Ouachitas are composed mainly of sandstone (<5% feldspar), shale, and chert, and their metamorphic counterparts, such as meta-quartzite, meta-argillite, phyllite, and slate (Goldstein and Reno, 1952). The Ouachitas also contain plentiful vein quartz (Miser, 1959).

The Arbuckle and Wichita Mountains of Oklahoma and Arkansas are good possible source areas for feldspars, because both of them contain granites and were positive elements during deposition of the CV clastics. Granite rocks of the Wichita



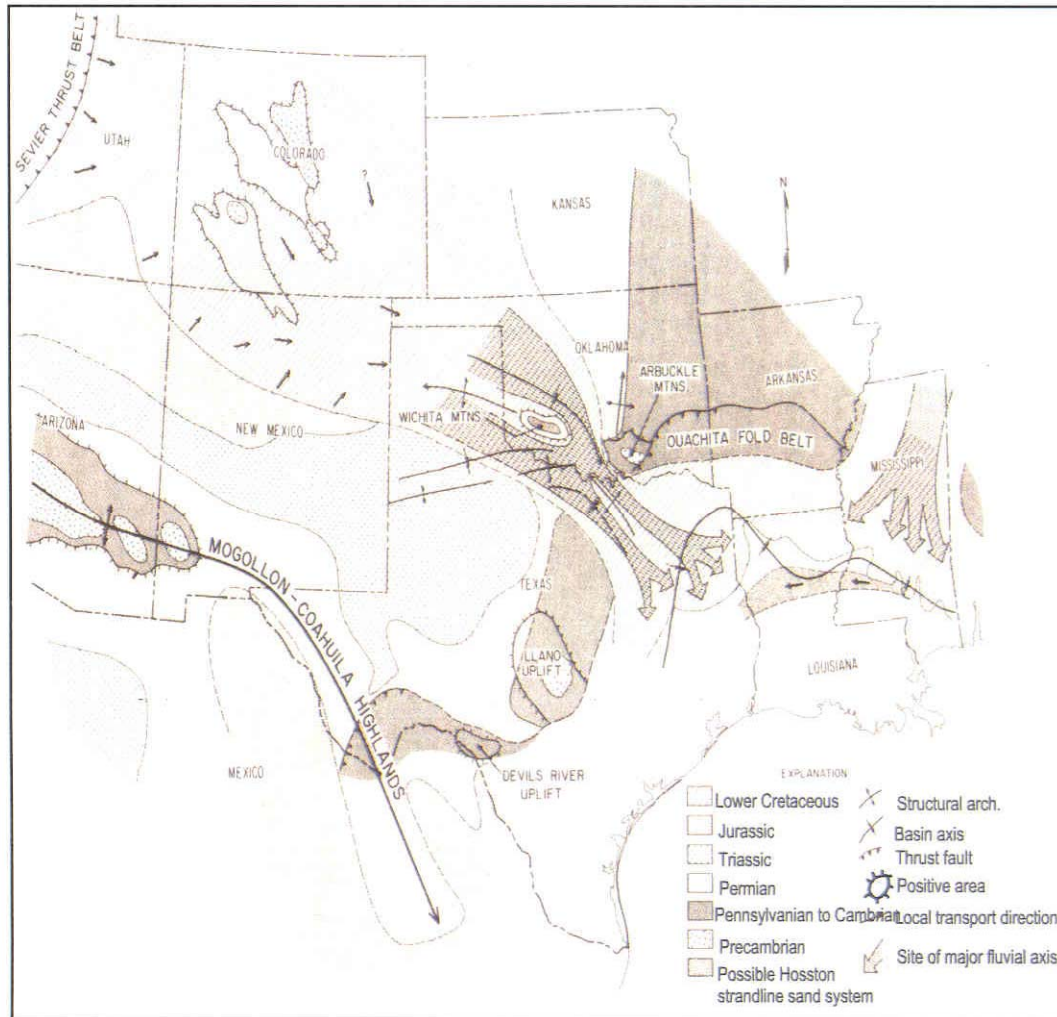


Figure 99: Paleogeographic map of the Early Cretaceous (Coahuilan) of the south-central and southwestern United States (From Saucier, 1985).

Province is characterized as perthite-quartz leucogranites. Virtually all are composed of about one-third quartz, two-thirds potassium feldspar that is mostly intergrown with plagioclase” Ham et al. (1964. pg.61). Feldspars in the CV are primarily K-feldspar, plagioclase and minor microcline and no perthite is observed. On the other hand, Ham et al. (1964. p. 130) mentioned that “Virtually all granites of the Eastern Arbuckle province are characterized by two feldspars, microcline and oligoclase, which distinguish these rocks petrographically from the perthite-rich low plagioclase leucogranites of the Wichita province”. He also reported the presence of orthoclase and plagioclase in the Arbuckle granites. Based on Ham (1964) `s observations, it is most likely that Arbuckle Mountains was a major source for CV feldspars. The Llano Region and Appalachian Mountains were not a source of detritus to the CV in my study area.

#### **4.7. Burial-Thermal History**

In order to understand the diagenetic history and porosity evolution of the Cotton Valley sandstones, it is essential to reconstruct the burial and thermal history through time. Genesis<sup>TM</sup> was used to generate time–temperature curves for four of the studied wells. Data used for the basin modeling were retrieved mainly from well logs, which include bottom-hole temperature, circulation times, stratigraphy, and gross lithology, and thickness of the penetrated formations. Available vitrinite reflectance (Ro) data were also used to interpret maximum temperature reached. Ro values for three shale samples from one well JA # 1 at depths 10262 ft., 9890 ft., and 9776 ft., are 1.24, 1.73, and 1.28 respectively. The burial history curve for all of the penetrated formations, including Travis Peak, Cotton Valley and Bossier formations, was plotted for four wells on top of

the Sabine uplift. These wells are Jones # 3, James Anderson # 1, Davidson Foundation # 1, Blocker Heirs # 1.

Figure 100 is a representative burial history curve for well Jones # 3. Dutton (1986, p. 117) reported two main erosional events in her study of Travis Peak sandstones in the East Texas Basin. The first one was associated with the movement of the Sabine Uplift at the beginning of Late Cretaceous time, when as much as 1825 ft (556 m) of pre-Austin Chalk deposits were removed between the end of Buda time and the beginning of Austin deposition (Halbouty and Halbouty 1982). The second erosional event was at

the end of Yegua time (Middle Eocene, 41 M.a) when about 1500 ft (450 m) of sediments were eroded (Dutton, 1986).

#### **4.8. Cements and replacive phases**

##### **4.8.1. General remarks**

Cements and replacive phases make up between 12 and 32% of the total sandstone volume. The amount of cementation in any rock is controlled primarily by the availability of pore space and the ability of the mineralizing fluids to go through the pores and by the availability of nucleation sites on the quartz grain in particular to precipitate quartz overgrowths. Facies with a high amount of clay matrix have a low percentage of cements. This because the clay matrix decreased the porosity and permeability of the sediments and allowed smaller volumes of fluids to pass through the rock. Also, there was less primary porosity to be filled. Additionally, detrital clay matrix and thick clay coatings reduced the availability of nucleation sites on detrital

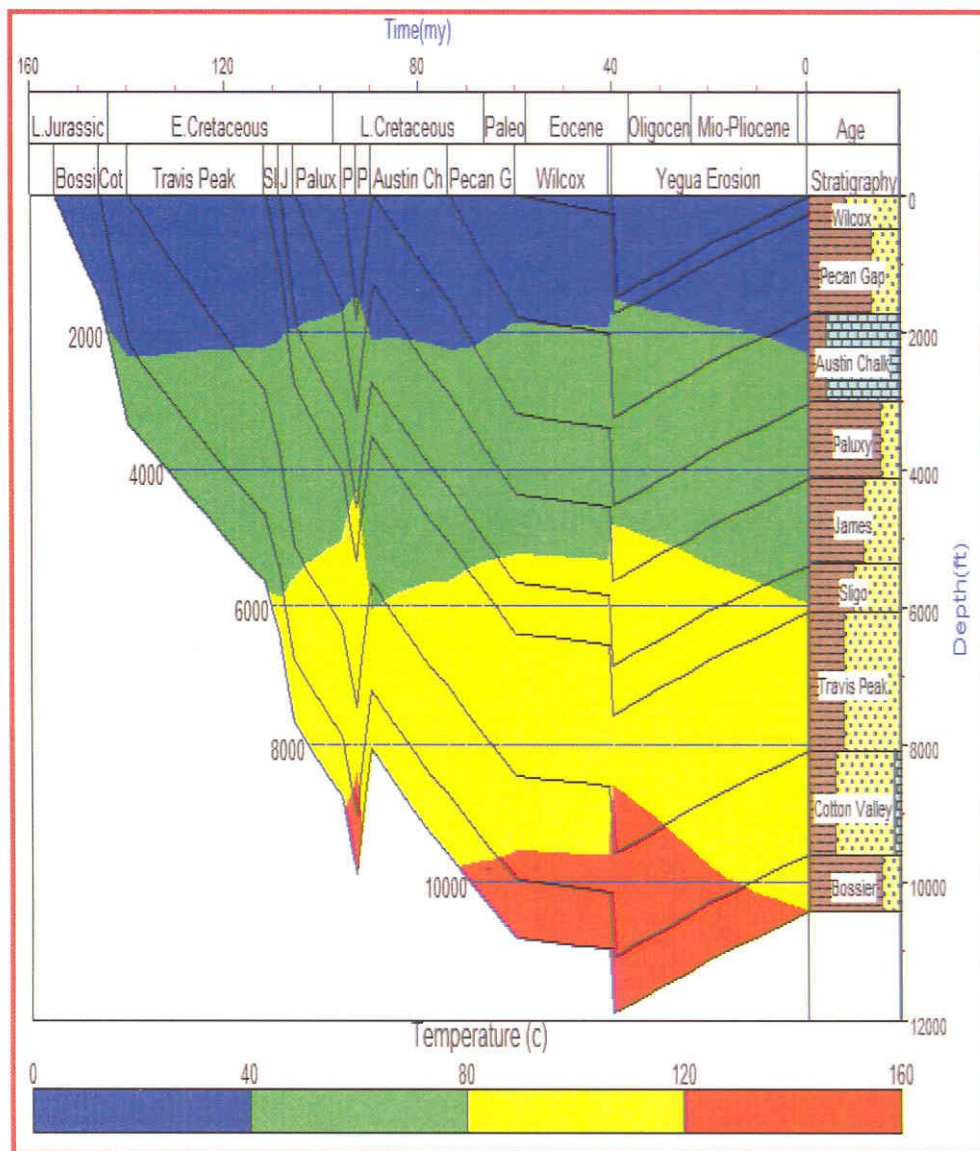


Figure 100: Burial and thermal model for the Cotton Valley Group and overlying formations in Jones well # 3.

quartz grains and retarded quartz cementation. The most abundant authigenic minerals in the Cotton Valley Sandstones are quartz, calcite, dolomite, illite, and chlorite. Less abundant authigenic minerals are kaolinite, feldspar, pyrite and anhydrite. Pyrobitumen, although not a mineral, fills intergranular as well as secondary intergranular pores. Dissolution of feldspars and a few rock fragments and heavy minerals was a pervasive process in the Cotton Valley sandstones. Albitization of detrital feldspar was also observed. Figure 101 shows the paragenetic sequence of various diagenetic events in the CVS and will be discussed later in this chapter.

#### **4.8.2. Quartz**

Quartz is the most abundant cement in Cotton Valley sandstones, averaging from 3.3% to 14.1% of individual facies (Table 4). Sandstones from storm-dominated shorefaces and bioturbated shorefaces have an average ranging from 3.3% to 5.9%, respectively; whereas the laminated and tidally influenced shoreface facies average 11.4% and 14.1%, respectively. Cryptobioturbated shoreface and sand flat sandstones have an average of 6% and 10.8% respectively. In matrix-free sandstones and sandstones with low amount of calcite cement, syntaxial quartz overgrowths completely occlude primary porosity and form interlocking quartz crystals (Fig. 102). In the bioturbated sandstones clay matrix and grain coatings decrease the amount of quartz cement and some primary porosity is preserved. Worden and Morad (2000) pointed out that quartz cementation is strongly controlled by primarily lithofacies because silica needs clean substrates to form: quartz cementation is most likely to be inhibited by the presence of grain coating clay, infiltrated clays and microquartz.

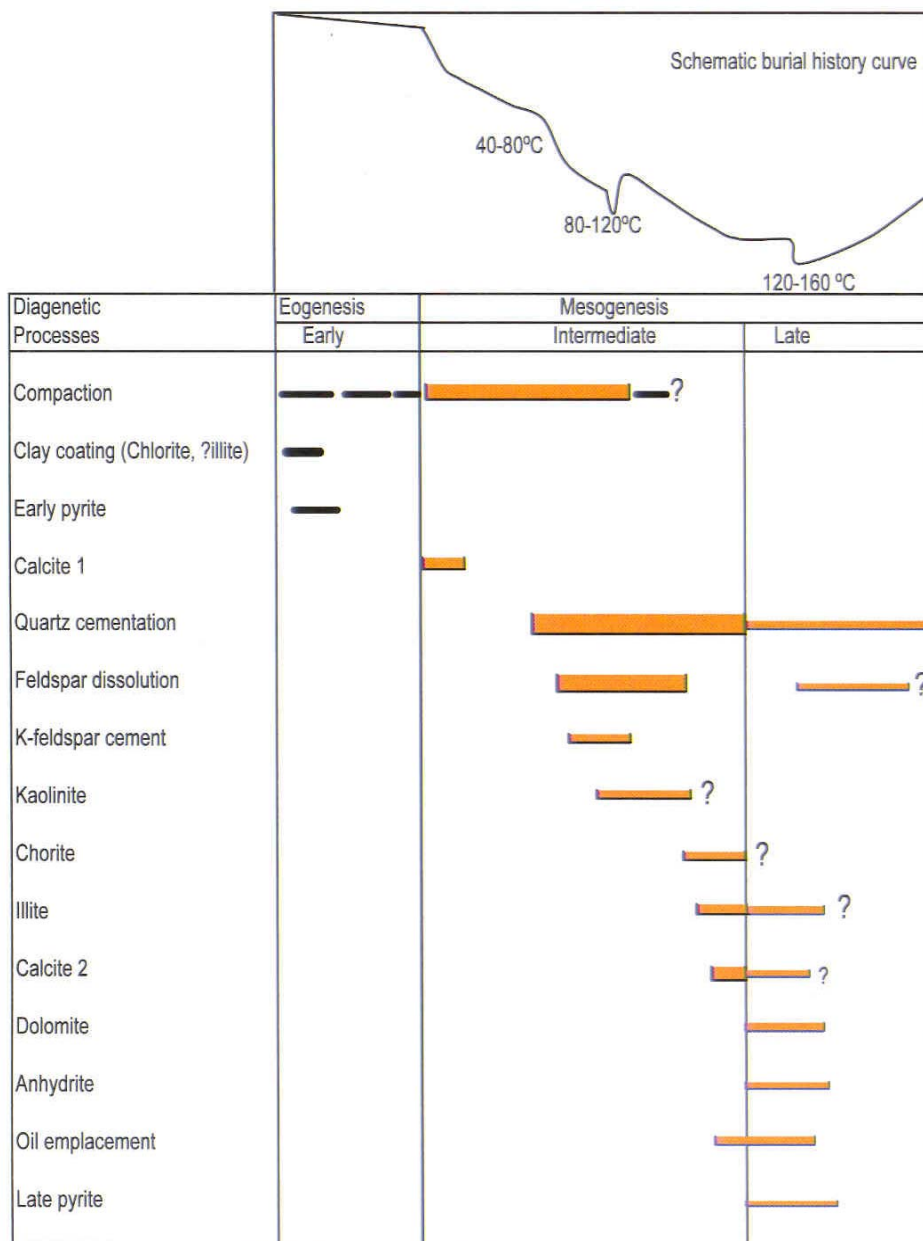


Figure 101: Schematic paragenetic sequence of diagenetic processes and products in Cotton Valley sandstones. Thickness of lines indicates relative importance of event.

Table 4: Distribution of cements in potential reservoir facies. n = number of samples. Values are percent of rock volume. F1 :Bioturbated SF, F2: Cryptobioturbated SF, F3: Laminated SF, F4: tidally influenced SF, F5: Storm-dominated SF, and F6: Sand flat.

Facies	*Qz	Total Carb.	Calcite	Dolomite	Kaol.	Anhy.	Pyr.	Illite	Chlor.	n
F1	5.9	4.3	3.5	0.8	0.6	0.0	1.1	0.5	1.0	16
F2	6.0	3.2	2.9	0.3	1.0	0.0	1.0	0.7	0.7	13
F3	11.4	7.7	6.7	1.0	0.9	0.0	2.0	1.9	1.0	27
F4	14.1	4	2.5	1.5	2.3	4.7	0.0	0.0	0.5	12
F5	3.3	27.4	27	0.4	1.4	2.2	0.0	0.0	0.4	3
F6	10.8	7.5	5.8	1.7	0.9	1.0	0.7	0.0	0.9	17

\*Quartz is corrected quartz cement percentage (quartz cement % from thin section + 40% of the quartz cement value).



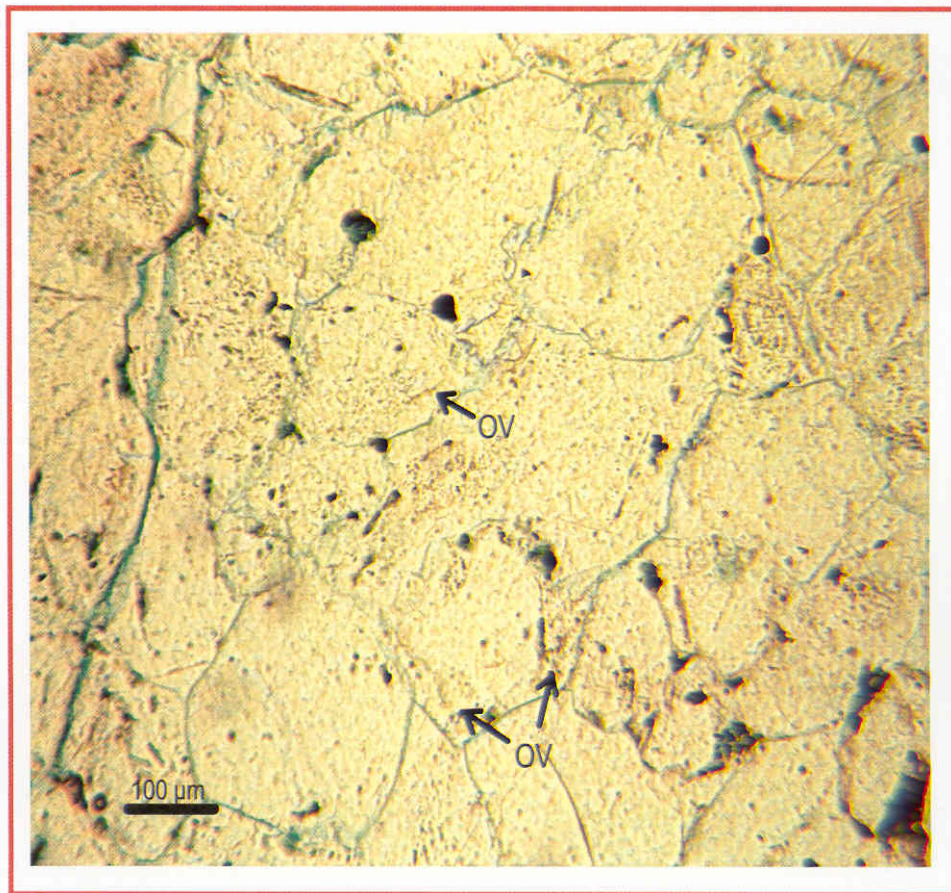


Figure 102: Quartz cement (OV) almost occludes primary porosity and destroyed reservoir quality in clean well sorted sandstones. BSH # 1, 8734 ft.

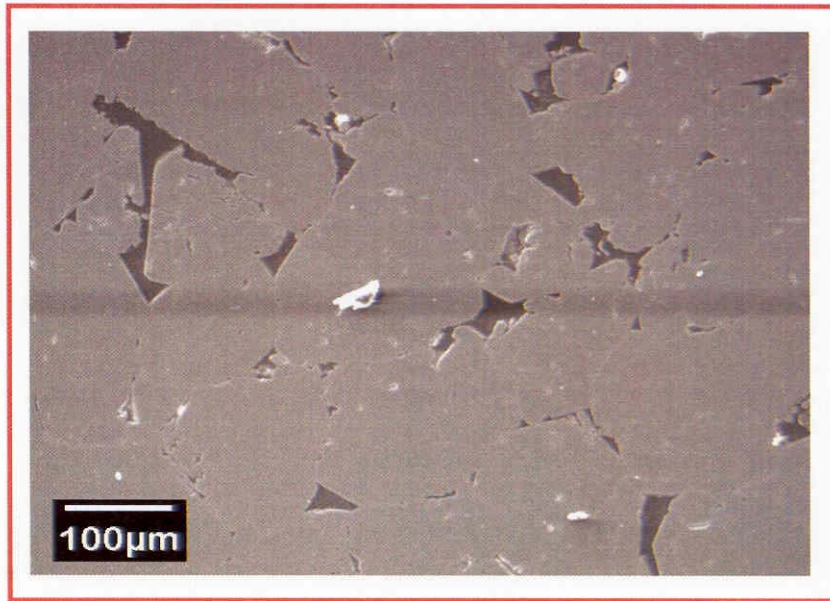
Dickinson and Milliken (1994), in their study of Etjo sandstones from Namibia pointed out that quartz grain fracturing and healing by quartz cement has been underestimated during sandstone petrographic analysis. CL imaging of the Cotton Valley sandstones show that grain fracturing is common and most of the fractures are healed with authigenic quartz (Fig. 103).

Point counts of quartz cement in thin section underestimated the true amount because of the absence of dustline on many grains. This resulted in a low IGV values in many of the samples. So, I determined a correction factor by comparing point-count data with CL imaging for 13 samples. The correction factor ranged from 35% to 60% (average of 40%) more than point-count data (Table 5). For example if the point counted quartz cement percentage from thin section is A. Then the corrected quartz cement percentage =  $A + (0.4 \times A)$ . Corrected quartz cement values are used in all calculations concerning quartz cement.

Twelve samples from different facies with variable amounts of quartz cement were analyzed for their oxygen isotopic composition using the technique of Land and Dutton (1984) as described earlier. The volume of quartz cement was counted for each sample from the thin section or using a grid on CL images.

The  $\delta^{18}\text{O}_{\text{SMOW}}$  for bulk samples (Table 6) was plotted versus quartz overgrowth/total quartz. The value for pure quartz overgrowths was obtained by extrapolating the regression line to 100 % overgrowth. The regression line extrapolates from a value of 13.5‰ (SMOW) for detrital quartz to 24.6‰ (SMOW) for quartz

A



B

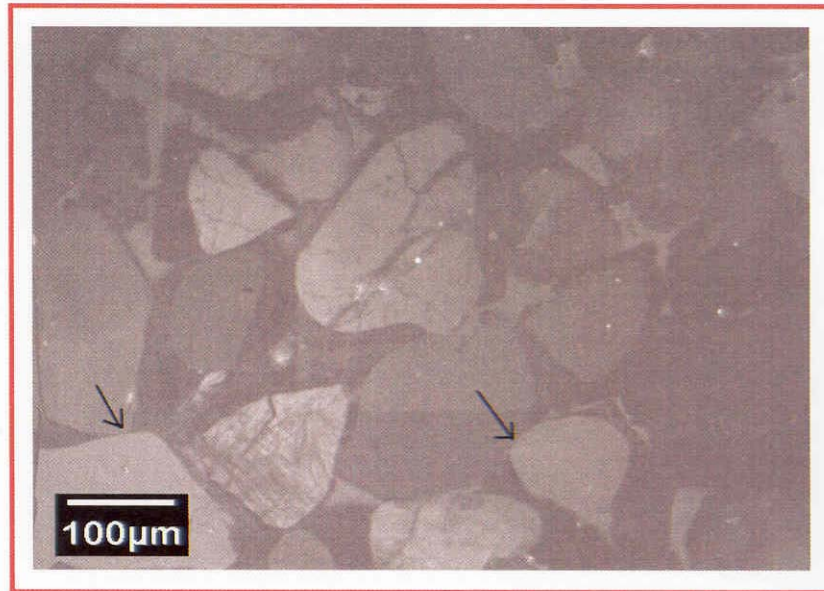


Figure 103: Combined electron secondary (A) and scanned CL (B) images reveals that quartz cement healed grain fractures. Note point grain contacts (arrows). XLC # 1, 9192.5

Table 5. Comparison between the amount of quartz cement determined by using and without using CL. Cement values are percent of total rock.

Sample	Facies	Qz cement (thin section)	Qz cement (CL)	Difference	% of difference
JA 10026B	Cryptobioturbated	5.5	7.5	2	36.4
JA 10026K	Cryptobioturbated	4.5	6	1.5	33.3
Jones 8753.5	Laminated	14	19	5	35.7
Blocker 9706	Laminated	10	13.5	3.5	35.0
Jones 8608	Tidal SF	12.5	17	4.5	36.0
Jones 8611	Tidal SF	9	13	4	44.4
Blocker 9745	Lagoon	0.7	1	0.3	42.9
Bsh 8693	Sand flat	10	13.5	3.5	35.0
Bsh 8935	Bay	3.5	5	1.5	42.9
Bsh 8722	Soil	4	6	2	50.0
Blocker 9328	Bioturbated	5	8	3	60.0
Jones 8428	Bioturbated	5	7	2	40.0

Table 6: Percentage of overgrowth of total quartz and Oxygen isotopic data for bulk quartz samples.

Sample	Cement/Total quartz (%)	$\delta^{18}\text{O}$ qtz (%)
JA9774	4	13.3
JA10026A	12.3	16.4
XLB8701	24.9	15.5
XLB9040	2.1	13.2
XLB9164.5	15.7	16.2
XLC9175	16.9	14.6
XLC9177.5	16.8	14.1
XLC9192.5	20.9	16.1
XLC9182.5	2.1	13.3
BS8584	4	13.7
BS8693	21	16.5
BH9311	12	13.5

cement. The cement value has a confidence interval of  $\pm 1.7\%$  (SMOW) and the data has a correlation coefficient of 0.8 (Fig. 104). Fluid inclusion analysis from three selected samples with abundant quartz cement revealed homogenization temperatures between 100°C-110°C. All data are primary inclusions at quartz overgrowth boundaries. Freezing temperatures of the liquid was about -14°C, which correlates with a salinity of 160 ‰ five times the salinity of sea water.

#### **4.8.2.1. Sources of silica**

Although quartz overgrowths are the dominant cement type in quartzose sandstones, their origin and the controls on its distribution are still subject to debate. Potential sources of silica have been summarized by McBride (1989). The most commonly proposed sources are pressure solution at grain contacts and stylolites, illitization of smectite clays, and dissolution of siliceous microfossils or spicules. Pressure solution of detrital quartz is considered by many authors as a significant source of quartz cement (Pittman, 1972, Füchtbauer, 1974; Houseknecht, 1984; Dutton, 1986, 1989; James et al., 1986; and McBride et al., 1987).

Although feldspar decomposition is a good source of silica for quartz cement (Fothergill, 1955; Hawkins, 1978; Land and Macpherson, 1992a; Bjørlykke and Egeberg, 1993; and Souza, 1999), the fact that feldspar dissolution in Cotton Valley sandstones postdates quartz cementation rules out this source of silica.

Two principal internal sources of silica in the Cotton Valley sandstones are intergranular pressure solution and dissolution along stylolites. A possible external source is silica-rich fluid expelled from the underlying Bossier shales. Factors that favor



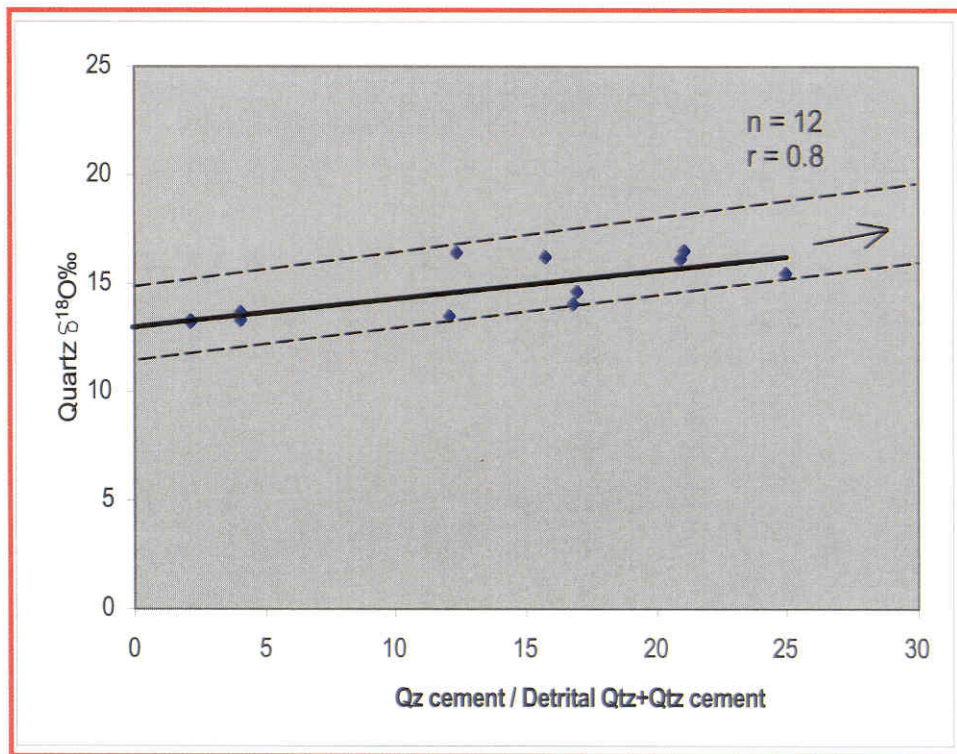


Figure 104: Oxygen isotope data for bulk quartz samples. Extrapolation of line to 100% quartz cement is used to estimate the isotopic composition of pure quartz overgrowths. The line extrapolates from 13.5‰ SMOW for detrital quartz to 24.7‰ SMOW for pure quartz cement. Dashed lines are 95% confidence level.



the development of one pressure solution phenomena over the others include clay content and distribution (Heald, 1955); degree of cementation (Heald, 1955); porosity (Wanless, 1979), grain size (Dunnington, 1967); and planar rock heterogeneity (Nelson, 1983).

An attempt was made to quantify the amount of quartz cement derived from pressure solution and stylolites in this study. The number of thin sections for each facies type is representative of the volume proportion of the facies types in the formation (Table 7). The average quartz cement in the Cotton Valley is 11% and the calculated amount of silica derived internally from both pressure solution and stylolites constitutes

48% of the total quartz cement (see below). The remaining 52% come from sources that could not be quantified. Other significant local sources of silica include dissolution of quartz grains at clay laminae and at contacts between sandstone and interbedded shales, and dissolution of micron-scale detrital quartz within interbedded shales and clay laminae. High content of clay laminae are observed in cores and shale interbeds constitute up to 35% of the total CV rock volume. These sources could not be quantified. A possible external source, a silica-rich fluid expelled from the Bossier shales. The amount of quartz cement derived from intergranular pressure solution was determined by point counting the amount of “overlap” quartz using CL images. Houseknecht (1984) defined overlap quartz as that portion of a detrital grain that is inferred to have been dissolved by intergranular pressure solution. The point-counted overlap quartz ranges from 0% to 3% with an average of 1.0% (Appendix D). The amount of quartz cement derived from intergranular pressure solution is only 9% of the

Table 7. Comparison between the percentage of thin sections of potential reservoir facies and the percentage of each facies in the analyzed cores.

Total no. of thin sections = 124		Total thickness 2098 ft		
Facies	No. of thin sections	% of sections	Facies thickness (ft)	% of Fm thickness
Bioturbated	16	13	330	15.9
Cryptobioturbated	13	10.4	200	10
Laminated	27	21	400	19
Tidally influenced	13	10.4	290	13
Storm dominated	3	2.4	100	4.7
Sand flat	18	15	400	19

total quartz cement (1.0/11). Thus, intergranular pressure solution was not a significant process in the Cotton Valley sandstones.

Stylolites are surfaces of dissolution which have serrated forms in cross section (Braithwaite, 1989). The surface accumulates clay and other insoluble material, such as heavy minerals, organic matter, and pyrite. Stylolites in Cotton Valley sandstones were examined in cores in an attempt to characterize their distribution and abundance with relative to various facies. The number of stylolites was counted in eight cores (Table 8 and appendix A). The constraint used to determine the stylolite density in cores is that it should be serrated surface (clay laminae are not counted) and continuous across the slabbed part of the core. No relationship found between the occurrence of stylolites and facies type. Stylolites occur in all facies. However, the abundance of stylolites per foot is variable. Sandstones from tidally influenced shoreface have a range from 5 stylolites/foot to 36 stylolites/foot with average of 20 stylolites/foot, whereas, storm-dominated sandstones have a range from 1 stylolite/foot to 2 stylolites/foot (average 1 stylolite/foot). Abundance of clay laminae within the tidally influenced shorefaces may explain the high density of stylolites in this facies. The highest amount of quartz cement in the tidally influenced shorefaces has no relation to the high density of stylolites. It is likely that stylolites formed at least in part, after the main phase of quartz cementation, because stylolites appear to cut both detrital grains and quartz overgrowths.

Generally, microscopic stylolites are subhorizontally aligned relative to bedding plane and have amplitudes of 1 mm to 5 mm (Fig. 105). Stylolites are mainly formed along clay laminae and less commonly within homogeneous sandstones (may be formed

Table 8. The number of stylolites/foot as determined from 8 cores for potential reservoir facies.

Facies	Range of number of stylolites/foot	Average	Total stylolites per facies	Total feet analyzed
Bioturbated SF	1/ foot – 12/ foot	6	194	330
Cryptobioturbated SF	4/foot - 9/ foot	6.5	132	200
Laminated SF	1/foot - 15/foot	8	400	400
Tidally influenced SF	5/foot - 36/foot	20	502	290
Sand flat	1/foot - 7/foot	4	511	400
Storm dominated SF	1/foot - 2/foot	1	10	100

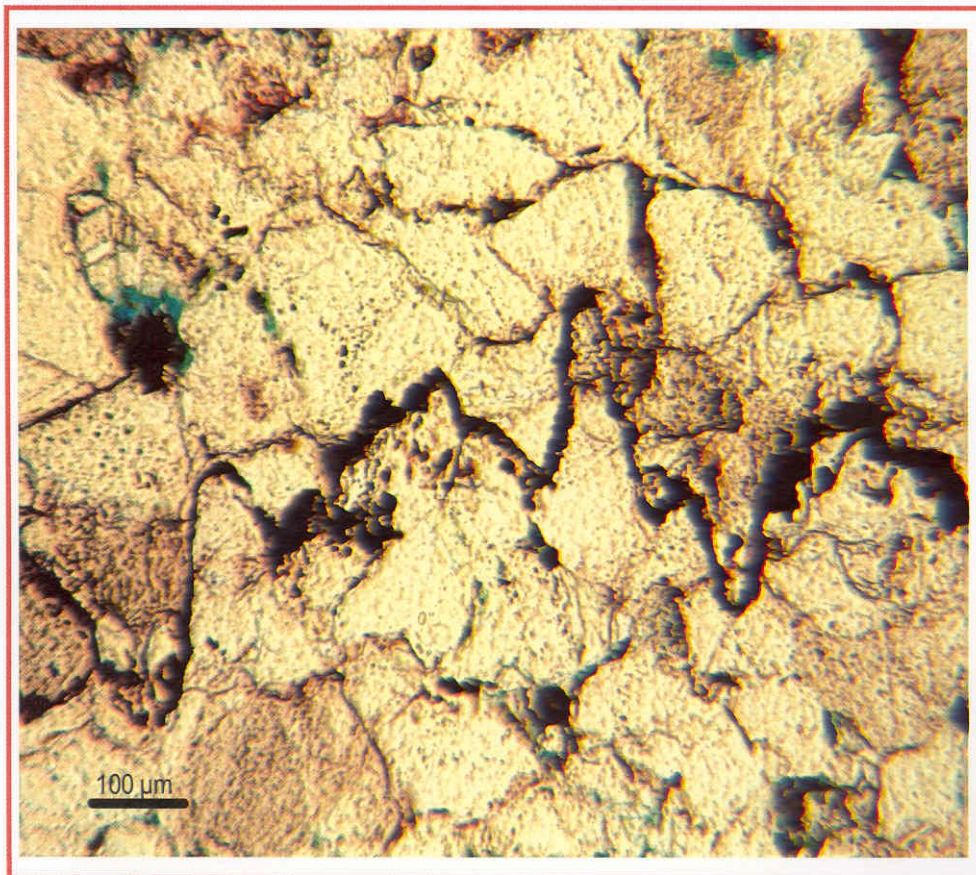


Figure 105: Photomicrograph shows moderate amplitude (0.5 mm) stylolite surface. GL # 1, 9434 ft.

along oyster shell fragments). The volume of silica that could have been derived from dissolution along stylolites was estimated from the number and amplitude of stylolites in thin sections using the method of Sibley and Blatt (1976). One assumes that stylolite frequency in the thin section is representative of the stylolite frequency in the formation. Of 170 total thin sections, 27 sections contain a total of 81 stylolites. The sum of the maximum column height of all stylolites is 22.1 mm, which is the minimum total thickness of rock that has been dissolved. Heald (1955) suggests that the estimated volume of dissolved rock based on stylolite amplitudes is 3 to 10 times less than estimates based on point counting of heavy mineral residues along stylolites. So, as much as 66.3 mm to 220 mm of rock may have been dissolved along stylolites. The total thickness represented in thin sections is 5100 mm (170 thin sections x 30 mm length of thin section), with an average of 11% quartz cement in all of the 170 thin sections. The volume of silica in quartz cement represents 561 mm (total thickness 5100 mm x 0.11 (average quartz cement)).

Therefore, by applying Heald's (1955) assumption, dissolution along stylolites in Cotton Valley sandstones accounts for 1.3% to 4.3% of 11% quartz cement or 11.8% to 39% of the total quartz cement (66.3 to 220 mm/561 mm).

The volume loss of quartz along stylolites was also estimated by calculating what thickness of sandstone having a normal texture and composition had to be dissolved to yield a given thickness of insoluble residue along stylolites. The assumption is that the stylolite collects insoluble residue including heavy minerals, feldspar, pyrite and organic matter that was once homogeneously distributed in the rock. The average thickness of

insoluble residue along stylolites in the thin sections is 0.3 mm, the average matrix counted is 7.5%.

Therefore  $(x \text{ mm}) \times 0.075 \text{ (amount of matrix)} = 0.3 \text{ mm (average thickness of insoluble residue)}$

Then  $x = 0.3/0.075 = 4 \text{ mm}$

So, to get 0.3 mm of insoluble residue we need to dissolve 4 mm of quartz. Thus, we need to dissolve from the sandstone 13 times the thickness of the stylolite residue (in mm) to get the thickness of the insoluble residue.

The sum of thicknesses of insoluble residue in measured stylolites is 8.5 mm. Then the minimum estimated thickness dissolved should be  $8.5 \times 13 = 110.5 \text{ mm}$ . Thus, of the total stratigraphic thickness represented by thin sections (5100 mm), 561 mm is quartz cement and 110.5 mm of quartz grains were dissolved at stylolites. This method indicates that dissolution at stylolites yielded 2.2% of 11 % quartz cement or 20% of the quartz cement volume.

So, if Heald's (1955) observations apply to Cotton Valley sandstones, the internal sources of silica account only for a maximum of about 48% of the total quartz cement, and an external source of silica is required. Location of stylolites was determined in the cores and 21 samples were taken and their distances to the nearest stylolite above and below each sample recorded. Figure 106 a shows the cross plot of quartz cement volume (corrected) and the distance from nearest stylolite in cm. Immediately adjacent to stylolites ( $< 5 \text{ cm}$ ), values of quartz cement range from 2 to 15% and then increases to 22% as distance from stylolite increases to 20 cm. At distance



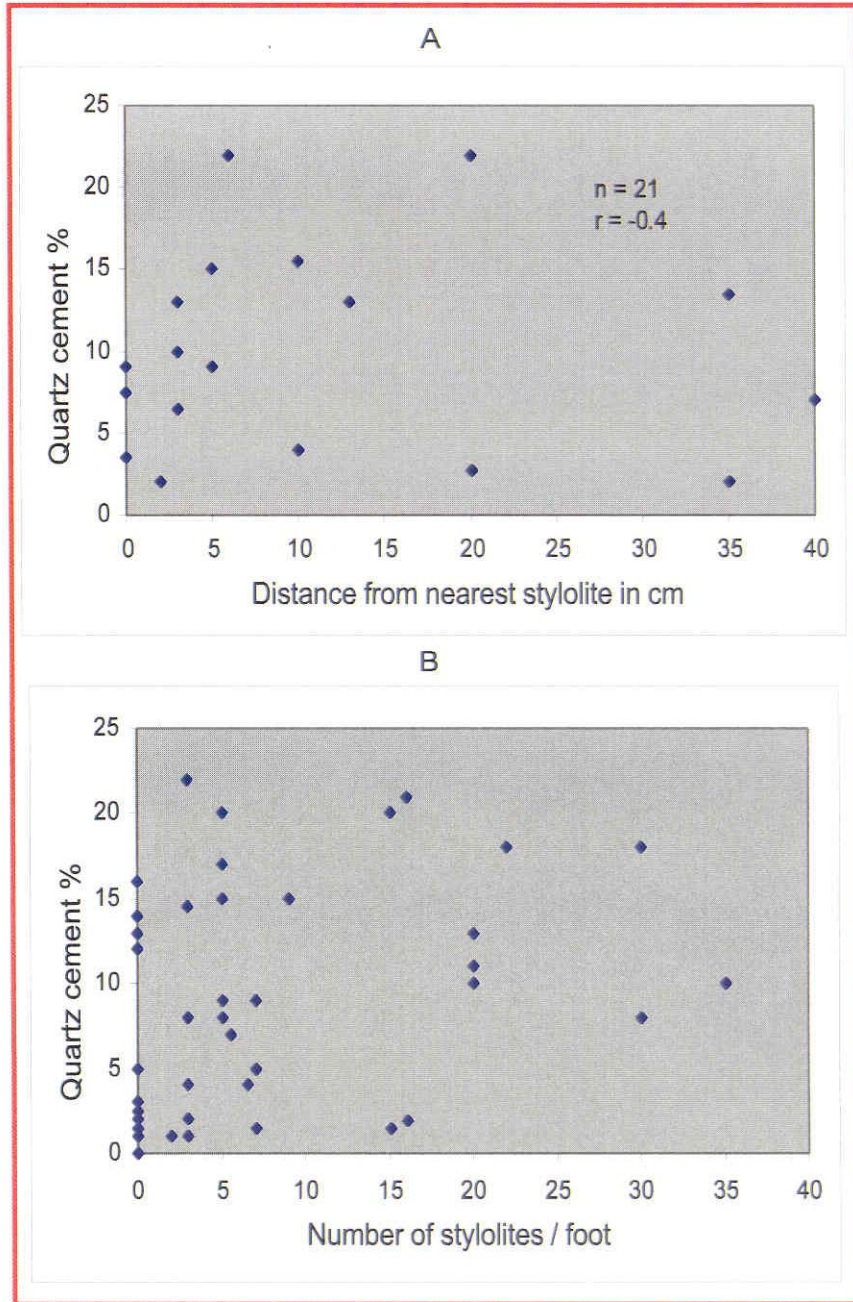


Figure 106: Cross plot between the quartz cement in a sample and the distance of the sample from nearest stylolite (A) and the number of stylolites /foot of core (B).

from 40 to 60 cm, quartz cement values vary between 2 and 10%. These data show a poor correlation ( $r = -0.4$ ) between the distance from nearest stylolite to the amount of quartz cement (Fig. 106a). Walderhaug and Bjørkum (2003) studied the effect of stylolite spacing on quartz cementation in the Lower Jurassic STØ Formation, southern Barents Sea, and found a good relationship between the amount of quartz cement and the distance to nearest stylolite. They concluded that the amounts of quartz cement decrease as the distance from stylolites increase. I did not find this relationship in my samples. The data of Walderhaug and Bjørkum (2003) is exceptional because of the lack of clay laminae along stylolites and the distance between stylolites reaches up to few meters.

A plot of the number of stylolites per foot versus quartz cement for 49 samples (Fig. 106b) also has a poor correlation ( $r = 0.4$ ). In parts of cores that lack stylolites, quartz cement ranges from 0 to 17%. I didn't find a relationship between the amount of quartz cement and either distance from nearest stylolite or number of stylolites per foot.

Dutton (1986), in her study of the Travis Peak Formation which overlies Cotton Valley Sandstones, concluded that dissolution of silica along stylolites accounted for only 12.5% of the total quartz cement (13.5%).

Spötl et al. (2000) summarized problems in all techniques that attempt to quantify the amount of silica derived from stylolites: (1) measuring the stylolite amplitudes systematically; this method give only the minimum volume and tends to overlook stylolites not visible macroscopically; (2) multiplying the stylolite amplitude by some poorly constrained correction factor (Heald, 1955; and Dutton and Diggs, 1990); (3) comparing the concentration of heavy minerals within and outside the stylolite

results in a large error if the original heavy mineral concentration is low or if some heavy minerals have dissolved); (4) comparing the concentration of clay minerals within and outside the stylolite can give a high estimate because many stylolites originated along mud drapes; and (5) comparing the concentration of immobile trace elements within and outside the stylolites generate possibly large errors if the abundance of the predominant carrier mineral is primarily low. In spite of these problems, my data strongly suggest that significant amounts of silica had to be imported to Cotton Valley sandstones.

Ascending silica-rich fluids that resulted from smectite to illite transformation within Bossier shales which underlies Bossier shale is a possible external source of silica for CVS. Dutton (1986) concluded that internal sources of silica for Travis Peak Formation are not enough and ascending fluids from underlying formations were the main external source of silica.

#### **4.8.2.2. Isotope geochemistry**

The  $\delta^{18}\text{O}_{\text{SMOW}}$  value for pure quartz overgrowths was obtained by extrapolating the regression line of  $\delta^{18}\text{O}$  versus quartz overgrowth/total quartz to 100 % quartz overgrowth is 24.6 ‰ with a correlation coefficient of 0.8. This is statistically significant at the 99% confidence level. If quartz precipitated from evolved marine water with  $\delta^{18}\text{O}$  of +4 to +5, the  $\delta^{18}\text{O}_{\text{SMOW}}$  of 24.7‰ indicates a temperature of precipitation between 100°C and 115°C (Fig. 107). These temperatures are close to the homogenization temperatures of primary fluid inclusions measured in three samples (110°C to 115°C). There is no data available to analyze the present day isotopic

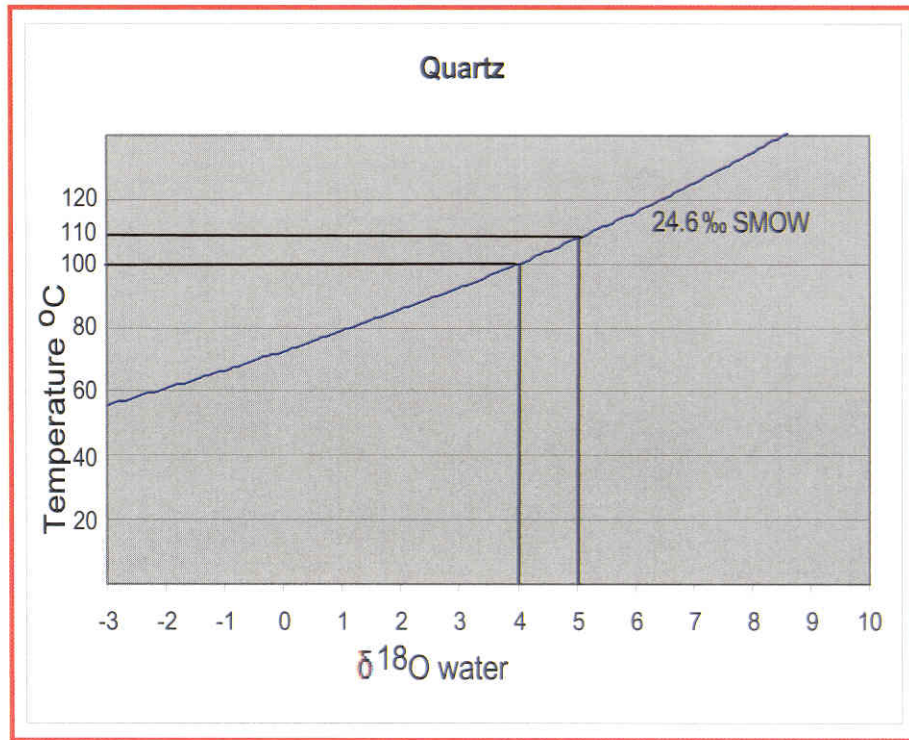


Figure 107: Temperature of quartz precipitation calculated from oxygen isotopic analysis assuming water isotopic composition ranging from +4 to +5 SMOW. Quartz-water fractionation equation from Friedman and O'Neil (1977).

composition of the formation water. The weak correlation coefficient ( $r^2 = 0.64$ ) of the oxygen isotopic regression line leads to an unquantified uncertainty of the calculated temperature of quartz precipitation.

### **4.8.3. Carbonates**

#### **4.8.3.1. Calcite**

Calcite and dolomite phases occur in Cotton Valley sandstones, but calcite is common. Total carbonates averages from 3.2% to 27.4% of the total rock volume in the different facies studied. Calcite constitutes about 98% of the total carbonates. Calcite occurs as concretions and completely cemented layers ranging in thickness from a few centimeters to 1 m. These layers commonly occur adjacent to limestone beds in the middle and upper parts of the CVS. However, calcite cement is not confined to sandstones adjacent to limestone beds, but it is also observed in all facies at various parts of the CVS. The abundance of calcite varies from one facies to another (Table 4). Storm-dominated shorefaces have the greatest amount of calcite (27%), probably because of the high content of oyster fragments at time of deposition. After burial, dissolution of shell fragments contributed to calcite cement. Sandstones from the tidally influenced shorefaces, bioturbated, and cryptobioturbated shorefaces average 2.5%, 3.5% and 2.9% respectively. Sand flat and laminated sandstones average 5.8% and 6.7% calcite, respectively. Calcite also occurs as a replacive phase. Calcitized feldspar grains range from 0 to 2.5% (average 1.5%) of the rock volume.

There are two main types of calcite:

1) Calcite type 1 occurs as blocky or poikilotopic cement that occludes all of the pores in layers reaching up to 1m thick and in spheroidal concretions of decimeter scale. Limitation of cores prevented me from determining whether the thicker calcite cemented sandstone bodies were large concretions or laterally extensive layers. Calcite cement type 1 ranges in abundance from 2% to 18% and averages 10% of total rock volume. Most of the calcitized feldspar grains (average 1.5% of rock volume) contain calcite type 1. IGV values for these samples range from 26.9% to 29.5% (with an average of 27.9%).

Petrographic evidence indicates that this calcite precipitated after significant compaction as indicated by the presence of long and rarely concavo-convex contacts (Fig. 108), and the IGV values. The depth of cementation of calcite type 1 was calculated by four ways. Firstly, by plotting the average IGV value (27.9%) on average porosity-depth curves for Atwater and Miller (1965) and Sclater and Christie (1980). Both curves reveal a depth of 2.2 kms. Secondly, by plotting the IGV value on IGV-depth curve of Paxton et al. (2002), which yielded a depth of 1.8 km. Thirdly, by using the temperature of precipitation of calcite type 1 from oxygen isotope data (see below). Genesis thermal reconstruction was also used as the basis for estimating the depth of formation of calcite 1 (about 1 km). The assumed temperature of precipitation of this calcite ranges from 52°C to 60°C. This calcite was most probably precipitated from sea water and assuming a sea floor temperature of 10°C and a geothermal gradient of 35.9°C/km (Dutton 1986), the calculated depth of cementation is 1-1.5 km. Thus, the depth of cementation of calcite type 1 ranges from 1.0 to 2.2 kms. Table 9 shows that

calcite type 1 has  $\delta^{18}\text{O}_{\text{PDB}}$  values of -5.9‰ to -6.8‰ (average = -6.4‰) and  $\delta^{13}\text{C}_{\text{PDB}}$  of -0.04‰ to -1.0‰ (average of -0.7‰). The carbon isotope values indicate that calcite 1 originated from the dissolution of marine shells or limestone which carries a sea water isotopic signature. Because the composition of the pore water at the time of calcite 1 precipitation is unknown, calculating the temperature of precipitation of this calcite requires some assumptions. Assuming that the original pore water was sea water, continuous water-rock interaction during burial would enrich it in  $\delta^{18}\text{O}$ . If  $\delta^{18}\text{O}$  reached values of +1‰ to +2‰ as expected from burial depth of 1-2.2 km, this calcite precipitated at 52°C to 60°C (Fig. 109a). Such temperatures are compatible with cementation at a burial depth of 1-2.2 km assuming 35.9°C/km as the geothermal gradient (Dutton, 1986) and a sea floor temperature of 10 °C. The source of Ca for calcite type 1 cement is the local dissolution and reprecipitation of the carbonate shell fragments in the sandstones and the oyster-rich lagoonal limestone beds interbedded with the sandstone.

2) Calcite Type 2 occurs as blocky and small crystals that fill primary and secondary pores. In cores I could not tell any specific megascopic distribution for this calcite. I only recognized its occurrence by using HCl. Calcite type 2 ranges in abundance from 2% to 7% and averages 5 % of total rock volume. Minor amount the calcitized feldspar grains (average 0.5% of total rock volume) contain calcite type 2. IGV values for these samples range from 20.2% to 27.9% with an average of 24%.

The depth of cementation of calcite type 2 ranges from 2.6 km to 3.2 km as calculated from plotting the average IGV value (24%) on the average porosity-depth curve of



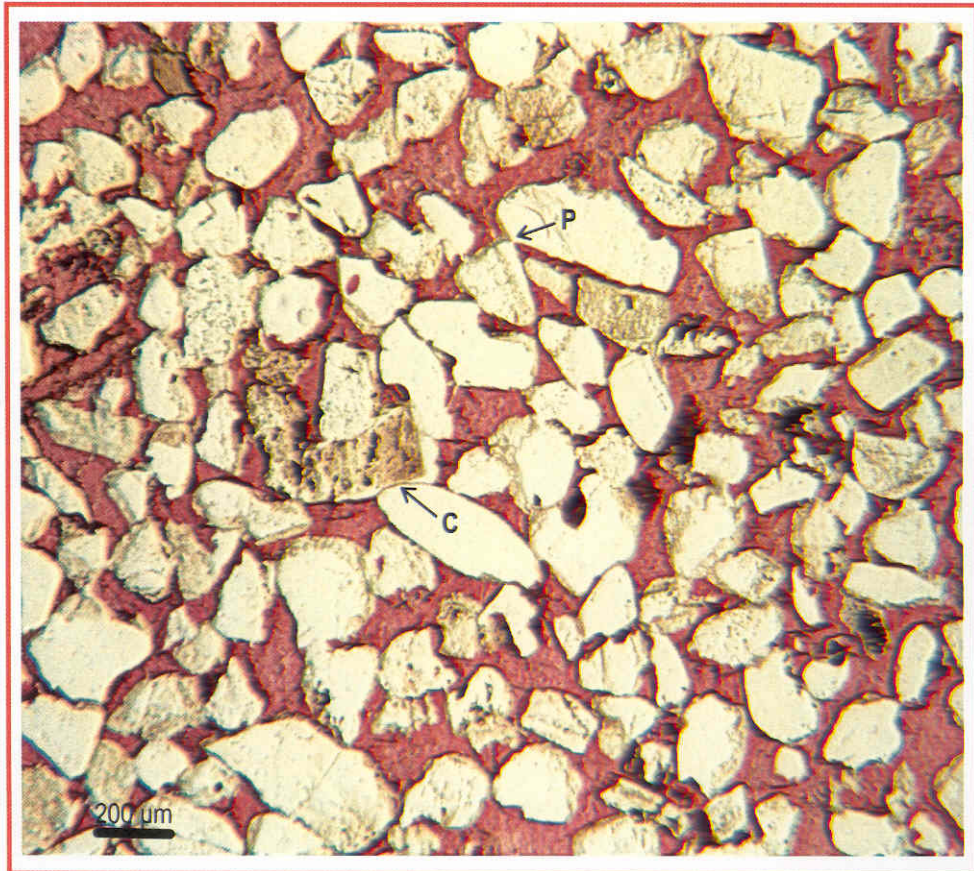


Figure 108: Calcite 1 (stained red). Note point (p) and concavo convex (C) grain contacts. Jones # 3, 8821 ft.

Table 9. Oxygen and Carbon isotopic data for bulk carbonate samples.

Carbonates	sample	$\Delta^{13}\text{C}$	$\delta^{18}\text{O}_{\text{PDB}}$	$\delta^{18}\text{O}_{\text{SMOW}}$
Calcite type 1	BS8584	-0.04	-5.9	24.5
Calcite type 1	BH9311	-0.7	-6.5	23.9
Calcite type 1	XLC9177.5	-0.3	-6.6	23.8
Calcite type 1	XLC9182.5	-0.7	-6.0	24.4
Calcite type 1	XLC9204.5	-1.0	-6.8	23.6
Calcite type 2	BS8679	-3.2	-10.1	20.3
Calcite type 2	BS8781	-3.5	-11.3	19.1
Calcite type 2	BS8852	-3.2	-11.4	19.0
Calcite type 2	BS8909	-2.5	-11.3	19.1
Calcite type 2	XLB9040	-2.4	-11.2	19.2
Dolomite	BS8679	-2.7	-10.2	20.2
Dolomite	BS8781	-3.1	-10.4	20.0
Dolomite	XLC9204.5	-2.0	-9.3	21.1
Dolomite	BS8584	-2.5	-6.7	23.7

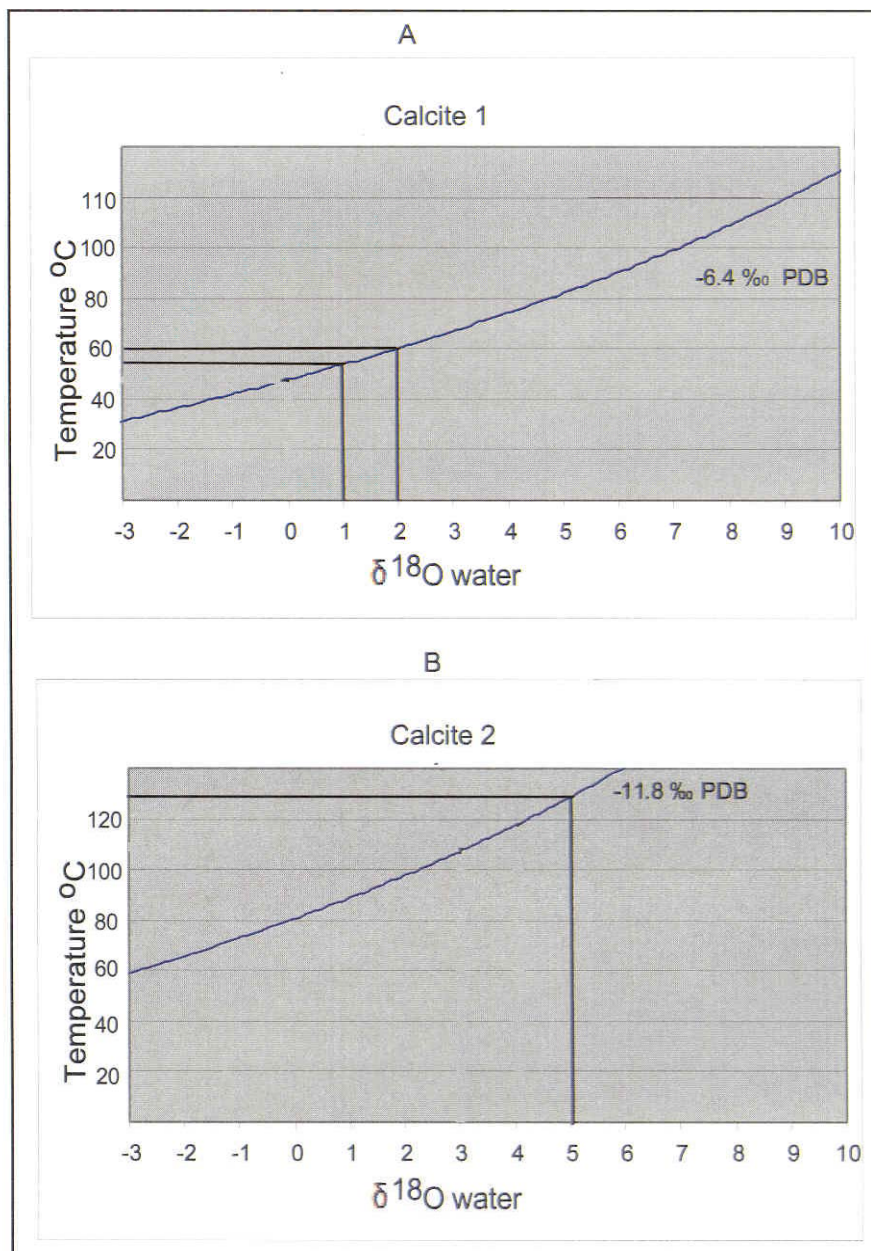


Figure 109: Range of possible temperatures and water isotopic composition for calcite type 1 (A) and calcite type 2 (B). Calculated from the calcite-water fractionation equation from Friedman and O'Neil (1977).

Sclater and Christie (1980) and Atwater and Miller (1965), respectively. Plotting the IGV value on the IGV-depth curve of Paxton et al. (2002) yield a depth of cementation of about 3.5 km. Using the same approaches to calculate the depth and temperature of cementation of calcite type 2 using IGV as was used for calcite type 1 yields temperatures of 130 °C and depth range from 2.6 to 3.5 km. Petrographic evidence indicates that this phase of calcite post-dated quartz cementation (Fig. 110). However, quartz cementation is a continuous processes and quartz could have been precipitated in other parts of the rocks.  $\delta^{18}\text{O}$  values of calcite type 2 cement range from -10.1‰ and -11.4‰ (average = -11.0 ‰) and  $\delta^{13}\text{C}$  values range from -2.4‰ to -3.5‰ (average = -3.0‰). The estimated temperature of precipitation of quartz cement ranges from 100°C and 115°C (see quartz cement section). Assuming that at this temperature  $\delta^{18}\text{O}$  pore water was between +4‰ and +5‰ and calcite type 2 should have formed deeper and hotter than quartz cement. Thus a value of +5 was assumed for  $\delta^{18}\text{O}$  pore water that precipitated this phase of calcite. Calcite type 2 precipitated at a temperature of about 130 °C (Fig. 109b).

$\delta^{13}\text{C}$  values range from -2.43‰ to -3.47‰ (average -3‰), which may reflect the mixture of some carbon from thermal decarboxylation with carbon from marine shells. Calcium derived from the dissolution and albitization of feldspars and from the marine carbonate-rich shales near the sandstones might be a source of calcite type 2.

#### **4.8.3.2. Dolomite cement**

The average volume of dolomite cement is 1%, but few samples contain abundant dolomite. Two samples in sand flat facies (DSF#1, 9511 ft (2882 m), and



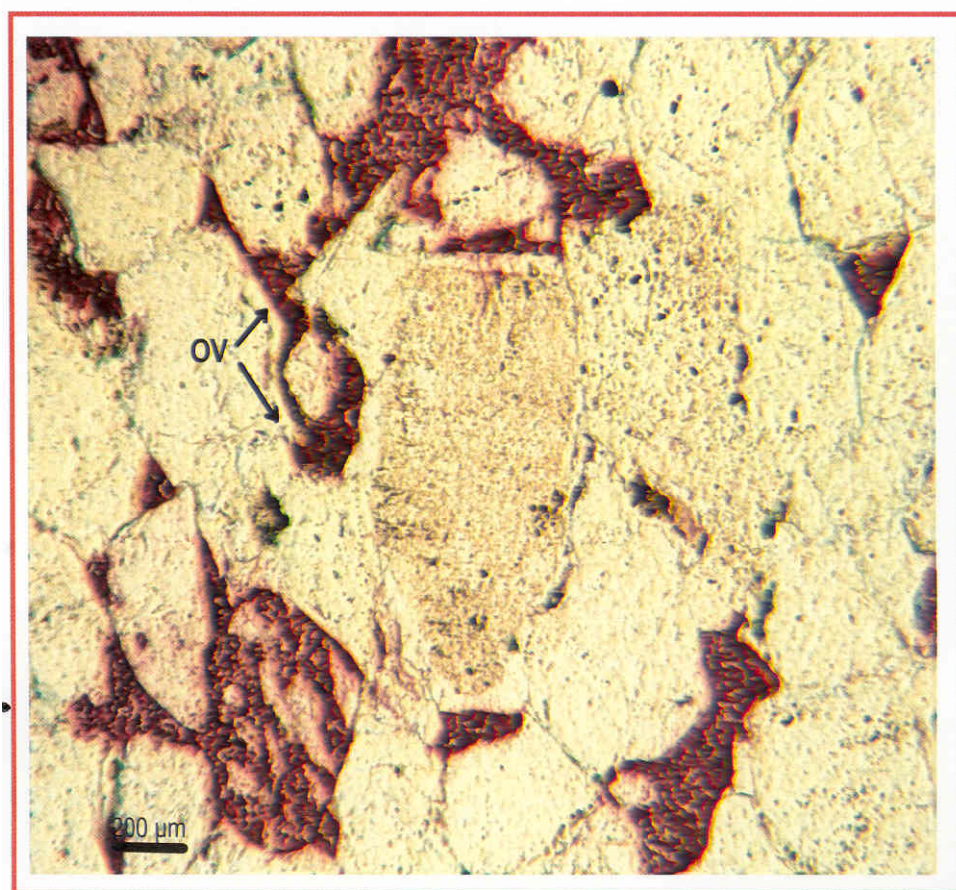


Figure 110: Calcite 2 cement (stained red) postdating quartz overgrowth (OV). BSH # 1, 9731 ft.

DSF # 1, 9514 ft (2883 m) contain 10% pore-filling dolomite. I could not recognize in cores dolomite cement. Dolomite rhombs are iron rich (as shown by EDS analysis) and commonly precipitated within detrital clay matrix or are recrystallized from calcite. In most samples calcite type 2 is surrounded by the later iron-rich dolomite, but in some samples calcite type 2 was replaced by iron-rich dolomite. Feldspar grains replaced by dolomite are minor.

The average isotopic composition of late diagenetic ferroan dolomite ( $n = 4$ ) is  $\delta^{18}\text{O}_{\text{PDB}} -9.1\text{‰}$  and  $\delta^{13}\text{C}_{\text{PDB}} -2.5\text{‰}$  (Table 9). Ferroan dolomite was precipitated at estimated temperatures between 155°C and 163°C assuming pore water with isotopic values between +5.0‰ and +6‰, which are values heavier than the pore water which precipitated calcite type 2 (Fig. 111). Magnesium for dolomite was most probably derived from detrital clay transformation. Dutton and Land (1985) pointed out that the reduction of iron compounds during organic maturation can provide reduced iron for ferroan dolomite. Boles and Franks (1979) believed that the amount of iron and magnesium necessary for converting calcite into ferroan dolomite can be derived in sufficient quantities and at appropriate temperature from adjacent shales and mudstone by the transformation of smectite to illite. Cotton Valley sandstones have an average of 20%-35% shales interbedded with the sandstones; these could be a good source for iron as well as carbonates and silica.

#### **4.8.4. Clay minerals**

##### **4.8.4.1. General Remarks**

Kaolinite, chlorite, and illite are the authigenic clay minerals identified in Cotton

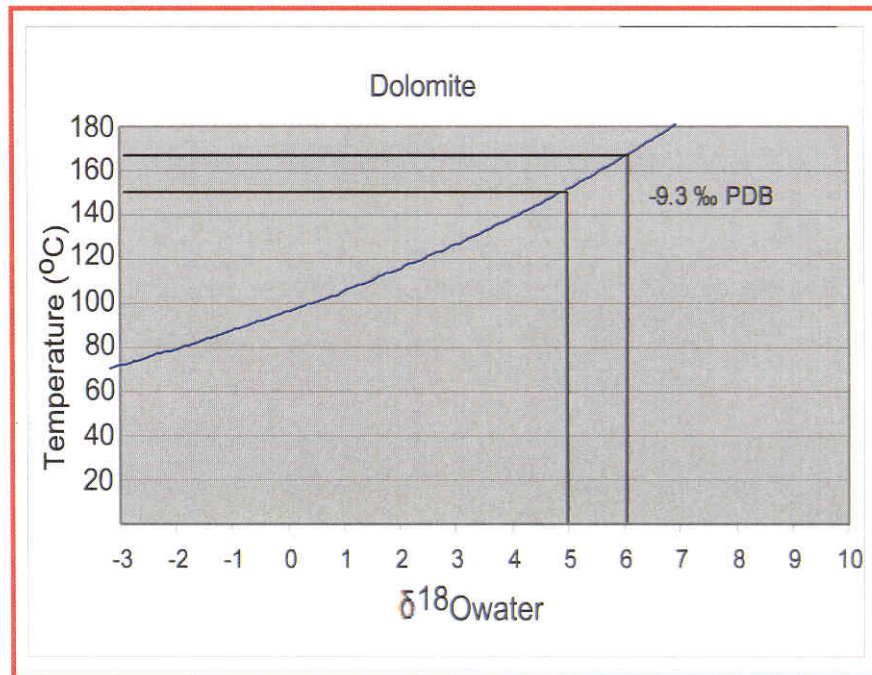


Figure 111: Possible temperature range and water isotopic composition for authigenic dolomite. Calculated from dolomite-water fractionation equation in Friedman and O'Neil (1977).



Valley sandstones. Kaolinite and chlorite are the most abundant authigenic clays with an average of 1.2% and 0.8% in the different facies studied (Table 4). Illite cement average 0.5% of the sandstone volume. These values based on point counts and some of that volume is micropores. Authigenic clays occur as pore-filling cements, replacive phases and clay coats. Galloway (1974) classified clay coats and clay rims on the basis of the clay crystal's orientation to its substrate. This distinction is difficult to make in thin sections and the general term "clay coats" is used here. In rare samples illite crystals was observed (SEM) oriented normal to quartz grain surfaces and the term illite rim is used. Except in illite section, the term clay coat will be used for both illite and chlorite coats. The original composition of clay coats is not known, but coats are most probably derived from recrystallization of previous detrital clays (chlorite and smectite). Direct precipitation from pore water is also possible.

The crystallization of authigenic clay minerals in sandstones during diagenesis is especially dependent upon pore-fluid chemistry (Bjørlykke, 1979; Galloway, 1984). In turn, the pore fluid composition is controlled by many factors, the most important of which include depositional environment, dissolution of detrital grains and cements, and the extent of fluid flow and mixing during diagenesis. Burley et al. (1986) suggested that not only can the composition, texture and geometry of original sedimentary deposits be expected to exert a controlling influence on clay authigenesis, but so can the gross physical and chemical environment. The availability of water within the sediment and its ability to move within the sediment are as important in diagenesis as the actual pore fluid composition.

#### **4.8.4.2. Kaolinite**

Kaolinite was observed in most of the samples. Authigenic kaolinite occurs in primary pores and secondary pores and commonly is associated with relicts of dissolved feldspar grains (Fig. 112a). Destruction of feldspars was the main source for kaolinite cement which either replaced feldspar grains or fill secondary pores after feldspar dissolution. Kaolinite precipitation overlapped quartz cement, but most appears to have precipitated after quartz cement. Kaolinite is well crystallized, face-to-face stacks of pseudo-hexagonal plates with abundant micropores (Fig. 112b).

Formation of kaolinite from saline water requires an acidic pH (Shelton, 1964), which can be accomplished by the dissolution of CO<sub>2</sub> released during organic matter maturation. Under these conditions the water becomes undersaturated with respect to chlorite and illite but, kaolinite is precipitated. The precipitation of kaolinite appears to be the first diagenetic event following carbonate dissolution (Fig. 113). Schwartz and Longstaffe (1988) suggested that, over the pH range of 3 to 6, calcite cement dissolves, which drives the solution pH to higher values. In contrast, the activity of aluminum drops by several orders of magnitude over the same increase in pH, leading to supersaturation of aluminum and precipitation of kaolinite.

Components for kaolinite in Cotton Valley sandstones were mostly derived from the dissolution of detrital feldspars. The larger amounts of kaolinite observed in close proximity to or within degraded feldspars support that origin. Al and Si may also have been derived from fluid expelled during the compaction of nearby shales.

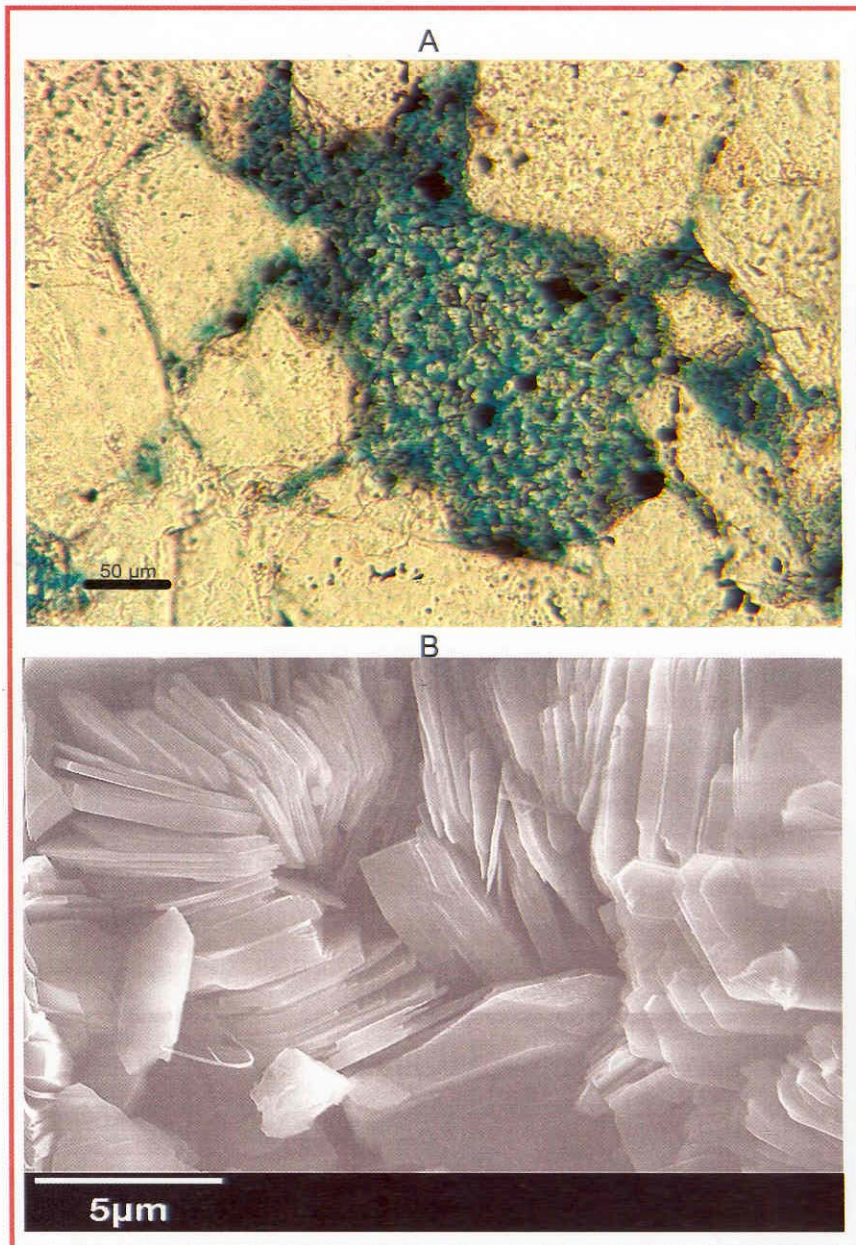


Figure 112: Shows kaolinite cement with micropores (A) and well formed pseudo-hexagonal plates of kaolinite. Samples are from BSH # 1, 8639 ft, and Jones # 3, 9606 ft respectively.

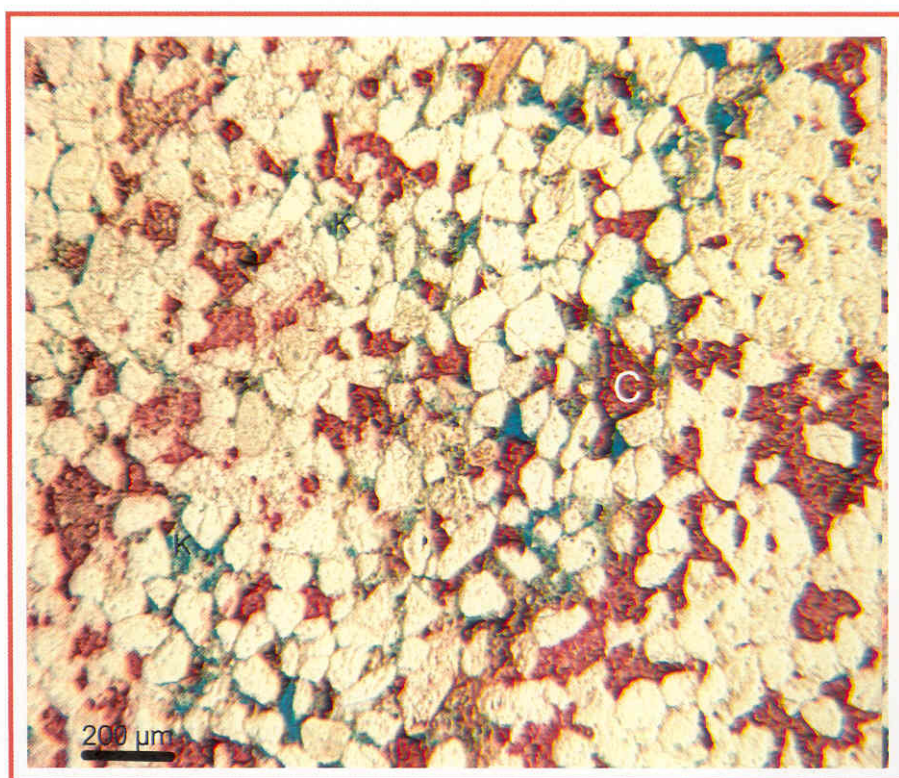


Figure 113: Dissolution of calcite (C) and precipitation of kaolinite (K). Note blue areas are porosity. BSH # 1, 8781 ft.

#### **4.8.4.3. Chlorite**

Fe-rich chlorite occurs as an early diagenetic grain coating and as a late diagenetic pore filling and replacement of feldspars. Chlorite cement ranges from 0.4% to 1% in the different facies studied. That the chlorite coating was early is suggested by its partial to complete coating of framework grains. Point counting of 200 grains per sample in 22 samples indicates chlorite coatings range from 1 % to 19% of rock volume with an average of 8.9% in different facies (Appendix E). Several sources of early chlorite coatings have been discussed in the literature. Longstaffe (1986) reported that early grain-coating Fe-rich chlorite occurs only within sedimentary facies that were very closely associated with marine to non-marine transitions. Schwartz and Longstaffe (1988) suggested that wave and /or current motion causes the concentric accretion of chlorite about the sand grains and that iron necessary for clay crystallization can be obtained from fresh water that fed into the system.

Other workers have favored the formation of early diagenetic chlorite from marine pore water in a low-energy environment (Rohrlich et al., 1969). Johnston and Johnson (1987) suggested that the formation of early chlorite coating may result either by infiltration of colloidal clay-rich waters or by in situ alteration of feldspars. Clay coating in the Cotton Valley Sandstones may have been recrystallized from detrital clay that entered the sandstone shortly after deposition.

Most pore-filling chlorite appears to have precipitated after quartz cement and averages 0.7% of total sandstone volume. Late diagenetic chlorite is also iron-rich

(chamosite) and usually consists of euhedral to subhedral crystal plates arranged in a haphazard face-to-edge card house (Fig. 114). Bell et al. (1993) pointed out that where  $K^+ / Mg^{2+}$  ratio and  $K^+ / Fe^{2+}$  ratios were initially low, the precipitation of iron-rich chlorite is favored. Iron and  $Mg^{2+}$  may be supplied to pore waters from the breakdown of detrital clays or smectite to illite transformation in the adjacent shales.

Clay coating plays an important role in controlling the amount of quartz cement in the Cotton Valley sandstones (Fig. 115) and hence strongly affected reservoir quality. Clay coatings predate quartz cement and where thick and continuous it can retard quartz cementation. When thin and discontinuous, clay coats form a dustline separating detrital quartz grains from authigenic cement.

Genuise (1991) reported that dissolved iron, magnesium, silica, and aluminum must be available to produce authigenic chlorite. He also pointed out that possible sources of these components include: dissolution of volcanic rock fragments, transformation of other authigenic clays, smectite to illite transitions in the interbedded shales, and dissolution of carbonate cements, iron oxides, and pyrite.

#### **4.8.4.4. Illite**

Illite in Cotton Valley sandstones ranges from 0% to 1.9% and averages 0.5% of the sandstone volume. It occurs as grain rims of tangentially to near vertically oriented crystals (Fig. 116a). Illite hairs also are oriented at high angles to grain surfaces to form meniscus-shape bridges between adjacent grains (Fig. 116b). In most samples illite rims are thin and did not prevent quartz cement. Where illite rims are thick enough they retarded the precipitation of quartz cement. Authigenic illite rims probably formed



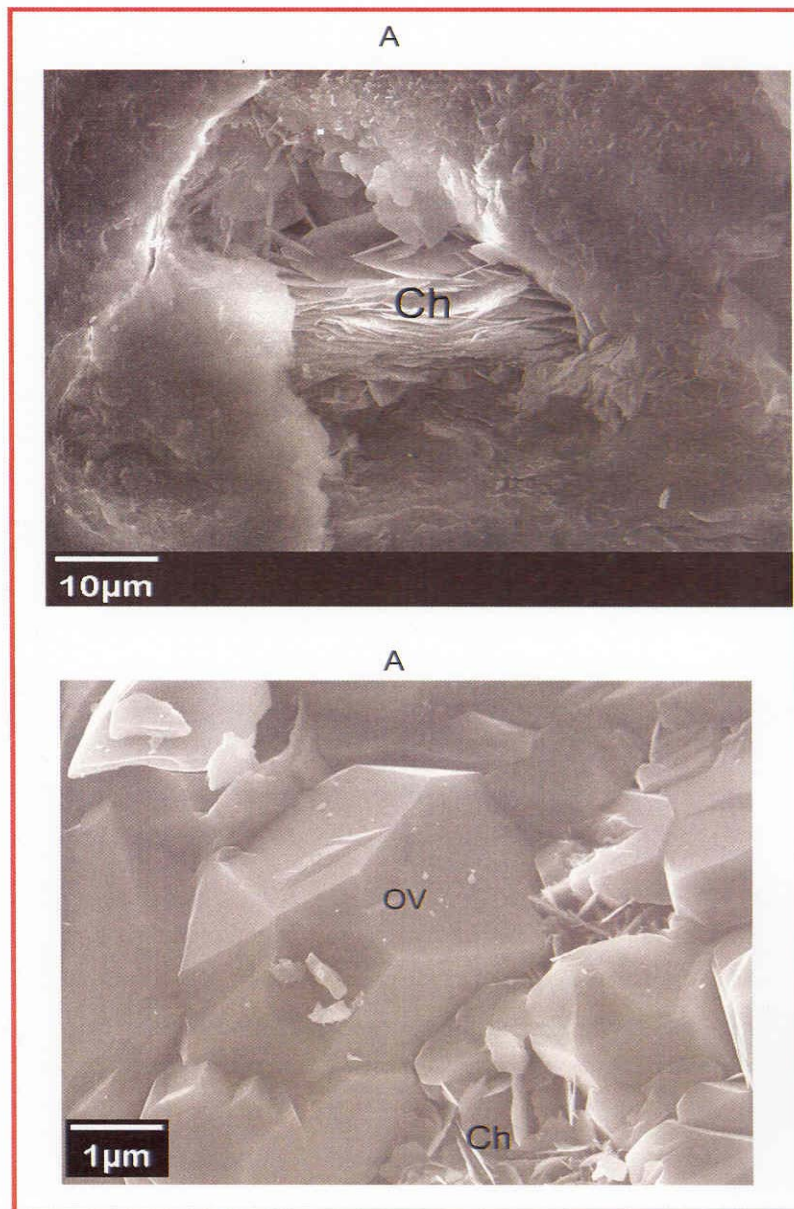


Figure 114: Pore filling chlorite (Ch). Note in B chlorite overlap and post date quartz cement (OV). JA # 1, 8958 ft.



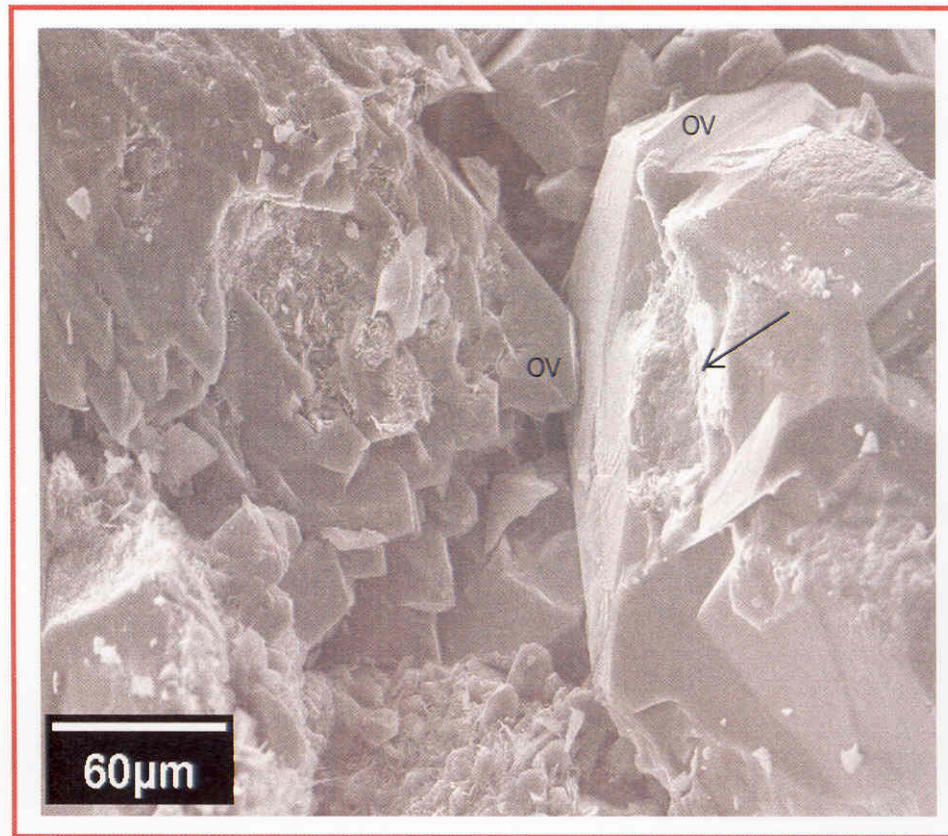


Figure 115: SEM image showing intensive quartz overgrowth cement (OV). Note thick clay coat locally prohibited quartz cementation (arrow). Jones # 3, 8753 ft.

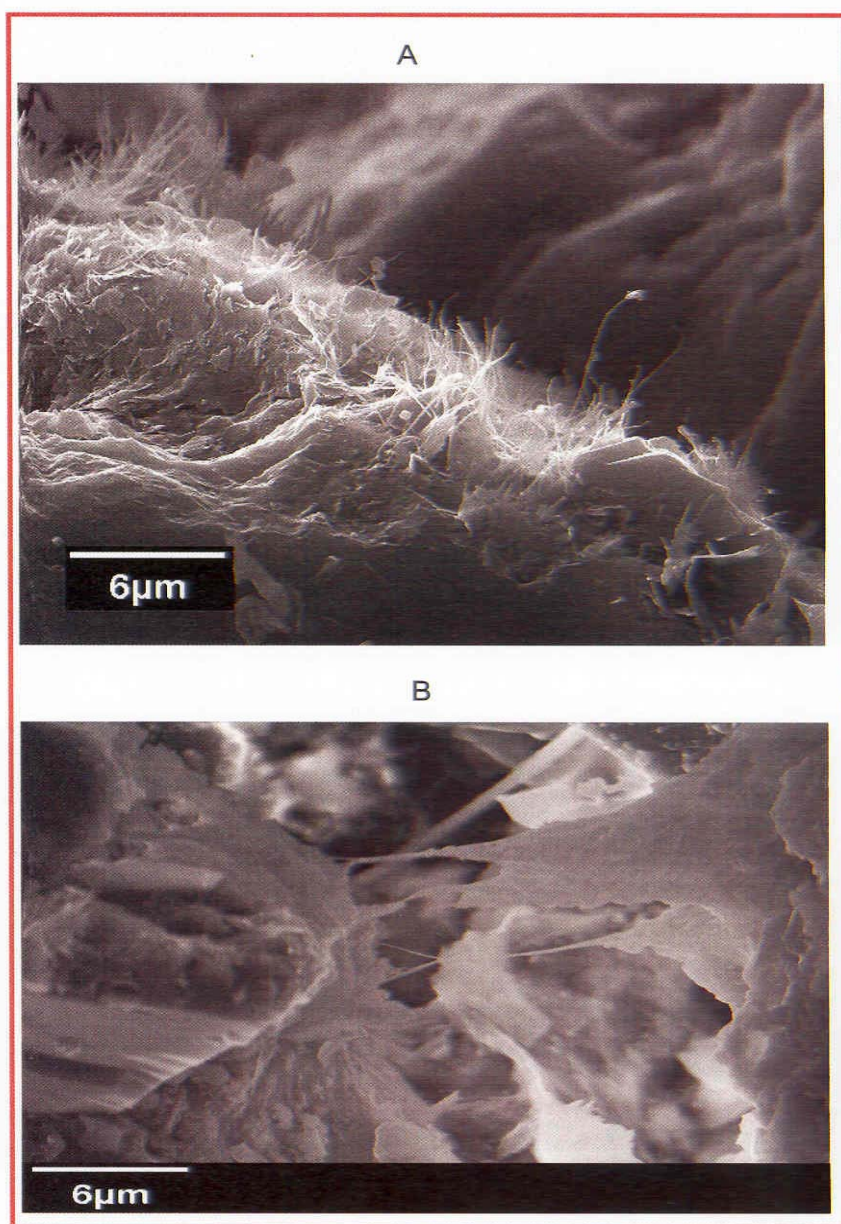


Figure 116: SEM images showing pore-bridging fibrous illite cement (A) and illite rimming detrital grains (B). Samples from Jones # 3, 9454 ft, and GL # 1, 9619 fy, respectively.

contemporaneously with or shortly after chlorite and pre-dated quartz cement, whereas pore-bridging illite post-dated quartz cement. Illite forms where the pore solution reaches a relatively high  $K^+/H^+$  ratio by a continuous release of  $K^+$  and consumption of  $H^+$ ; under these conditions kaolinite is unstable. Muscovite, the only mica present, shows evidence of dissolution and accounts for additional source of  $K^+$ . Illite may also be a result of illitization of smectite or recrystallization from previous detrital clay. The origin of early grain lining or late pore bridging illites is not known. Illite could form from many precursor minerals (kaolinite, smectite, recrystallization of detrital clay minerals) at various temperatures. Bjorkum (1988) suggested that illitization of kaolinite could be formed at temperatures as low as 50 °C. Bjørlykke (1984) suggested that illite in closed system could be formed at temperatures from 130-150°C. Hurst and Irwin (1982) suggested that in open system illite could be formed at temperatures lower than 120°C. Based on my paragenetic sequence, I infer that illite in the CV formed between 120-130 °C

#### **4.8.5. Other authigenic minerals**

##### **4.8.5.1. Feldspars**

Authigenic feldspar is a minor component and ranges from 0.1% to 1% of framework grains in various facies. K-feldspar occurs as external overgrowths, whereas albite occurs as internal growths within the partially dissolved feldspar grains. Authigenic albite occurs as partial pseudomorphic replacements of detrital feldspars and SEM and BSE show that albitized feldspars are composed of abundant euhedral crystals (10-80 microns) that grew mostly along the detrital host feldspar grains. This authigenic albite does not luminesce

under CL. Microprobe analyses of diagenetic feldspars (appendix C1) show a nearly pure albite has a composition of > 95 mole % Ab.

Detrital K-feldspars have an average composition of > 93 mole % orthoclase. Many plagioclase grains show albite twinning; other grains show chessboard twinning that is the product of albitization (Gold, 1984). Albite is present in selected samples from four wells having a depth range from 8693 ft (2634 m) to 10112 ft (3064 m). No trend of degree of albitization was found over this narrow range. However, albitization was extensive in sample BSH 8693 ft., near the top of the formation (appendix C). Dutton (1986) explained the more complete albitization near the top of Travis Peak Formation which overlies CVS, as a result of the movement of hydrocarbon-transporting fluids at the very top of the formation. In CVS, there is a significant production of gas from the upper few hundred feet of the formation (stacked barrier islands below Knowls Limestone, which is a good sealing rock). Later fluid that emplaced the hydrocarbons in sandstones at top of the formation may also caused albitization. K-feldspar overgrowths formed at the same time or before quartz cement,

because calcite type 2 post-dated feldspar overgrowths. However, I can not tell the relative timing and temperature of precipitation of albite. Kaiser (1984) argued that albitization in the Frio Formation (Oligocene) occurred at a much lower temperature range, from 50°C to 85°C. Dutton (1984) indicated that albitization in the Travis Peak Formation started at 80°C. CVS is deeper and hotter than Travis Peak formation and a temperature of 90°C is assumed for the precipitation of albite. Dissolution of K-feldspar and muscovite contributed to K-feldspar overgrowths. Na required for albitization was

most likely derived from Na-Cl brines that were mobilized during Early Cretaceous time by salt dome dissolution. The Al was most probably derived from the dissolution and replacement of silicates in sandstone.

#### **4.8.5.2. Pyrite**

Pyrite is a minor but ubiquitous diagenetic component. It ranges in abundance from 0% to 2% of the total rock volume in different studied facies. It commonly occurs as disseminated subcubic crystals, framboids (Fig. 117a and b) and scattered clusters that precipitated within the pores. Pyrite also replaced framework grains. Textural relationships suggest that there are two stages of pyrite formation, early pyrite that largely filled primary pores, and late pyrite associated with the emplacement of hydrocarbons.

Berner (1970) pointed out that pyrite clusters which display clear framboidal texture is probably a result of recrystallization from colloidal solution. Schwartz and Longstaffe (1988) indicated that early diagenetic pyrite is formed close to the sediment-water interface, where the depletion and destruction of solid organic by aerobic bacteria takes place. The reduction of  $\text{Fe}_2\text{O}_3$  to FeO and sulfate-reducing bacteria liberate bicarbonate ions into the pore water and continue to reduce pH by the production of  $\text{H}_2\text{S}$  gas. Some of the  $\text{H}_2\text{S}$  gas may diffuse upward to the sediment-water interface, while the remainder reacts with iron to form early diagenetic pyrite (Schwartz and Longstaffe, 1988). Early diagenetic pyrite occurs as fine framboidal grains and aggregates (Einsele, 1992). Folk (1998) interpreted some framboids as the pyritized corpses of nannobacterial cells which indicated that precipitation of iron sulfide was



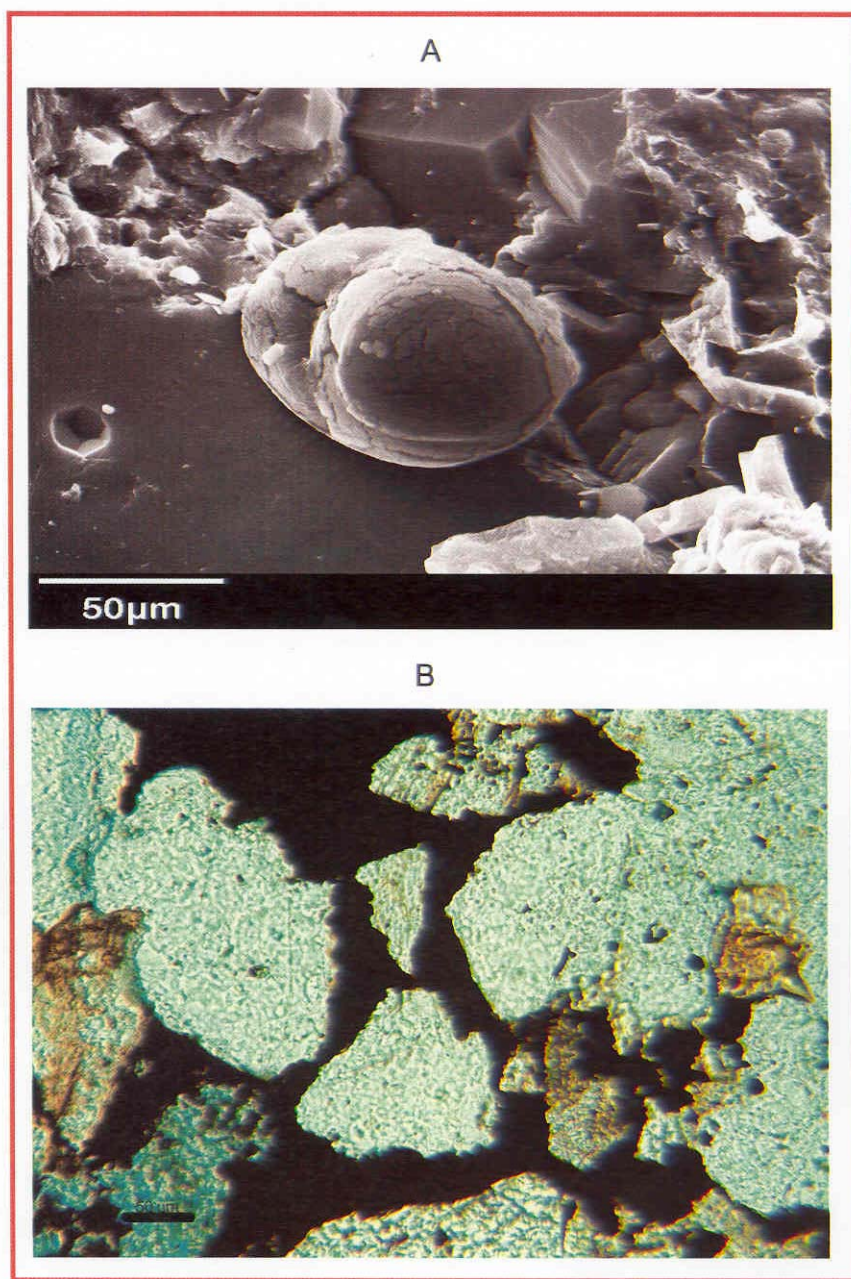


Figure 117: Framboidal pyrite (A), and early pore-filling (B). Note corroded margins of quartz grains (arrows). Samples are from GL # 1 9591 ft and BSH # 1, 8652 ft, respectively.

performed by these dwarf forms of bacteria, often associated with decaying organic matter. Late diagenetic pyrite most probably formed during the emplacement of hydrocarbons bearing H<sub>2</sub>S.

#### **4.8.5.3. Anhydrite**

Anhydrite is a minor component in the CVS. It was recognized only in one core (Cargil gas unit # 15) as fracture-filling cement. Anhydrite cement in this core was identified in 12 thin sections from different facies (appendix B); most samples contain less than 2.8% anhydrite, but one sample from Cargil gas unit # 15 (9358.5 ft; 2835.9 m) has 26.5% anhydrite cement. Anhydrite replaces framework grains and calcite type 2. Petrographic evidence indicates it precipitated after quartz overgrowths and probably after iron-rich dolomite. Both anhydrite occurrences are interpreted as late diagenetic phases. It is most probably a precipitate from brine fluids that entered the sandstones from the underlying salt beds.

### **4.9. Porosity and permeability**

#### **4.9.1. General remarks**

The amount of porosity visible in thin sections is quite variable, ranging from 0 to 7.5%. Thin section porosity was divided into primary and secondary types; primary porosity in the studied facies ranges from 0 to 2.5% with average of 1% (Table 10). Secondary porosity results from dissolution of framework grains (mainly feldspars) and cements (calcite) and ranges in all studied facies from 0 to 5% and averages 3.4%. Secondary porosity constitutes up to 75% of the total porosity, but averages 68.1%. The retention of higher primary porosity (4-4.5%) in some sandstone like GL # 1, 9510 ft.,



(2881 m) and JA # 1, 10026 ft., (3038 m) suggests that quartz cementation was not extensive in these samples and this is because of the presence of thick chlorite coats around detrital grains. The distribution of visual porosity is largely controlled by facies; bioturbated and cryptobioturbated shoreface sandstones have the highest porosity values of 6.5% and 7.5%, respectively (Table 10). Storm-dominated and laminated sandstones have visual porosity values of 2% and 3.5%, respectively. Tidally influenced shorefaces and sand flat sandstones have porosity values of 5% and 6%, respectively.

Most of the secondary porosity appears to have formed by dissolution of feldspar grains. Minor dissolution of calcite cement also contributed to secondary porosity (Fig. 118). Sandstones from the bioturbated, cryptobioturbated shorefaces and sand flat environments have the highest average values of secondary porosity, 4.5%, 5%, and 4%, respectively. Sandstones from the tidally influenced, storm-dominated, and laminated sandstones have average secondary porosities of 2.5%, 3% and 1.5%, respectively.

Porosimeter porosity values range from 2.5% to 9% with average of 6% in the different studied facies (Table 10). Sandstones from the cryptobioturbated and bioturbated shorefaces have the highest average measured porosity of 9% and 8%, respectively, whereas, storm-dominated and laminated shoreface sandstones have the lowest average porosity values of 2.5% and 4%, respectively (Table 10). The correlation coefficient between porosimeter and point-counted values is 0.90 (Fig. 119). Point-counted porosities are less than equivalent core analysis porosities owing to the presence of micropores between authigenic clay crystals and within clay matrix.

Table 10. Porosity and permeability data in potential reservoir facies. md = millidarcy.

Facies	Primary porosity (%)	Secondary porosity (%)	Total visual porosity (%)	Measured porosity (%)	Micro-porosity (%)	Permeability (md)
Bioturbated	2.0	4.5	6.5	8.0	1.5	0.01-10
Cryptobioturbated	2.5	5.0	7.5	9.0	1.5	0.01-10
Laminated	1.0	2.5	3.5	4.0	0.5	0.01-0.05
Tidal shoreface	2.0	3.0	5.0	6.0	1.0	0.01-0.03
Storm shoreface	0.5	1.5	2.0	2.5	0.5	0.01-0.1
Sand flat	2.0	4.0	6.0	7.0	1.0	0.01-1.0

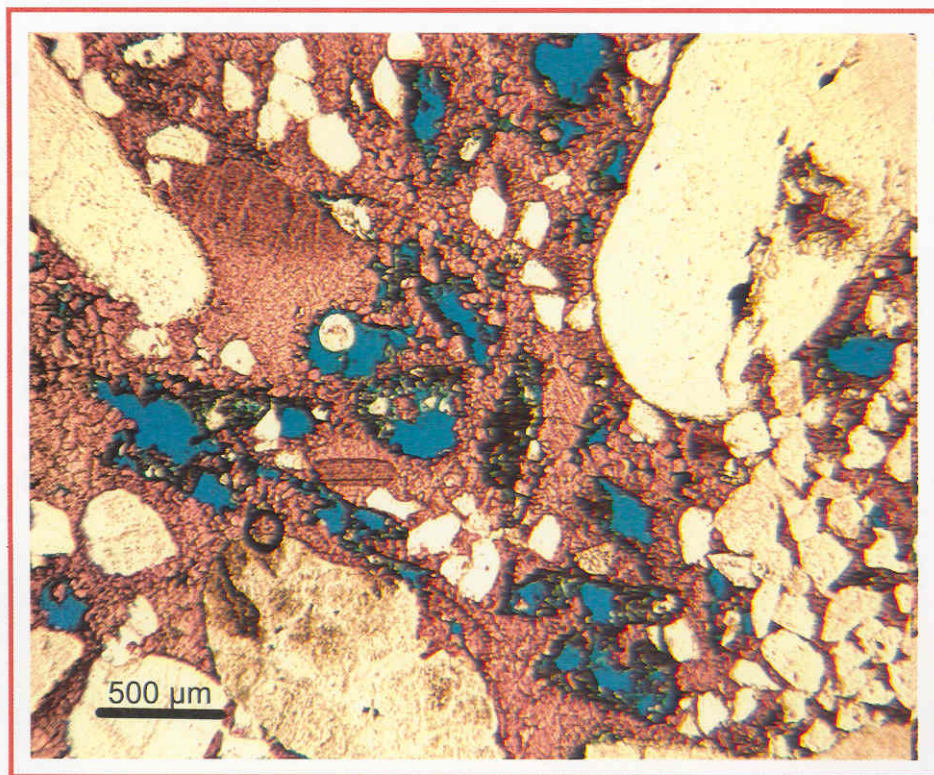


Figure 118: Secondary porosity formed after calcite dissolution. Calcite is stained red and blue areas are porosity. BH # 1, 9811 ft.

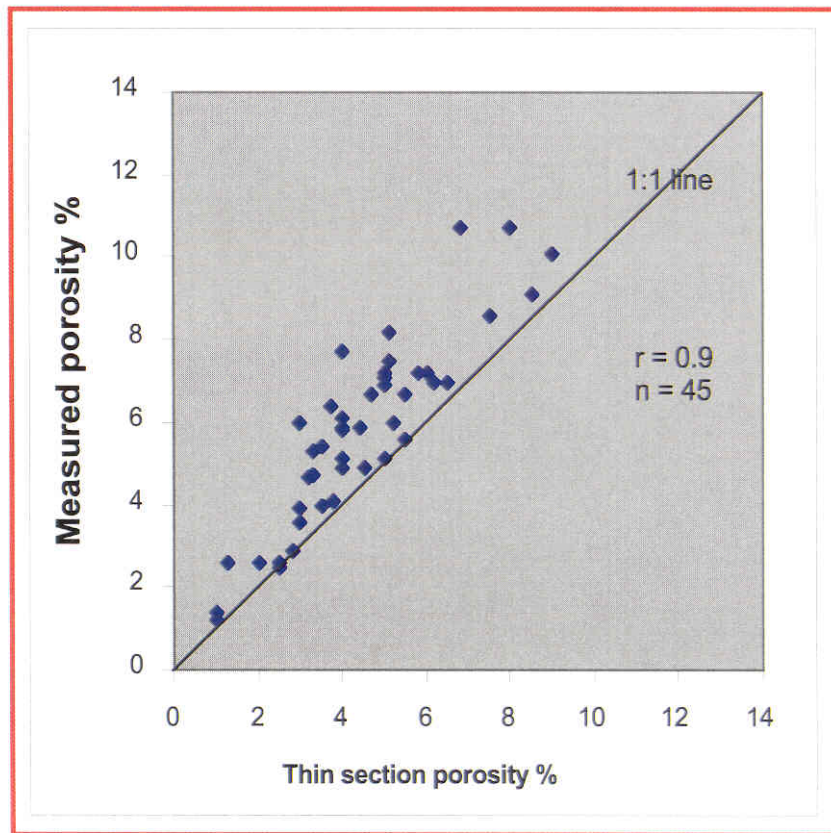


Figure 119: Cross-plot of porosimeter porosity versus point-counted porosity.

Microporosity (the difference between visual and measured porosities) is an important porosity type, especially in gas reservoirs and usually is underestimated or overlooked in thin-section. Significant microporosity occurs in clay-rich sandstones. Bioturbated shoreface sandstones have the highest average values (1.5%) of microporosity among all facies (Table 10). Sandstones from tidally influenced shoreface and sand flat environments have an average microporosity of 1%. Laminated shoreface sandstones have the least amount of microporosity with an average of 0.5%.

#### **4.9.2. Major pore types**

Types of pores observed in the Cotton Valley sandstones are intergranular, intragranular, moldic, oversized, and micropores (Fig. 120). Intragranular pores include all pores within partially dissolved feldspars, chert grains and heavy minerals. It ranges from 0% to 5.5% in all studied facies and averages 1.6% (appendix B). Complete dissolution of the detrital grains produces moldic or oversized pores. Moldic pores are common and range from 0.3% to 3% and average 1.4% in all studied facies, whereas oversized pores are rare. A visual micropore is any existing micropore between clay platelets, mainly associated with kaolinite and can be seen at high optical magnification. For this study, all intergranular pores are considered to be primary. Oversized pores are a combination of primary and secondary; one third of the oversized pores is assumed to be primary and two thirds secondary. However oversized pores are not common in the CVS. Secondary porosity is the sum of moldic porosity, intragranular porosity, and two thirds of the oversized pores.

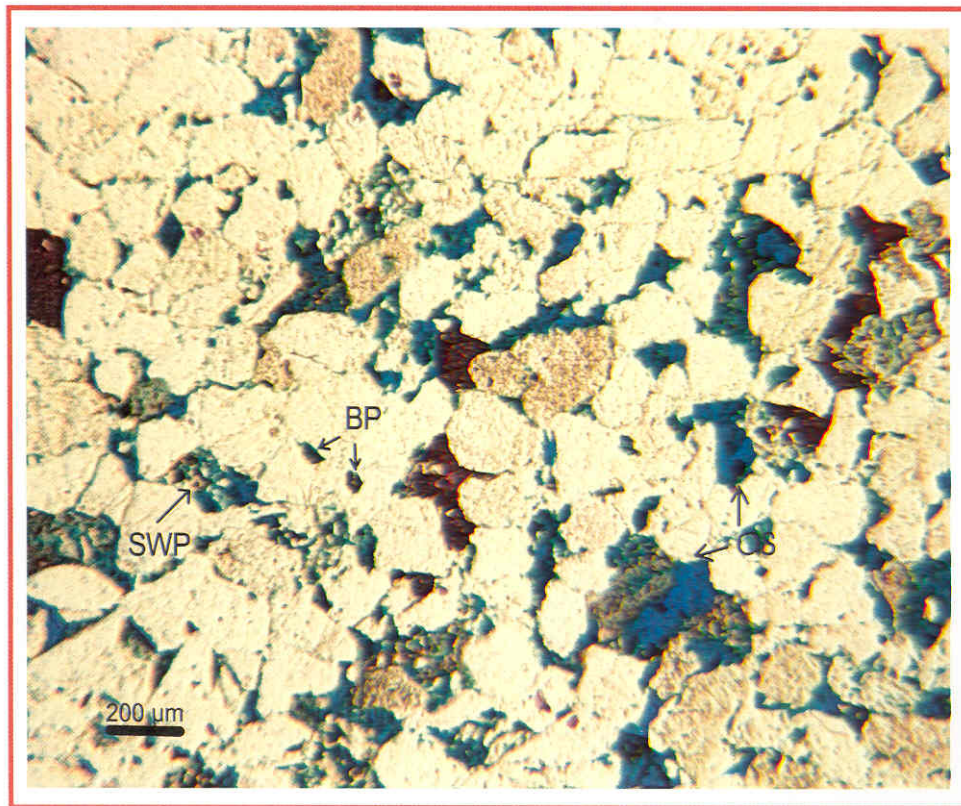


Figure 120: Various pore types, intergranular pores (BP) is minor and secondary intergranular pores (SWP) is significant. Note oversized pores (OS). Bsh #1, 8683 ft.

## **4.10. Secondary porosity development**

### **4.10.1. General remarks**

Grain dissolution was a pervasive diagenetic process in Cotton Valley sandstones. Feldspar grains were most affected by dissolution (Fig. 121), whereas carbonate (calcite) dissolution was minor. Several mechanisms have been proposed for the origin of dissolution porosity in sandstones: (1) carbonic acid from thermal breakdown of organic matter in hydrocarbon source rock; (2) inorganic carbonic acids; (3) organic acids; and (4) meteoric water.

### **4.10.2. Carbonic acids from thermal breakdown of organic matter**

Thermal maturation of organic matter in source rocks can generate CO<sub>2</sub> and carboxylic acids (Surdam et al., 1984; 1993). Schmidt and McDonald (1979b) emphasized that feldspars and early diagenetic carbonate cements are the main constituents dissolved from sandstones, and the necessary acid solutions are generated as a by-product of organic matter reactions in shale. Generation of CO<sub>2</sub> from kerogen in sediments occurs from approximately 60°C to 140°C (Johnston and Johnston, 1987). Hunt (1979) suggested that thermal decarboxylation of organic matter occurs during burial and diagenesis of shales at temperatures between 80° and 120°C can supply significant amounts of carbon dioxide to pore water. Such acidic solution can reach pH of 3 or lower (Curtis, 1983) and cause dissolution of carbonates and silicates.

Curtis (1983) reported that the silicate dissolution reaction is evidenced by the precipitation of kaolinite, whose solubility decreases as neutral pH is approached.

However, Giles and Marshall (1986) argued that clay mineral reactions within shales



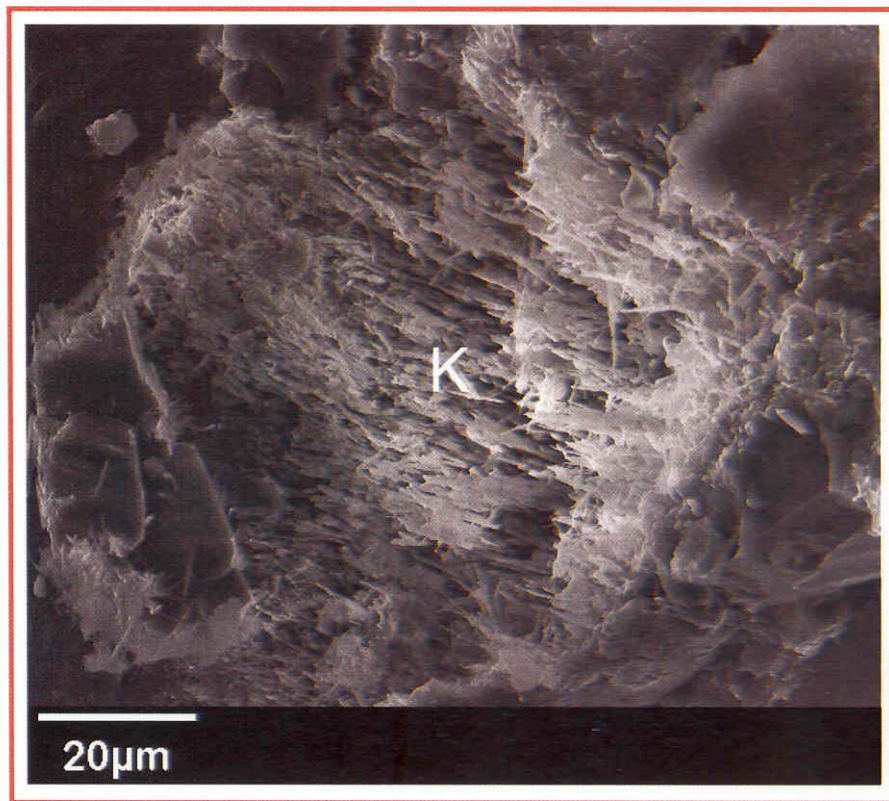


Figure 121: SEM image shows intensive leaching of K-feldspar grain (K). Jones # 3, 9454 ft.

will neutralize acidic fluids before they escape from the source rock. I found no available CO<sub>2</sub> analyses of the Cotton Valley formation water to examine the CO<sub>2</sub> question.

#### **4.10.3. Inorganic carbonic acids**

Acid fluids can also result from CO<sub>2</sub> that formed inorganically through chloritization of kaolinite (Bjørlykke, 1984; Lundegard and Land, 1986; Schwartz and Longstaffe, 1988; Hutcheon and Abercrombie, 1990a). Schwarz and Longstaffe (1988) suggested that, the reaction of minerals with carbonates during deep burial diagenesis provides a powerful mechanism for generation of large quantities of CO<sub>2</sub> of inorganic origin. Another processes invoked to explain subsurface dissolution involves hydrolysis reactions. Hutcheon and Abercrombie (1990a and b) suggested that silicate hydrolysis with increasing temperatures in burial diagenesis generates H<sup>+</sup> that can be expected to promote dissolution of feldspars and carbonates.

#### **4.10.4. Organic acids**

Surdam et al. (1984) pointed out that organic acids expelled as a result of thermal maturation of organic matter are highly effective in dissolving feldspars and complexing aluminum released during dissolution. Geochemical analysis for few CV shale samples indicates that organic matter is mainly type I and type II kerogen. Type I kerogen is hydrogen rich, whereas type II is oxygen rich and hydrogen deficient (Tissot and Welte, 1978). So, type II is oxygen rich and would yield more CO<sub>2</sub> and more organic acids. However, because the CV is sand-rich and most shales interbeds are organic-poor, it is not likely that all the CO<sub>2</sub> necessary to account for the secondary porosity in the CV would have been generated from interbedded shales. Additional CO<sub>2</sub>

may have been derived from deeper formations, such as the Bossier. Dutton (1986) concluded that acidic fluids generated from Bossier shales coincided with the main phase of feldspar dissolution in the Travis Peak Formation. So, Bossier shales may be also a good source of acidic fluids for CVS.

Lind and Heim (1975) indicated that the presence of organic acids (oxalate) in soils increases the Al solubility by several orders of magnitude. However, Kharaka et al. (1986) and Morton and Land (1987) pointed out that concentrations of dissolved aluminum in the Gulf Coast formation waters is below 1.0 mg/l, which raises doubts about the complexation of aluminum as a significant processes in Al transport.

#### **4.10.5. Meteoric water**

Galloway (1984) indicated that meteoric water in the Gulf Coast today extends to depths as great as 5000 ft (1.5 km) along the fluvial axes of the Catahoula Formation.

The paleogeographic setting of the East Texas area in Early Cretaceous should have permitted equally deep or deeper meteoric circulation (Dutton, 1986) during shallow burial owing to highlands to the north.

Meteoric water might have played a role in dissolving feldspar grains in Cotton Valley sandstones. Fluid inclusion data in the quartz overgrowths indicates at least some cement precipitated from saline fluids, so any meteoric water in the sandstones had been flushed by that time. Salt beds occur below the Cotton Valley and not above it. Moreover the sediments are deposited in a shallow marine setting with a high rate of subsidence as indicated by the preservation of the upper shoreface sediments. However, water might

infiltrate back barrier facies during deposition and early post-depositional history and may be during lowstand too.

Fresh water had a negligible effect on the marine reservoir facies in the Cotton Valley Sandstones in East Texas Basin (Wescott, 1983). A fluctuating shoreface environment consisting of alternating sand and shale combined with rapid subsidence and burial may effectively seal off the sands from meteoric water. A similar conclusion was made by Janks et al. (1985) for the CV in southern Mississippi.

#### **4.11. Permeability**

Cotton Valley sandstones are tight gas sandstones, defined as having in-situ permeabilities less than 0.1 md. Permeability was measured at surface conditions (200 psi); those measurements (n=350) are referred to as unstressed horizontal permeability. Vertical permeability data were not used in this study. Air permeability measurements were also made at different parts of six pieces of whole core (having large trace fossils) using an electronically-based permeameter using a soft probe tip (mini-permeameter). Mini-permeameter measurements were carried out within trace fossils and in adjacent host rock and range from 0.1 to 1 md. Sandstones from all of the non-bioturbated facies have permeability values < 1.0 md, which is typical for tight gas sandstones. Relatively high permeability values up to 10 md were recognized in the bioturbated and cryptobioturbated sandstones. These relationships will be discussed in the reservoir quality section.

Core analysis data for all of the studied wells provide good clues about distribution of porosity and permeability (Figs. 122-128). Measured porosity in all

samples ranges from 1% to 13.5% and permeability from 0.001 to 10 md. There is a weak relationship between porosity and permeability for all facies ( $r = 0.75$ ), a relationship typical of sandstones with several percent micropores in clay of all origins.

About 30% of the analyzed bioturbated *Ophiomorpha*-dominated sandstones have permeabilities greater than 0.1 md, and 5.7% of the samples have permeability values between 1 and 10 md (Fig. 123). In sandstones from cryptobioturbated sandstones about 75% of the samples have permeabilities less than 0.1 md, 8% of samples have values less than 1.0 md and 17% of the samples have a permeability range between 1 and 10 md (Fig. 124). 95% of the sand flat sandstones have permeability values less than 0.1 md and only 5% of the samples have permeability values between 0.1 and 2 md (Fig. 125). In laminated shoreface sandstones only 4% of the samples have permeability  $>0.1$  md (Fig. 126) and only 3% of the samples from storm dominated shoreface have permeability  $>0.1$  md (Fig. 127). Figure 126 indicates that 44% of the tidally influenced shoreface sandstones have permeability  $> 0.1$  md, but never reach 1 md. Mini-permeameter measurements show 0.3 md permeability in the laminated sandstone is, whereas in bioturbated layers it ranges from 0.6 to 0.7 md (Fig. 129). Figure 130 indicates that permeability values within the trace fossil (*Teichichnus*) are 3 times higher than the highly cemented host rock. A permeability value of 1 md is in the bioturbated layer in figure 131 is 10 times greater than in the non-bioturbated one. A comparison of permeability measurements in the massive, clean sandstone and bioturbated sandstone indicated that the latter has up to 10 times greater permeability than the massive one.

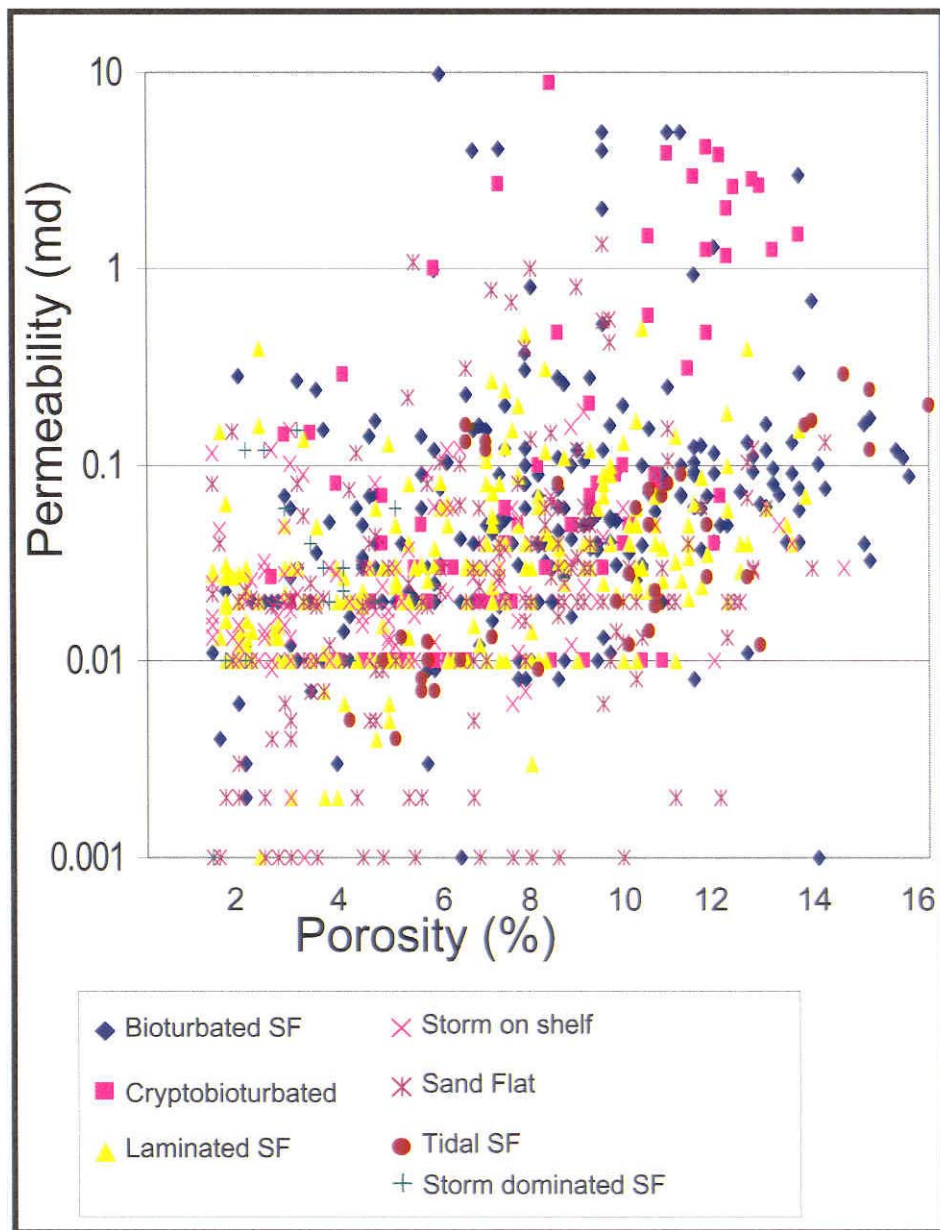


Figure 122: Cross-plot of Helium porosity and permeability for all studied facies. Values for each facies were identified from depth and core description.

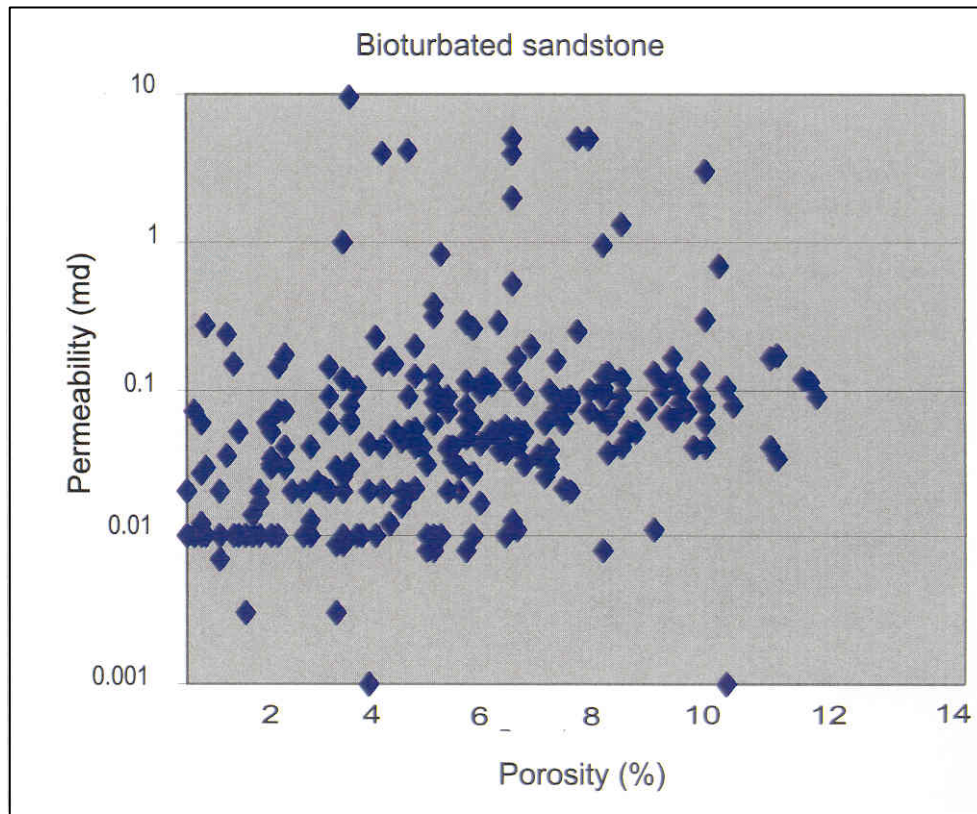


Figure 123. Cross-plot of measured porosity and permeability for the bioturbated Ophiomorpha-dominated sandstones. About 35% of the samples have permeability  $>0.1$  md and only 5.7% of the samples have permeability  $>1.0$  md.



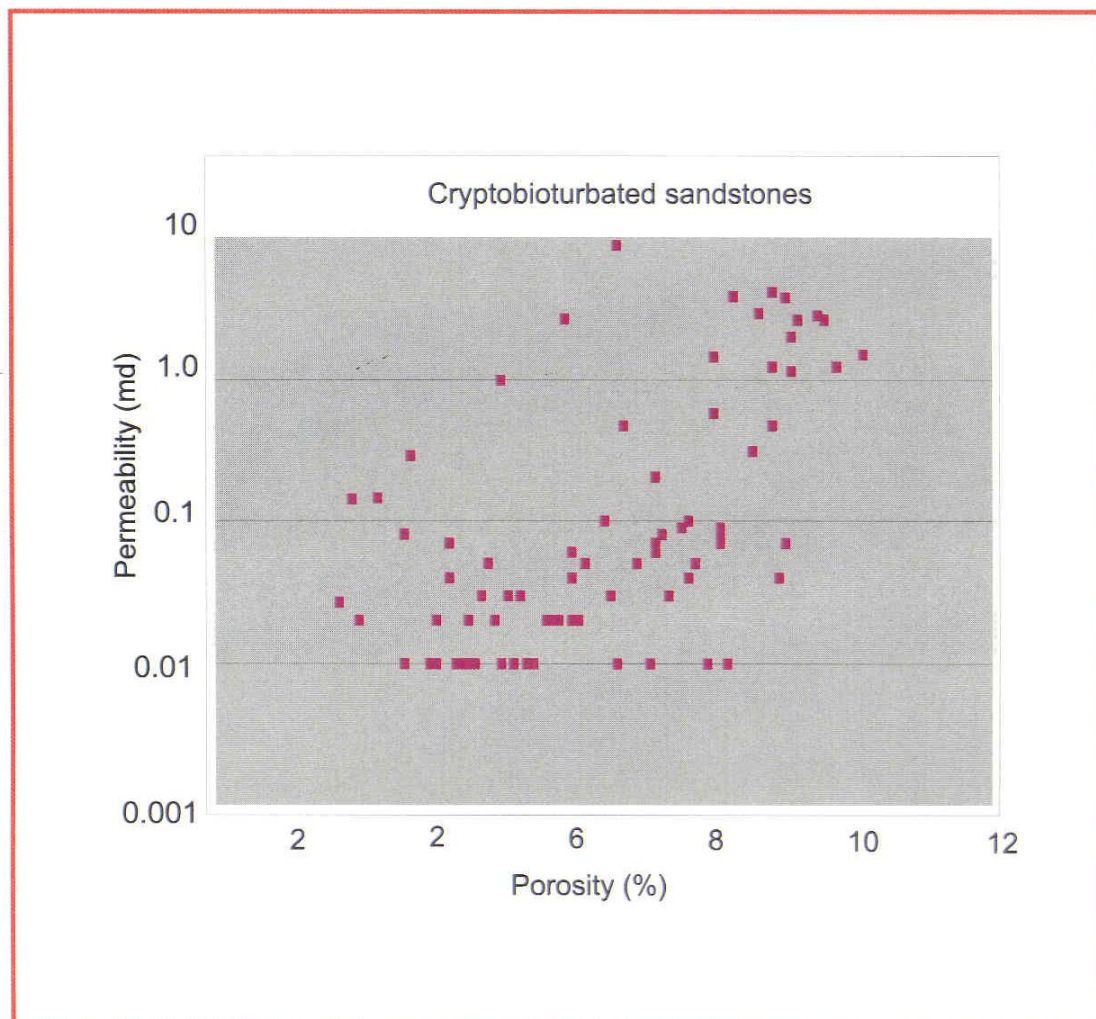


Figure 124: Cross-plot of measured porosity and permeability for the bioturbated Ophiomorpha-dominated sandstones. About 8% of the samples have permeability >0.1 md and 17% of the samples have permeability >1.0 md.

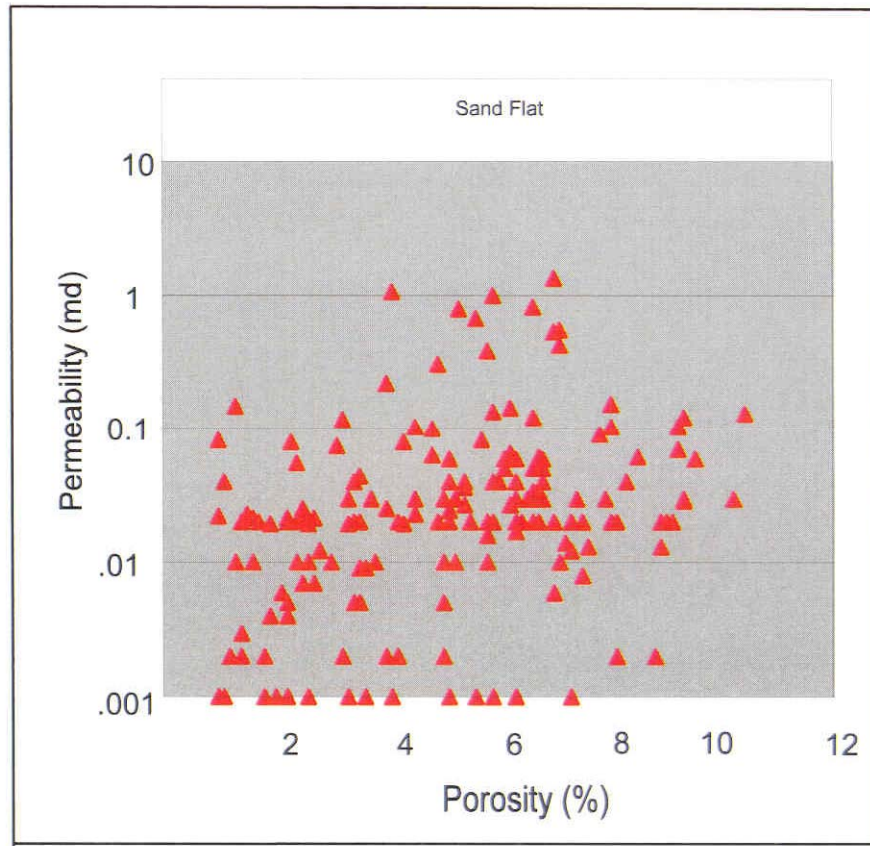


Figure 125. Cross-plot of measured porosity and permeability for the sand flat sandstones. About 17% of the samples have permeability  $>0.1$  md and only 2% of the samples have permeability  $>1.0$  md but never reach 3 md.

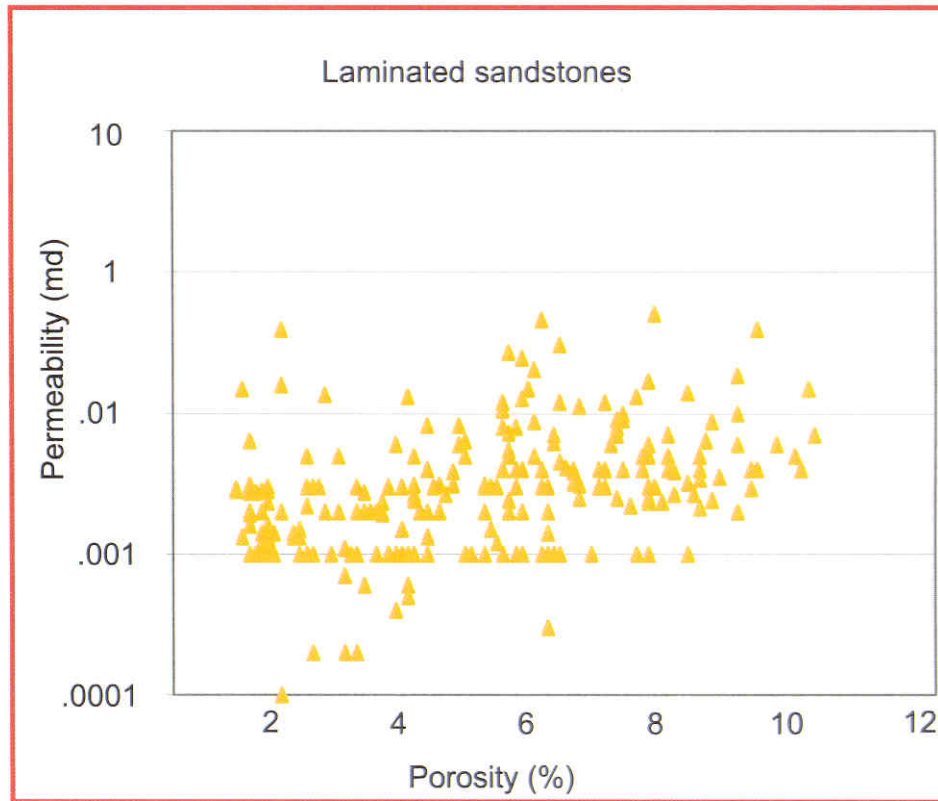


Figure 126. Cross-plot of measured porosity and permeability for the Laminated sandstones. Only 4% of samples have permeability > 0.1 md.

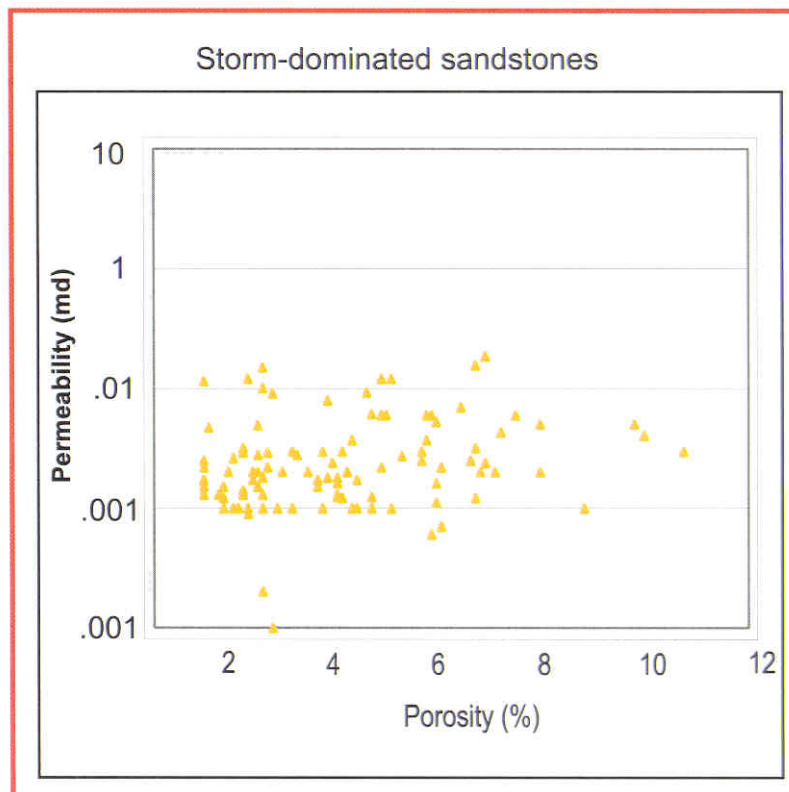


Figure 127 Cross-plot of measured porosity and permeability for the storm-dominated sandstones. 3% of samples have permeability  $> 0.1$  md.

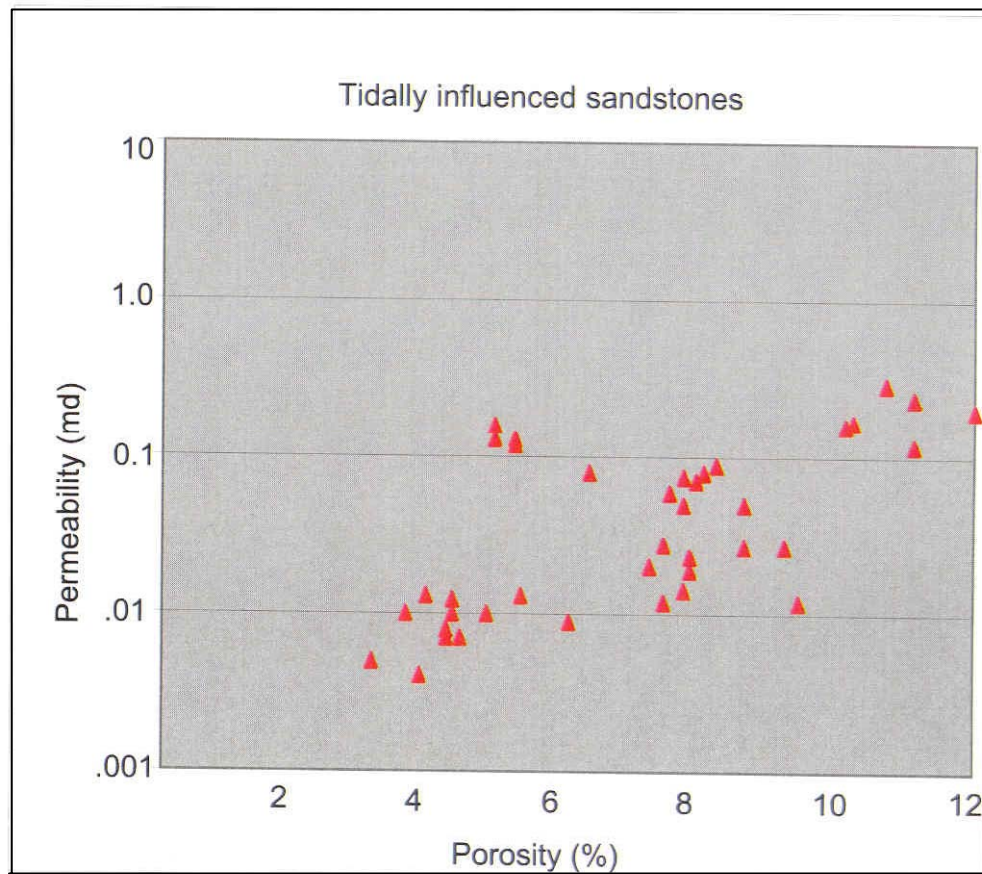


Figure 128. Cross-plot of measured porosity and permeability for the tidally influenced sandstones. 44% of samples have permeability > 0.1 md.



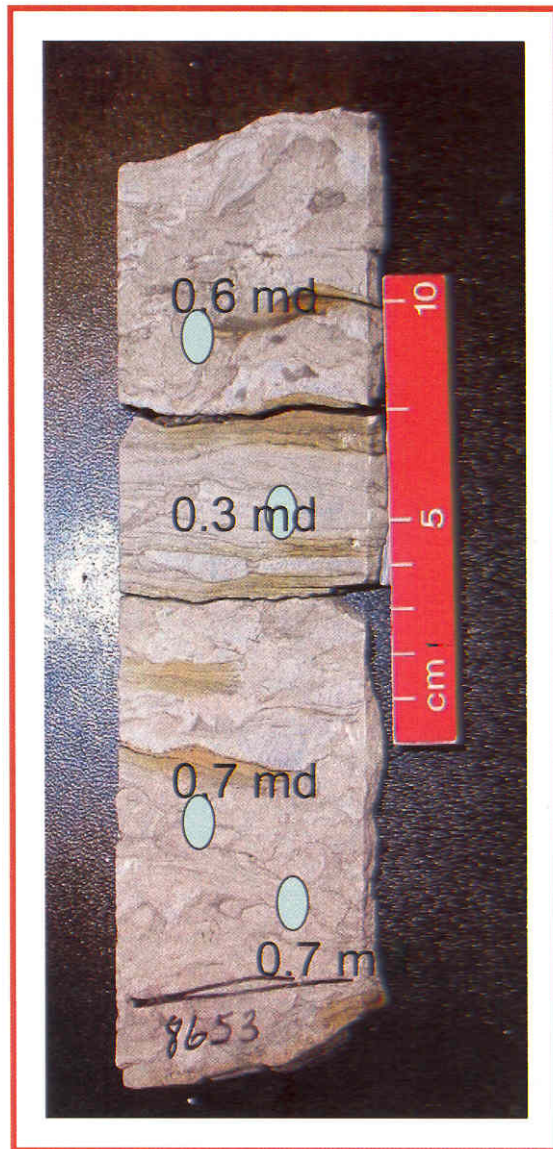


Figure 129. Probe permeability data measured at different parts of the laminated-scrambled facies. Permeability values in the bioturbated sandstones is double that in the laminated sandstone.



Figure 130: Probe permeability data measured within and outside the trace fossils.



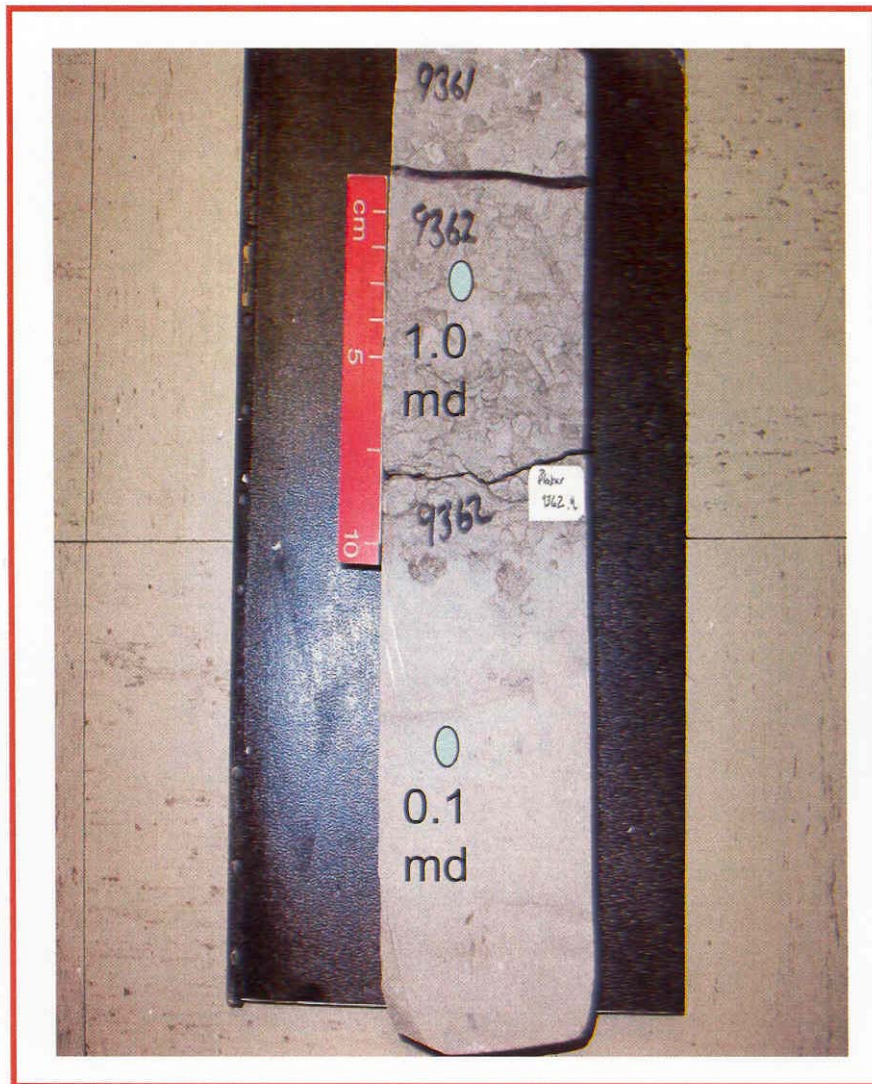


Figure 131. Permeability measurements within the bioturbated layer is 10 times greater than the non-bioturbated one.

#### **4.12. Diagenetic evolution and parasequences**

Diagenesis has a strong impact on Cotton Valley sandstones. Original porosity decreased from 40% to as less as 5%, the framework grain composition has been changed through dissolution and replacement, and various types of cements have been introduced into pores. The diagenetic processes are divided into two main types: 1) physical processes, which include compaction, and 2) chemical processes, which include dissolution, precipitation and replacement processes. The integrated paragenetic sequence of authigenic phases in the Cotton Valley sandstones is shown in figures 101 and 132.

Schmidt and McDonald (1979a) defined eogenesis as all those processes occurring at or near surface conditions and controlled by the chemistry of the depositional environment. Mesogenesis is defined as all of the processes that take place after burial without influence of the surface environment. Eogenetic events in the CV include: 1) the development of clay coatings around the detrital grains (chlorite and illite); and 2) early pore filling pyrite. In this shallow-marine environment the original pore water composition was most probably sea water.

The main diagenetic events during mesogenesis include: 1) calcite 1 precipitation; 2) quartz cement; 3) dissolution of unstable grains mostly feldspar. 4) K-feldspar overgrowths; 5) kaolinite and chlorite cement; 6) oil emplacement; 7) illite; 8) calcite 2; 9) dolomite and anhydrite; and 10) late diagenetic pyrite. Compaction started early and probably minimized or stopped after quartz cementation.

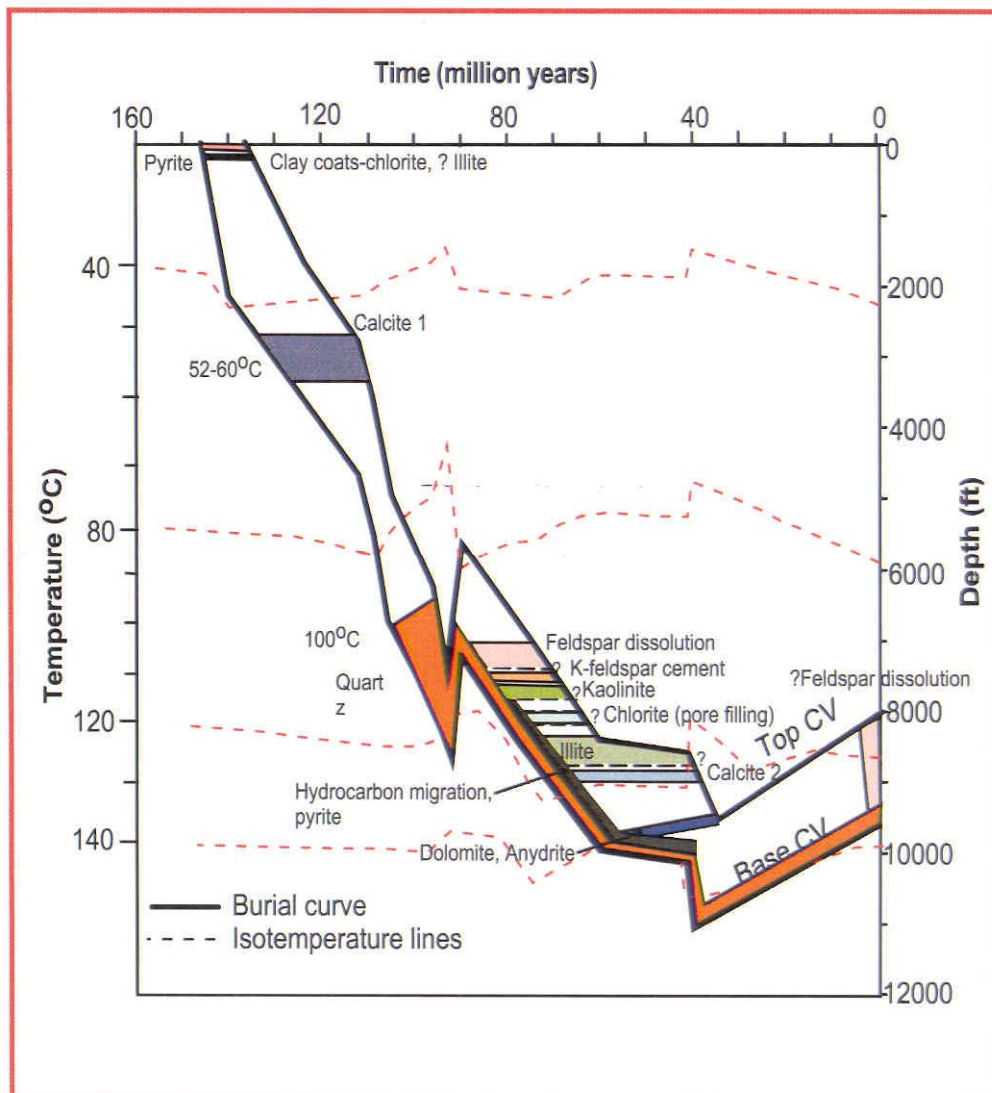


Figure 132: Burial-history curve for Jones # 3, showing interpreted times and depths at which major diagenetic events occurred.

Bailey (1983) studied the Terryville sandstones in East Texas Basin (stratigraphically equivalent to the Cotton Valley Sandstones, but not the same rocks in this study) and constructed a paragenetic sequence that differs from the mine. His sequence of events was; 1) calcite cement; 2) illite/chlorite cement; 3) compaction; 4) plagioclase cement; 5) quartz cement; 6) dolomite and ferroan calcite cement; 7) pressure solution/illite recrystallization/ feldspar alteration; 8) carbonate dissolution; 9) barite cement; 10) chlorite cement; 11) hydrocarbon emplacement/pyrite cement; 12) ferroan dolomite cement; and 12) quartz cement. I and Bailey (1983) agree on the occurrence of the same authigenic minerals, but we disagree on their relative timing.

The main differences between the two sequences are: 1) I document two phases of calcite instead of one; 2) Bailey did not include kaolinite cement in his sequence and he interpreted two phases of quartz cementation. Illitization of kaolinite in Bailey's rocks may explain the absence of kaolinite in his paragenetic sequence.

Wescott (1983) also studied the diagenesis of CVS in East Texas and Terryville sandstones in East Texas Basin and he constructed another paragenetic sequence that differs from mine. His sequence of events include: 1) development of clay coats on grains; 2) formation of quartz overgrowth; 3) dissolution of unstable grains followed by precipitation of phyllosilicates; 4) precipitation of calcite; and replacement of grains by calcite. The main differences between Wescott's paragenetic sequence and mine are: 1) Wescott did not include pyrite, albite, K-feldspar overgrowths, and iron-rich dolomite; and 2) I recognized two types of calcite.

#### **4.13. Porosity evolution: Compaction and cementation porosity loss**

Sandstone reservoir quality is controlled by diagenetic processes that either reduce or enhance porosity. Among these diagenetic processes, mechanical compaction, intergranular pressure solution, cementation, framework grain dissolution and cement dissolution have been documented. Atkins and McBride (1992) documented that an original porosity of 40-45% is observed in many depositional environments in well sorted Holocene sands. An original porosity of 40% is assumed in this study.

Pittman and Larese (1991) divided compaction into physical and chemical processes. Physical processes or mechanical compaction include (1) grain rearrangement; 2) breakage of grains; and 3) ductile deformation. Chemical compaction occurs in the form of intergranular pressure solution and stylolites. Houseknecht (1987) defined mechanical compaction as the bulk volume reduction due to processes other than framework grain dissolution. Chemical compaction is defined as the bulk volume reduction caused by the dissolution of framework grains at points of contact (Füchtbauer, 1967; Houseknecht, 1987).

Mechanical compaction was a significant porosity reducing agent in the Cotton Valley Sandstones. From the previous discussion about calcite 1, I indicated that the IGV value was reduced from an initial value of 40% to an average of 27.9% by compaction at the time of calcite 1 cementation. The cross plot of cement volume (corrected values of quartz cement are used) versus intergranular volume of the Cotton Valley Sandstones (Fig. 133) indicates that original porosity loss by compaction was much more than that lost by cementation in the bioturbated sandstones (bioturbated

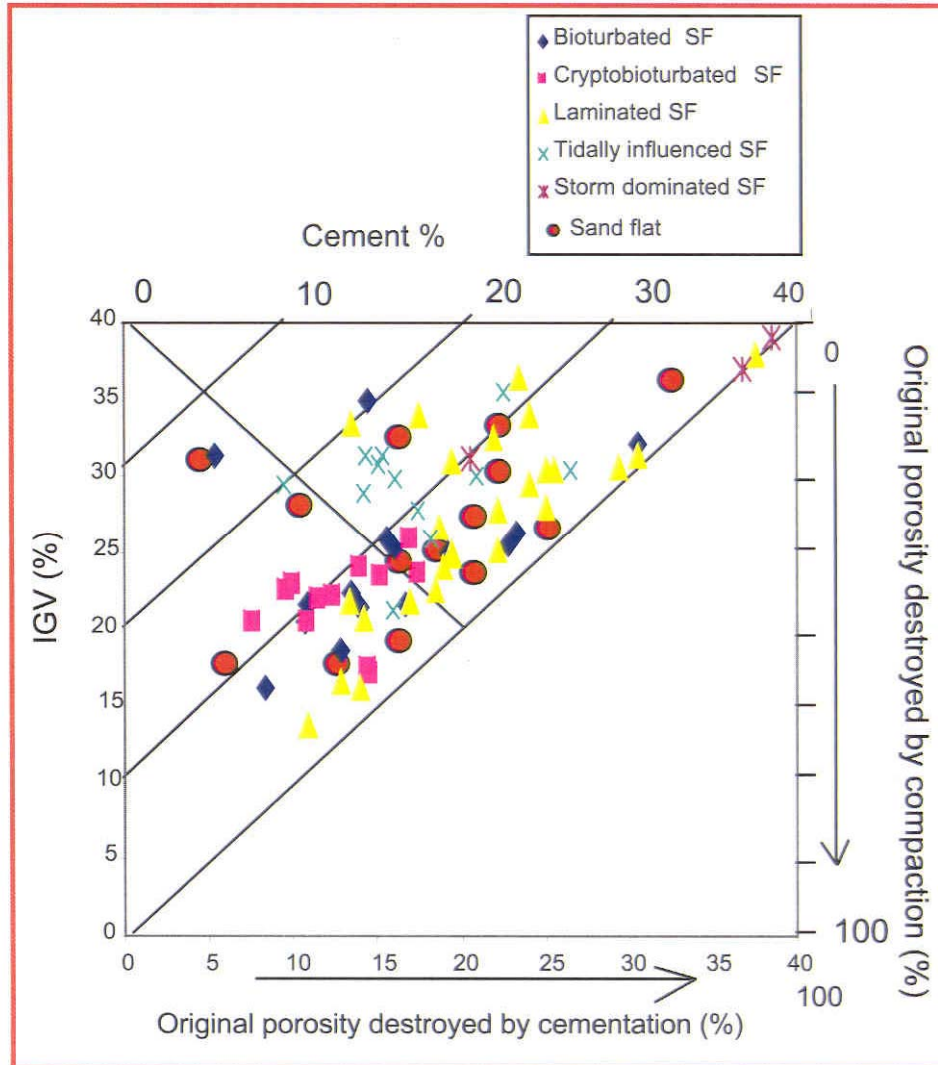


Figure 133: Houseknecht's (1987) plot illustrating intergranular volume (IGV) vs. cement abundance for potential reservoir facies of CVS.

*Ophiomorpha*-dominated sandstones and cryptobioturbated sandstones). In the bioturbated and cryptobioturbated sandstones porosity loss due to compaction was much more important than cementation in about 80% and 90% of the samples, whereas porosity loss by cementation was more significant in the nonbioturbated sandstones. In sandstones from the laminated, tidally influenced shorefaces and sand flat environment about 85%, 90%, 100%, and 75% of the samples showed that porosity loss due to cementation was greater than that lost by compaction.



## **CHAPTER 5**

### **RESERVOIR QUALITY**

The major objective of the following discussion is to illustrate the impact of depositional environment and diagenesis on reservoir quality and show the relationship between them. A better understanding of the depositional environment in relation to reservoir geometry and internal facies relations, in conjunction with a better understanding of the diagenetic overprint and its control on porosity and permeability development and retention, is essential for any further hydrocarbon exploration of the Cotton Valley Sandstones in the East Texas Basin.

Wescott (1983) indicated that diagenesis in the Cotton Valley Sandstones is controlled by (1) rock composition and texture, and (2) the composition and nature of pore waters and that depositional environment exerted an essential control on the composition and texture of the sandstone and therefore influenced subsequent diagenesis. My work confirms those conclusions and shows that depositional environment was the single most important parameter.

Depositional environment controlled the amount of clay grain coats and matrix, which in turn controlled the degree of quartz cementation, the amount of porosity lost by compaction, and the amount of carbonate cement. The general consensus is that bioturbation in most settings disturbs lamination and introduces detrital clay to the sandstone and hence, decreases the reservoir quality. In the Cotton Valley tight sandstone reservoirs this scenario is correct only for sandstones where bioturbation

introduced more than 15% clay matrix (Fig. 134). Sandstones with less than 10% matrix and (Fig. 135) and high percent of clay coats have good values of porosity and the highest values of permeability. These sandstones I identified as clean bioturbated sandstones a term introduced for the first time in this study. Davis (1979) indicated that the amount of detrital clay strongly controls the amount of quartz cement and that 15% or more detrital clay can result in less than 10% quartz cement.

The second important factor that controlled reservoir quality is the amount of quartz cement. Normalizing average values of quartz cement in the studied facies to 100%, figure 136 shows that the non-bioturbated sandstones have 22% to 30% quartz cement, whereas the bioturbated sandstones have only 12%. Other cements are less important, but carbonates are locally significant (up to 27%). The third significant element is the amount of clay coating. Clay coating plays an important role in retarding quartz cement and in preserving some porosity (Wilson and Pittman, 1976; Moraes and De Ros, 1990; and Storvoll et al., 2002). The abundance of clay coatings (percent of free grain surface coated by clay) is variable in Cotton Valley Sandstones. Bioturbated sandstones have a range from 1.4% to 19% with average of 11%, which is the highest average in the studied facies. Other facies have a range from 4% to 9% (appendix E).

Taking into account that Cotton Valley sandstones were deposited in a barrier island-coastline setting, there are two main types of sandstones: higher energy, well sorted and relatively coarser grained upper-shoreface sandstones, and low-energy fine-grained, clay-rich bioturbated sandstones. The higher energy clean sandstones had good

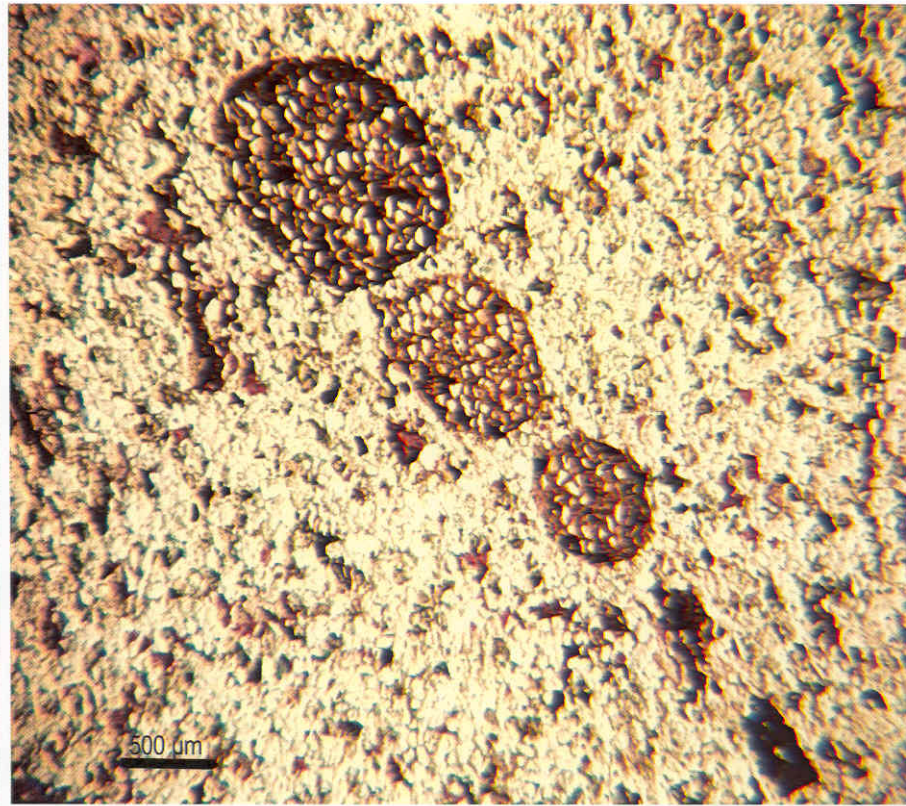


Figure 134: Bioturbated sandstone with more than 10% detrital clay. Note absence of visual pores. GL # 1, 9619 ft.

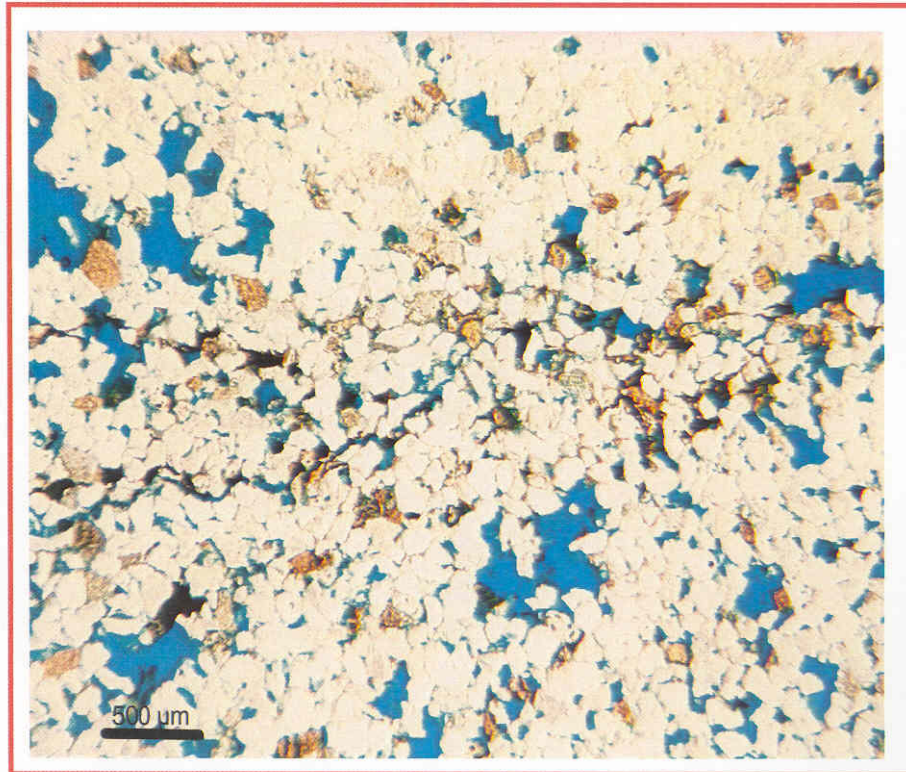


Figure 135: Photomicrograph of bioturbated sandstone with <10% detrital clay and high percent of clay coating. Note good porosity (blue areas). BH # 1, 9328 ft.

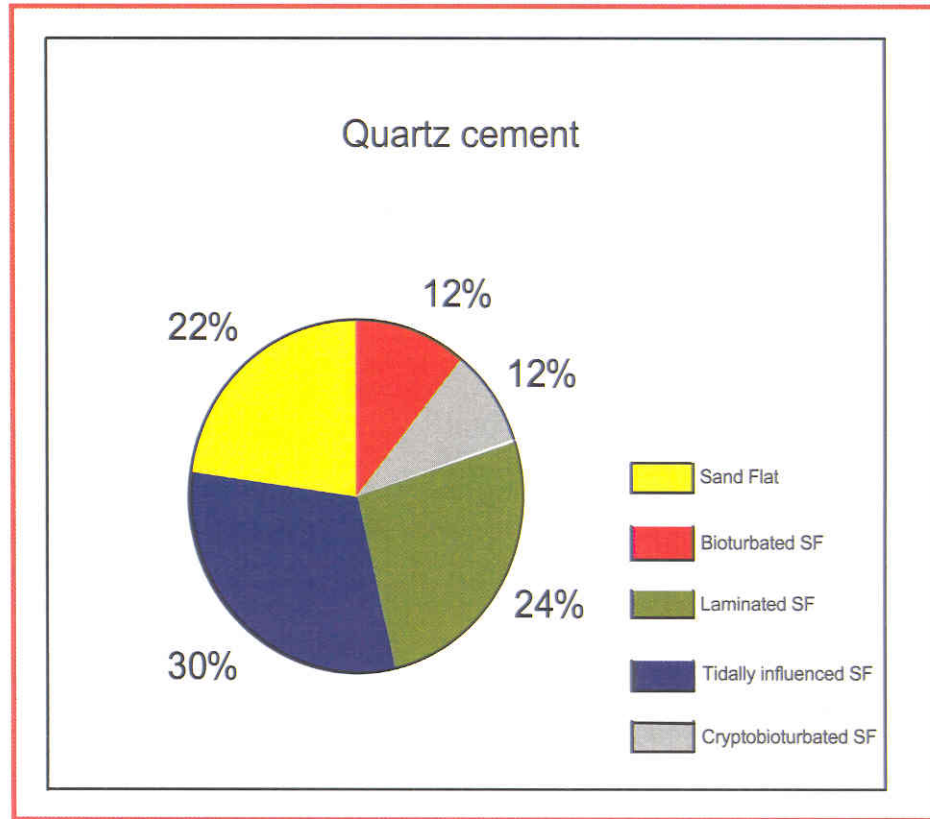


Figure 136: Distribution of quartz cement in various facies.  
Bioturbated sandstones have the least quartz cement.

initial porosity and permeability and after burial they would still be a good conduit for the migration and storage of pore fluids. The probability of cementation for these sandstones is very high, because there was more pore space for all cements and much larger quartz grain surface areas and nucleation sites for quartz cement. The distribution of quartz cement and total cement in different facies supports this concept and explains why loss of porosity due to cementation was much more significant than compaction in non-bioturbated sandstones.

Wescott (1983) studied Cotton Valley sandstones in Harrison and Panola Counties in the East Texas Basin and recognized four types of reservoir rocks in the Cotton Valley Sandstones; (1) tight rocks with a high percentage of quartz and calcite cements; (2) rocks with high clay content possessing high microporosity and low permeability; (3) rocks with good secondary porosity due to dissolution of feldspars, rock fragments and cements; and (4) rocks having the best reservoir quality with highest porosity and permeability.

I divided the Cotton Valley Sandstones into three main rock reservoir types: (1) clean bioturbated sandstones with less than 10% clay matrix and high percentage of clay coats which are the best reservoir facies; (2) intermediate quality bioturbated sandstones with more than 15% clay matrix and high microporosity; and (3) poor reservoir quality sandstones with abundant cement, mainly quartz. Bioturbated sandstones (in shorefaces or back barrier) with less than 10% clay matrix have the best reservoir quality in the Cotton Valley Sandstones (Fig. 137). This is because of the relatively high content of detrital clay



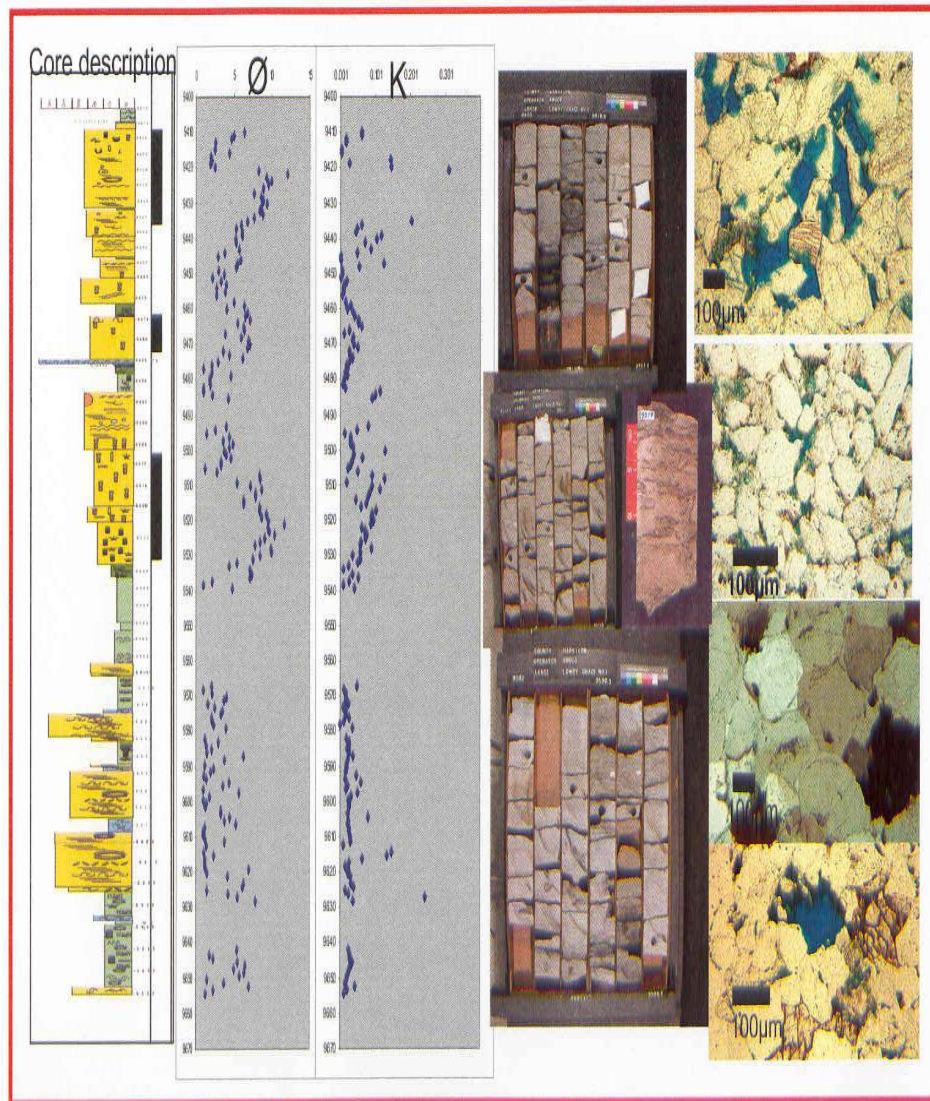


Figure 137: Integration of core description, core photos, porosity and permeability data with depth, and thin section images. Bioturbated sandstones have the best porosity and permeability.



matrix which decreased porosity and increased the clay coatings enveloping the quartz grains and consequently decreased nucleation sites for quartz cement.

Best reservoir quality sandstones have a range of porosity from 5% to 12% and permeability range from 1.0 to 10 md. Mini-permeameter data (permeability section) support this conclusion, where permeability values within trace fossils were up to 10 times greater than in the nonbioturbated host rock.

Intermediate reservoir quality sandstones having clay matrix from 10 to 15% result in low visual porosity (primary+secondary) and permeability. However, these sandstones still have a significant amount of microporosity that might be useful for gas reservoirs. Poor reservoir quality sandstones have either a high percentage of cements (mainly quartz) or > 15% clay matrix that occludes all of the pores and destroys permeability. This type of reservoir commonly has porosity < 5% and permeability <0.1% and requires fracturing to yield gas.

The organic geochemical studies necessary to know the source of Cotton Vally hydrocarbons are beyond the scope of this study. However, three main possibilities are: 1) carbonate mudstones of lower Smackover Formation (Sassen et al., 1986a); 2) dark basinal shales of the Bossier Formation (Collins, 1980); and 3) shale interbeds in the Cotton Valley.

Laminated carbonate mudstones of the lower Smackover have been identified as the source rock for Smackover reservoirs (Sassen et al., 1986a). However, evaporites of the overlying Buckner Formation probably acted as a seal that prevented migration of

Smackover oil up-dip. Shales within the CV are not probably the source rock because the CV is sand-rich and most shales interbeds are organic-poor (total organic content <1%). Bossier Formation (about 900 ft., 272 m), which consists of dark basinal shales (Collins, 1980), is the offshore marine equivalent of Cotton Valley clastics (Stewart, 1984) and is most likely the source for hydrocarbons in the CV. Dutton (1986) also concluded that Bossier shales are the source of hydrocarbons for both Cotton Valley and Travis Peak (overlies CV) formations.

## **Conclusions**

The Cotton Valley Sandstone in East Texas is composed of thirteen parasequence sets that combine to form six third-order sequences composed of highstand, transgressive and/or lowstand systems tracts. The distribution of the parasequence sets within the lowstand, transgressive and highstand system tracts reflect type-1 sequences deposited in a basin with a shelf margin. Twenty three facies (F1 to F 23) are recognized and have been grouped into four facies associations that represent fully marine (FA1), marginal marine (FA2 and FA3), and back barrier/coastal plain (FA4) environments of deposition.

FA1 facies were deposited in a lower-shoreface to inner-shelf environment that was affected by periods of storm activity. Facies of FA2 were deposited within wave-dominated upper shoreface and foreshore environments in which tidal influence on the sediments was observed. The facies succession of FA3 is the product of tidal inlet migration and lateral accretion of the adjacent spit platform. FA4 is interpreted to be back-barrier and coastal-plain deposits.

Net sand maps along with core descriptions indicate deposition of prograding shorefaces (probably wave-dominated delta) in the highstand system tracts and barrier island/lagoon-shelf systems in the transgressive systems tract. A close relationship is observed between the distribution of net-sand thickness of the pre-existing highstand system tract sediments and the respective overlying transgressive systems tract sandstones. Barrier island sandstones are consistently deposited directly above net sand “thicks” of the underlying highstand system tract. Redeposition of the underlying

highstand system tract and lowstand system tract sediments contributed to the volume of sediments deposited in the overlying barrier systems of the transgressive system tract. Major sediment contribution was remobilized from underlying sediments from beneath the transgressive surface in the Cotton Valley Sandstones.

The barrier islands are interpreted to be mesotidally influenced. This interpretation is inferred on the presence of short barriers with tidal flats and tidal marshes and is based on the net sand maps and core data interpretation. The average net sand thickness of the barriers is 70 feet (21m). The tidal inlets are closely associated with the barrier island sandstone bodies. Flood tidal deltas and tidal inlets are interpreted from cores. The outer banks of North Carolina are believed to be the present day analogue for the transgressive system tract CVS depositional system.

The detrital composition of sandstones was intensely modified through diagenesis. Dissolution and replacement mainly of feldspars transformed arkoses and sub-arkoses into subarkoses and quartzarenites.

Much of the diagenesis in CVS took place in sea water and meteoric water had no or negligible effect. Quartz cement, volumetrically the most important authigenic phase in the Cotton Valley sandstones, precipitated from water with a  $\delta^{18}\text{O}$  composition range from +4 to +5‰ (SMOW) at estimated temperatures that ranged from about 100°C to 110°C at depths from 8930 to 10226 ft (2706 to 3098 m). The main control on quartz cementation was temperature and the availability of detrital quartz grains surface area. The available grain surface area was controlled by the clay coating.

The amount of silica derived internally from both pressure solution and stylolites constitute up to 48% of the total quartz cement. The remaining 52% come from sources that could not be quantified. Other significant local sources of silica include dissolution of quartz grains at clay laminae and at contacts between sandstone and interbedded shales, and dissolution of micron-scale detrital quartz within interbedded shales and clay laminae. High content of clay laminae are observed in cores and shale interbeds constitute up to 35% of the total CV rock volume. These sources could not be quantified. A possible external source, a silica-rich fluid expelled from the Bossier shales.

Albitization of K-feldspar was observed in the CVS, but no trend for decrease or increase of the degree of albitization was found over the studied narrow depth range (600 m). However, albitization of feldspars in some samples was near complete at the top of the CV.

Carbonates (mainly calcite) are less abundant but locally significant. There are two main types of calcite. Calcite 1 was most probably precipitated at temperature range from 52°C to 60°C, assuming  $\delta^{18}\text{O}_{\text{water}}$  between +1‰ and +2‰ at depth range from 1-2.2 km. Calcite 2, interpreted as a later event than type 1 and its estimated temperature of precipitation from water with  $\delta^{18}\text{O}$  composition of +5 at temperatures from 120°C to 130°C, at depths from 2.6 to 3.5 km. The main source of Ca for calcite cement is the local dissolution and precipitation of carbonate shell fragments in the sandstones and the oyster-rich lagoonal mudstone beds interbedded with the sandstones supplemented by dissolution and albitization of feldspars and from marine carbonate-rich shales near

by the sandstones. Late diagenetic ferroan-dolomite cement was minor and precipitated from water with  $\delta^{18}\text{O}$  composition range from +5 and +6‰ at estimated temperature range of 155°C and 163°C.

Kaolinite, chlorite and illite are the main authigenic clays observed in the Cotton Valley sandstones. Kaolinite cement was mostly derived from the dissolution of detrital feldspars which supply the essential elements ( $\text{Al}^{3+}$  and  $\text{Si}^{4+}$ ) for kaolinite. Chlorite occurs as early diagenetic grain coatings and late diagenetic pore-filling cement as well as a replacive phase. Chemical dissolution of feldspar would have released plentiful supplies of  $\text{Al}^{3+}$  and  $\text{Si}^{4+}$  in solution and iron and magnesium might be supplied to pore waters from the breakdown of chloritic and illitic detrital clays or smectite to illite transformation in the adjacent shales. Shale interbedded with CVS (20%-35%) could be a good source of iron, carbonates and silica. Illite cement commonly rims grains and forms bridges between adjacent grains. Dissolution of mica flakes (muscovite) is commonly observed and may account for adding significant amount of  $\text{K}^{+}$  to the pore water. Illite may also be resulted from illitization of smectite or recrystallization of previous detrital clay.

Pyrite is ubiquitous authigenic cement and occurs as an early diagenetic pore filling and a late diagenetic phase associated with residual hydrocarbons. Anhydrite cement is a minor component that post-dates quartz cement and probably iron-rich dolomite.

Original porosity loss by compaction was much more than that lost by cementation in the bioturbated *Ophiomorpha*-dominated sandstones and crypto-

bioturbated sandstones, whereas porosity loss by cementation was greater in the cleaner sandstones of the laminated, tidally influenced shorefaces and sand flat.

Porosity and permeability of these tight gas sandstones vary with depositional environment. Bioturbated sandstones (including bioturbated *Ophiomorpha*-dominated and cryptobioturbated sandstones) possess good porosity and the highest permeability values whereas, laminated shoreface sandstones have the lowest porosity and permeability values.

The most important parameters that influenced reservoir quality other than composition are (1) the degree of bioturbation, percentage of clay coats and the volume of clay matrix; (2) the amount of quartz cement; and (3) the percentage of clay coating. Depositional environment controlled the amount of clay matrix/coats, the degree of bioturbation and the amount of carbonate cements.

Cotton Valley Sandstones are divided into three main reservoir types: (1) clean bioturbated sandstones with less than 10% clay matrix these are the best reservoir facies; (2) intermediate quality bioturbated sandstones with 10-15% clay matrix and high microporosity; and (3) poor reservoir quality sandstones with abundant cement, mainly quartz and > 15% clay matrix.

Hydrocarbons in the CVS could not have been generated in the shales interbedded with CV reservoirs because those shales are organic poor (TOC < 1%). The source rocks for CV hydrocarbons are the shales of the Bossier Formation.



## **Appendix A: Core description:**

### **LEGEND:**

F1: Inner-mid shelf

F2: Bioturbated Ophiomorpha-dominated shoreface

F3: Storm-dominated shoreface

F4: Cryptobioturbated shoreface

F5: Laminated shoreface

F6: Tidally influenced shoreface

F7: Tidal flat (sand flat, mixed flat, marsh, and mud flat)

F8: Lagoon-bay mud and sand

F9: Storm beds on shelf

F10: Soil










F11: LAG DEPOSITS

F12: Transitional to lower shoreface

Appendix A.1: Core description for Blocker Heirs well # 1,  
Harrison County, Blocker field.


SED. STRUCTURES						DEPTH (F)	LITHOFACIES	ENVIRONMENT	BIOTURBATION	OYSTERS	NO. OF STYLOLITES
CLASTIC GRAIN SIZE											
Gravel	Coarse	Medium	Fine	V.fine	Mud						
Top at 9310 ft						-9310	F1	inner shelf			
							F11	shell lag			
						-9315	F2	lower shoreface to transitional			
						-9320	F1	inner shelf to mid shelf			
						-9325	F2	middle-lower shoreface			
						-9330	TS				
						-9335	F5	middle to upper shoreface			15
							F11	storm bed			
						-9340	F5	middle to upper shoreface			35
						-9345					

Appendix A.1: Core description for Blocker Heirs well # 1, Harrison County, Blocker field.

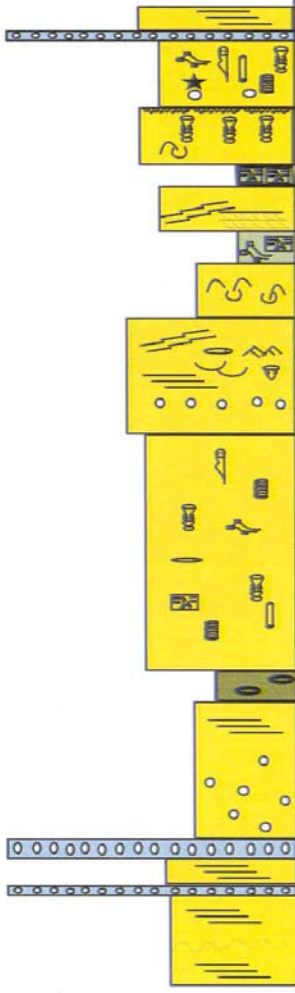
SED. STRUCTURES						DEPTH (F)	LITHOFACIES	ENVIRONMENT	BIOTURBATION	OYSTERS	NO. OF STYLOLITES
CLASTIC GRAIN SIZE											
Gravel	Coarse	Medium	Fine	V.fine	Mud						
						-9345	F4	lower shoreface			
						-9350	F1	inner shelf			
						-9350		middle shelf			
						MFS	F13	transitional to lower shoreface			
						-9360	F2	lower shoreface			
						-9365	F5	middle-upper shoreface			
						-9370					
						-9380	F4	middle-upper shoreface very clean ss, with cryptic bioturbation			20
						-9382.5					
						-9695	F1	inner shelf			
						-9700					
						-9705	F11	transgressive lag			
						-9710	F5	middle-upper shoreface			30

333

Appendix A.1: Core description for Blocker Heirs well # 1 Harrison County, Blocker field.

SED. STRUCTURES						DEPTH (FT)	LITHOFACIES	ENVIRONMENT	BIOTURBATION	OYSTERS	NO. OF STYLOLITES
CLASTIC GRAIN SIZE											
Gravel	Coarse	Medium	Fine	V.fine	Mud						
						9710	F5	middle-upper shoreface			
							F11	storm bed/shell hash			
						9715					
Flooding surface						9720	F5	middle-upper shoreface			
						9725		lower shoreface			
						9730	F1	inner shelf			
						9735	F11	storm lag			
						9740	F7	intertidal-subtidal sand flat with ray feeding trace			30
						9745	F11	storm bed			
						9750					
						9755	F7	intertidal-subtidal sand flat			
<i>Thalassinoides</i>						9760	F8	restricted lagoon			
						9765	F7	back barrier			

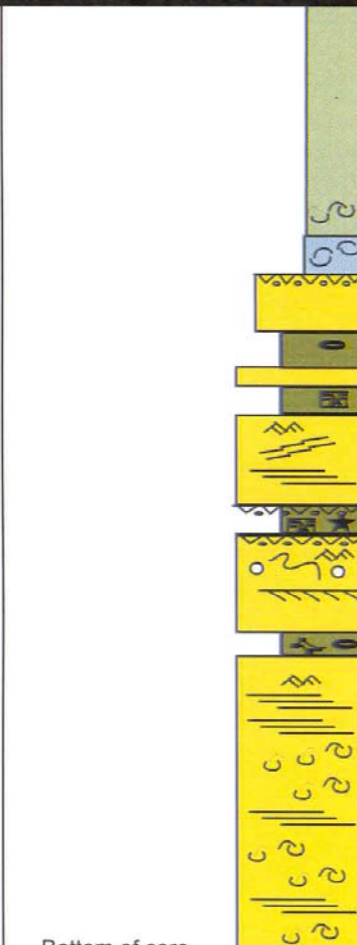
Appendix A.1: Core description for Blocker Heirs well # 1 Harrison County, Blocker field.

SED. STRUCTURES						DEPTH (FT)	LITHOFACIES	ENVIRONMENT	BIOTURBATION	OYSTERS	NO. OF STYLOLITES
CLASTIC GRAIN SIZE											
Gravel	Coarse	Medium	Fine	V.fine	Mud						
						9765	F5	middle shoreface			
						9770	F2	lower shoreface			
						9775	F2	middle shoreface			
						9780	F5	lower shoreface			
						9785	F1	inner shelf			
						9790	F4	lower shoreface			
						9795	F3	middle shoreface			
						9800	F2	lower shoreface			
						9805	F1	inner shelf			
						9810	F3	lower shoreface to transition			
						9815	F11	lag deposits			
						9820	F3	storm-dominated middle to upper shoreface			

Appendix A.1: Core description for Blocker Heirs well # 1 Harrison County, Blocker field.



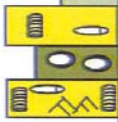

SED. STRUCTURES						DEPTH (FT)	LITHOFACIES	ENVIRONMENT	BIOTURBATION	OYSTERS	NO. OF STYLOLITES
CLASTIC GRAIN SIZE											
Gravel	Coarse	Medium	Fine	V.fine	Mud						
						9820	F3	storm-dominated middle to upper shoreface			9
						9825					
						9830					
						9840					
						9845	F13	lower shoreface to transition			
						9850	F1	inner to transitional middle shelf			
						9855					
						9860					
						9865	F1	middle-outer shelf <i>Helmenthopsis</i> in some silt beds			
						9870					
						9875					
						9880	F9	storm derived oysters on shelf			
						9885	F1	<i>Chondrites</i> -dominated inner shelf			

Appendix A.1: Core description for Blocker Heirs well # 1 Harrison County, Blocker field.

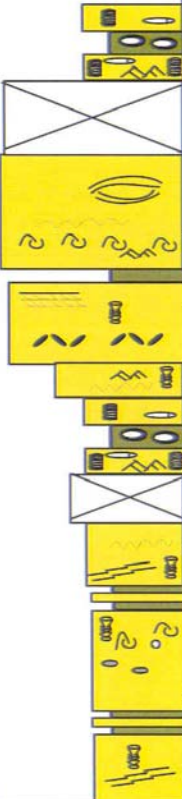
SED. STRUCTURES						DEPTH (FT)	LITHOFACIES	ENVIRONMENT	BIOTURBATION	OYSTERS	NO. OF STYLOLITES
CLASTIC GRAIN SIZE											
Gravel	Coarse	Medium	Fine	V.fine	Mud						
						-9885					
						-9890					
						-9895	F1	Chondrites-rich inner shelf			
						-9900	F11	lag deposits			
						-9905	F5	lower shoreface			
						-9910	F4	cryptobioturbated middle shoreface			
						-9915	F13	transition to lower shoreface			
						-9920					
						-9925	F6	shelly middle shoreface smal bivalves, cryptic massive bioturbation, tidal mud drapes			
						-9930					
						-9935					
Bottom of core						-9939					



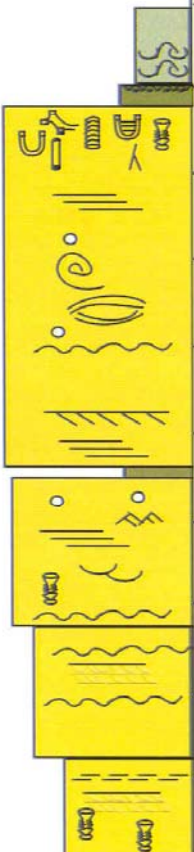
Appendix A.2: Core description of Burnett Brothers well # 1,  
Panola County, Carthage field.

SED. STRUCTURES						DEPTH (FT)	LITHOFACIES	ENVIRONMENT	BIOTURBATION	OYSTERS	NO. OF STYLOLITES
CLASTIC GRAIN SIZE											
Gravel	Coarse	Medium	Fine	V.fine	Mud						
Top at 9418						9418					
						9420	F8	lagoon			
						9425					
						9430					
						9435					
						9440					
						9445					
						9450					
						9455					
						9460					
						9475					
						9480	F13	transition to lower shoreface			
9485											












Appendix A.2: Core description for Burnett Brothers #1,  
Panola County, Carthage field.

SED. STRUCTURES						DEPTH (F)	LITHOFACIES	ENVIRONMENT	BIOTURBATION	OYSTERS	NO. OF STYLOLITES
CLASTIC GRAIN SIZE											
Gravel	Coarse	Medium	Fine	V.fine	Mud						
						-9485					
						-9490	F13	transition to lower shoreface			
						-9495					
						-9500	F5	middle-upper shoreface			5
						-9505					
						-9510	F2	lower shoreface			1
						-9515	F13	transition to lower shoreface			
						-9520	F2	lower shoreface			40
						-9525					
						-9530					
						-9535					
Base at 9537											

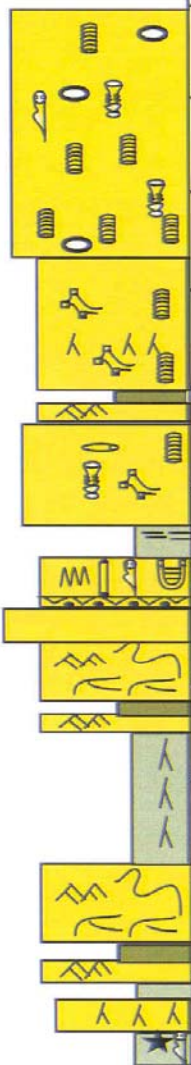
Appendix A.2: Core description for Burnett Brothers #1,  
Panola County, Carthage field.

SED. STRUCTURES						DEPTH (FT)	LITHOFACIES	ENVIRONMENT	BIOTURBATION	OYSTERS	NO. OF STYLOLITES
CLASTIC GRAIN SIZE											
Gravel	Coarse	Medium	Fine	V.fine	Mud						
						-8640	F1	shelf			
						-8645	TS F13	lower shoreface to transitiona			
						-8650	F4	upper shoreface-Beach <i>Ophiomorpha</i> and <i>Cryptio</i> -bioturbation			
						-8655					
						-8660					7
						-8665					
						-8670					
						-8675					29
						-8680					
						-8685	F2	lower shoreface			
						-8690					

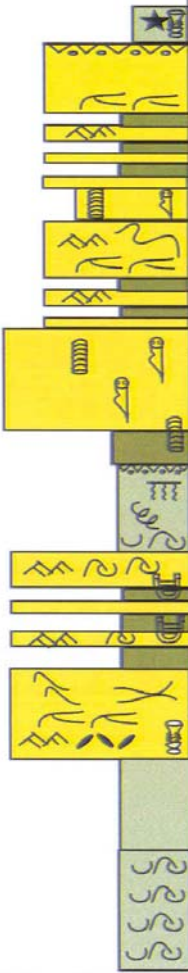
Appendix A.3: Core description of Bradshaw well # 1,  
Harrison County, Woodlawn field.

SED. STRUCTURES						DEPTH (FT)	LITHOFACIES	ENVIRONMENT	BIOTURBATION	OYSTERS	NO. OF STYLOLITES
CLASTIC GRAIN SIZE											
Gravel	Coarse	Medium	Fine	V.fine	Mud						
						8690	F7	inter-subtidal point bar			3
						8695					
						8700					
						8705	F10	soil zone, marsh mud, no traces, just roots and carbonaceous matter			1
						8710					
						8715	F7	inter-subtidal Mixed flat			2
						8720					
						8725					
						8730	F10	soil zone, marsh mud, no traces, just roots and carbonaceous matter			
						8740					
						8745	F7	mixed flat			
						8750	F8	bay fill/subtidal flat			
							F7	mud flat			
							F8	subtidal flat			

Appendix A.3: Core description of Bradshaw well # 1,  
Harrison County, Woodlawn field.

SED. STRUCTURES						DEPTH (FT)	LITHOFACIES	ENVIRONMENT	BIOTURBATION	OYSTERS	NO. OF STYLOLITES
CLASTIC GRAIN SIZE											
Gravel	Coarse	Medium	Fine	V.fine	Mud						
						8750					
						8755		subtidal flat flood tidal delta			
						8760					
						8765	F7	mixed flat/back barrier subtidal fully marine			
						8770					
						8775		subtidal flat flood tidal delta			
						8780	F8	bay mud			
						8785	F7	sand flat  mixed flat			
						8790	F10	mud flat, rooted, mottled, fractured marsh mud			
						8795	F7	mixed flat			
						8800		bay mud/back barrier thin sand flat rooted on top			
						8810	F8	bay mud, with <i>Diplochraterion</i> , <i>Ophiomorpha</i>			

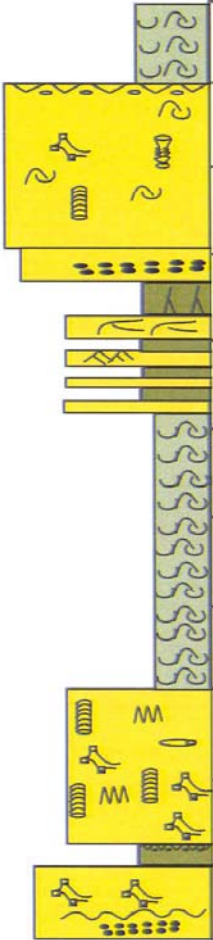
Appendix A.3: Core description of Bradshaw well # 1,  
Harrison County, Woodlawn field.

SED. STRUCTURES						DEPTH (F)	LITHOFACIES	ENVIRONMENT	BIOTURBATION	OYSTERS	NO. OF STYLOLITES
CLASTIC GRAIN SIZE											
Gravel	Coarse	Medium	Fine	V.fine	Mud						
						8810					
						F8	bay mud				
							subtidal sand flat, with chloritic stained sand				

242































Appendix A.3: Core description of Bradshaw well # 1,  
Harrison County, Woodlawn field.

SED. STRUCTURES						DEPTH (FT)	LITHOFACIES	ENVIRONMENT	BIOTURBATION	OYSTERS	NO. OF STYLOLITES
CLASTIC GRAIN SIZE											
Gravel	Coarse	Medium	Fine	V.fine	Mud						
						-8865					
						F8	oyster-rich lagoon				
						F7	subtidal flat, fully marine above sand bar, with some scattered oysters				
						F10	marsh, subaerial exposure				
						F7	mixed sand-mud flat				
						F8	lagoon, oyster- dominated mud				
						F7	subtidal flat				

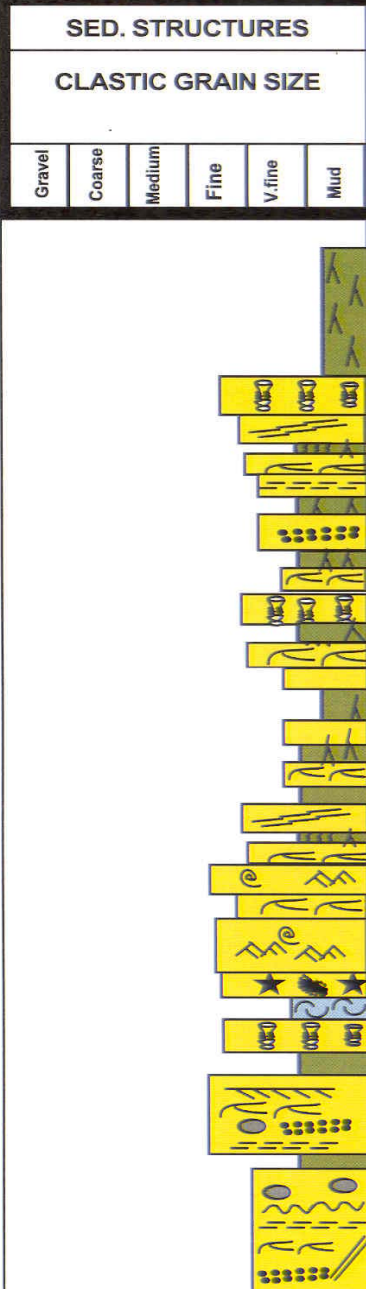


Appendix A.3: Core description of Bradshaw well # 1,  
Harrison County, Woodlawn field.

SED. STRUCTURES						DEPTH (FT)	LITHOFACIES	ENVIRONMENT	BIOTURBATION	OYSTERS	NO. OF STYLOLITES
CLASTIC GRAIN SIZE											
Gravel	Coarse	Medium	Fine	V.fine	Mud						
						-8920	F7	sand flat			15
						-8925	F8	bay sand/inter-subtidal tidal flat, climbing ripples, flasers, mud drapes and various types of fauna			
						-8930					
						-8935					
						-8940					
						-8945					
						-8950					
						-8955	F7	subtidal flat			
						-8960					
						-8965	F8	bay sand/tidal flat			
						-8970	F7	subtidal flat			
						-8975					
						-8980	F8	bay sand/tidal flat			
						-8985					

Bottom at 8984

Appendix A.4: Core description of Davidson Foundation # 1,  
Harrison County, Woodlawn field.

SED. STRUCTURES						DEPTH (FT)	LITHOFACIES	ENVIRONMENT	BIOTURBATION	OYSTERS	NO. OF STYLOLITES
CLASTIC GRAIN SIZE											
Gravel	Coarse	Medium	Fine	V.fine	Mud						
						9445	F7				
						9450		mud flat			
								sand flat			
						9455		mixed flat			
								marsh			
						9460		sand flat			
								marsh			
						9465		mixed flat			
								marsh			
						9470					
								mixed flat			
						9475					
							sand flat				
						9480					
							bay mud				
						9585 TS	F11	oyster lag			
								mixed flat			
						9490	F7	sand flat			
						9495					
						9500					


#### Appendix A.4: Core description of Davidson Foundation # 1, Harrison County, Woodlawn field.

SED. STRUCTURES						DEPTH (FT)	LITHOFACIES	ENVIRONMENT	BIOTURBATION	OYSTERS	NO. OF STYLOLITES
Gravel	Coarse	Medium	Fine	V fine	Mud						
						9500					
						9510					
						9515	F7	sand flat			
						9520					
						9525					60
						9530	F11	oyster lag			
						9535	F7	subtidal lower shoreface			
						9540					
						9545	F8	bay mud			
						9550					
						9555	F7	mixed flat			
						9560		sand flat			15

Appendix A.4: Core description of Davidson Foundation # 1,  
Harrison County, Woodlawn field.

SED. STRUCTURES						DEPTH (FT)	LITHOFACIES	ENVIRONMENT	BIOTURBATION	OYSTERS	NO. OF STYLOLITES
CLASTIC GRAIN SIZE											
Gravel	Coarse	Medium	Fine	V.fine	Mud						

Appendix A.4: Core description of Davidson Foundation # 1,  
Harrison County, Woodlawn field.

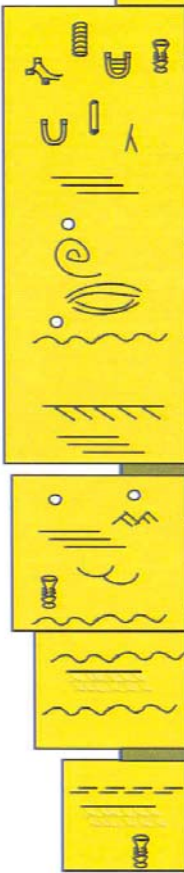
SED. STRUCTURES						DEPTH (Ft)	LITHOFACIES	ENVIRONMENT	BIOTURBATION	OYSTERS	NO. OF STYLOLITES
CLASTIC GRAIN SIZE											
Gravel	Coarse	Medium	Fine	V.fine	Mud						
						9615	F8	bay mud			
						9620	F7	sand flat			
						9625	F8	bay mud-sand			
						9630	F7	subtidal lower shoreface			
								mud flat			
								subtidal lower shoreface			
						9635	F7	subtidal-intertidal sand body			
						9640					
						9645					67
						9650	F8	distal bay center mud			
						9655	F7	mixed Flat			
						9660	F8	marine bay mud			
						9665	F7	subtidal lower shoreface fully marine			
						9670	F8	marginal bay sand			30

Appendix A.4: Core description of Davidson Foundation # 1,  
Harrison County, Woodlawn field.

SED. STRUCTURES						DEPTH (FT)	LITHOFACIES	ENVIRONMENT	BIOTURBATION	OYSTERS	NO. OF STYLOLITES
CLASTIC GRAIN SIZE											
Gravel	Coarse	Medium	Fine	V.fine	Mud						
						9670					
						9675	F7	mixed flat			
						9680	F8	marine mud in the mouth of the bay			
						9685	F7	sand flat			
							F8	bay mud			
						9690	F7	sand flat			
								mixed bay mud-sand			
						9695					
						9700	F7	<i>Teichichnus</i> -dominated sand flat			
						9705		<i>Ophiomorpha</i> -dominated sand flat			
							F8	bay mud			
						9710	F7	sand flat			
							F8	<i>Teichichnus</i> -dominated bay mud			
						9715	F7	sand flat			
								mixed flat			
						9720		sand flat			
						9725		mixed flat			



### Appendix A.5: Core description of Grace Lowry # 1, Harrison County, Woodlawn field.

SED. STRUCTURES						DEPTH (Ft)	LITHOFACIES	ENVIRONMENT	BIOTURBATION	OYSTERS	NO. OF STYLOLITES
CLASTIC GRAIN SIZE											
Gravel	Coarse	Medium	Fine	V. fine	Mud						
Top at 9410 ft						9410	F8	lagoon			
						9415	F11	lower shoreface to transitional			
						9420	F2	upper shoreface <i>Ophiomorpha</i> and <i>Cryptic</i> bioturbation			
						9425	F4				
						9430					
						9435					
						9440					7
						9445	F5	laminated upper shoreface			
						9450					
						9455					
						9460					29
						9465					



Appendix A.5: Core description of Grace Lowry # 1,  
Harrison County, Woodlawn field.

SED. STRUCTURES						DEPTH (FT)	LITHOFACIES	ENVIRONMENT	BIOTURBATION	OYSTERS	NO. OF STYLOLITES
CLASTIC GRAIN SIZE											
Gravel	Coarse	Medium	Fine	V.fine	Mud						
						-9465					
						-9470	F2	lower shoreface			
						-9475	F1	transition to inner shelf			
						-9480	F2	lower shoreface			
						-9485 TS	F11	transgressive lag Lagoon, Very restricted fauna			
						-9490	F8	brackish bay			
						-9495	F5	middle-upper shoreface with few 2 cm diame- ter chert pebbles and 10 cm diameter con- cretion			
						-9500					30
						-9505	F2	proximal lower shoreface <i>Ophiomorpha</i> -dominated			
						-9510					
						-9515					
						-9520					


Appendix A.5: Core description of Grace Lowry # 1,  
Harrison County, Woodlawn field.

SED. STRUCTURES						DEPTH (F)	LITHOFACIES	ENVIRONMENT	BIOTURBATION	OYSTERS	NO. OF STYLOLITES
CLASTIC GRAIN SIZE											
Gravel	Coarse	Medium	Fine	V.fine	Mud						
						-9520					
						-9525	F2	proximal lower shoreface <i>Ophiomorpha</i> -dominated			
						-9530		<i>Astrosoma</i> , <i>Teichichnus</i> - dominated lower shoreface to distal shoreface			
						-9535					
						-9540	F1	inner shelf			
						-9545	MFS	middle-outer shelf with big oysters			
						-9550					
						-9555					
						-9560		middle-outer shelf with big oysters			
						-9565					
						-9570	F9	storm beds			

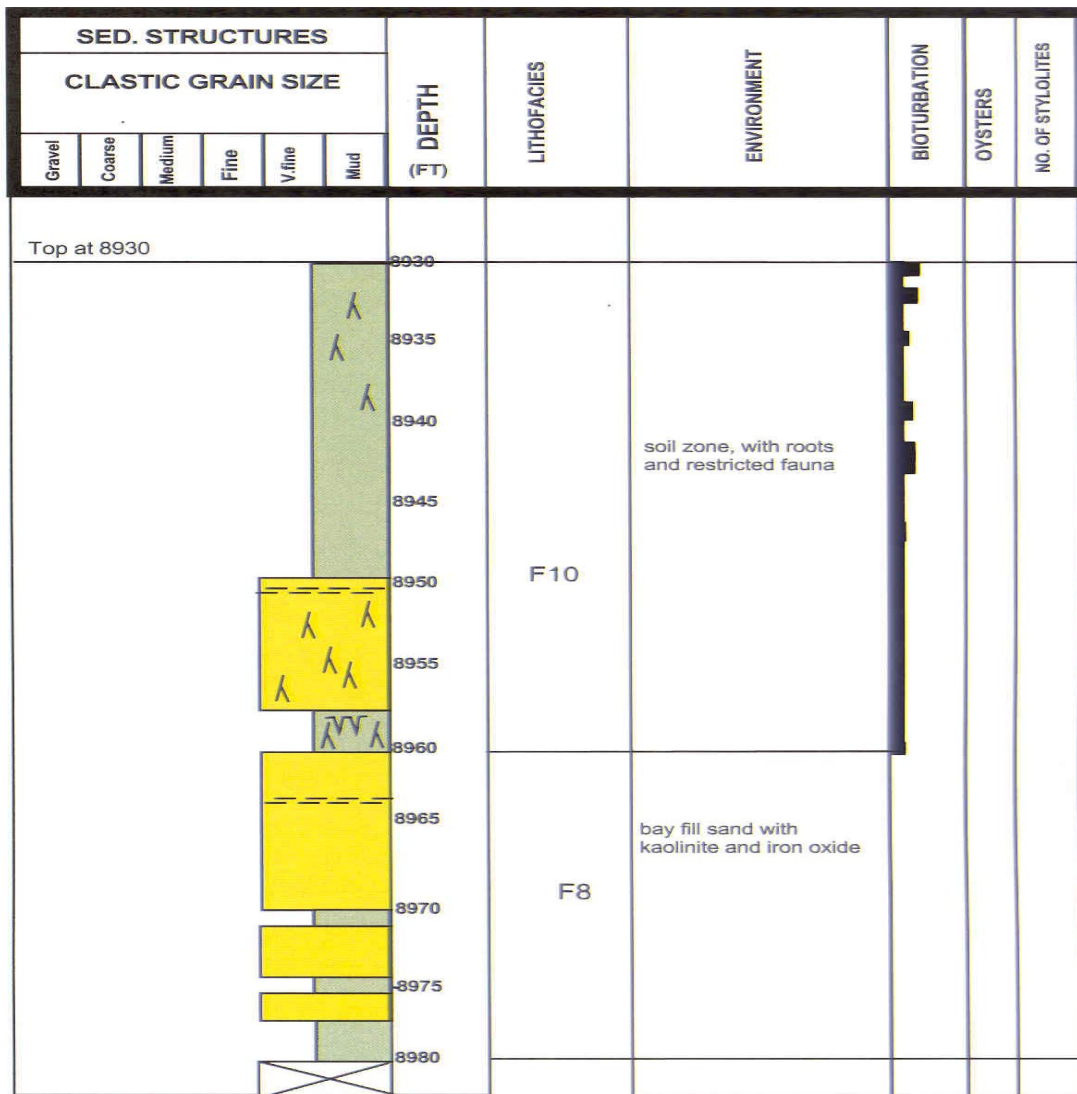
Appendix A.5: Core description of Grace Lowry # 1,  
Harrison County, Woodlawn field.

SED. STRUCTURES						DEPTH (FT)	LITHOFACIES	ENVIRONMENT	BIOTURBATION	OYSTERS	NO. OF STYLOLITES
CLASTIC GRAIN SIZE											
Gravel	Coarse	Medium	Fine	V.fine	Mud						
						-9570					
						-9575	F1	inner-middle shelf interrupted with few storm events			
						-9580					
							Transgressive lag				
						-9585	F5	lower-middle shoreface			
						-9590	F9				2
						-9595	F5	storm-dominated inner shelf			
						TS					
						-9600	F11	transgressive lag			
						-9605	F3	lower-middle shoreface with amalgamated storm beds.			
						-9610					
						-9615	F11	transgressive lag/ storm deposits on inner shelf			
						-9620	F3	storm dominated shoreface			

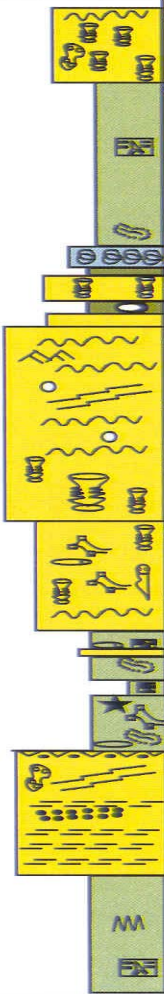
Appendix A.5: Core description of Grace Lowry # 1,  
Harrison County, Woodlawn field.

SED. STRUCTURES						DEPTH (F)	LITHOFACIES	ENVIRONMENT	BIOTURBATION	OYSTERS	NO. OF STYLOLITES							
CLASTIC GRAIN SIZE																		
Gravel	Coarse	Medium	Fine	V.fine	Mud													
						-9620	F3	amalgamated storm-dominated shelf with storm beds										
						-9625												
						-9630												
						-9635	F9	storm-dominated inner shelf. The fairweather deposits are clay, silt and very fine-grained sandstone, which are thoroughly btd by different types of ichnofossils. Periodically punctuated by storm events derived fine sand with bioclasts and sharp based storm derived events.										
						-9640												
						-9645	F1											
						-9650												
						-9655	F9											
Bottom																		

Appendix A.6: Core description of James Anderson # 1,  
Harrison County, Woodlawn field.

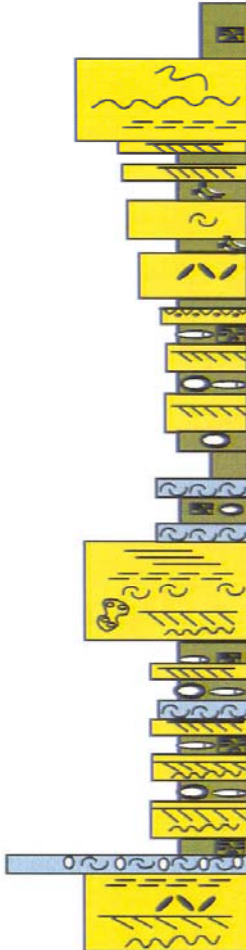


Appendix A.6: Core description of James Anderson # 1,  
Harrison County, Woodlawn field.

SED. STRUCTURES						DEPTH (FT)	LITHOFACIES	ENVIRONMENT	BIOTURBATION	OYSTERS	NO. OF STYLOLITES
CLASTIC GRAIN SIZE											
Gravel	Coarse	Medium	Fine	V.fine	Mud						
						9755	F2	<i>Ophiomorpha</i> -dominated lower shoreface			22
						9760	F1	inner shelf			
						9765					
						9770					
						TS	F11	gastropodes lag			
						9775	F13	lower shoreface to transition			
						9780	F5	middle-upper shoreface			20
						9785					12
						9790					15
						9795					20
						9800	F2	lower shoreface			15
						9805	F1	inner shelf-transition			
						9810		inner shelf			
						9815	F6	middle shoreface			
						9820	F1	inner to middle shelf			
						9825					
						9830					

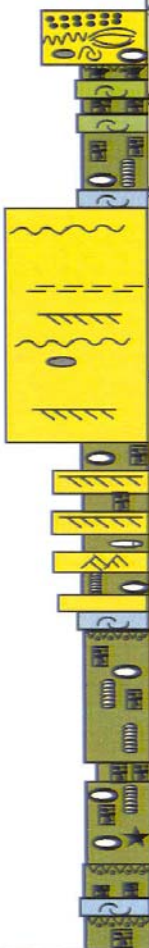


Appendix A.6: Core description of James Anderson # 1,  
Harrison County, Woodlawn field.

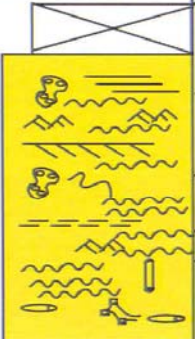


SED. STRUCTURES						DEPTH (FT)	LITHOFACIES	ENVIRONMENT	TUBURBATION	YSTERS	NO OF STYLOLITES
CLASTIC GRAIN SIZE											
Gravel	Coarse	Medium	Fine	V. fine	Mud						
						9830	F1	inner to middle shelf			
						9835	F6	lower to middle shoreface			12
						9840		lam-scrum lower shoreface			
						9845					
						9850	F13	transition to lower shoreface			
						MFS					
						9855	F1	middle-inner shelf			
							F11	oyster lag			
							F1	inner shelf			
						TS	F11	oyster Lag			
						9860	F4	middle shoreface			15
						9865	F1	transition to inner shelf			
							F11	oyster lag			
						9870	F1	transition to inner shelf			10 19 15
						9875	F11	oyster lag			
							F6	middle shoreface			10
						9880					



Appendix A.6: Core description of James Anderson # 1,  
Harrison County, Woodlawn field.

SED. STRUCTURES						DEPTH (Ft)	LITHOFACIES	ENVIRONMENT	BIOTURBATION	OYSTERS	NO. OF STYLOLITES
CLASTIC GRAIN SIZE											
Gravel	Coarse	Medium	Fine	V.fine	Mud						
						9880	F6	lower shoreface			20
						9885	F1	inner shelf			
						9890	F11	oyster lag			
						9895	F5	middle shoreface			3
						9900					3
						9905	F13	lam-scrum transition to lower shoreface			
						9910					
						9915	F11	oyster lag			
						9920	F1	inner-mid shelf			
						9925		mid-inner shelf			
						9930	F11	oyster lag			
							F1	distal-midshelf			


Appendix A.6: Core description of James Anderson # 1,  
Harrison County, Woodlawn field.

SED. STRUCTURES						DEPTH (FT)	LITHOFACIES	ENVIRONMENT	BIOTURBATION	OYSTERS	NO. OF STYLOLITES
CLASTIC GRAIN SIZE											
Gravel	Coarse	Medium	Fine	V.fine	Mud						
						10010					
						10020	F6	middle-upper shoreface with tidal influence			30
						10025					20
						10030					30
						10035					30
						10040					20
						10035					
						10040	F7	subtidal flat/flood tidal delta			27
						10045					5
						10050					30
						10055					18
						10060					20
						10065	F8	lagoon			
10070											

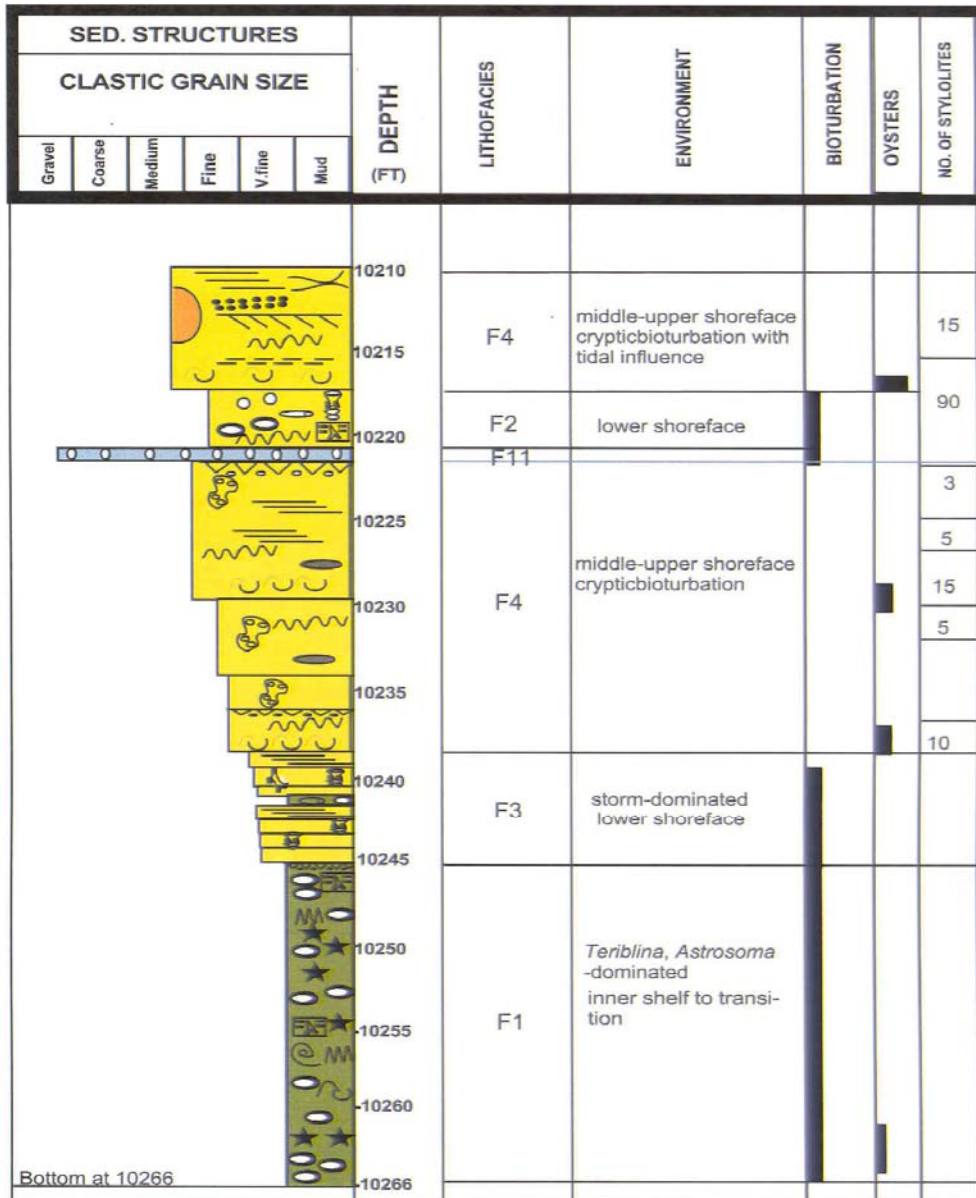
Appendix A.6: Core description of James Anderson # 1,  
Harrison County, Woodlawn field.

SED. STRUCTURES						DEPTH (F)	LITHOFACIES	ENVIRONMENT	BIOTURBATION	OYSTERS	NO. OF STYLOLITES
CLASTIC GRAIN SIZE											
Gravel	Coarse	Medium	Fine	V.fine	Mud						
						10110					
							F11	lag deposits			
						10115	F5	middle shoreface			
						10120	F2	lower shoreface			20
						10125	F1	middle shelf			
							F11	TS Lag			
							F1	inner-middle Shelf			
						10130	F2	middle shoreface			
						10135	F11	lag deposits			
						10140	F6	middle shoreface			30
						10145					50
						10150					66
						10155	F13	inner shelf to transition			
						10160	F1	inner shelf			

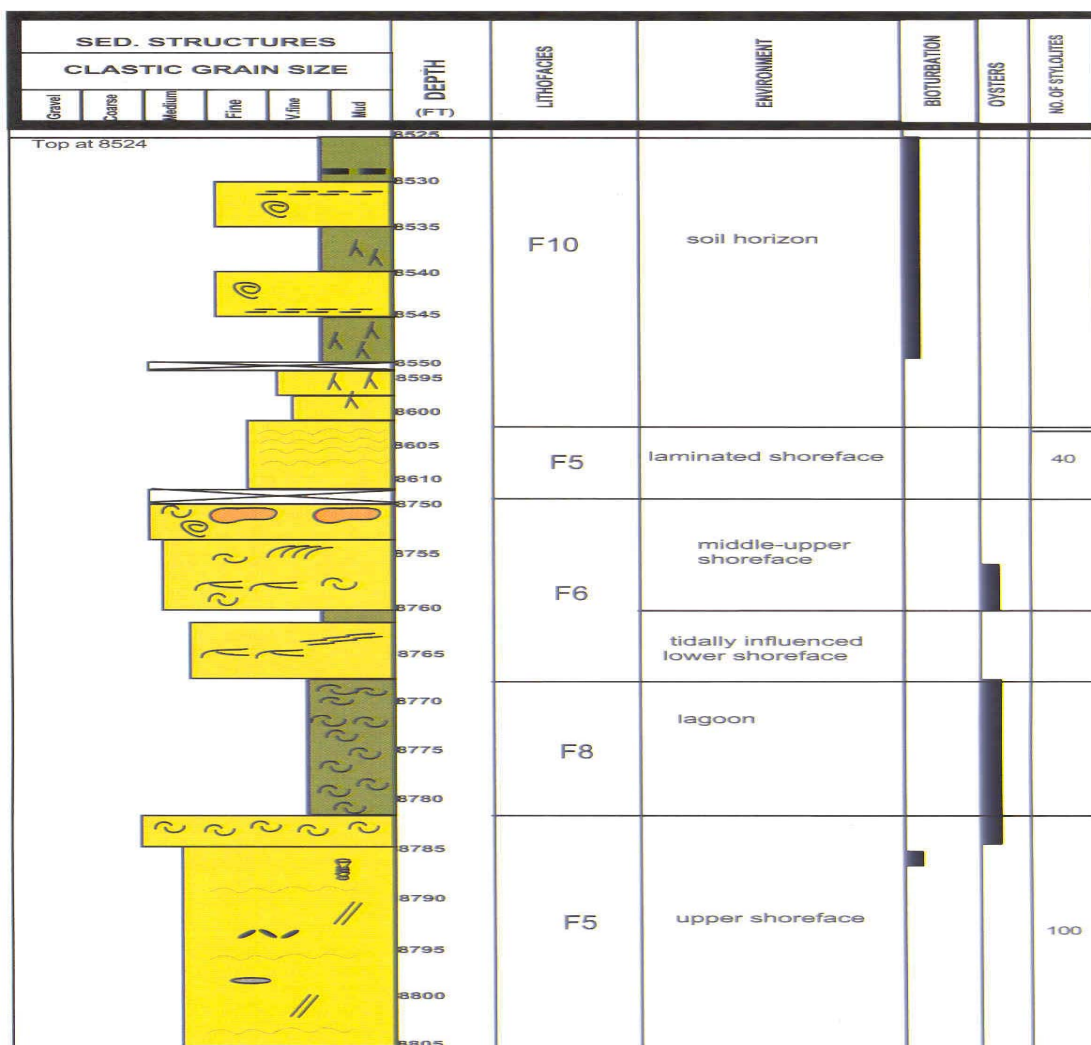
Appendix A.6: Core description of James Anderson # 1,  
Harrison County, Woodlawn field.

SED. STRUCTURES						DEPTH (FT)	LITHOFACIES	ENVIRONMENT	BIOTURBATION	OYSTERS	NO. OF STYLOLITES
CLASTIC GRAIN SIZE											
Gravel	Coarse	Medium	Fine	V.fine	Mud						
						10160	TS F11	Ts lag			
						10165					
						10170	F2	lower shoreface			
						10175	F1	inner shelf to transition			
						10180					
						10185	F2	lower shoreface			31
						10190					
						10195	F1	open shelf			
						10200					
						10205	F1	lower shoreface			
						10210					
						10215	F2	lower shoreface			
						10220	F1	transitional to inner shelf			20
						10225					
						10230	F11	Ts Lag			
						10235	TS				
						10240	F6	middle-upper shoreface			
						10245					

Appendix A.6: Core description of James Anderson # 1,  
Harrison County, Woodlawn field.



Appendix A.7: Core description of Jones # 1,  
Harrison County, Woodlawn field.










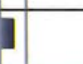




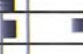





Appendix A.7: Core description of Jones # 1,  
Harrison County, Woodlawn field.

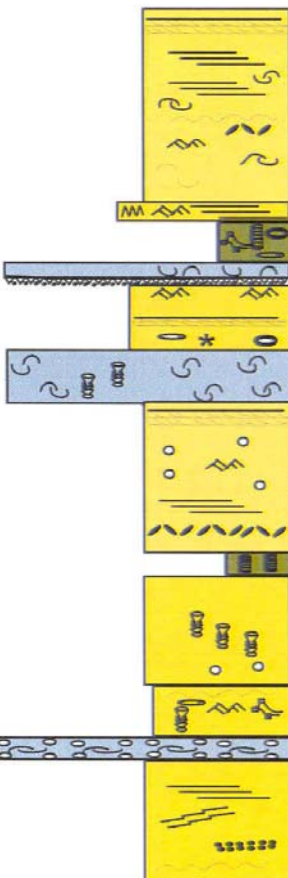
SED. STRUCTURES						DEPTH (FT)	LITHOFACIES	ENVIRONMENT	BIOTURBATION	OYSTERS	NO. OF STYLOLITES
CLASTIC GRAIN SIZE											
Gravel	Coarse	Medium	Fine	V.fine	Mud						
						8805	F5	upper shoreface			30
						8810 TS	F11	oyster lag			
						8815	F13	transition to lower shoreface			8
										20	
						8820				50	
						9400	F2	lower shoreface			
						9405	F11	storm bed			
						9410	F2	lower shoreface			
						9410	F11	storm bed			
						9415	F2	lower shoreface			
						9420					
						9425					
						9430					
						9435					
						9440					19
9445	F13	transition to lower shoreface									
9450					16						
Base at 9554 ft.											




Appendix A.8: Core description of Cargill well # 15,  
Harrison County, Waskom field.

SED. STRUCTURES						DEPTH (FT)	LITHOFACIES	ENVIRONMENT	BIOTURBATION	OYSTERS	NO. OF STYLOLITES						
CLASTIC GRAIN SIZE																	
Gravel	Coarse	Medium	Fine	V.fine	Mud												
						-9017	F8	lagoon									
						-9020											
						-9025											
						-9030											
						-9035											
												-9040					
												-9200					
												-9205	F8	restricted lagoon, <i>Teichichnus</i> -dominated			
												-9210	F5	upper shoreface			
						-9215											
						-9220	F2	middle to lower shoreface									
						-9222.5	F11	transgressive lag									
						-9222.5	F8	restricted bay									


Appendix A.7: Core description of Jones # 1,  
Harrison County, Woodlawn field.

SED. STRUCTURES						DEPTH (Ft)	LITHOFACIES	ENVIRONMENT	BIOTURBATION	OYSTERS	NO. OF STYLOLITES
CLASTIC GRAIN SIZE											
Gravel	Coarse	Medium	Fine	V.fine	Mud						
						-9222.5	F5	upper shoreface large scale x-bedding, planar bedding and small bivalves			10
						-9225					
						-9230					
						-9235	MFS F1	storm-dominated lower shore face			
						-9240		open shelf			
						-9240	F11	transgressive lag			
						-9240	F5	lower to middle shoreface			
						-9245	F11	transgressive lag with oysters and <i>ophiomprpha</i>			
						-9250	F6	middle shoreface			
						-9255	F8	restricted lagoon, <i>Teichichnus</i> -dominated			
						-9260	F2	middle Shoreface			5
						-9260		lower shoreface			
						-9265	F11	storm deposits			
						-9270	F6	lower shoreface			38
						-9272.5					15

Appendix A.7: Core description of Jones # 1,  
Harrison County, Woodlawn field.

SED. STRUCTURES						DEPTH (FT)	LITHOFACIES	ENVIRONMENT	BIOTURBATION	OYSTERS	NO. OF STYLOLITES
CLASTIC GRAIN SIZE											
Gravel	Coarse	Medium	Fine	V.fine	Mud						
						-9272.5					
						-9275	F5	lower-middle shoreface			
							F11	storm bed			
							F5	lower-middle shoreface			
						-9280	F11	storm			5
							F5	lower shoreface			
							F11	lag deposits			
						-9285	F6	middle-upper shoreface			45
							F11				
						-9290	F6	middle-upper shoreface			35
						-9295					
						-9300					5
						-9305					22
								lower-middle shoreface			11
						-9310	F11	storm deposits			
							F6	lower-middle shoreface			14
							F11	storm deposits			
						-9315	F13	inner shelf to toe of shoreface			
						-9320					
						-9325					15

Appendix A.7: Core description of Jones # 1,  
Harrison County, Woodlawn field.

SED. STRUCTURES						DEPTH (FT)	LITHOFACIES	ENVIRONMENT	BIOTURBATION	OYSTERS	NO. OF STYLOLITES
CLASTIC GRAIN SIZE											
Gravel	Coarse	Medium	Fine	V.fine	Mud						
						-9325					
						-9330	F6	lower to middle shoreface			20
						-9335					
						-9340	F13	transitional from inner shelf to the toe of lower shoreface			
						-9345	F1				
							F9				
							F1				
						-9350	F9				
						-9355	F9	inner shelf pyrite which replace some shell fragments			
						-9360	F1				
Bottom at 9366 ft											



## Appendix B: Point count Table.

Well	Depth (ft)	Size (mm)	sorting	Roundness	Quartz		K-feldspar			Plag.			RF	H	
					Polyxll.	Monoxll.	Fresh	Replaced	Leached	Fresh	Replaced	Leached			
1- Storm on shelf															
Lowry#1	9555.4	SILT	PS	SA		30					1			0.2	
Lowry#1	9591	SILT	PS	SA		60.8	3	1	0.4	2	1.1				
Lowry#1	9597.5	F	MS	SA	1	53	6	2	5	0.5	3	1.5	2		
Lowry#1	9640.5	SILT	MS	SR	0.1	52.4				1	0.7	1.1			
SFE	9358.5		storm-shrff			58.5	0.5			0				5	
SFE	9364		storm-shelf			17.5	0.5			5.5				0.5	
2- Transitional-Lower shoreface															
Jones#3	8821	F	MS	SR		1.5	62			0.5	6			0.5	
Jones#3	9447	F	MS	SR	1.8	62.6	0.2	0.5	0.1	2.2	0.3	0.2		0.8	
Jones#3	9454	FU	WS	SR	2	69.9	3.7	0.1	0.2	2	0.1	0.1	1.4		
SFE	9333.2	F	MS	SR		65	2			3.5		0.5	1.5		
SFE	9341.3	F	MS	SR		46.5				5		1			
3- Bioturbated Ophiomorpha-dominated shoreface															
Blocker#1	9328	F	WS	SA-SR		65	4.5	0.2	3.5	1	2.5	0.2			
Blocker#1	9768	F	MS-PS	SA-SR	3.2	63				7	2	1.2	2.2		
Blocker#1	9796	VF	PS	SA-SR	2	61.5	1.7	1	3	4.5	0.5	1	1.4		
DSF#1	9595	F	MS	SA-SR	2.5	67.5	1.7	0.8	4	1	2	0.7	0.2		
Lowry#1	9434	F	MS	SR	4	68				1.1	1	3	0.2		
Lowry#1	9505	F	WS	SR	2.2	64	3	1.4	3	1	2	1.1	4.5		
Lowry#1	9510	F	MS	SA	1	68.5	6	1	1.7	2	0.5	1	3		
BSH#1	8760	F	MS	SA-SR	1.9	69	1	1	3	3	1	0.5	0.2		
BSH#1	8909	F	WS	SA-SR	2.7	64.6				2	0.8	2.2	1.1		
BSH#1	8981	F	PS	SA	3	59.9	2	0.8	1.1	1	0.2	0.2	0.5		
Jones#3	9399	F	MS	SR	1.5	69	4.5	0.4	0.2	4	1	0.8	2		
Jones#3	9400	F	MS	SR	1.2	68	3	1.1	0.3	4	1	0.5	1.6		
Jones#3	9409	F	WS	SR	2.3	69	2.2	0.6	0.2	1.4	0.2	0.1	1.4		
Jones#3	9409.5	PEBBLE	PS	SR	15	55.6	1.4	1.1		0.5	0.2		2.5		
Jones#3	9428	F	MS	SR	1.5	69.7	1.4	0.5	0.3	3	1.1	0.2	0.8		
SFE	9260.6	F	MS	SR		65	0.5			2		0.5	0.5		
4- Cryptobioturbated Shoreface															
Blocker#1	9344	F	PS-MS	SA-SR		62.5	5	1	4.7	0.8	1	3			
Blocker#1	9924	VF	MS	SA-SR	1	69.3	1.1	0.1	4	2	0.5	0.6	1.9		
Blocker#1	9939	VF	WS	SA-SR		59.1	7	2	7	1.2	0.5	0.5	0.2		
JA#1	10026.08B	F	WS	SA-SR	0.9	66	3	2.4	3	1	2	1.2	0.5		
JA#1	10026.16C	F	WS	SA-SR		64.5	5	1.5	3	1	2	0.7	0.8		
JA#1	10026.3E	F	MS	SA-SR	0.1	60	5	2.4	2.5	1	2	1.8	0.8		
JA#1	10026.4F	F	MS	SA-SR	2.8	59	3	2	3	1.5	3	1	0.2		
JA#1	10026.5G	F	PS-MS	SA-SR	3.7	69	4	2	2	1	0.5	0.5	1.1		
JA#1	10026.58H	F	WS	SA-SR	2.2	69	4.4	1.4	3	1	3	0.4	2.2		
JA#1	10026.66I	F	MS	SA-SR	2.2	66.9	0.8			2.2	1.2	2	0.8		
JA#1	10026.75J	F	MS	SR		68.5	3	2.5	2	3	1	1	2.8		
JA#1	10026.88K	F	MS	SR	2.2	65	4	2.1	3	2	0.9	1.7			
JA#1	10226	SLT	WS	SR		50					1.3				
5- Laminated shoreface															
Blocker#1	9706	VF	MS	SR		59.9	1	1	0.8	3	1	1.1	2.8		
Blocker#1	9761	F	WS	SR	0.8	62.5	0.5			4	1	2	0.8		
Blocker#1	9779	LIMESTONE													
Blocker#1	9905	VF	PS	SA-SR	2	63.5				6	8		2		
Blocker#1	9908	F	PS	SA-SR	4	57.7	1	1	0.8	1	4	1	2.8		
JA #1	10143	F	MS	SA-SR	1	51				2.2	8		3		
Lowry#1	9445	F	WS	SA-SR	2.5	61.5	6	1.7	2	2	0.5	1.5	1.4		
Lowry#1	9459	F	PS	SA-SR	2	58.9	9	1	4	1	1	0.8	0.5		
Lowry#1	9470	F	PS	SA	2	50.9				2.8	1.4	2	1.7		
Lowry#1	9497	F	MS	SA-SR	0.9	61.5	6.5	1	3	4	1	0.5	2		
Lowry#1	9589	SILT	WS	SR		33				2			0.5		
Jones#3	8753.5	F	WS	SR	0.1	64				4	2.8	1.1	0.2		
Jones#3	8797	ML	WS	SR	1.5	70				2.2	1.7	1.7	0.2		
Jones#3	8808	FU	PS	SR	1.2	58				3.5	1	3.1	0.8		
Jones#3	8809	FU	PS	SR	2.5	59				0.2	0.8	1.7	3		
SFE	9207.5	F	MS	SA-SR		57.5	1	0.5		7.5	0.5	0.5	1		
SFE	9210.5	F	MS	SA-SR		59.5	3.5	1		8		1	2		
SFE	9218.4	F	MS	SA-SR		59	1.5	0.5		3.5		1			
SFE	9232	F	MS	SA-SR		60	4.5		0.5	7		1	3.5		
SFE	9240.9	F	MS	SA-SR		59	1.5			3	1		1		
SFE	9249.5	F	MS	SA-SR		59	2			4.5			1		
SFE	9252.5	F	MS	SA-SR		54.5	1	0.5	0.5	4.5	0.5	2	5.5		
SFE	9275.6	F	MS	SA-SR		61	1.5	1	0.5	2.5	1	1	3		
SFE	9281.1	F	MS	SA-SR		58.5	1		1	7.5		1.5	1		
SFE	9322.9	F	MS	SA-SR		52				4		0.5	1.5		

Appendix B: Point count Table. (Continued).

Heavy Minerals	Det. Clay	Bioclasts	Feld. Over	*Qz cement	Cements					
					Calcite	Dolomite	Anhydrite	Pyrite	Kaolinite	Illite
	48.7	5		0.1	7.5	0.5		5		
0.5	15			1.2	13	0.5		0.8		
0.5	2.2			5	8	1.7		2.8		
	20	0.2		0.5	23			0.2		
	1.5			7			26.5			
	67						2	7		
	2			2.5	25					
	3.4			13.5	12	0.5				
	2.6			17		0.2				
	7.5			19			1			
	30.5			1.5	12.5			3		
1.2	6			8	0.2			0.2		
	2	1.1		9	3.1			1	0.2	
	5.1			7.5	4				0.8	
1	6.8	1		6				0.8		
0.8	7.7	2		5.5		0.5	0.5	0.2	0.5	
0.2	3.8	0.5		3	6			2	1.3	
	3.1		0.5	4	1.5	0.7		0.5		
1.1	6			5	1				0.5	
	7		1	4.5	5	2		0.8	1.6	
	25			2.5				2.8		
1	4.7	1		7	1.4			0.3		
1	5	1.3		8	3	0.2				
1.5	8	3		5	2				0.6	
	4.7	0.5		8	10			0.5		
	4.4	2		7	6	0.8				
	20	0.5		5	3			2		
0.5	4.5			9				2	0.5	
	4.8		1	6	3.4			0.8		
0.1	2.8			7	1.1			0.5		
	5.1			5	2				1.4	
	4.7			6	3.4			0.2	0.4	
	5.2			7	3.6				0.8	
	4			6	2.5			0.5	1	
1.3	4.2		0.3	5	2.5			0.5	2.2	
1.5	3.3			6	0.5		0.8	0.5	0.8	
	1.1			5.5	9			0.5		
	4.2		1	4	2		0.5		0.5	
	6			6	2.5	0.3		0.5		
	15	2			30				1.7	
	4	0.5		13.5	4.8			1.1		
0.1		0.5		11	7.1			0.2	1	
2.3	2.2			6	1				1	
	6		0.5	16	1			0.2	0.5	
		4.1		0.2	30	0.5				
0.2	4			12			1.1		0.8	
0.1	2.8		0.5	11.5	2.7	0.5				
	18	2.8		3.7	11	1		1.7		
	0.8		1	10.5	1	0.5	2.8			
0.1	0.2	33		0.1	30.4			0.7		
0	3.7			19	0.5	1.4			1.3	
	2.7			16	0.5	0.5				
	4		0.1	18	0.5	2.2		0.3	0.8	
8	1.9			17	2	0.2		0.2		
	4.5			14	6					
	4			12.5	2.5					
	9	0.5		13.5	9.5			0.5		
1	2.5			14.5	0.5					
0.5	16			11.5	3			2		
	2	3		14.5	5.5					
	8			13.5	2			1		
	1.5	0.5		22	1	2				
	0.5			2.5	26			0.5		
	31			1			2.5	5		

Appendix B: Point count Table. (Continued).

Illite	Chlor.	Visual Porosity				SUM	Core Analysis		Gr. dens.	IGV
		Intergran.	Mouldic	Intra	Fracture		He Porosity	Horiz. Perm		
		2				100				
		0.5	0.2			100				
		2		3.8		100	2	0.02	2.65	24.7
		0.8				100				
	1					100				36
						100				
						100	4.1	0.01		29.5
		0.7		1.2		100	3.6	0.01		30.1
		0.2	0.5			100				20
						100				27.5
						100				
		2	3	2.5		100	8.6	0.7		21.4
	2	1	1	1		100	3.9	0.39		26.3
	0.8	1.2	2	2		100	6	0.04		25.9
		2	2			100	4.9	0.23	2.65	21.6
		3	2			100				20.4
		0.5		0.5		100	1.2	0.02	2.67	17.1
		4.5		0.2	0.3	100	7.2	0.09	2.64	18.8
		3	2	0.8		100	7.2	0.03	2.64	22.5
	1	1	2	0.5	0.2	100	7.7	0.07	2.65	25.9
		0.5		0.5		100	1.4	0.02	2.66	
		1.2				100				21.6
		0.5		0.3		100	5.8	0.2		24.7
		1		1.5		100	2.5	0.04		23.1
						100				32.2
		0.5		0.8		100	2.6	0.02		25.7
	0.5	0.5				100				
		1.5	2	2		100	5.6	0.02		23.5
	0	1	1	1.5		100	4	0.02		23
		1	4	1	5	100				20.4
			4	2.5		100				20
			2.8	4		100				22
			4	1	2.8	100				22.6
			4	1	5.5	100				23
			0.2			100				17.4
						100				17.1
			5	2.8		100				25.1
			2	2		100				23.7
			3	0.8		100				22.3
						100				
		1.5	2	2		100	6.7	0.04		24.9
		2.5	3	3		100	9.1	0.04		21.8
						100				
	6					100	1.4	0.02		16.2
	0.5	0.5	0.5	1		100	2.6	0.02		25.2
						100				30.7
		0.8	2			100	2.9	0.02	2.64	18.7
		2		1.7		100	6.4	0.03	2.64	20
		1				100	7.1	0.07	2.65	
		1		2		100	3.6	0.03	2.64	17.6
						100	1.2	0.02	2.68	
		1.4		0.5		100				27.3
		2	1			100	6	0.01		21.7
		3.4		3.1		100	7	0.09		29.3
		2		1.5		100	5.4	0.01		23.3
5		1		1		100				30.5
5				1		100				24
	0.5			1		100				33
3	0.5	1		0.5		100				22
	1			0.5		100				33.5
5	0.5	2.5		0.5		100				30
	3	2.5		1		100				30
		1.5				100				28
						100				29.5
		1		1.5		100				



Appendix B: Point count Table. (Continued).

SFE	9326	F	MS	SA-SR		52.5	2			8		1	3
SFE	9329	F	MS	SA-SR		55				13.5			2
<b>6- Tidally influenced shoreface</b>													
Blocker#1	9370	F	WS	SA-SR		58	3	0.5	2.3	0.2	1.6	2	0.8
Blocker#2	9380	F	WS	SR		61.3	4	1.2	3	0.5	0.6	2	1.7
Jones#3	8602	F	MS	SA		62.1				2.2	0.2	2.5	0.5
Jones#3	8605	F	MS	SA	0.1	61				3.7	0.5	2	1.4
Jones#3	8605.5	F	MS	SA	1.2	62.4				3.4	0.8	1.7	0.5
Jones#3	8606	F	MS	SR	0.9	61.5				1.9	1.8	2.2	
Jones#3	8606.5	F	MS	SA-SR	0.6	57.5				1.1	1.7	3.4	
Jones#3	8607.5	F	WS	SR	0.7	66.8				1.3	0.8	0.4	0.2
Jones#3	8608	F	PS-MS	SA	0.2	67				1.4	0.2	0.4	0.8
Jones#3	8609	F	MS	SA-SR	0.2	64				3.7	0.2	2	
Jones#3	8611	F	MS	SR	0.1	60				2.8	0.2	3	1.1
SFE	9270		MS	SR		67	0.5			0.5			0.5
SFE	9295		MS	SR		59.5	3.5			4		1	1.5
<b>7- storm dominated shoreface</b>													
Blocker#1	9829	F	WS	SR		52.8	3	2.1					1.7
Lowry#1	9619	F	MS	SA	2	56				3	1.7	3	0.8
SFE	9310.5	F	MS	SR		66.5	1			1	0.5	1	
<b>8- Sand Flat</b>													
Blocker#1	9731	F	WS	SR	1.4	65	0.5			1	4.5	0.5	0.8
Blocker#1	9749	VF	WS	SR		58	7.6	0.8	4	1.5	2	0.2	
DSF#1	9040	F	MS	SR	1	66.7				1.4	6	2	0.4
DSF#1	9412	F	WS	SR		65.2				2.2		0.5	1.1
DSF#1	9496	F	WS	SR	3.1	68				4	1	1	0.8
DSF#1	9511	F	MS	SR		59.1	0.2	2		1.1	4.8	1.1	0.5
DSF#1	9514	F	MS	SR	1.4	64.3				1.6	1.7	1.1	1.7
DSF#1	9576	F	MS	SA-SR	1.4	64	1.4			2.2	0.8	2	
DSF#1	9617	F	WS	SR	1.9	69	0.5	0.5	2.5	1.1			0.5
DSF#1	9719	F	PS	SA-SR	1.2	63.1	2.8			1.7	0.2	0.5	1.6
BSH#1	8652	F	PS	SA	0.7	60	1	0.2	0.5	3	1.7	4	0.2
BSH#1	8693	F	WS	SR-R	1.1	65.5	1.4	0.7	2	1	1	0.9	0.5
BSH#1	8711	F	MS	SR	2	69				0.8	1	1.2	0.5
BSH#1	8734	F	WS	SR	0.6	69.5	0.2	0.8	2	2	0.5	0.8	2.7
BSH#1	8817	F	MS	SR	2.7	66	0.2	0.5	0.5	0.6	1.2	0.1	1.6
BSH#1	8852	F	MS	SA-SR	2.5	54.7				1.1	2.8	3.1	2
BSH#1	8888	VF	PS-MS	SA-SR	1	58.5				1.1	2.2	3.7	1.1
DSF#1	9641	F	WS	SR	2	64				2.2	0.8	2	0.8
<b>9- Lag deposits</b>													
Blocker#1	9745	PEBBLE	PS	SR-R	53.7	10					0.2		3.4
JA#1	10135.5	F	PS	SA-SR	0.7	57.7				2.8	6		1.1
Blocker#1	9338	VF	PS	SA-SR	9.2	35.9				1	2.2		1.7
Blocker#1	9811	PEBBLE	PS	R	48	17.2				0.5			3
JA#1	10113	PEBBLE	PS	SR	39	31				0.8	0.7	1	1.1
Jones#3	9405	F	PS-MS	SA-SR	1.7	63	1	0.4		6	1.8		5
Lowry#1	9476	PEBBLE	PS	SR	25	15				0.2			6
SFE	9280.6	F	PS	SR		63	2			4	0.5	1	0.5
<b>10- Bay</b>													
JA # 1	9974	F	WS	SA		32							
DSF#1	9668	F	MS	SR	3	68.8	1.4	1.2	3	2	0.5	0.6	0.6
Lowry#1	9537.9	VF	PS	SA	0.7	50	6	1.7		2	0.2		1.4
BSH#1	8739	F	MS	SA-SR	1.5	65	0.2	0.5	0.2	1.4	1	1	1.4
BSH#1	8741	F	MS	SA-SR	1.5	62.1	0.5		0.3	2	0.5	4	1.1
BSH#1	8781	F	WS	SR	2	68.3				1	2.5	2	1
BSH#1	8935	VF	MS	SA-SR	2	59	3	0.4	4	2	0.7	1	1.1
BSH#1	8965	F	MS	SA-SR	1.1	63	2	1	2				1.4
<b>11- Lagoon</b>													
SFE	9028.4	BIO MICRITE				12							
SFE	9034.5					19				0.5			
<b>12- Soil</b>													
JA # 1	8958	F	WS	SA-AR	2.3	65				1.1		1.8	1.1
BSH#1	8722	VF	WS	SR	2	64	1.8	0.7	2	3	1	1.7	1
Jones#3	8523.5	F	WS	SA-SR	2.5	67				0.5	0.2	2	
Jones#3	8535.5	F	PS	SA		57.3				2	0.5	0.5	0.5
Jones#3	8548	F	PS	SA		63.8				1.4	0.2	0.4	0.2

Appendix B: Point count Table. (Continued).

	17			8.5			1	
	4			14.5		0.5		
	3			18	3			
0.5	3		0.2	15	2			
	11			12	0.5			
	11			10	1.5	2		0.8
1	8.8			12	0.8		0.2	1.2
0.3	11			11.5	0.8	3		
0.2	8			13.5	1.4	2.2		5.4
	6			15.5	2.1	0.8		1.1
	6			17	2.4		0.5	2
	7			15	0.3	0.3	0.5	
	8.2			13	0.2	1.4		2.5
	3.5	2		10	15			
				21		1		
		11.4		2	26	0.4		0.2
0.3	4.5	2	0.1	7.5	11		0.5	1.4
	1.5	1	1	0.5	26			
	0.2	0.2		16	9.1			
				13	0.2		1.2	1
	2.7			15	0.2		0.5	0.8
	23			4				
	2.2			16				0.7
0.2	0.2			2	14.8	10		
0.5	0.2			3.5	9	10		0.3
	3.7			17	1			0.5
0.3	2.2			15			0.6	0.8
0.3	24			2			1.4	0.2
	13	0.1		4			3	2.2
0.1	3		0.3	13.5	1		1	2
	3			12	5			1.7
	7			9.5				
0.6	2			19	1.5			
	14			6	10		0.5	0.8
	3.8			12	8.5		0.8	1.1
0.1	1.1			15	5	2.5	0.2	0.3
		2		1	29.5		0.2	
	0.2	0.2	0.2	3	27			
		28	1	2	18	0.5		
		1.3			24			0.2
		0.3		3	21.5			
	6		0.5	10	4	0.4		
		25			28.8			
	18.5			4.5	4	1	0.5	
	15	46				6.5	0.5	
0.3	3.6			9				
0.1	35			0.2	0.5		1.4	
	2.8			7	9		1	
	5			10				
	1.3			7	12		0.2	0.5
0.1	17			5	1			1
	2.3			11	1.5	0.1	9	1.4
	25.5	24			34.5	1	3	
	29	15			35		1.5	
	21			5				
	14			6	2			
	4.4			18	3.7	2.5		
	34			2				
	29			1		0.8	0.5	

Appendix B: Point count Table. (Continued).

SFE	9326	F	MS	SA-SR		52.5	2			8		
SFE	9329	F	MS	SA-SR		55				13.5		
<b>6- Tidally influenced shoreface</b>												
Blocker#1	9370	F	WS	SA-SR		58	3	0.5	2.3	0.2	1.6	2
Blocker#2	9380	F	WS	SR		61.3	4	1.2	3	0.5	0.6	2
Jones#3	8602	F	MS	SA		62.1				2.2	0.2	2.5
Jones#3	8605	F	MS	SA	0.1	61				3.7	0.5	2
Jones#3	8605.5	F	MS	SA	1.2	62.4				3.4	0.8	1.7
Jones#3	8606	F	MS	SR	0.9	61.5				1.9	1.8	2.2
Jones#3	8606.5	F	MS	SA-SR	0.6	57.5				1.1	1.7	3.4
Jones#3	8607.5	F	WS	SR	0.7	66.8				1.3	0.8	0.4
Jones#3	8608	F	PS-MS	SA	0.2	67				1.4	0.2	0.4
Jones#3	8609	F	MS	SA-SR	0.2	64				3.7	0.2	2
Jones#3	8611	F	MS	SR	0.1	60				2.8	0.2	3
SFE	9270		MS	SR		67	0.5			0.5		
SFE	9295		MS	SR		59.5	3.5			4		
<b>7- storm dominated shoreface</b>												
Blocker#1	9829	F	WS	SR		52.8	3	2.1				
Lowry#1	9619	F	MS	SA	2	56				3	1.7	3
SFE	9310.5	F	MS	SR		66.5	1			1	0.5	
<b>8- Sand Flat</b>												
Blocker#1	9731	F	WS	SR	1.4	65	0.5			1	4.5	0.5
Blocker#1	9749	VF	WS	SR		58	7.6	0.8	4	1.5	2	0.2
DSF#1	9040	F	MS	SR	1	66.7				1.4	6	2
DSF#1	9412	F	WS	SR		65.2				2.2		0.5
DSF#1	9496	F	WS	SR	3.1	68				4	1	1
DSF#1	9511	F	MS	SR		59.1	0.2	2		1.1	4.8	1.1
DSF#1	9514	F	MS	SR	1.4	64.3				1.6	1.7	1.1
DSF#1	9576	F	MS	SA-SR	1.4	64	1.4			2.2	0.8	2
DSF#1	9617	F	WS	SR	1.9	69	0.5	0.5	2.5	1.1		
DSF#1	9719	F	PS	SA-SR	1.2	63.1	2.8			1.7	0.2	0.5
BSH#1	8652	F	PS	SA	0.7	60	1	0.2	0.5	3	1.7	4
BSH#1	8693	F	WS	SR-R	1.1	65.5	1.4	0.7	2	1	1	0.5
BSH#1	8711	F	MS	SR	2	69				0.8	1	1.2
BSH#1	8734	F	WS	SR	0.6	69.5	0.2	0.8	2	2	0.5	0.4
BSH#1	8817	F	MS	SR	2.7	66	0.2	0.5	0.5	0.6	1.2	0.1
BSH#1	8852	F	MS	SA-SR	2.5	54.7				1.1	2.8	3.1
BSH#1	8888	VF	PS-MS	SA-SR	1	58.5				1.1	2.2	3.1
DSF#1	9641	F	WS	SR	2	64				2.2	0.8	2
<b>9- Lag deposits</b>												
Blocker#1	9745	PEBBLE	PS	SR-R	53.7	10					0.2	
JA#1	10135.5	F	PS	SA-SR	0.7	57.7				2.8	6	
Blocker#1	9338	VF	PS	SA-SR	9.2	35.9				1	2.2	
Blocker#1	9811	PEBBLE	PS	R	48	17.2				0.5		
JA#1	10113	PEBBLE	PS	SR	39	31				0.8	0.7	
Jones#3	9405	F	PS-MS	SA-SR	1.7	63	1	0.4		6	1.8	
Lowry#1	9476	PEBBLE	PS	SR	25	15				0.2		
SFE	9280.6	F	PS	SR		63	2			4	0.5	
<b>10- Bay</b>												
JA # 1	9974	F	WS	SA		32						
DSF#1	9668	F	MS	SR	3	68.8	1.4	1.2	3	2	0.5	0.1
Lowry#1	9537.9	VF	PS	SA	0.7	50	6	1.7		2	0.2	
BSH#1	8739	F	MS	SA-SR	1.5	65	0.2	0.5	0.2	1.4	1	
BSH#1	8741	F	MS	SA-SR	1.5	62.1	0.5		0.3	2	0.5	
BSH#1	8781	F	WS	SR	2	68.3				1	2.5	
BSH#1	8935	VF	MS	SA-SR	2	59	3	0.4	4	2	0.7	
BSH#1	8965	F	MS	SA-SR	1.1	63	2	1	2			
<b>11- Lagoon</b>												
SFE	9028.4	BIO MICRITE				12						
SFE	9034.5					19				0.5		
<b>12- Soil</b>												
JA # 1	8958	F	WS	SA-AR	2.3	65				1.1		1.1
BSH#1	8722	VF	WS	SR	2	64	1.8	0.7	2	3	1	1.1
Jones#3	8523.5	F	WS	SA-SR	2.5	67				0.5	0.2	
Jones#3	8535.5	F	PS	SA		57.3				2	0.5	0.1
Jones#3	8548	F	PS	SA		63.8				1.4	0.2	0.1



Appendix C: Electromicroprobe analyses of detrital and Authigenic feldspars.

Sample	Na2O	SiO2	K2O	Al2O3	CaO	BaO	Total	Ab mole%	Or mole %	An mole %	Lable
BSH 8693	11.36	67.79	0.09	19.28	0.06	0.00	98.57	99.21	0.49	0.31	ab
	11.24	67.59	0.04	20.20	0.78	0.02	99.88	96.07	0.23	3.70	ab
	9.94	65.57	0.65	20.97	1.41	0.01	98.55	89.14	3.85	7.01	ab
	9.30	64.12	0.17	22.27	3.34	0.01	99.21	82.60	0.99	16.41	ab
	11.52	67.35	0.03	19.22	0.11	0.00	98.23	99.31	0.15	0.54	ab
	10.55	67.09	0.07	19.89	0.53	0.00	98.13	96.91	0.41	2.69	ab
	10.79	67.56	0.04	19.53	0.08	0.01	98.01	99.37	0.21	0.42	ab
	11.00	68.00	0.02	19.51	0.03	0.00	98.56	99.74	0.13	0.14	ab
	10.82	67.80	0.03	19.42	0.03	0.02	98.11	99.68	0.18	0.14	ab
	11.56	68.38	0.01	19.48	0.00	0.00	99.43	99.95	0.04	0.01	ab
	10.93	65.40	0.92	21.02	0.91	0.00	99.18	90.79	5.03	4.18	ab
	8.77	63.56	0.13	22.74	4.10	0.01	99.32	78.83	0.78	20.38	ab
	0.46	64.04	15.89	18.12	0.01	0.00	98.52	4.22	95.73	0.05	potash
	10.68	67.38	0.10	19.39	0.34	0.00	97.88	97.71	0.59	1.70	ab
	10.11	64.28	0.37	21.81	3.08	0.02	99.66	83.85	2.05	14.10	ab
	10.00	64.59	0.30	21.70	2.90	0.02	99.52	84.73	1.69	13.59	ab
	0.49	63.42	15.42	17.99	0.07	0.18	97.57	4.60	95.06	0.35	potash
BSH 8722	0.35	63.07	14.93	19.63	0.11	0.03	98.12	3.42	95.97	0.61	potash
BSH 8935	0.55	65.08	16.07	18.15	0.00	0.44	100.28	4.93	95.07	0.00	potash
	0.55	64.58	15.56	17.45	0.02	0.40	98.56	5.12	94.79	0.09	potash
	0.60	65.76	14.96	16.97	0.00	0.21	98.50	5.75	94.24	0.01	potash
	0.75	59.94	13.66	17.88	0.10	0.05	92.37	7.66	91.80	0.54	potash
	0.68	64.80	15.72	18.45	0.01	0.61	100.28	6.20	93.75	0.05	potash
	0.39	63.33	16.42	17.85	0.00	0.14	98.13	3.47	96.53	0.00	potash
	0.54	62.95	15.96	17.76	0.01	0.15	97.36	4.85	95.09	0.06	potash
	0.46	62.50	16.50	17.40	0.02	0.01	96.89	4.04	95.84	0.11	potash
	0.69	62.19	15.80	17.59	0.05	0.43	96.74	6.17	93.60	0.22	potash
	1.28	62.03	15.55	17.29	0.03	0.24	96.43	11.13	88.71	0.16	potash
	0.39	63.20	16.25	17.88	0.07	0.13	97.91	3.47	96.20	0.33	potash
BH 9516	0.72	64.29	15.78	18.31	0.02	0.07	99.17	6.44	93.49	0.07	potash
	0.40	64.04	16.11	18.56	0.06	0.24	99.42	3.65	96.04	0.31	potash
	0.56	63.79	15.79	18.21	0.00	0.00	98.34	5.08	94.91	0.01	potash
	2.10	65.11	13.88	18.53	0.03	0.08	99.73	18.65	81.18	0.17	potash
	1.98	65.13	13.89	18.41	0.04	0.10	99.55	17.74	82.07	0.19	potash
JA10112	11.40	69.30	0.58	19.40	0.04	0.00	100.72	98.77	1.03	0.21	ab
	11.70	67.40	0.05	20.10	0.04	0.00	99.29	98.87	1.03	0.10	ab
	11.50	68.40	0.02	18.90	0.75	0.00	99.57	99.90	0.00	0.10	ab
	0.51	65.10	15.10	18.30	0.01	0.00	99.02	4.26	95.74	0.00	potash
	0.32	66.20	15.60	18.20	0.00	0.00	100.32	2.17	97.83	0.00	potash
	0.65	66.10	15.10	18.27	0.00	0.00	100.12	6.25	93.75	0.00	potash
	0.94	66.80	14.70	18.60	0.00	0.00	101.04	5.26	94.74	0.00	potash
JA 10260	0.76	65.20	14.90	18.20	0.00	0.00	99.06	96.94	3.06	0.00	ab

Appendix D: Point count data: Quartz overlap and quartz cement by using CL.

Well	Sample	Detrital Quartz	Quartz cement %	Overlap %	Others
BSH # 1	8847.5	73.5	13.5	3	10
JA # 1	10014	79	10.5	2.5	8
JA # 1	10045	80	10	1	9
BSH # 1	8871	78	12	0.5	9.5
XLC # 1	9192.4	79	11	0	10
XLC # 1	9177.5	77	13	1	9
JA # 1	10026	79	9	1	11
BSH # 1	8693	75	13	0.5	11.5
BSH # 1	8722	77	8	0	15
BSH # 1	8935	73	7	1	19
BSH # 1	8693	75	16	1	8

Appendix E: Percent of free grain surface coated by clay in potential reservoir facies.

Facies	Sample	% clay coats
Bioturbated SF	GL 9505	15.3
Bioturbated SF	GL 9510	7.5
Bioturbated SF	DSF 9595	10
Bioturbated SF	Jones 9409	11.8
Bioturbated SF	Jones 9428	6
Bioturbated SF	Bsh 8981	19
Bioturbated SF	Bh 9328	1.4
Bioturbated SF	Bh 9797	6.4
Average		11
Cryptobioturbated SF	JA 10027	3.4
Cryptobioturbated SF	Bsh 9344	6.7
Cryptobioturbated SF	Bh 9370	1
Cryptobioturbated SF	Bh 9924	5.3
Average		4.1
Sand flat	Bsh 8693	6.2
Sand flat	DSF 9641	8
Sand flat	DSF 9412	13
Average		9
Tidal SF	Jones 8602	11
Tidal SF	Jones 8605	12
Tidal SF	Jones 8608	7
Tidal SF	Jones 8609	4.5
Tidal SF	Jones 9400	10
Tidal SF	Bsh 9760	7
Tidal SF	Bsh 9739	7.9
Average		8.4
Average for all facies		8.6

## References

- Atkins, J.E., and McBride, E.F., 1992, Porosity and packing of Holocene river, dune, and beach sands: American Association of Petroleum Geologists Bulletin, v. 76, p. 339-355.
- Atwater, G.I., and Miller, E.G., The effects of decrease in porosity with depth on future development of oil and gas reserves in south Louisiana (abs.): American Association of Petroleum Geologists Bulletin, v. 69, p. 334.
- Aylon, A., and Longstaffe, F.G., 1990, Isolation of diagenetic silicate minerals in clastic sedimentary rocks for oxygen isotope analysis: A summary of methods; Israel: Journal of Earth Science, v. 39, p. 139-148.
- Bailey, J.W., 1983, Stratigraphy, environments of deposition, and petrography of the Cotton Valley Terryville Formation in Eastern Texas: The University of Texas at Austin, Master's thesis, 229p.
- Bartberger, C.E., Dyman, T.S., and Condon, S.M., 2002, Is there a basin-centered gas accumulation in the Cotton Valley sandstones, Gulf Coast, U.S.A.?: Geologic studies of basin centered gas systems: U. S Geological Survey Bulletin 2184-D, p. 1-38.
- Beard, D.C., and Weyl, P.K., 1973, Influence of texture on porosity and permeability of unconsolidated sand: American Association of Petroleum Geologists Bulletin, v. 57, p. 349-369.
- Bell, D.A., Siegrist, H.G., and Buurman, J.D., 1993, Paragenesis and reservoir quality within a shallow combination trap: Central West Virginia: American Association of Petroleum Geologists Bulletin, v. 77, p. 1077-2091.
- Berner, R.A., 1970, Sedimentary pyrite formation: American Journal of Science, v. 268, p. 1-23.
- Bjørkum, P.A., and Gjelsvik, N., 1988, An isochemical model for formation of authigenic kaolinite, K-feldspar and illite in sediments, Journal of Sedimentary Petrology, v. 58, p. 506-511.
- Bjørlykke, K., 1979, Discussion, cementation of sandstones: Journal of Sedimentary Petrology, v. 49, p. 1358-1359.



- Bjørlykke, K., 1980, Clastic diagenesis and basin evolution: *Revista del Instituto de Investigaciones Geologicas. Diputacion Provincial, Universidad de Barcelona*, v. 34, p. 21-44.
- Bjørlykke, K., 1984, Formation of secondary porosity: how important is it? in McDonald, D.A., and Surdam, R.C., eds., *Clastic Diagenesis: American Association of Petroleum Geologists Memoir 37*, p. 277-286.
- Bjørlykke, K., 1988, Sandstone diagenesis in relation to preservation, destruction and creation of porosity, in Chilingarian, G.V., and Wolf, K.H., eds., *Diagenesis*, 1: Elsevier, Oxford, p. 555-588.
- Bjørlykke, K., 1994, Fluid-flow processes and diagenesis in sedimentary basins, in Parnel, J., ed., *Geofluids: Origin, Migration, and Evolution of fluids in Sedimentary Basins: Geological Society Special Publication 78*, p. 127-140.
- Bjørlykke, K., and Egeberg, P.K., 1993, Quartz cementation in sedimentary basins: *American Association of Petroleum Geologists Bulletin*, v. 77, p. 1538-1548.
- Black, C.E., and Berg, R.R., 1987, Fan-delta reservoirs in the Lower Cotton Valley Group (Jurassic), Kildare field, northeast Texas: *Gulf Coast Association of Geological Societies Transactions*, v. 37, p. 35-42.
- Block, S., 1994, Importance of reservoir quality prediction in exploration, in Michel, Wilson, M.D., ed, *Reservoir quality assessment and prediction in clastic rocks: Society for Sedimentary Geology (SEPM) Short Course no. 30*, p. 5-8.
- Boles, J.R., 1982, Active albitization of plagioclase, Gulf Coast Tertiary: *American Journal of Science*, v. 282, p. 165-180.
- Boles, J.R., and Franks, S.G., 1979, Clay diagenesis in Wilcox sandstones of southwest Texas: implications of smectite diagenesis on sandstone cementation: *Journal of Sedimentary Petrology*, v. 49, p. 55-70.
- Bonnell, L.M., and Lander, R.H., 2002a, Reservoir quality prediction, from deep water to tight gas sandstones. GCAGS 2002 short course notes, Austin, Texas (unpublished).
- Bonnell, L.M., Lander, R.H., and Sundhaug, C., 1998a, Grain coatings and reservoir quality preservation: role of coating completeness, grain size and thermal history (abs.): *American Association of Petroleum Geologists Annual convection Extended Abstracts*, v. 1, p. A. 81.

- Bonnell, L.M., Lowray, C.J., and Bray, A.A., 1999, The timing of illitization, Haltenbamken, mid-Norway (abs.): American association of Petroleum Geologists Annual Convection Program, p. A14.
- Braithwaite, C.J.R., 1989, Stylolites as open fluid conduits: *Marine and Petroleum Geology*, v. 6, p. 93-96.
- Brint, J.F., Hamilton, P.J., Fallick, A.E., Haszeldine, S., and Brown, S., 1991, Oxygen isotopic analysis of diagenetic quartz overgrowths from Brent Sands: a comparison of two preparation methods: *Journal of Sedimentary Petrology*, v. 61, p. 527-533.
- Brown, L.F., and Fisher, W.L., 1977, Seismic-stratigraphic interpretation of depositional systems: examples from Brazilian rift and pull-apart basins, in *American Association of Petroleum Geologists Bulletin*, Memoir 26, p. 213-248.
- Buffler, R.T., Watkins, J.S., Shaub, F.J., and Worzel, J.L., 1980, Structure and early geologic history of the deep central Gulf of Mexico, in *Proceedings, Symposium on the origin of the Gulf of Mexico and the early opening of the central North Atlantic Ocean*: Baton Rouge, Louisiana State University, School of Geosciences, p. 3-16.
- Burgess, W.J. 1976, Geologic evolution of the mid-continent and Gulf Coast Areas-Aplate tectonic view. *Transactions Gulf Coast Association of Geological Societies*, v. 26, p. 132-143. Block, S., 1994, Importance of reservoir quality prediction in exploration, in Michel, Wilson, M. D., ed, *Reservoir quality assessment and prediction in clastic rocks*: Society for Sedimentary Geology (SEPM) Short Course no. 30, p. 5-8.
- Burley, S.D., 1993, Models of burial diagenesis for deep exploration plays in Jurassic fault TRAPS OF THE Central and Northern North Sea. In: *Petroleum Geology of Northwest Europe: Proceedings of the 4<sup>th</sup> Conference*, Parker, J.R., ed, Geological Society of London, p. 1353-1375.
- Burley, S. D., Kantorowicz, J.D., and Waugh, B., 1986, Clastic diagenesis, in Brenchley, P., J., and Williams, B.P.J., eds., *Sedimentology: Recent developments and application aspects*, Geological Society of America Special Publication no. 18, p.189-226.
- Burley, S.D., Mullis, J., and Matter, A., 1989, Timing diagenesis in the Tartan reservoir (UK North Sea): constraints from a combined cathodoluminescence microscopy and fluid inclusions studies: *Marine and Petroleum Geology*, v. 6, p. 21-42.
- Byrnes, A.P., 1994, Empirical methods of reservoir quality prediction, in Wilson, M.D., ed., *Reservoir Quality Assessment and Prediction in Clastic Rocks*: Society for Sedimentary Geology (SEPM) Short Course 30, p. 9-22.

- Canals, M., and Meunier, J.D., 1995, A model for porosity reduction in quartzite reservoirs by quartz cementation. *Geochemica et Cosmochemica Acta*, v. 59, no. 4, p. 699-709.
- Cecil, C.B., and Healds, M.T., 1971, Experimental investigation of the effects of grain coatings on quartz growth: *Journal of Sedimentary Petrology*, v. 41, p. 582-584.
- Clifton, H.E., and J.K., Thompson, 1978, *Macaronichnus segregates*- a feeding structure of shallow marine polychaetes: *Journal of Sedimentary Petrology*, v. 48, p. 1293-1302.
- Coleman, J.L., Jr., 1985. Diagenesis of Cotton Valley sandstone (Upper Jurassic), east Texas: Implications for tight gas formation pay recognition: discussion: *Americas Association of Petroleum Geologists Bulletin*, v. 69, no. 5, p. 813-815.
- Coleman, J.L. Jr., and Coleman, C.J., 1981, Stratigraphic, sedimentologic and diagenetic framework for the Jurassic Cotton Valley Terryville massive sandstone complex, Northern Louisiana: *Gulf Coast Association of Geological Societies Transactions*, v. 31, p. 71-79.
- Collins, S.E., 1980, Jurassic Cotton Valley and Smackover reservoir trends, east Texas, north Louisiana, and south Arkansas: *Americas Association of Petroleum Geologists Bulletin* v. 64, no. 7, p. 1004-1013.
- Curran, H.A., 1985, The trace fossil assemblage of a Cretaceous nearshore environment: Englishtown Formation of Delaware, U.S.A. In: H. A. Curran (editor): *Society of Economic Paleontologists and Mineralogists Special Publication no. 35*, p. 261-276.
- Curtis, C.D., 1983, A link between aluminum mobility and destruction of secondary porosity: *Americas Association of Petroleum Geologists Bulletin* v. 67, p. 380-384.
- Davis, J.C., 1973, *Statistics and data analysis in geology*; New York, John Wiley and Sons, Inc. 550p.
- Davies, D.K., 1979, *Quality of sandstone reservoirs: Lunnock, Texas*, D.K. Davis, Inc., 51p.
- Davies, J.P., Prediction of in-situ permeability: significance of rock type identification in reservoir characterization of tight gas sandstones, (abs.): *American Association of Petroleum Geologists*, v. 5, p. 33.

- Dewers, T., and Ortoleva, P., 1990, A coupled reaction/transport/mechanical model for intergranular pressure solution, stylolites, and differential compaction and cementation in clean sandstones: *Geochemica et Cosmochemica Acta*, v. 54, p. 1609-1625.
- Dewers, T., and Ortoleva, P., 1990a, Pressure solution during diagenesis: a unified model for intergranular pressure solution, stylolites and differential compaction/cementation, in I. Meshri and P. Ortoleva, eds., *Prediction of reservoir quality through chemical modeling: American Association of petroleum Geologists Memoir* (in press).
- Dickinson, W.W., and Milliken, K.L., 1994, The diagenetic role of brittle deformation in compaction and pressure solution, Etjo sandstone, Namibia: *The Journal of Geology*, v. 103, p. 339-347.
- Dickenson, K.A., Berryhill H.L., and Holmes C.W., 1972, Criteria for recognizing ancient barrier coastlines, In: J.K. Rigby and W.K. Hamblin (eds.), *Recognition of ancient sedimentary environments: Society of Economic Mineralogists and Paleontologists, Special Publication no. 16*, p. 192-214.
- Dott, H.R., Jr. 1983, SEPM Presidential Address: Episodic Sedimentation – How normal is average? How rare is rare? Does it matter?: *Journal of Sedimentary Petrology* v. 53, p. 5-23.
- Dott, H. R. Jr. 1988, An episodic view of shallow marine clastic sedimentation in: Debar P. L., vanGelder A., and Nio S.D. (eds.), *Tide-Influenced Sedimentary Environments and Facies*, D. Reidel Publishing Company, Dordrecht, p. 3-12.:
- Duke, W.L., 1985, Hummocky cross-stratification, tropical hurricanes, and intensive winter storms, *Sedimentology*, v. 32, p. 167-194.
- Duke, W.L., Arnott R.W.C., and Cheel R.J., 1991, Shelf sandstones and hummocky cross stratification: new insights on a stormy debate, *Geology*, V. 19, p. 625-628.
- Dunnay, M.A., 1981, Porosity and permeability reduction in the Cotton Valley sandstones, east Texas: Master's thesis, University of Missouri-Columbia, 127p.
- Dunnington, H.V., 1967, Aspects of diagenesis and shape change in stylolitic limestone reservoirs: *Seventh World Petroleum Congress*, p. 337-352.
- Dutton, S.P., 1986, Diagenesis and burial history of the Lower Cretaceous Travis Peak Formation, east Texas: Ph.D. Dissertation, The University of Texas, Austin, 165p.
- Dutton, S.P., 1987, Diagenesis and burial history of the lower Cretaceous Travis Peak Formation, East Texas: The University of Texas at Austin, Bureau of Economic Geology Report of Investigation No. 164, 58p.

- Dutton, S.P., and Diggs, T. N., 1990, History of quartz cementation in the Lower Cretaceous Travis Peak Formation, East Texas: *Journal of Sedimentary Petrology*, v. 60, no. 2, p. 190-202.
- Dutton, S.P., and Land, L.S., 1985, Meteoric Burial diagenesis of Pennsylvanian arkosic sandstones, southwestern Anadarko basin, Texas: *American Association of Petroleum Geologists Bulletin*, v. 69, p. 22-38.
- Dutton, S.D., Clift, S.J., Hamilton, D.S., Hamlim, H.S., Hentz, T.F., Howard, W.E., Akhter, M.S., and Laubach, S.E., 1992, Atlas of major low-permeability sandstone gas reservoirs in the continental United States: Bureau of Economic Geology, The University of Texas at Austin, Gas Research Institute, Contract no. 5082-211-0708, 460p.
- Einsele, G., 1992, *Sedimentary basins, evolution, facies, and sediment budget*, Springer Verlag, Berlin, 628p.
- Elshayeb, T., and Henk, B., 2003, The tight gas sands of the Cotton Valley Formation: A core workshop integrating the sedimentology, ichnology, and rock properties data for a comprehensive understanding of the depositional environments, sequence stratigraphy, reservoir characterization, and log Interpretation (low resistivity pay): Core Workshop, Bureau of Economic Geology.
- Eversull, L.G., 1985, Depositional systems and distribution of Cotton Valley blanket sandstones in north Louisiana: *Gulf Coast Association of Geological Society Transaction*, v. 35, p. 49-57.
- Eubanks, D.L., 1985, Depositional and diagenetic history of Terryville sandstones, Cotton Valley Group (Upper Jurassic), Carthage field, Panola County, Texas: Master's Thesis, Stephen F. Austin State University, 113p.
- Finley, R.J., 1986, An overview of selected blanket-geometry, low permeability gas sandstones in Texas, in Spencer, C.W., and Mast, R.F., eds., *Geology of tight gas reservoirs: Americas Association of Petroleum Geologists Studies in Geology* no. 24, p. 69-85.
- Fisher, R.S., 1982, Diagenetic history of Eocene Wilcox sandstones and associated formation waters, south-central Texas: Ph.D. Dissertation, The University of Texas at Austin, Texas, 185p.
- Folk, R.L., 1974, *Petrology of sedimentary rocks* Austin, Texas: Hemphill Publishing CO.
- Folk, R.L., 1998, Nannobacteria and the precipitation of pyrite as framboids and large

- crystals: some comparisons with cooper minerals: Geological Society of America Southeastern Section, 47. the Annual Meeting Charleston, W.V, abstracts with programs, v. 30, no. 4, p. 12.
- Fothergill, C.A., 1955, The cementation of oil reservoir sands and its origin: Fourth World Petroleum Congress, Rome, Proceedings, Section 1, p. 301-314.
- Franks, R.L., and Forester, R.W., 1984, Relationship among secondary porosity, pore-fluid chemistry and carbon dioxide, Texas Gulf Coast, in McDonald, D.A., and Surdam, R.C., eds., *Clastic Diagenesis: Americas Association of Petroleum Geologists Memoir 37*, p. 63-79.
- Frazier, D.E., 1974, Depositional episodes: their relationship to the Quaternary stratigraphic framework in the northwestern portion of the Gulf Basin: University of Texas, Austin, Bureau of Economic Geology Geological Circular 71-1.
- Friedman, M., 1954, Miocene orthoquartzite from New Jersey: *Journal of Sedimentary Petrology*, v. 24, p. 235-241.
- Friedman, G.M., 1971, *Staining: Procedures in Sedimentary Petrology*: Wiley-Interscience Publisher, New York, p. 511-530.
- Friedman, I., and O'Neil, J. R., 1977, Compilation of stable isotopic fractionation factors of geochemical interest, in Fleischer, M., ed., *Data of Geochemistry*, 6<sup>th</sup> edition: United States Geological Survey, USGS, Professional paper no. 440-KK, 12p.
- Füchtbauer, H., 1967, Influence of different types of diagenesis on sandstone porosity: 7<sup>th</sup> World Petroleum Congress Proceedings, v. 2, p. 353-369.
- Füchtbauer, H., 1974, *Sediments and Sedimentary Rocks 1*: John Wiley and Sons, New York, 464p.
- Galloway, W.E., 1984, Hydrologic regimes of sandstone diagenesis, in McDonald, D.A., and Surdam, R.C., eds., *Clastic diagenesis: American Association of Petroleum Geologists Memoir no. 37*, p. 3-13.
- Galloway, W.E., 1989a, Genetic stratigraphic sequences in basin analysis I: architecture and genesis of flooding surface bounded depositional units: *American Association of Petroleum Geologists Bulletin*, v. 73, p. 125-142.
- Galloway, W.E., and Cheng, E.S., 1985, Reservoir facies architecture in a microtidal barrier system-Frio Formation, Texas Gulf Coast: The University of Texas at Austin, Bureau of Economic Geology Report of investigations no. 144, 36p.
- Galloway, W.E., and Hobday, D.K., 1983, *Terrigenous clastic depositional systems-applications to petroleum, coal, and uranium exploration*: New York, Springer-Verlag, 423p.

- Galloway, W.E., and Hobday, D.K., 1996, Terrigenous Clastic Depositional S, 2<sup>nd</sup> edition: New York, Springer-Verlag, pp. 490.
- Galloway, W.E., Ewing, T.E., Garrett, C.M., Tyler, N., and Bebout, D. G., 1984, Atlas of major oil reservoirs: The University of Texas at Austin, Bureau of Economic Geology, Special publication, 193p.
- Gaupp, R., Matter, A., Platt, J., Ramseyer, K., and Walzebuck, J., 1993, Diagenesis and fluid evolution of deeply buried Permian (Rotliegende) gas reservoirs, northwest Germany: American Association of Petroleum Geologists Bulletin, v. 77, p. 1111-1128.
- Genuise, J.J., Petrography and geochemistry of authigenic chlorite from Cretaceous and Oligocene sandstones of the Texas/Louisiana Gulf Coast: Master's Thesis, The University of Texas, Austin, 191p.
- Giles, M.R., and Marshall, J.D., 1986, Constraints on the development of secondary porosity in the subsurface: reevaluation of processes: Marine and Petroleum Geology, v. 3, p. 243-255.
- Gold, P.B., 1984, Diagenesis of Middle and Upper Miocene sandstones, Louisiana Gulf Coast: The University of Texas at Austin, Master's thesis, 115p.
- Goldstein, A., Jr. and Reno, D.H., 1952, Petrography and metamorphism of sediments of Ouachita facies: American Association of petroleum Geologists Bulletin, v 36, p. 2275-2290.
- Halbouty, M.T., and Halbouty, J.J., 1982, Relationships between East Texas Field Region and Sabine Uplift in Texas: American Association of Petroleum Geologists Bulletin, v. 66, n. 8, p. 1042-1054.
- Hall, C.D., Janks, J.S., and Ladle, G.H., 1984, Sedimentology and diagenesis of the Cotton Valley sandstone in the Amoco No. 1 Cullers Well, Rusk County, Texas, in Presley, M.W. ed., The Jurassic of East Texas, East Texas Geological Society, p. 127-140.
- Ham, W.E., Denison, R.E., and Merritt, C.A., 1964, Basement rocks and structure evolution of southern Oklahoma: Oklahoma Geological Survey, Bulletin 95, 302p.
- Haq, B.U., Hardenbol, J., and Vail, P.R., 1987, Chronology of fluctuating sea levels since the Triassic (250 million years ago to the present): Science, v. 235, 1156-1167.
- Hawkins, P.J., 1978, Relationship between diagenesis, porosity reduction, and oil emplacement in Late Carboniferous sandstone reservoirs, Bothamsall oilfield, E. Midland: Journal of the Geological Society of London, v. 135, p. 7-24.



- Heald, M.T., 1955, Stylolites in sandstones: *Journal of Geology*, v. 63, p. 101-114.
- Heald, M.T., 1956, Cementation of Simpson And St. Peter sandstones in parts of Oklahoma, Arkansas, and Missouri: *Journal of Geology*, v. 58, p. 624-633.
- Heald, M.T., 1959, Significance of stylolites in permeable sandstones: *Journal of Sedimentary Petrology*, v. 29, p. 251-253.
- Henk, B., and Elshayeb, T., 2004, The tight gas sands of the Cotton Valley Formation: A core workshop integrating the sedimentology, ichnology, and rock properties data for a comprehensive understanding of the depositional environments, sequence stratigraphy, reservoir characterization, and log Interpretation (low resistivity pay): Core Workshop, Bureau of Economic Geology.
- Heron, S.D., Jr., Moslow, T.F., Berelson, W.M., Herbert, J.R., Steele, G.A., III, and Susman, K. R., 1984, Holocene sedimentation of a wave-dominated barrier islan shoreline: Cape Lookout, North Carolina: *Marine Geology*, v. 60, p. 413-434.
- Hogg, A.J.C., Sellier, E., and Jourdan, A.J., 1992, Cathodoluminescence of quartz cements in Brent Group Sandstones, Alwyn South, UK North Sea., in Morton, A.C., Haseldine, R.S., Giles, M.R., and Brown. S., *Geology of the Brent Group*, Geological Society of London Special Publication no. 61.
- Houghton, H.F., 1980, Refined techniques for staining plagioclase and alkali feldspars in thin section: *Journal of Sedimentary Petrology*, p. 629-631.
- Houseknecht, D.W., 1984, Influence of grain size and temperature on intergranular pressure solution, quartz cementation, and porosity in quartzose sandstone: *Journal of Sedimentary Petrology*, v. 54, p. 348-361.
- Houseknecht, D.W., 1987, Assessing the relative importance of compaction processes and cementation to reduction of porosity in sandstones: *American Association of Petroleum Geologists Bulletin*, v. 71, p. 633-642.
- Howard, J.D., 1972, Trace fossils as criteria for recognizing shorelines in stratigraphic record. In: Rigby J.K. and Hamblin W. K. (eds.), *Recognition of Ancient Sedimentary Environments*. Society of Economic Paleontologists and Mineralogists Special Publication, n. 16, p. 215-225.
- Howard, J.D. 1975. The sedimentological significance of trace fossils. In: R. W. Frey (editor), *the study of trace fossils*, Springer-B Verlag, New York, p. 131-146.
- Howard, J.D., and Frey R.W., 1975, Estuaries of the Georgia coast, U.S.A.: sedimentology and biology: *Senckenbergiana Maritima*, v. 7, p. 1-13
- Hoyt, J.H., 1967, Barrier island formation: *Geological Society of America Bulletin* 78, p. 1123-1136.

- Hoyt, J.H., and Henry V.J., 1967, Influence of inlet migration on barrier island sedimentation: Geological Society of America Bulletin, V. 78, p. 77-86.
- Hubbard, S.M., Pemberton S.G., and Howard E.A., 1999, Regional geology and sedimentology of the basal Cretaceous Peace River Oil Sand deposit north Central Alberta: Bulletin Canadian Society of Petroleum Geologists, v. 47, p. 270-297.
- Hunt, J.M., 1979, Petroleum Geochemistry and Geology, W.H. Freeman and CO., San Francisco, 617p.
- Hurst, A., and Irwin, H., 1982, Geological modeling of clay diagenesis in sandstones: Clay and Clay Minerals, v. 17, p. 5-22.
- Hutcheon, I., and Abercrombie, H.J., 1990a, Carbon dioxide in clastic rocks and silicate hydrolysis: Geology, v. 18, p. 541-544.
- Hutcheon, I., and Abercrombie, H.J., 1990b, Fluid-rock interactions in thermal recovery of bitumen, Tucker Lake Pilot, Cold Lake, Alberta, in Meshri, I.D., and Ortoleva, P.J., eds., Prediction of Reservoir Quality through Chemical Modeling: American Association of Petroleum Geologists Memoir 49, p. 161-170.
- Imlay, R.W., 1943, Jurassic formations of the Gulf region: American Association of Petroleum Geologists Bulletin, v. 27, no. 11, p. 1407-1533.
- Jackson, M.L.W., and Lauback, S.E., 1991, Structure history and origin of the Sabine arch, east Texas and northwest Louisiana: University of Texas at Austin, Bureau of Economic Geology, Geological Circular 91-3, 47 p.
- James, W.C., Wilmar, G.C., and Davidson, B.G., 1986, Role of quartz type and grain size in silica diagenesis, Nugget Sandstone, south-central Wyoming: Journal of Sedimentary Petrology, v. 65, p. 657-662.
- Janks, J.S., Sanness, T., and Rasmussen, B.A., 1985, Diagenesis of the Cotton Valley sandstones, Catahoula Creek Field, Southern Mississippi: Gulf Coast Association of Geological Societies transaction volume 35, p. 415-423.
- Jervey, M.T., 1988, Quantitative geological modeling of siliclastic rock sequences and their seismic expressions, in C.K. Wilgus et al., eds., Sea level changes: an integrated approach: Society of Economic Paleontologists and Mineralogists Special Publication 42, p. 47-69.
- Johnston, D.D., and Johnson, R.J., 1987, Depositional and diagenetic controls on reservoir quality in First Wilcox Sandstone, Livingston Field, Louisiana: American Association of Petroleum Geologists Bulletin, v. 71, p. 1152-1161.

- Kaiser, W.R., 1984, Predicting reservoir quality and diagenetic history in the Frio Formation (Oligocene) of Texas, in McDonald, D. A., and Surdam, R. C., eds., *Clastic diagenesis: American Association of Petroleum Geologists Memoir no. 37*, p. 195-215.
- Karaka, Y.K., Leroy, M.L., Carothers, W.W., and Goerlitz, D.F., 1986, Role of organic species dissolved in formation waters from sedimentary basins in mineral diagenesis, in Gautier, D.L., ed., *Roles of Organic Matter in Sediment Diagenesis: Society of Economic Paleontologists and Mineralogists Special Publication 38*, p. 111-122.
- Kast, J.A., 1978, Depositional environment of the Schuler Formation (Late Jurassic) in Upshure County, Texas: Master's Thesis: Southern Methodist University, Dallas, Texas.
- Mcmanus, M.M., and Tibbetts, S.D., 1993, Sequence stratigraphy and depositional controls on reservoir quality of Upper Jurassic Cotton Valley sandstones, Carthage field, East Texas (abs.): *American Association of Petroleum Geologists*, v. 1993, p. 149.
- Kosters, E.C., Bebout, D.G., Seni, S.J., Garrett, C.M., J.R., Brown, L.F., Jr., Hamlin, H.S., Dutton, S.P., Ruppel, S.C., Finley, R.J., and Tyler, N., 1989, *Atlas of major Texas gas reservoirs: The University of Texas at Austin, Bureau of Economic Geology*, 161 p.
- Kreitler, C.W., Collins, E.W., Fogg, G.E., Jackson, M.P.A., and Seni, S.J., 1983, Hydrogeologic characterization of the saline aquifers, East Texas Basin- Implications to nuclear waste storage in East Texas salt domes: The University of Texas at Austin, Bureau of Economic Geology, report prepared for U. S. Department of Energy under contract no. DE-AC97-80ET46617, 54p.
- Kvale, E.P., and Archer, A.W., 1991, Characteristics of two, Pennsylvanian-age, semidiurnal tidal deposits in Illinois Basin, U.S.A., in Smith D. G. ed., *Clastic tidal sedimentology. Canadian Society of Petroleum Geologists Memoir 16*, p. 179-188.
- Land, L.S., 1984, Frio sandstone diagenesis, Texas Gulf Coast: a regional isotopic study, in McDonald, D.A., and Surdam, R.C., eds., *Clastic diagenesis: American Association of Petroleum Geologists Memoir 37*, p. 37-62.
- Land, L.S., and Macpherson, G.L., 1992a, Origin of the saline formation waters, Cenozoic section, Gulf of Mexico sedimentary basins: *American Association of Petroleum Geologists Bulletin*, v. 76, p. 1344-1362.

- Land, L.S., and Milliken, K.L., 1981, Feldspar diagenesis in the Frio Formation, Brazoria County, Texas: *Geology*, v. 9, p. 314-318.
- Land, L.S., Milliken, K.L., and McBride, E.F., 1987, Diagenetic evolution of Cenozoic sandstones, Gulf of Mexico sedimentary basin: *Sedimentary Geology*, v. 50, p. 195-225.
- Lander, R.H., Felt, V., Bonnell, L., 1997b, Sensitivity/risk assessment with basin models: approach and case example from a frontier setting (abs.): American association of Petroleum Geologists Annual convection Program, p. A66.
- Lander, R.H., Felt, V., Bonnell, L., and Walderhaug, O., 1997a, Utility of sandstone diagenetic modeling for basin history assessment (abs.): American association of Petroleum Geologists Annual convection Program, p. A66.
- Lander, R.H., and Walderhaug, O., 1997, An empirically calibrated model for sandstone reservoir prediction (abs.): American association of Petroleum Geologists Annual convection Program, p. A66.
- Lander, R.H., and Walderhaug, O., 1999, Predicting porosity through simulating sandstone compaction and quartz cementation: American association of Petroleum Geologists Bulletin, v. 83, p. 433-449. Annual convection Program, p. A66.
- Lander, R.H., Walderhaug, O., Bonnell, L., and 1997c, Application of sandstone diagenetic modeling to reservoir quality prediction and basin history assessment: *Memorias del I Congreso Latinoamericano de Sedimentologica*, Soc. Venezolana de Geólogos, Tomo I, p 373-386.
- Lauback, S.E., and M.L.W. Jackson, 1991, Origin of arches in the northwestern Gulf of Mexico Basin: *Geology*, v. 18, p. 595-598.
- Leder, F., and Park, W.C., 1986, Porosity reduction in sandstone by quartz overgrowth: *American Association of Petroleum Geologists Bulletin*, v. 70, p. 1713-1728.
- Lee, M., and Savin, S.M., 1985, Isolation of diagenetic overgrowths on sand grains for oxygen isotope analysis: *Geochemica et Cosmochemica Acta* v. 49, p. 497-501.
- Lerand, M.M., Nelson, H.R., and Schmidt, V. 1976, Reduction of porosity in reservoir sandstones by authigenic minerals: Geological Association of Canada, Mineralogical Association of Canada, and Canadian Geophysical Union, Joint Annual Meeting Program with Abstracts, v. 1, p. 50
- Lind. C., and Heim, J., 1975, Effects of organic solutes on chemical reactions of aluminum: United States Geological Survey, Water Supply Paper 1827-G, 82p.

- Longstaffe, F.J., 1986, Oxygen isotope studies of diagenesis in the basal Belly River sandstone, Pembina I-Pool, Alberta: *Journal of Sedimentary petrology*, v. 65, p. 78-88.
- Longstaffe, F.J., 1989, Stable isotopes as tracers in clastic diagenesis, in Hutcheon, I.C., ed., *Burial Diagenesis Mineralogy Association of Canada Short course Handbook* no. 15, p. 197-199.
- Longstaffe, F.J., 1993, Meteoric water and sandstone diagenesis in the western Canada sedimentary basin, in Horbury, A.D., and Robinson, A.G., eds., *Diagenesis and basin Development: American Association of Petroleum Geologists studies in Geology* 36, p. 49-68.
- Loutit, T.S., Hardenbol, J., Vail, P.R., and Baum, G.R., 1988, condensed sections: the key to age dating and correlation of continental margin sequences, in Wilgus, C.K., Hastings, B.S., Kendall, C.G., Posamentier, H.C., Ross, C. A., and Van Wagoner, J.C., eds., *Sea-level changes: an integrated approach: Society of Economic Paleontologists and Mineralogists Special Publication* 42, p. 183-216.
- Lundergard, P.D., and Land, L.S., 1986, Carbon dioxide and organic acids: their role in porosity enhancement and cementation, *Paleogene of the Texas Gulf Coast*, in Gautier, D.L., ed., *Roles of Organic Matter in Sediment Diagenesis: Society of Economic Paleontologists and Mineralogists Special Publication* 38, p. 129-146.
- Lyon, I.C., Burley, S.D., McKeever, P.J., Saxton, J.M., and Macaulay, C., 2000, Oxygen isotope analysis of authigenic quartz in sandstones: a comparison of ion microprobe and conventional analytical techniques: in R.H. Worden, and S. Morad, eds., *Quartz cementation in sandstones: Special publication for the international Association of Sedimentologists*, no. 29, p. 299-316.
- MacEachern, J.A., and S.G., Pemberton, 1992, Ichnological aspects of Cretaceous shoreface successions and shoreface variability in the western interior of seaway of North America. In: Pemberton, S.G. ed., *Applications of Ichnology to Petroleum Exploration: a core workshop*, no. 17, p. 169-198.
- Mann, C.J., and Thomas, W.A., 1964, Cotton Valley Group (Jurassic) nomenclature, Louisiana and Arkansas: *Gulf Coast Association of Geological Societies Transactions*, v. 14, p. 143-152.
- McBride, E.F., 1985, Diagenetic processes that affect provenance determination in sandstones, in Zuffa, G.G., ed., *Provenance of Arenites: NATO Advanced Studies Institute, Series C: Mathematical and Physical Science*, v. 148, D. Reidel Publishing Company, Boston, p. 95-114.
- McBride, E.F., 1989, Quartz cement in sandstones: a review: *Earth Science Reviews*, 26, p. 69-112.

- McBride, E.F., Land, L.S., and Mack, 1987, Diagenesis of eolian and fluvial feldspathic sandstones, Norphlet Formation (Upper Jurassic), Rankin County, Mississippi, and Mobile County, Alabama: American Association of Petroleum Geologists Bulletin, v. 71, p. 1019-1034.
- McDevitt, M.C., 1983, Petrology and diagenesis of the Terryville sandstones (Cotton Valley), Northwestern Louisiana: University of New Orleans, Master's thesis, 82p.
- McGowen, M.K., and Harris, D.W., 1984, Cotton Valley (Upper Jurassic) and Hosston (Lower Cretaceous) depositional systems and their influence on salt tectonics in the East Texas Basin: University of Texas, Bureau of Economic Geology, Geological Circular 84-5, 41p.
- Milliken, K.L., 1988, Loss of provenance information through subsurface diagenesis in Plio-Pliocene sandstones, Northern Gulf of Mexico: Journal of Sedimentary Petrology, v. 58, p. 992-1002.
- Milliken, K.L., 1989, Petrography and composition of authigenic feldspars, Oligocene Frio Formation, South Texas: Journal of Sedimentary Petrology, v. 59, p. 361-374.
- Milliken, K.L., 2003, Microscale distribution of kaolinite in Breathitt Formation sandstones (middle Pennsylvanian): Implications for mass balance: International Association of Sedimentologists, Special Publication no. 34, p. 343-360.
- Milliken, K.L., Land, L.S., and Loucks, R.G., 1981, History of burial diagenesis determined from isotopic geochemistry, Frio Formation, Brazoria CO., Texas: American Association of Petroleum Geologists Bulletin, v. 65, p. 1397-1413.
- Milliken, K.L., McBride, E.F., and Land, L.S., 1989, Numerical assessment of dissolution versus replacement in the subsurface destruction of detrital feldspars, Oligocene Frio Formation, South Texas: Journal of Sedimentary Petrology, v. 59, p. 740-757.
- Miser, H.D., 1959, Structure and vein quartz of the Ouachita Mountains of Oklahoma and Arkansas, in Cline, L.M., Hilseweck, W.J., and Feray, D.E., (eds.), The geology of the Ouachita Mountains, a symposium: Dallas and ARDMORE GEOLOGICAL SOCIETIES. P. 30-43.
- Mitchum, R.M. Jr., and Vail, P.R., 1977, Seismic stratigraphy and global changes in sea level, part 7: Seismic stratigraphic interpretation procedure, in Payton, C.E., ed., Seismic stratigraphy-applications to hydrocarbon exploration: American Association of Petroleum Geologists Bulletin, Memoir 26, p. 135-143.

- Moraes, M.A.S., and De Ros, L., 1989, Infiltrated clays in fluvial Jurassic sandstones of Reconcavo Basin, Northeastern Brazil: *Journal of Sedimentary Petrology*, v. 60, no. 6, p. 809-819.
- Morad, S., Bergin M., Knarud, R., and Nystuen, J.P., 1990, Albitization of detrital plagioclase in Triassic reservoir sandstones from the Snorre Field, Norwegian North Sea: *Journal of Sedimentary Petrology*, v. 60, p. 411-425.
- Morad, S., De Ros, L.F., Nystuen, J.P., and Bergan, M., 1998, Carbonate diagenesis and porosity evolution in sheet-flood sandstone: evidence from the Middle and Lower Lunde Members (Triassic) in the Snorre Field, Norwegian North Sea, in Morad, S., ed., *Carbonate Cementation in Sandstones: International Association of Sedimentologists Special Publication 26*, p. 53-85.
- Morton, R.A., 1979, Temporal and spatial variations in shoreline changes and their implications, examples from the Texas Gulf Coast: *Society of Economic Paleontologists and Mineralogists* v. 49, p. 1101-1111.
- Morton, R.A., and Land, L.S., 1987, Regional variations in formation water chemistry, Frio Formation (Oligocene): Texas Gulf Coast: *American Association of Petroleum Geologists Bulletin*, v. 71, p. 191-206.
- Nelson, R.A., 1983, Localization of aggregate stylolites by rock properties. *American Association of Petroleum Geologists Bulletin*, v. 67, p. 313-322.
- Oehler, J.H., 1984, Carbonate source rocks in the Jurassic Smackover trend of Mississippi, Alabama, and Florida, in Palacas, J.G., ed., *Petroleum geochemistry and source rock potential of carbonate rocks: Tulsa: American Association of Petroleum Geologists Studies in Geology*, v. 18, p. 63-69.
- Oelkers, E.H., Bjørkum, P.A., and Murphy, W.M., 1996, A petrographic and computational investigation of quartz cementation and porosity reduction in North Sea sandstones: *American Journal of Science*, v. 296, p. 420-452.
- Park, W.C., and Scott, E.H., 1968, Stylolites: their nature and origin. *Journal of Sedimentary Petrology*, v. 38, p. 175-191.
- Paxton, S.T., Szabo, J.O., Ajdukiewicz, and Klimentidis, R.E., 2002, Construction of an intergranular volume compaction curve for evaluating and predicting compaction and porosity loss in rigid-grain sandstone reservoirs: *American Association of Petroleum Geologists Bulletin*, v. 86, no. 12, p. 2047-2067.
- Pettijohn, F.J., Potter, P.E., and Siever, R., 1987, *Sand and Sandstone*, 2<sup>nd</sup> edition, Springer-Verlag, New York, 553p.
- Pemberton, S.G., and Frey R.W., 1985, The *Glossifungites* ichnofacies: modern examples



- from the Georgia coast, U.S.A: in H.A. Curran, ed., *Biogenic Structures: Their Use in Interpreting Depositional Environments*. Society of Economic Paleontologists and Mineralogists Special Publication 35, p. 237-259.
- Pemberton, S.G., and MacEachern J.A., 1997, The ichnological signature of storm deposits: the use of trace fossils in event stratigraphy. In: C.E. Brett, and G.C. Baird, eds., *Palaeontological events*. Columbia University Press, New York: p. 74-109.
- Pemberton, S.G., MacEachern, J.A., and Ranger M.J., 1992, Ichnology and event stratigraphy: the use of trace fossils in recognizing tempestites. In S. G. Pemberton (editor), *Applications of ichnology to petroleum exploration: a core workshop*. SEPM, p. 85-117.
- Pemberton, S.G. and Wightman D.M., 1992, Ichnological characteristics of brackish water deposits: in S. G. Pemberton ed., *Applications of Ichnology to Petroleum Exploration: a core workshop*. SEPM, core workshop Notes 17: 141-167.
- Pemberton, S.G., Spila, A.J. Pulham, T. Saundres, J. MacEachern, D. Robbins, and I. Sinclair, 2001, Ichnology and sedimentology of shallow to marginal marine systems-Ben Nevis and Avalon reservoir, Jeanne d' Arc Basin, Geological Association of Canada, Short Course Notes 15, 353p.
- Pittman, E.D., 1970, Plagioclase feldspar as an indicator of provenance in sedimentary rocks: *Journal of Sedimentary Petrology*, v. 40, p. 591-598.
- Pittman, E.D., 1972, Diagenesis of quartz in sandstones as revealed by scanning electron microscopy: *Journal of Sedimentary Petrology*, v. 42, p. 507-519.
- Pittman, E.D., 1979, Porosity, diagenesis and productivity capability of sandstone reservoirs in Scholle, P.A., and Schluger, P.R., eds., *Aspects of Diagenesis*: Society of Economic Paleontologists and Mineralogists Special Publication no. 26, p. 159-174.
- Pittman, E.D., and Larese, R.E., 1991, Compaction of lithic sands: experimental results and applications: *American Association of Petroleum Geologists Bulletin*, v. 75, p. 1279-1299.
- Posamentier, H.W., and Vail, P.R., 1988, Eustatic controls on clastic deposition II sequence and system tract models, in Wilgus, C.K., Hastings, B.S., eds., *Sea-level changes: an integrated approach*: Society of Economic Paleontologists and Mineralogists Special Publication 42, p. 109-124.
- Posamentier, H.W., Jervey, M.T., and Vail, P.R., 1988, Eustatic controls on clastic

- deposition I-conceptual framework, , in Wilgus, C.K., Hastings, B. S., eds., Sea-level changes: an integrated approach: Society of Economic Paleontologists and Mineralogists Special Publication 42, p. 125-154.
- Presely, M.W., and Reed, C.H., 1984, Jurassic exploration trend of East Texas, in Presley, M.N., ed., The Jurassic of East Texas: East Texas Geological Society, Tylor, Texas, p. 11-22.
- Pryor, W.A., 1973, Permeability-porosity patterns and variations in some Holocene sand bodies: American Association of Petroleum Geologists Bulletin, 57, p. 162-189.
- Rampino, M.R., and J.E. Sanders, 1980, Holocene transgression in south-central Long Island, New York: Journal of Sedimentary Petrology, v. 4, p. 1063-1080.
- Ramseyer, K., Boles, J.R., and Lichtner, P.C., 1992, Mechanism of plagioclase albitization: Journal of Sedimentary Petrology, v. 62, p. 349-357.
- Reineck, H.E and Singh I.B., 1968, Depositional sedimentary environments with reference to terrigenous clastics, Springer-Verlag, New York, 281p.
- Renard, F., Brosse, E., and Gratier, J.P., 2000, The different processes involved in the mechanism of pressure solution in quartz-rich rocks and their interactions, , in Worden, R.H., and Morad, S., eds., Quartz cementation in Sandstones: International Association of Sedimentologists, Special Publication no. 29, p. 67-78.
- Riezebos, P.A., 1974, Scanning electron microscopical observations of weakly cemented Miocene sands: Geologie en Mijnouw, v. 53, p. 109-122
- Robinson, A., and Gluyas, J., 1992, Model calculations of loss of porosity in sandstones as a result of compaction and quartz cementation: Marine and Petroleum Geology, v. 9, p. 319-323.
- Rohrlich, V., Price, N.B., and Calvert, S.E., 1969, Chamosite in recent sediments of Loch Etive, Scotland: Journal of Sedimentary Petrology, v. 39, p. 624-631.
- Rose, P.R., 1987, Dealing with risk and uncertainty in exploration: how can we improve?: American Association of Petroleum Geologists Bulletin, v. 71, p. 1-16.
- Roy, P.S., Cowell, P.J., Ferland, M.A. and Thom, B.G., 1994, Wave dominated coasts, In: R.W. G. Carter and C. D. Woodroffe (eds.), Coastal Evolution, Late Quaternary Shoreline Morphodynamics, Cambridge University Press, p. 91-186.
- Salvador, A., 1987, Late Triassic-Jurassic paleogeography and origin of Gulf of Mexico Basin: Association of Petroleum Geologists Studies in Geology v. 71, no. 4, p. 419-451.

- Sassen, R., Moore, C.H., and Meendsen, F.C., 1987a, distribution of hydrocarbon source potential in the Jurassic Smackover Formation: *Organic Geochemistry*, v. 11, p. 379-383.
- Saucier, A.E., Finely, R.J., and Dutton, S.P., 1985, The Travis Peak (Hosston) Formation of East Texas and North Louisiana, in *Proceedings, 1985 Society of Petroleum Engineers/Department of Energy Joint Symposium on Low Permeability Reservoirs*, SPE/DOE Paper no. 13850, p. 15-22.
- Saunders, T., MacEachern J.A., and Pemberton, S.G., 1994, Cadotte Member sandstone: progradation in a boreal basin prone to winter storms, In: S. G., Pemberton, D. P. James and D. M., Wightman (eds.), *Canadian Society of Petroleum Geologists Mannville Core Conference*, p. 331-349.
- Schmidt, V., and McDonald, D.A., 1979a, The role of secondary porosity in the course of sandstone diagenesis , in Scholle, P.A., and Svhluger, P.R., eds., *Aspects of Diagenesis: Society of Economic Paleontologists and Mineralogists Special Publication no. 26*, p. 175-207.
- Schmidt, V., and McDonald, D.A., 1979b, Texture and recognition of secondary porosity in sandstones, in Scholle, P.A., and Svhluger, P.R., eds., *Aspects of Diagenesis: Society of Economic Paleontologists and Mineralogists Special Publication no. 26*, p. 209-225.
- Schwartz, F.W., and Longstaffe, F.J., 1988, Ground water and clastic diagenesis, in Back, W., Rosenshein, J. S., and Seaber, eds., *Hydrology: Boulder, Colorado: Geological Society of America, The Geology of North America*, v. 0-2, p. 413-434.
- Sclater, J.G., and Christie, P.A.F., 1980, Continental stretching: an explanation of the post-mid-Cretaceous subsidence of the central North Sea basin: *Journal of Geophysical Research*, v. 85, p. 3711-3739.
- Scotchman, I., Johnnes, L.H., and Miller, R.S., 1989, Clay diagenesis and oil migration in Brent Group sandstones of NW Hutton field, UK North Sea: *Clay Minerals* v. 24, p. 339-374.
- Seni, S.J., and Jackson, M.P.A., 1983, Evolution of salt structures, East Texas diapir province, part 1: sedimentary record of halokinesis: *Association of Petroleum Geologists Studies in Geology* v. 67, no. 8, p. 1219-1244.
- Shearer, H.K., 1938, Developments in South Arkansas and North Louisiana: *American Association of Petroleum Geologists Bulletin* v. 22, p. 719-727.
- Shelton, J.W., 1964, Authigenic kaolinite in sandstones: *Journal of Sedimentary Petrology*, v. 34, p. 102-111.

- Sibley, D.F., and Blatt, H., 1976, Intergranular pressure solution and cementation of the Tuscarora Orthoquartzite: *Journal of Sedimentary Petrology*, v. 46, p. 881-896.
- Siebert, R.M., Moncure, G.K., and Lahann, R.W., 1984, A theory of framework dissolution in sandstones, in McDonald, D.A., and Surdam, R.C., eds., *Clastic Diagenesis: Association of Petroleum Memoir 37*, p. 163-175.
- Siever, R., 1962, Silica solubility, 0-200°C, and the diagenesis of siliceous sediments: *Journal of Geology*, v. 70, p. 127-150.
- Siever, R., and Stone, W.N., 1994, Quantitative petrologic constraints on basin paleohydrologic models (abs.): American Association of Petroleum Geologists Annual Convention Program and Abstracts, p. 258-259.
- Sippel, R.F., 1968, Sandstone petrology, evidence from luminescence petrography: *Journal of Sedimentary Petrology* v. 38, p. 530-554.
- Soeder, D.J., and Chowdiah, P., 1990, Pore geometry in high- and low-permeability sandstones, Travis Peak Formation, East Texas: *Society of Petroleum Engineers Formation Evaluation*, v. 5, no. 4, p. 421-430.
- Souza, R.S., 1999, Integrated diagenetic modeling and reservoir quality assessment and prediction of the Agua Grande sandstones, Early Cretaceous, Reconcavo Basin, Northeast Brazil: PhD. Thesis, University of Texas at Austin, 386p.
- Spencer, C.W., 1987, Hydrocarbon generation as a mechanism for overpressuring in Rocky Mountain region: *American Association of Petroleum Geologists Bulletin*, v. 71, p. 368-388.
- Spötl, C., Houseknecht, D.W., and Riciputi, L.R., 2000, High temperature quartz cement and the role of stylolites in a deep gas reservoir, Spiro Sandstone, Arkoma Basin, U.S.A., in Worden, R. H., and Morad, S., eds., *Quartz cementation in sandstones: International Association of Sedimentologists, Special publication no. 29*, p. 281-297.
- Stewart, S.K., 1984, Smackover and Haynesville facies relationships in north-central East Texas, in Persely, M.W., ed., *The Jurassic of East Texas: East Texas Geological Society*, p. 56-62.
- Stone, W.N., and Siever, R., 1996, Quantifying compaction, pressure solution and quartz overgrowth cementation in moderately- and deeply-buried quartzose sandstones from the Greater Green River Basin, Wyoming: *SEPM Special publication No. 55*, p. 129-149.
- Storvoll, V., Bjørlykke, K., Karlsen, D., and Sagial, G., 2002, Porosity preservation in

- reservoir sandstones due to grain-coating illite: a study of the Jurassic Garn Formation from the Kristin and Lavrans fields, offshore Mid-Norway: *Marine and Petroleum Geology*, v. 19, p. 767-781.
- Surdam, R.C., Boese, S.W., and Crossey, L.J., 1984, The chemistry of secondary porosity, in McDonald, D.A., and Surdam, R.C., eds., *Clastic Diagenesis: American Association of Petroleum Geologists Memoir 37*, p. 127-149.
- Surdam, R.C., Jiao, Z.S., and MacGowan, D.B., 1993, Redox reactions involving hydrocarbons and mineral oxidants: a mechanism for significant porosity enhancement in sandstones: *American Association of Petroleum Geologists Bulletin*, v. 77, p. 1509-1518.
- Swain, F.M., 1944, Stratigraphy of Cotton Valley Beds of Northern Gulf Coastal Plain: *American Association of Petroleum Geologists Bulletin*, v. 28, p. 577-614.
- Swain, F.M., 1949, Upper Jurassic of northeastern Texas: *American Association of Petroleum Geologists Bulletin*, v. 33, p. 1206-1250.
- Swift D.J.P., 1975, Barrier island genesis: evidence from the Middle Atlantic shelf of North America: *Sedimentary Geology* v. 14, p. 1-43.
- Swift, D.J.P., A.G. Figueiredo, G.L. Freeland, and G.F. Oertel, 1983, Hummocky cross-stratification and mega ripples: a geological double standard? *Journal of Sedimentary Petrology*, V. 53, p. 1259-1317.
- Syers, J.K., Chapman, S.L., Jackson, M.L., and Rex, R.W., 1968, Quartz isolation from rocks, sediments and soils for determination of oxygen isotopic composition: *Geochemica et Cosmochemica Acta*, v. 32, p. 1022-1025.
- Tissot, B.P., and Welte, D.H., 1978, *Petroleum formation and occurrence*: New York, Springer-Verlag, 538p.
- Thomas, W.A., and Mann, C.J., 1966, Late Jurassic depositional environments, Louisiana and Arkansas: *American Association of Petroleum Geologists Bulletin*, v. 50 no. 1, p. 178-182.
- Trojan, M., 1985, Effects of diagenesis on reservoir properties and log response, upper Jurassic Taylor sandstone, Cotton Valley Group, Licolin Parish, Louisiana: *Gulf Coast Association of Geological Societies Transaction*, v. 35, p.515-524
- Turabian, K.L. 1987. *A Manual for Writers of Term Papers, Thesis, and Dissertations*. 5th ed. Chicago: The University of Chicago Press.
- Turner, J.R., 1997, Recognition of low resistivity, high permeability reservoir beds in the Travis Peak and Cotton Valley of east Texas: *Gulf Coast Association of Geological Societies Transaction*, v. 47, p. 585-593.

- Turner, P., Burley, S.D., Rey, D., and Prosser, J., 1995, Burial history of the Penrith Sandstone (Lower Permian) deduced from the combined study of fluid inclusions and palaeomagnetic data: *Palaeomagnetic Applications in Hydrocarbon Exploration and Production*, Geological Society of London Special Publication no. 98, p. 43-78.
- Vail, P.R., 1987, Seismic stratigraphy interpretation procedure, in Bally, A.W., ed., *Atlas of Seismic stratigraphy*: American Association of Petroleum Geologists Studies in Geology 27, p. 1-11.
- Vail, P.R., and Wornardt, W. Jr., 1991, An integrated approach to exploration and development in the 90's: well log-seismic sequence stratigraphy analysis: *Transactions-Gulf Coast Association of Geological Societies*, v. 41, p. 630-650.
- Varva, C.L., Scheihing, M.H., and Klein, J.D., 1990, Reservoir geology of the Taylor sandstone in the Oak Hill Field, Rusk County, Texas; integration of petrology, sedimentology, and log analysis for delineation of reservoir quality in a tight gas sand: American Association of Petroleum Geologists, *Proceedings of the 1<sup>st</sup> Archie Conference*, p. 130-158.
- van Wagoner, J.C., Mitchum, R.M., Campion, K.M., and Rahmanian V.D., 1990, Siliclastic sequence stratigraphy in well logs, core, and outcrops: concepts for high-resolution correlation of time and facies: *American Association of Petroleum Geologists Methods in Exploration Series*, no. 7, The American Association of Petroleum Tulsa, OK, 55p.
- van Wagoner, J.C., Posamentier, H.W., Mitchum, R.M., Vail, P.R., Sarg, J.F., Loutit, T.S., and Hardenbol, J., 1988, An overview of the fundamentals of sequence stratigraphy and key definitions, in Wilgus, C. K., Hastings, B. S., Kendall, C.G., Posamentier, H.C., Ross, C.A., and van Wagoner, J.C., eds., *Sea-level changes: an integrated approach*: Society of Economic Paleontologists and Mineralogists Special Publication 42, p. 39-45.
- Walderhaug, O., 1996, Kinetic modeling of quartz cementation and porosity loss in deeply buried sandstone reservoirs: *American Association of Petroleum Geologists Bulletin*, v. 80, p. 731-745.
- Walderhaug, O., Lander, R.H., Bjørkum, P.A., and Oelkers, E.H., Bjørlykke, K., and Nadeau, P.H., 2000, Modeling quartz cementation and porosity in reservoir sandstones: example from the Norwegian continental shelf, in Worden, R.H., and Morad, S., eds., *Quartz cementation in Sandstones*: International Association of Sedimentologists, Special Publication no. 29, p. 39-49.
- Walker, G., and Burley, S.D., 1991, Luminescence petrography and stereoscopic studies

- of diagenetic minerals, in, Luminescence Microscopy: in Barker, C. E., and Kopp, O. C., eds., Quantitative and Qualitative applications, Society of Economic Paleontologists and Mineralogists Special Publication no. 25, p. 83-92.
- Wanless, H.R., 1979, Limestone response to stress: pressure solution and dolomitization: *Journal of Sedimentary Petrology*, v. 49, p. 437-362.
- Weimer, R.J., Howard, J.D., and Lindsay, D.R., 1982, Tidal flats, in Scholle, P. A., and Spearing, D., eds., *Sandstone Depositional environments: American Association of Petroleum Geologists Memoir 31*, p. 191-246.
- Wescott, W.A., 1983, Diagenesis of Cotton Valley Sandstones (Upper Jurassic), East Texas: implications for tight gas formation pay recognition: *American Association of Petroleum Geologists Bulletin*, v. 67, p. 1002-1013.
- Wheatcroft, R.A., 1990, Preservation potential of sedimentary event layers: *Geology*, v. 18, p. 843-845.
- Wilkinson, B.H., 1975, Matagorda Island, Texas: the evolution of the Gulf Coast barrier complex: *Geological Society of America Bulletin* 86, p. 959-967.
- Williams, L.B., and Hervig, R.L., 1994, Correlating cathodoluminescence and oxygen isotopic compositions of detrital and diagenetic quartz: *Geological Society of America Annual meeting, Abstracts with Programs*, v. 26, p. 490.
- Williams, L.B., Hervig, R.L., and Dutton, S.P., 1997, Constrains on Paleofluid compositions in the Travis Peak Formation, East Texas: Evidence from microanalysis of oxygen isotopes in diagenetic quartz, in I. P. Montanez, J. M., Gregg, and K. L. Shelton, eds., *Basin wide diagenetic pattern: Integrated petrologic, geochemical, and hydrologic considerations*, Society of Sedimentary Geology Special Publication no. 57, p. 269-280.
- Williams, R., and Mitchum R.M., 1997, Sequence stratigraphic controls on Cotton Valley tight gas sandstones, Carthage Field, Panola County, Texas: in Shanley, R. A., ed., *Shallow marine and nonmarine reservoirs: Gulf Coast Section*, Society of Economic Paleontologists and Mineralogists Foundation 18<sup>th</sup> Ann. Res. Conf Proceedings, 409-425.
- Williams, R.A., Robinson M.C., Fernandez E.G., and Mitchum R.M., 2001, Cotton Valley/Bossier of East Texas: sequence stratigraphy creates depositional history: *Gulf Coast Association Geological Society Transaction*, V. 51, p. 379-388.
- Wilson, D.A., and Hensel, W.M., 1984, The Cotton Valley Sandstone of east Texas: A log-core study, in Presley, M.W., ed., *The Jurassic of East Texas: Tylor, Texas*, East Texas Geological Society, p. 141-152.



- Wilson, M.W., and Pittman, E.D., 1977, Authigenic clays in sandstones: recognition and influence on reservoir properties and paleoenvironmental analysis: *Journal of Sedimentary Petrology*, v. 47, no. 1, p. 3-31.
- Wood, J.R., and Brynes, A.P., 1994, Alternate and emerging methodologies in geochemical and empirical modeling, in Wilson, M. D., ed., *Reservoir Quality Assessment and Prediction in Clastic Rocks*: Society of Economic Paleontologists and Mineralogists Short Course no. 30, p. 395-400.
- Worden, R.H., and Morad, S., 2000, Quartz cementation in oil field sandstones: a review of the key controversies, in Worden, R.H., and Morad, S., eds., *Quartz cementation in Sandstones*: International Association of Sedimentologists, Special Publication no. 29, p. 1-20.
- Worrall, D.M., and Snelson, S., 1989, Evolution of the northern Gulf of Mexico, with emphasis on Cenozoic growth faulting and the role of salt, in Bally, A.W., and Palmer, A.R., eds., *The Geology of North America; An Overview*: Geological Society of America, *The Geology of North America Series*, v. A, p. 97-138.

## **Vita**

Tarek Abu Serie Elshayeb was born in Cairo, Egypt, on April 20, 1967, the son of Abu Serie. Tarek received his B.S. degree in geology from the Cairo University, Egypt, in 1988. After graduating, he started his academic career teaching sedimentary petrology and researching sandstone sedimentology and diagenesis as a faculty member of the department of Geological Sciences, Cairo University, Egypt. In the fall of 1996, he got his M.S. degree in geology with honors from Cairo University, Egypt. In the fall of 1999 he enrolled in graduate program at the Department of Geological Sciences at the University of Texas at Austin as part of his expertise improvement plan sponsored by the Egyptian Cultural and Educational Bureau. Tarek will teach in the Geology department, Cairo University, Egypt after graduation.

Permanent address:  
4 Toman Buy Street, Burg Samah  
6th Floor, apartment no. 35  
Zaitun, Cairo, Egypt.

This dissertation was typed by the author.